Dissertation zur Erlangung des Doktorgrades

der Fakultät für Chemie und Pharmazie

der Ludwig-Maximilians-Universität München

Advanced labeling methods and probe design for DNA-based super-resolution microscopy

Sebastian Strauß

aus Pfaffenhofen an der Ilm, Deutschland

2021

Erklärung

Diese Dissertation wurde im Sinne von § 7 der Promotionsordnung vom 28. November 2011 von Herrn Prof. Dr. Ralf Jungmann betreut und von Herrn Prof. Dr. Veit Hornung von der Fakultät für Chemie und Pharmazie vertreten.

Eidesstattliche Versicherung

Diese Dissertation wurde eigenständig und ohne unerlaubte Hilfe erarbeitet.

München, 08.06.2021

Sebastian Strauß

Dissertation eingereicht am 09.06.2021

1. Gutachter: Prof. Dr. Veit Hornung

2. Gutachter: Prof. Dr. Ralf Jungmann

Mündliche Prüfung am 14.07.2021

List of publications

Peer-reviewed publications that are part of this cumulative thesis:

S. Strauss, P. C. Nickels, M. T. Strauss, V. J. Sabinina, J. Ellenberg, J. D. Carter, S. Gupta, N. Janjic, R. Jungmann

Modified aptamers enable quantitative sub-10-nm cellular DNA-PAINT imaging

Nature Methods 15, 685-688 (2018)

O. K. Wade*, J. B. Woehrstein*, P.C. Nickels*, **S. Strauss***, F. Stehr, J. Stein, F. Schueder, M. T. Strauss, M. Ganji, J. Schnitzbauer, H. Grabmayr, P. Yin, P. Schwille, R. Jungmann (* equal contribution)

124-Color Super-resolution Imaging by Engineering DNA-PAINT Blinking Kinetics

Nano Letters, 19 (4), 2641-2646 (2019)

S. Strauss, R. Jungmann

Up to 100-fold speed-up and multiplexing in optimized DNA-PAINT

Nature Methods, 17, 789–791 (2020)

Other peer-reviewed publications:

F. Schueder, M. T. Strauss, D. Hoerl, J. Schnitzbauer, T. Schlichthaerle, **S. Strauss**, P. Yin, H. Harz, H. Leonhardt, R. Jungmann

Universal Super-Resolution Multiplexing by DNA Exchange

Angewandte Chemie International Edition, 56 (14), 4052-4055 (2017)

A. Auer, M.T. Strauss**, S. Strauss**, R. Jungmann

nanoTRON: a Picasso module for MLP-based classification of super-resolution data

Bioinformatics, 36 (11), 3620-3622 (2020)

M. I. E. Harwardt, M. S. Schröder, Y. Li, S. Malkusch, P. Freund, S. Gupta, N. Janjic, **S. Strauss**, R. Jungmann, M. S. Dietz°, M. Heilemann°

Single-Molecule Super-Resolution Microscopy Reveals Heteromeric Complexes of MET and EGFR upon Ligand Activation

International Journal of Molecular Sciences, 21 (8), 2803, (2020)

A. Dasgupta, J. Deschamps, U. Matti, U. Hübner, J. Becker, **S. Strauss**, R. Jungmann, R. Heintzmann, J. Ries

Direct supercritical angle localization microscopy for nanometer 3D superresolution

Nature Communications, 12, 1180 (2021)

M. Ganji*, T. Schlichthaerle*, A. S. Eklund, **S. Strauss**, R. Jungmann

Quantitative assessment of labeling probes for super-resolution microscopy using designer DNA nanostructures

ChemPhysChem, 22 (11), 911-914 (2021)

Table of Contents

List of publications ..... **v**

Summary ..... **ix**

Abbreviations ..... **xi**

1 Introduction **1**

1.1 Introduction to fluorescence microscopy *1*

1.1.1 Fluorescence 1

1.1.2 Fluorescence microscope 3

1.1.3 Resolution in optical microscopy and diffraction limit 5

1.1.4 TIRF and HILO microscopy: Detection of single molecules 6

1.2 Super-resolution microscopy *9*

1.2.1 STED microscopy 9

1.2.2 Single molecule localization microscopy 10

1.3 DNA-PAINT microscopy *14*

1.3.1 Principle of DNA-PAINT 14

1.3.2 DNA hybridization kinetics in DNA-PAINT 15

1.3.3 Variations and advances of DNA-PAINT 16

1.3.4 Improving the imaging speed of DNA-PAINT 18

1.4 DNA nanotechnology for super-resolution microscopy *22*

1.4.1 DNA structure 22

1.4.2 Basics of DNA nanotechnology and DNA origami 23

1.5 Labeling approaches for DNA-PAINT super-resolution microscopy *25*

1.5.1 Labeling for fluorescence microscopy 25

1.5.2 Binder property requirements for super-resolution microscopy 26

1.5.3 Binder categories: Chances and limitations in super-resolution microscopy 28

1.5.4 Protein-DNA conjugation strategies 34

1.5.5 Detecting single mRNA molecules using FISH 36

2 Aims and objectives 38

3 Publications 40

3.1 Publication I: Modified aptamers enable quantitative sub-10-nm cellular DNA-PAINT imaging 40

3.2 Publication II: 124-Color Super-resolution Imaging by Engineering DNA-PAINT Blinking Kinetics 70

3.3 Publication III: Up to 100-fold speed-up and multiplexing in optimized DNA-PAINT 107

4 Outlook 137

5 References 141

Acknowledgements 152

Summary

Light microscopy has become an essential tool for biological research and clinical diagnostics. Fluorescence microscopy enables high-resolution imaging with high contrast and specificity. With the emergence of super-resolution microscopy, features below the diffraction limit of light became visible, leading to a more detailed understanding of cellular structures and biomolecular localizations. Ever since, a multitude of super-resolution techniques has been developed including STED, STORM, and PALM.

DNA-PAINT is one of the latest super-resolution techniques and is based on transient hybridization of a short dye-labeled DNA strand with a DNA strand attached to the target molecule. The on- and off-binding of the DNA strands create a blinking pattern that is subsequently reconstructed to a super-resolved image. DNA-PAINT has three unique advantages compared to other super-resolution techniques: 1) A spatial resolution down to the single molecule level on artificial DNA nanostructures (< 5 nm) can be achieved; 2) Unique DNA sequences can serve as barcodes that can then be used for theoretically unlimited multiplexing independent of spectrally distinct fluorophores; 3) Predictable hybridization kinetics enable precise quantification of molecules (qPAINT). However, the spatial resolution achieved *in vitro* cannot be easily translated to cellular imaging, since the target protein requires labeling with a small probe to achieve minimal distance between the target protein and the binder carrying the DNA sequence. Moreover, DNA-PAINT's slow image acquisition speed sets a practical time limit for high-scale multiplexing and its applicability to resolve biological questions with relevant statistics.

In this thesis, I targeted both limitations by extending the binder portfolio, designing novel DNA probes for parallelized multiplexing, and designing new sequences to speed up DNA-PAINT.

First, to overcome the limitation of binder size and availability, new molecules were explored for applications in fluorescence microscopy to replace the commonly used large antibodies. In a collaboration with the company SomaLogic, I established modified aptamers (called SOMAmers) as novel binders for super-resolution microscopy (**Publication I**). SOMAmers are small, DNA-based binder molecules with improved binding affinities compared to traditional aptamers. I developed a protocol to specifically label membrane and extracellular

proteins with SOMAmers. By combining SOMAmers and DNA-PAINT microscopy, I demonstrated a spatial resolution better than 10 nm - for the first time - in a cellular context. Furthermore, their superiority to antibodies as labeling probes was demonstrated with respect to resolution and quantitative imaging.

The second part of this thesis introduces a kinetic barcoding approach incorporated to DNA-PAINT to enable multiplexed imaging in a single image acquisition round while using a single fluorophore (**Publication II**). This was achieved by labeling target molecules with DNA probes with different binding times and frequencies. The target molecules were distinguished by post-processing identification of their characteristic kinetic fingerprint.

The third part of this thesis targets the slow image acquisition of DNA-PAINT by improving the DNA sequence design (**Publication III**). In a previous study, the hybridization kinetics were increased by 10-fold by optimizing the sequence of the docking and imager strand pair and imaging buffer conditions. However, this approach was only applicable to a single target and a finite speed limit had not been achieved at this point. As a follow-up study, I introduced repetitive sequence motifs with overlapping binding sites. The imaging speed thereby increased proportionally to the number of repeats. As a result, the image speed was increased up to 100-fold and speed-optimized multiplexing is possible with up to six targets only by changing the sequences.

Abbreviations

BSA	bovine serum albumin
CDR	complementary determining region
CRISPR	clustered regularly interspaced short palindromic repeats
DARPin	designed ankyrin repeat proteins
DBCO	dibenzocyclooctyne
DNA	deoxyribonucleic acid
dSTORM	direct stochastic reconstruction microscopy
EMCCD	electron multiplying charge coupled device
FISH	fluorescence in situ hybridization
FWHM	full width at half maximum
GFP	green fluorescent protein
HILO	highly inclined and laminated optical sheet
Ig	immunoglobulin
kDa	kilodalton
NA	numerical aperture
NHS	N-hydroxysuccinimide
PAINT	point accumulation for imaging in nanoscale topography
PALM	photo-activated localization microscopy
PSF	point spread function
RNA	ribonucleic acid
sCMOS	scientific complementary metal–oxide–semiconductor
SELEX	systematic evolution of ligands by exponential enrichment
SMLM	single molecule localization microscopy
SOMAmer	slow-off rate modified aptamer
STED	stimulated emission depletion
STORM	stochastic reconstruction microscopy
TCEP	tris(2-carboxyethyl)phosphine
TIRF	total internal reflection fluorescence

1 Introduction

1.1 Introduction to fluorescence microscopy

Fluorescence microscopy has evolved into one of the most widely used tools in biological research, with countless applications in cell biology and clinical diagnostics. It enables researchers to detect and observe specific molecules and subcellular structures in a wide range of living and fixed specimens such as single cells, tissue slices, and whole organisms. The following sections will introduce the concept of fluorescence microscopy and imaging modalities that enable the detection of single molecules.

1.1.1 Fluorescence

Fluorescence corresponds to the emission of photons upon absorption of light by molecules called fluorophores. The process of absorption and fluorescence can be schematically depicted in a Jablonski diagram (Figure 1) [1]. An electron residing in a ground state S_0 absorbs light and is excited into a higher energy state (S_1). While residing in the S_1 state the electron relaxes to a lower vibrational state by non-radiative energy loss. When the electron returns to its ground state, S_0, it releases energy by emitting a photon. This emission of light is called fluorescence. Due to the non-radiative relaxation in the S1 state fluorescence emits photons at a longer wavelength compared to the absorbed light; a phenomenon referred to as the Stokes shift. Alternatively, the electron can move from S_1 into a triplet state (T_1) via intersystem crossing. This state is a longer lasting dark state of the fluorophore from where the electron finally relaxes back to the ground state emitting photons as phosphorescence.

Fluorophores absorb and emit light at a range of wavelengths that are depicted in their absorption and emission spectra, with characteristic maximum values at their peaks. Typically, the absorption and emission spectra are approximately mirror imaged to each other.

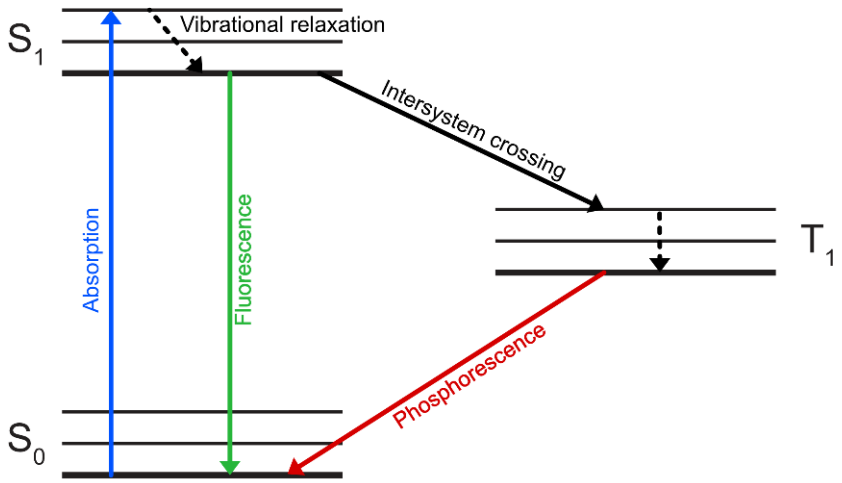

Figure 1: Jablonski diagram: Bold lines represent the different energy levels, and the thin lines represent the respective higher vibrational energy levels within the energy levels. An electron of a molecule absorbs a photon and jumps from energy state S_0 to S_1 (blue arrow). Non-radiative vibrational relaxation by external perturbation decreases the vibrational energy level of the electron (black dashed arrows). When an electron relaxes back to S_0 a photon is released via fluorescence (green arrow). Alternatively, after sustained excitation the electron can enter a dark triplet state (T1) by intersystem crossing. When relaxing from T_1 to S_0 energy is released as phosphorescence (red arrow).

Besides the absorption and emission spectra there are further photophysical properties describing a fluorophore. The extinction or attenuation coefficient (ε) is defined by the probability of a fluorophore to absorb photons at a given wavelength. The quantum yield is defined by the ratio of emitted photons to absorbed photons. In addition, each fluorophore has a characteristic fluorescence lifetime which is defined by the average time the molecule spends in the excited state before returning to the ground state. Typical fluorescence lifetimes are in the range of 1 – 10 ns [2]. Exemplary photophysical properties of the fluorophores Cy3B and ATTO 655 are listed in Table 1.

Table 1: Spectral properties of fluorophores Cy3B [3] and ATTO 655 (ATTO-TEC GmbH, Siegen, Germany).

	Cy3B	**ATTO 655**
Absorption maximum	558 nm	663 nm
Emission maximum	572 nm	680 nm
Extinction coefficient	130,000 M^{-1} cm^{-1}	125,000 M^{-1} cm^{-1}
Quantum yield	67 %	30 %
Fluorescence lifetime	2.8 ns	1.8 ns

1.1.2 Fluorescence microscope

The absorption and fluorescence characteristics of fluorophores can be employed to perform optical microscopy. In fluorescence microscopy, a light emitting fluorophore is attached to a molecule of interest, e.g. protein, DNA or RNA, and detecting its fluorescence provides specificity and high contrast to the non-fluorescent background. The fluorophore is excited by a certain wavelength and emits light that is detected through a sensitive camera or point detector. Figure 2a shows an exemplary image that was recorded using fluorescence microscopy.

A schematic representation of the major components of a fluorescence microscope setup are depicted in Figure 2b. First, fluorescence microscopy requires an intense excitation light source with a narrow chromatic range. In modern microscope setups common light sources include LEDs or monochromatic light produced by lasers.

Due to the Stokes shift, it is possible to separate excitation light from fluorescent light by using filters. A filter set is typically composed of three components: bandpass filters for excitation and fluorescence light, and a dichroic beam splitter or dichroic mirror. A bandpass filter lets a narrow color ranges pass but blocks other colors. A dichroic mirror is an interference filter that enables light of a small range of colors to pass through while reflecting other colors. In fluorescence microscopy, these mirrors direct the excitation beam to the sample and let fluorescence wavelengths pass through to a detector.

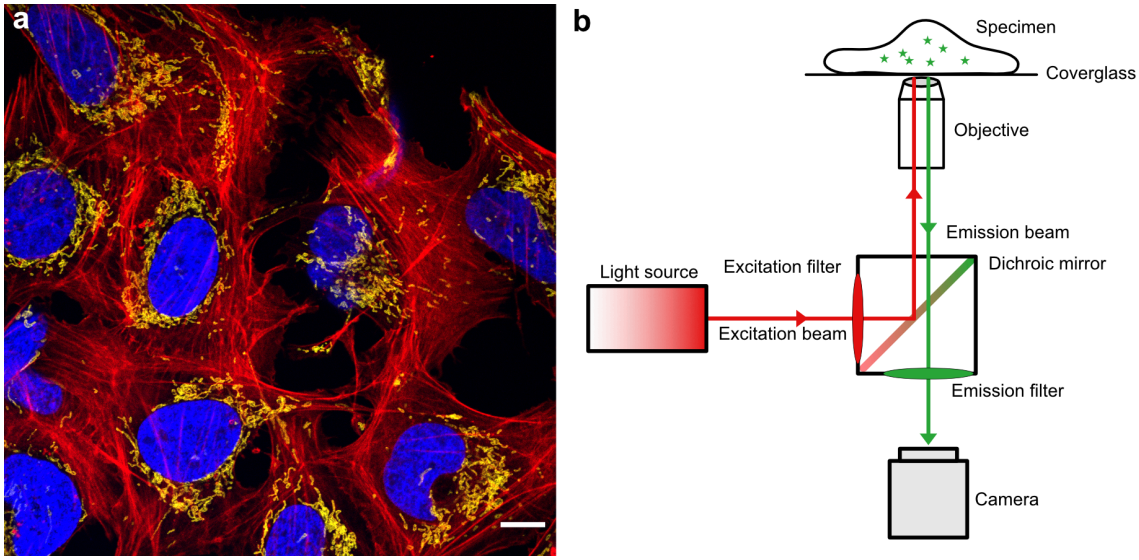

Figure 2: a) Example of a fluorescence microscopy image**.** The image was recorded using a confocal laser scanning fluorescence microscope. Nucleus, mitochondria, and actin were visualized in U-2 OS cells. Blue: Nuclear DNA (DAPI), Yellow: Mitochondria (TOM20, Alexa Fluor 488) Red: Actin cytoskeleton (SiR-Actin). Scale bar: 10 µm. b) Schematic of a fluorescence microscope setup. A light source, e.g. laser, is used to excite fluorophores inside the specimen. The excitation beam (red line) is reflected at the dichroic mirror and guided to the sample through the objective lens. Fluorescence emitted by the specimen (green line) is collected through the objective, passes through the dichroic mirror, and is detected by a camera. Excitation and fluorescence are filtered through excitation and emission filters, respectively.

An objective lens is used to focus excitation light on the sample and collect fluorescence signals. It is a critical component that determines the magnification and resolution of the created image. Magnification strengths are typically 10-fold for air objectives, ~60-fold for water immersion and 100 to 150-fold for oil immersion objectives. The resolution contribution of the objective will be discussed in section 1.1.3.

There are two basic modalities in fluorescence microscopy – widefield and confocal laser scanning microscopy. They mainly differ in their light source, sample illumination, signal detection and image generation. In widefield microscopy the whole specimen volume is illuminated, and the signal is either detected directly through an eyepiece by the observer or the fluorescence is captured by a camera and visualized on a monitor. Typically used cameras include charged coupled devices (CCDs), scientific complementary metal–oxide–semiconductor (sCMOS) cameras, and electron multiplying CCDs (EMCCDs) for low signal applications. Since the entire volume is illuminated, strong background signal will be detected from out-of-focus volumes that can cause blurry images.

In confocal laser scanning microscopy, a focused beam of light is used to point-scan the sample. Out-of-focus signal is blocked by the addition of a pinhole into the detection path. The fluorescence intensity is detected by point detectors such as photomultiplier tubes (PMT) or avalanche photodiodes (APD).

While widefield microscopy is a simple and fast implementation that is particularly suitable for live-cell imaging and thin samples, confocal microscopy is preferred for thick samples and applications where optical sectioning with minimal out-of-focus signal is required. However, the scanning approach leads to longer image acquisition times and higher laser intensities at the focal laser beam, thus it is less suitable for imaging living cells.

1.1.3 Resolution in optical microscopy and diffraction limit

Any optical system has a fundamental resolution limit caused by the diffraction of light. In 1873, Ernst Abbe postulated that the resolution depends on the wavelength and numerical aperture (NA) of the objective lens [4]. The NA is calculated by the refractive index n of the medium between the lens and the object, and the sine of the half-angle of the cone of light that can enter the objective. Therefore, it is a direct measurement of the maximum angle at which the objective can detect light.

$$NA = n \sin \alpha$$

Given the NA and the wavelength and assuming a perfect optical system, the achievable spatial resolution (r) according to Ernst Abbe is given by

$$r = 0.5 \frac{\lambda}{NA}$$

For instance, applying a 488 nm laser and an oil immersion objective with an NA of 1.49, will result in a theoretical lateral resolution of approximately 164 nm.

Other definitions of resolution in light microscopy are the Rayleigh criterion and full width at half maximum (FWHM) [5, 6]. Both measurements are based on the geometry of the point spread function (PSF). The PSF mathematically describes the diffraction pattern that appears when a point emitter is imaged with a microscope. The x-y plane contains a central bright spot referred to as the Airy disk, which is surrounded by lower intensity concentric rings. The

Rayleigh resolution limit ($r_{Rayleigh}$) is defined by the radius of the Airy disk and its FWHM (r_{FWHM}) are calculated as follows:

$$r_{Rayleigh} = 0.61 \frac{\lambda}{NA}$$

$$r_{FWHM} = 0.51 \frac{\lambda}{NA}$$

The FWHM can be experimentally determined from the PSFs obtained by imaging single emitters such as fluorescent beads. Besides the wavelength and the NA of the objective, the FWHM will be affected by aberrations or imperfections of individual microscopes.

1.1.4 TIRF and HILO microscopy: Detection of single molecules

Using a fluorescence microscope to observe single molecules requires bright fluorophores, sensitive optics, and an illumination pattern providing a high signal-to-noise ratio. Total internal reflection fluorescence (TIRF) microscopy is based on fluorophore excitation using an evanescent field that illuminates a specimen close to the glass surface (in the range of 50 – 200 nm) which significantly increases the signal-to-noise ratio. The creation of an evanescent field is based on the refraction of light and different refractive indices of the media at the interface.

The refractive index (n) of an optical medium describes how an electromagnetic wave propagates within this medium. If a wave passes through a medium with a higher refractive index the speed of the wave propagation slows down. When the incident angle differs from normal, the refracted wave is bent at the interface. Consequently, n also determines how much the light is bent when entering another medium. The refraction of a transmitted beam can be described by Snell's Law, with refraction indices n_1 and n_2, and angles of incidence θ_1 and θ_2 (Figure 3):

$$\sin \theta_1 \cdot n_1 = \sin \theta_2 \cdot n_2$$

If n_1 is larger than n_2, the refracted ray is perpendicular to the axis of incidence (θ_2 = 90 °) at a certain critical angle θ_c.

$$\theta_c = \sin^{-1}\frac{n_2}{n_1}$$

If the incident ray exceeds this critical angle, it is totally internally reflected within the higher refractive medium. At the interface, a thin electromagnetic field or evanescent wave is generated which penetrates the low refraction index medium.

The penetration depth d of an evanescent field is calculated with the following equation [7]:

$$d = \frac{\lambda}{4\pi\sqrt{n_1^2 \sin^2 \theta - n_2^2}}$$

It is determined by the angle of incidence and the refractive indices n_1 and n_2. It increases with higher wavelengths λ and decreases with higher incident angles θ. The intensity of the evanescent field decays exponentially with increasing distance from the coverglass.

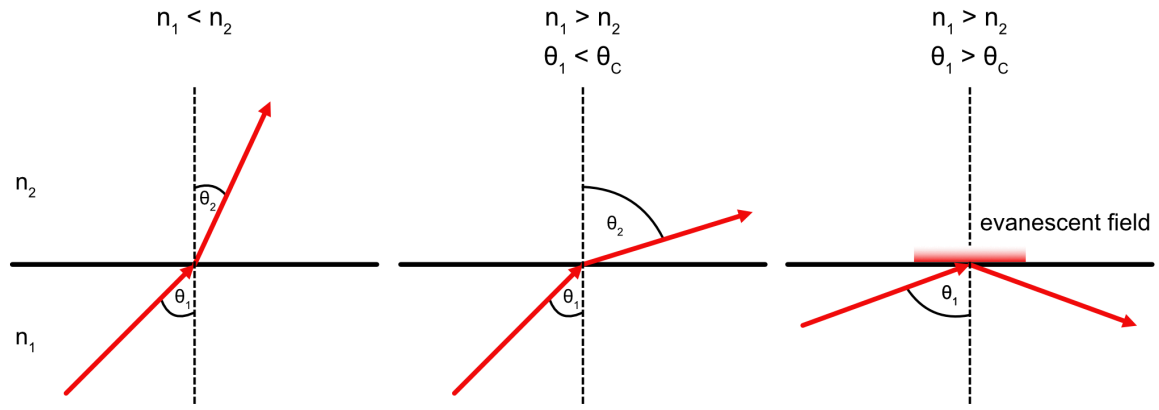

Figure 3: Refraction of light according to Snell's law. When an incident beam propagates into a medium with a different refractive index it is bent at the interface. When n_2 is smaller than n_1 and the incident angle exceeds the critical angle θ_c, the beam is reflected at the interface and a thin evanescent field is generated.

The described evanescent field is used as an excitation source for TIRF microscopy to reduce background fluorescence. This makes it suitable to investigate the dynamics of immobilized single molecules or super-resolution imaging of structures close to the surface. There are two common ways to create a total internal reflection of the excitation beam. One way is to insert a prism on top of the sample to generate a high incident angle in an upright widefield microscope [8]. Secondly, the objective can be used to create a high incident angle (Figure 4) [9, 10]. For that, the objective requires a high NA (>1.45) to allow an angle of incidence greater than the critical angle. The advantage of an objective-based TIRF microscope is the flexibility

to change the angle of incidence and so the illumination depth by focusing the laser spot in different areas of the back focal plane. A modern objective used for TIRF microscopy has a 100× magnification and a high NA of 1.49. With these objective properties, an angle of incidence of up to 79.4 ° can be achieved [11]. Using this angle and an excitation wavelength of 561 nm at a glass/water interface (n_1 = 1.52, n_2 = 1.33), the possible minimum penetration depth is approximately 66 nm.

If the specimen requires imaging further away from the coverslip such as intracellular proteins, TIRF cannot be applied. Highly inclined and laminated optical sheet (HILO) microscopy enables cellular single-molecule imaging providing up to eightfold higher signal-to-noise ratio compared to epi-illumination (Figure 4) [12]. An incident laser beam is strongly refracted at the glass/specimen interface and enters the specimen side as a laminated optical sheet. A sheet thickness of ~7 µm was experimentally measured for an illumination diameter of 30 µm by Tokunaga et al. [12].

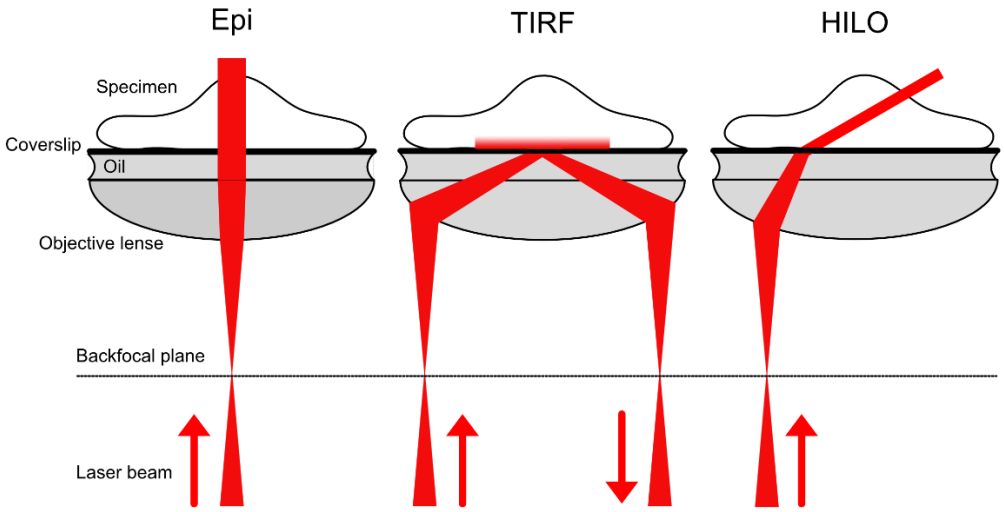

Figure 4: Illumination modes on a widefield microscope setup. Epi-illumination: The laser beam passes through the center of the objective lens without being refracted. TIRF: The laser passes through the side of the objective lens and is refracted such that it exceeds the critical angle at the coverslip/specimen interface. Consequently, the laser beam it is reflected at the coverslip/specimen interface and an evanescent wave excites the volume close to the surface. HILO: By moving the excitation beam away from the center it is refracted and appears as a laminated optical sheet at the specimen's side.

1.2 Super-resolution microscopy

The diffraction limit as described by Abbe is a fundamental limit that had prevented deeper insights into smaller details of cellular structures and proteins for many years. This section introduces two basic concepts that surpassed this long-existing barrier – STED and SMLM. Both techniques were rewarded with a joint Nobel prize in chemistry in 2014.

1.2.1 STED microscopy

Stimulated emission depletion (STED) microscopy described by Stefan Hell in 1994 was the first concept to fundamentally overcome the diffraction limit of light [13] and was first applied for biological imaging in 2000 [14]. STED is based on introducing an illumination pattern with sub-diffraction limited features. Practically, this is achieved by using a donut-shaped laser beam (called STED laser) that switches off the fluorescence around the excitation beam and effectively reduces the size of the PSF (Figure 5). The quenching of fluorescence is accomplished by stimulated emission. The STED laser is a near-infrared laser with a wavelength that is comparable to the energy difference of the ground and excited states of the fluorophore. When the excited fluorophore encounters photons of the STED laser it returns to its ground state through stimulated emission. Spontaneous fluorescence emission and stimulated emission have different wavelengths and can thus be separated by optical filters.

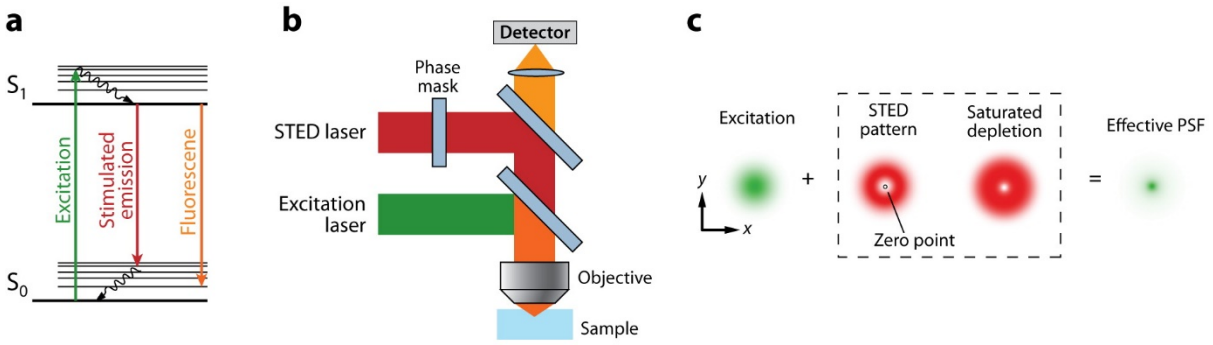

Figure 5: Principle of STED microscopy: a) Stimulated emission: A fluorophore at the ground state (S0) can absorb a photon by the excitation light and jumps to an excited state (S1). Spontaneous fluorescence emission brings the fluorophore back to its ground state. Stimulated emission happens when an excited fluorophore encounters a photon with a comparable wavelength compared to the energy gap between the ground and excited states. b) Schematic of a STED microscope. Excitation and STED lasers are aligned and focused through the objective into the sample. The donut shape of the STED laser is created by inserting a phase mask into the light path. c) x-y profile of the excitation and STED laser. The zero point of the STED laser is aligned with the intensity maximum of the excitation laser. Saturated depletion leads to suppression of spontaneous fluorescence around the zero point and therefore decreases the size of the effective PSF. Reprinted with permission from Annual Reviews [15], copyright (2009).

The spatial resolution that can be achieved with STED depends on the size of the effective PSF. With a higher degree of saturation, the PSF can be decreased, meaning high STED laser power densities are required. Using a STED laser intensity of ~1 GW/cm² the resolution obtained is approximately 20 nm [16]. The resolution Δr can be mathematically described as follows [16]:

$$\Delta r = \frac{0.45\lambda}{NA\sqrt{1+\frac{I}{I_S}}}$$

Here, λ corresponds to the wavelength of the excitation laser, I to the peak intensity of the depletion laser, I_S to the saturation intensity of the fluorophore. The quotient $\frac{I}{I_S}$ describes the degree of saturation.

1.2.2 Single molecule localization microscopy

The positions of fluorescent molecules can be localized precisely when the signal derives from a single molecule. By fitting the PSF emerging from a single emitter its centroid position can be determined with up to ~1 nm precision [17, 18]. However, when imaging a biological sample, single fluorophores are typically not separated such that each of them can be localized

with that precision. In the concept of single molecule localization microscopy (SMLM) the fluorescent state of probes is spatiotemporally separated. This is achieved by activating a subset of probes such that their PSFs are not overlapping (Figure 6). The coordinates of this subset of molecules are then localized and the molecules are either bleached or sent back into a dark state, followed by the activation of another set of probes. This process is iterated until each fluorescent probe has been localized at least once. The localizations obtained in each imaging frame are collected in a coordinate list and can be reconstructed to generate a final super-resolved image. The spatial resolution (Δr) of SMLM approaches depends on the localization precision of the PSF centroid, thus on the number of photons (N) collected from a fluorophore in a single frame:

$$\Delta r \approx \frac{PSF}{\sqrt{N}}$$

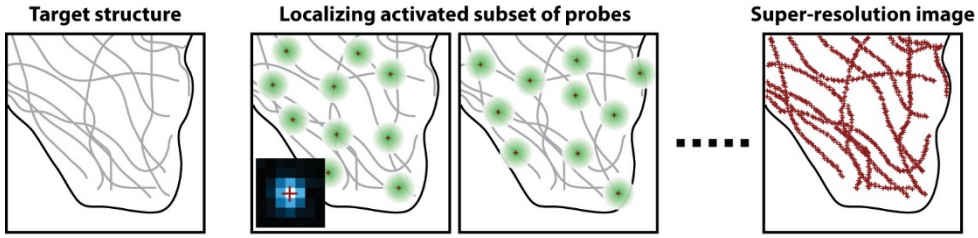

Figure 6: Scheme of single molecule localization microscopy. Only a subset of fluorophores is activated such that their PSFs are not overlapping and can be precisely localized. This procedure is iterated over many frames until ideally each fluorophore has been activated and localized. The resulting coordinates of the probe molecules are then reconstructed to create a super-resolved image. Reprinted with permission from Annual Reviews [15], copyright (2009).

Several techniques can achieve the required on and off-switching of fluorophores. Photo-activated localization microscopy (PALM) uses photoactivatable fluorescent proteins (e.g. PA-GFP) that can be activated by irradiation with a UV laser and then illuminated with a blue laser until they are photobleached [19]. Photoswitchable fluorescent proteins such as Dronpa can be reversibly converted between a bright and dark state upon appropriate laser excitation [20].

Stochastic optical reconstruction microscopy (STORM) uses small photoswitchable fluorophores such as the Cy3-Cy5 pair switch that can convert between bright and dark states up to hundreds of times [21]. To accomplish this a strong red laser pulse sends all fluorophores to the dark state. Then, a green laser is used to switch on a small fraction of fluorophores. With

a following red laser excitation, the activated fluorophores emit fluorescence until they are switched off and their positions localized.

Under reducing imaging buffer conditions and appropriate laser excitation wavelengths conventional photoswitchable fluorophores such as Alexa Fluor 647 or Cy5 can be switched between bright and dark states [22]. This approach is called direct STORM (dSTORM) since it does not require an activator molecule in proximity like Cy3 in the Cy3-Cy5 pair switch.

In 2017, Balzarotti et al. introduced the concept of MINFLUX that combines the approach of SMLM and patterned excitation [23]. It is a novel localization concept that uses a donut-shaped excitation pattern to probe fluorophores with a local intensity minimum and therefore obtaining high localization precision with fewer photons. Furthermore, it provides fast and precise single particle tracking and imaging with a localization precision of approximately 1 nm. This technique has been further expanded to three-dimensional multicolor imaging, within larger field of views using iterative MINFLUX [24].

Emitters can also be localized in the z-direction by engineering the shape of the PSF depending on the z-position relative to the focal plane of the objective. Huan et al. applied the astigmatism imaging method [25] for 3D STORM imaging [26]. A weak cylindrical lens was inserted into the imaging part that changes the orientation and ellipticity of the image of a fluorophore depending on the z-position (Figure 7). The x and y coordinates of a fluorophore are obtained by fitting the image with a 2D elliptical Gaussian function. By measuring the peak widths w_x and w_y, the z-position can be determined. Therefore, a calibration curve is measured using immobilized beads carrying fluorophores. With the astigmatism approach, the z-coordinate can be measured in a range of approximately 1 µm

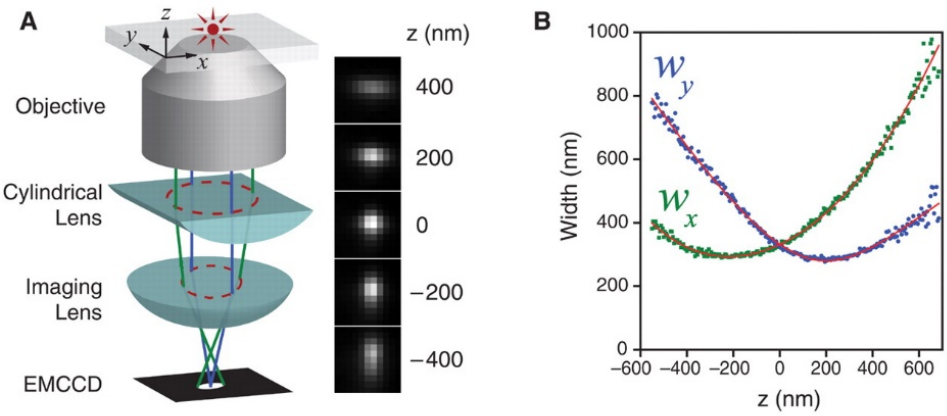

Figure 7: 3D single molecule localization super-resolution microscopy using astigmatism: A) A cylindrical lens is added into the detection path to shape the fluorophore images relative to the z-position of the focal plane. It creates an elliptical shape in the horizontal direction when the emitter is below the focal plane or vertically when the emitter is above the focal plane. B) Calibration curve that measures the image width w_y and w_x as a function of the z-position of the fluorophore. Reprinted with permission from AAAS [26], copyright (2008).

1.3 DNA-PAINT microscopy

1.3.1 Principle of DNA-PAINT

Point Accumulation for Imaging in Nanoscale Topography (PAINT) is an alternative SMLM approach to create blinking by introducing diffusing probes in solution that specifically and transiently interact with the molecular target. This concept was introduced by Sharonov et al. who used an environment-sensitive dye Nile Red to image supported lipid bilayers [27]. The broad applicability of this approach was limited by the availability of probes that specifically bind their respective targets with binding kinetics suitable for PAINT.

Another approach based on PAINT providing improved applicability and controlled kinetics was introduced in 2010 by Jungmann et al. as DNA-PAINT [28]. In this technique, short fluorophore coupled oligonucleotides (called imager strands) transiently hybridize to their complementary target sequence (called docking strand) that is attached to the molecule of interest (Figure 8). The predictable kinetics of DNA hybridization offers full control over the binding and unbinding kinetics of the imager strand and is applicable to any target molecule that can be labeled with a short DNA strand. Here, the blinking density is adjusted by the imager strand concentration and hybridization time. Another benefit is that photobleaching of fluorophores becomes less relevant since the docking strand can be replenished with an unlimited supply of diffusing imager strands in solution. On the downside, these imagers are non-fluorogenic, thus generating fluorescent background upon excitation. This implicates that a TIRF microscope setup or another selective plane illumination method is needed to suppress the background of diffusing imager strands. In addition, longer camera integration times (>50 ms) are beneficial, as they average out background signal.

Through repetitive binding of the imager strands, DNA-PAINT achieves high photon counts and sampling statistics. Therefore, sub-5 nm spatial resolution with a localization precision of approximately 1 nm has been achieved under optimized imaging conditions on artificial DNA-origami structures [29, 30].

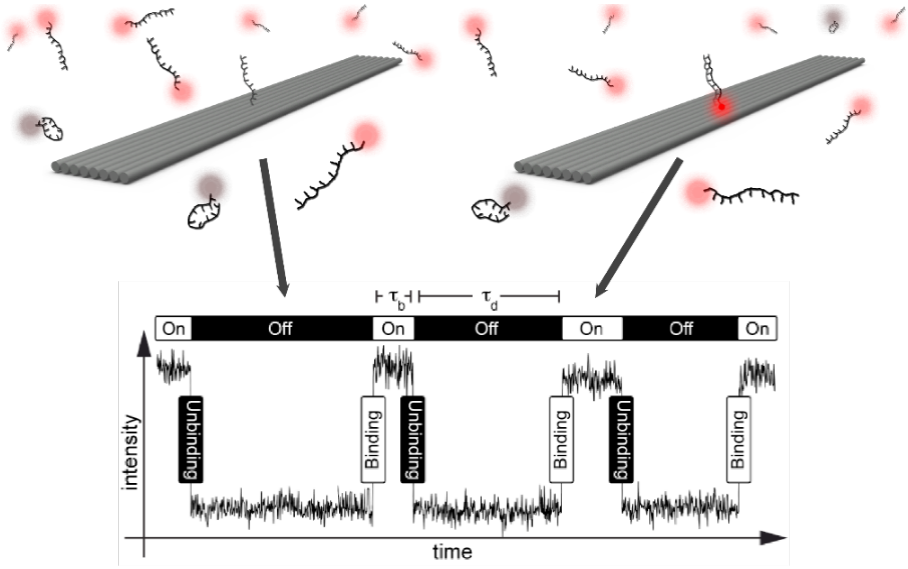

Figure 8: DNA-PAINT concept: Short fluorophore-coupled oligonucleotides (imager strands) are freely diffusing in solution and bind to their complementary sequence (docking site), here incorporated in a DNA origami structure. The binding and unbinding of imager strands create the on/off fluorescent switching patterns as seen in the intensity vs. time trace (bottom). The duration an imager strand is bound to the docking site is denoted as bright time (τ_B) and the time between two binding events is referred to as dark time (τ_B). Reprinted with permission from American Chemical Society [28], copyright (2010).

1.3.2 DNA hybridization kinetics in DNA-PAINT

The hybridization kinetics between the docking and imager strand can be described by a second order kinetic model with imager and docking strand concentrations c_i and c_d, respectively, and association rate (k_{on}) and dissociation rate (k_{off}).

$$[c_i] + [c_d] \underset{k_{off}}{\overset{k_{on}}{\rightleftarrows}} [c_i c_d]$$

The association rate of the imager and docking strands can be calculated using the mean time between binding events (dark time, τ_D) and imager strand concentration (c_i) as follows:

$$k_{on} = \frac{1}{c_i \cdot \tau_D}$$

The association rate depends on various parameters. It changes with salt concentration, temperature, imager sequence, and diffusion properties [31]. A typical imager/docking strand pair with nine complementary nucleotides, in 600 mM NaCl at 23 °C has an association rate of

$2.3 \cdot 10^6$ M^{-1} s^{-1} [28]. Since the imager strand is in solution, the association rate is ultimately limited by diffusion which is in the range of 10^9 M^{-1} s^{-1} [32].

The dissociation rate (k_{off}) is independent of the imager and docking strand concentrations and can be directly determined by measuring the time during which the imager is bound to the docking site (bright time, τ_b).

$$k_{off} = \frac{1}{\tau_b}$$

The bright time depends on the thermodynamic stability of the DNA duplex under the conditions the measurement is conducted including the length and GC content, temperature, and buffer salinity.

1.3.3 Variations and advances of DNA-PAINT

Exchange-PAINT

Imaging of multiple targets in fluorescence microscopy is mostly achieved by using fluorophores that can be separated by the absorption and emission spectrum. Since the spectrum of visible light is relatively narrow (350 – 800 nm), the total number of targets that can be imaged in the same sample is limited. In addition, emissions at various wavelengths are causing aberrations, various detection efficiencies, and crosstalk between channels, which can all lead to quantification inconsistencies and would require more control measurements.

In DNA-PAINT, the target identity or 'color' is encoded in the DNA sequence; consequently, it is decoupled from the fluorophore's emission spectrum. Exchange-PAINT uses the sequence identity to sequentially read out an arbitrary number of binding sites (Figure 9) [33]. Therefore, in Exchange-PAINT, the multiplexing capacity is not limited by the amount of spectrally distinguishable fluorophores but is expanded to the number of orthogonal DNA sequences that can be designed. In a cell imaging experiment, all labels e.g. DNA-coupled antibodies are introduced simultaneously, followed by sequentially alternating imaging and washing steps. The advantage of this method is that each channel can be measured using the same best performing fluorophore to obtain similar resolutions for different targets, whilst avoiding optical aberrations and crosstalk. Agasti et al. designed and tested 52 different docking site sequences and tested their orthogonality using a DNA-origami cross-talk assay [34]. They also

demonstrated 8-color DNA-PAINT imaging in cells by labeling with primary antibodies directly coupled to a DNA-PAINT docking strand. DNA-based multiplexing has also been established for other imaging methods, such as diffraction-limited confocal microscopy, STED, and STORM [35-37].

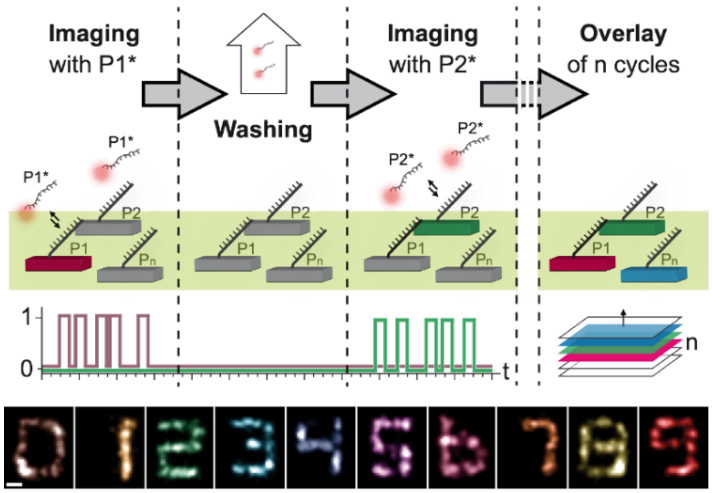

Figure 9: Concept of Exchange-PAINT with n number of targets labeled with orthogonal docking strands. First, imager strands carrying the sequence P1* are introduced and interact with their complementary docking site P1. After image acquisition, P1* imager strands are washed off the sample followed by the introduction of the next imager strands with the sequence P2* that interact exclusively with docking site P2. This cycle is repeated until all n sequences are imaged. To obtain a final multiplexed super-resolution image, the images acquired in each channel are overlayed, aligned and assigned to a pseudocolor. Reprinted with permission from Springer Nature [33], copyright (2014).

Quantitative PAINT (qPAINT)

Despite the high spatial resolution of DNA-PAINT, dense molecular clusters in cells cannot always be resolved and quantification based on spatial separation would not be possible. Nevertheless, the predictable binding kinetics of DNA-PAINT imager strands can be used to count integer numbers of molecules within non-resolved areas. This approach has been introduced by Jungmann et al. as quantitative PAINT (qPAINT) [38].

The influx rate (ζ) of binding events depends on an intrinsic association rate of the imager strand (k_{on}) and the imager concentration (c_i).

$$\zeta = k_{on} \cdot c_i$$

The influx rate is calibrated using isolated targets or DNA origami structures with defined number of docking sites. To obtain the number of docking sites of a certain region, the mean dark time between binding events (τ_D) is measured. With a known influx rate and a measured τ_D, the number of docking sites (n) can be calculated as follows:

$$n = \frac{1}{\zeta \cdot \tau_D}$$

For precise quantification, the influx rate can be adjusted according to the density of the regions of interest. Thus, dense regions require a lower imager concentration for a more precise count whereas sparse regions are counted with higher precision when higher imager concentrations are used. The adaptability of qPAINT to various molecular densities makes it broadly applicable for biological questions. For example, DNA-PAINT in combination with qPAINT were used to precisely quantify ryanodine receptor nanodomains [39].

1.3.4 Improving the imaging speed of DNA-PAINT

The imaging speed of DNA-PAINT is limited by the diffusion of the imager and the background fluorescence. In theory, the imaging speed can be arbitrarily increased by reducing the binding time of the imager strand while increasing the imager strand concentration. However, with increasing imager concentration, the background fluorescence becomes higher which decreases the signal-to-noise ratio and thereby decreases the resolution. In this section, recent approaches used to speed up DNA-PAINT by decreasing the background fluorescence and increasing the association rate of the imager strand to the docking strand will be discussed.

FRET-PAINT

One approach, introduced by two research groups, uses Fluorescence Resonance Energy Transfer (FRET) based DNA-PAINT probes to decrease the background fluorescence of imager strands in solution [40, 41]. In one approach introduced by Auer et al., an acceptor fluorophore is attached to the docking strand and is activated when the imager with the donor fluorophore binds and transfers its energy via FRET (Figure 10 a). The fluorescence of the acceptor dye will only be emitted and detected once the imager strand binds to the donor strand. Unbound imager strands are not detected, and thus the imager concentration can be arbitrarily increased. Alternatively, to avoid photobleaching of the acceptor dye over time, the donor and acceptor dye can be attached to separate DNA strands that transiently bind to an extended docking strand [40, 41]. In this case, the signal is detected when both strands are binding the docking strand simultaneously.

FRET-PAINT has been further optimized concerning camera speed, choice of fluorophores, and dissociation rate of imagers. Ultimately, imaging with 40 nm resolution has been achieved in a few tens of seconds [42]. Despite the significant speed enhancements, a spatial resolution below 20 nm has not been demonstrated using FRET-PAINT due to a reduced energy transfer efficiency and direct excitation of the acceptor. Overall, FRET-PAINT is suitable for applications where fast imaging is desirable and a spatial resolution of ~40 nm is sufficient when using standard widefield optics.

Improved sequence design and buffer conditions

Another approach to obtain faster DNA-PAINT imaging is to optimize the hybridization kinetics of the imager and docking strand, in particular the association rate. Schickinger et al. developed a tethered multifluorophore motion assay which they applied to study DNA hybridization kinetics on a single molecule level [43]. They found that the concentration of monovalent salt in the range of 0.15 M – 1 M NaCl influences the association rate without having a significant impact on the dissociation rate. Furthermore, they measured a strong sequence dependency on the association rate. The sequences with the highest association rates depicted a low propensity for secondary structures or hairpin formation of which the highest association rate was achieved with the sequence CCTCCTCC.

Research carried out by Schueder et al. optimized the previously mentioned sequence to make it applicable for DNA-PAINT imaging (Figure 10 b) [44]. Several sequences were designed and screened on DNA origami structures to achieve a high association rate (k_{on}) with a bright time suitable for DNA-PAINT (0.1 s – 1 s) and narrow distributions of dark and bright times. In this study, TCCTCCC was identified as the best performing docking sequence with a five-times enhanced k_{on} compared to the P1 sequence (AGATGTAT), frequently used in earlier DNA-PAINT studies. Moreover, the association rate was improved two-fold by increasing the concentration of $MgCl_2$ in the imaging buffer from 10 mM – 75 mM. The combination of using increased $MgCl_2$ concentrations with the optimized sequence design led to a 10-fold increase in k_{on} ($\sim 10^7\ M^{-1}\ s^{-1}$) compared to P1 imaging with 10 mM $MgCl_2$ ($\sim 10^6\ M^{-1}\ s^{-1}$). The optimized sequence was used for high-throughput imaging of microtubules over a large field of view (>1 mm^2) within eight hours and with a resulting localization precision of ~8 nm. However, a limitation of this approach is that the improvements based on the sequence design can only be applied for a single target molecule since the presented sequences in that study are not orthogonal.

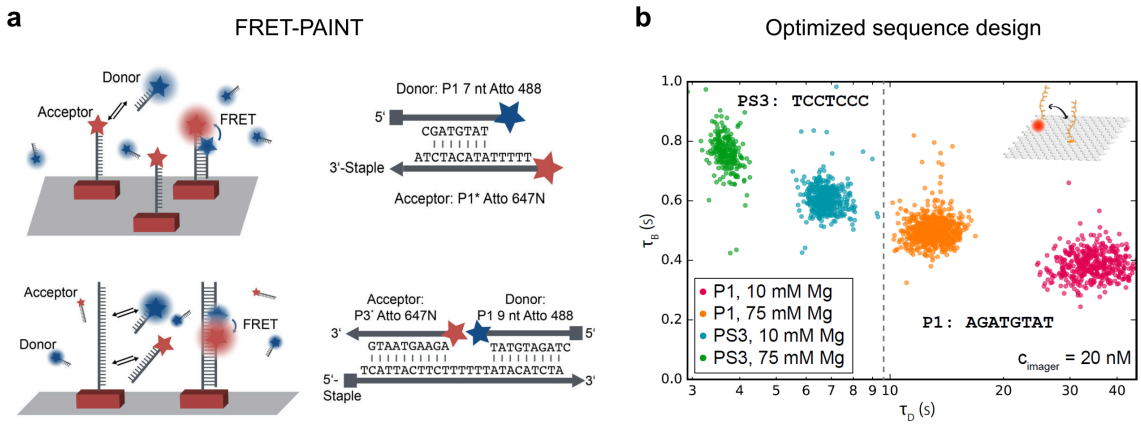

Figure 10: Different approaches tackling the imaging speed of DNA-PAINT. a) FRET-PAINT probes can decrease background fluorescence: The docking strand is attached to a FRET acceptor dye (ATTO 647N) that fluoresces upon binding of the imager strand coupled to a donor dye (ATTO 488). Bottom: Both FRET donor and acceptor dyes are attached to separate imager strands that bind to an extended docking strand. Signal is detected when both imager strands are bound. Reprinted with permission from American Chemical Society [40], copyright (2017) b) Speed optimization of DNA-PAINT by optimizing sequence design and salt concentration: Ideal sequences for DNA-PAINT have a low dark time (τ_D) and a bright time in the range of (0.1 and 1 s). The PS3 sequence measured in 75 mM $MgCl_2$ displays an approximate 10-fold decreased dark time. Reprinted with permission from Springer Nature [44], copyright (2019).

Argonaut PAINT

Filius et al. attached an argonaut (Ago) protein to the imager strand to increase the hybridization rate (Ago-PAINT) [45]. The Ago protein functions as a guide for a short DNA sequence (guideDNA) to find its complementary sequence. In the presented study, a wild-type CbAgo protein [46] was coupled to the imager strand, leading to prearrangement of the guide DNA into a helical conformation and making the hybridization to the docking site more favorable. Therefore, this approach leads to a 10-fold improved association rate in the range of $\sim 10^7$ M^{-1} s^{-1}. However, the applicability of Ago-PAINT for cellular imaging has not been demonstrated.

Fluorogenic probes for DNA-PAINT

Chung et al. introduced a fluorogenic DNA imager probe that is fluorescent in a bound state but dark when unbound [47]. This imaging probe consists of a non-fluorescent quencher at the 3'-end and a fluorophore on the 5'-end of the imager strand. In solution, the oligonucleotide is flexible where the quencher and fluorophore are in proximity, thereby leading to a dark state. Upon hybridization to the target sequence, quencher and dye become separated and fluorescence from the dye can be detected. To ensure that the signal is not quenched in a bound

state, the imager strand is 15 nt long and includes mismatches to the target sequence to destabilize its hybridization and enable transient binding. In contrast to previously described molecular beacons, the sequence is designed such that there is no stable stem formation in the unbound state, which would slow down the association rate of the probe to its docking strand. This probe design is compatible with epi-illumination instead of TIRF and achieved high spatial resolution with short camera integration times of 5 ms.

1.4 DNA nanotechnology for super-resolution microscopy

1.4.1 DNA structure

Deoxyribonucleic acid (DNA) is the carrier molecule of the genome. It is a polymeric molecule composed of different nucleotides, each comprises a sugar group (deoxyribose), a phosphate group, and a nucleobase. The genetic code is built up from the sequence of the four nucleobases: adenine (A), thymine (T), guanine (G) and cytosine (C). In 1953, J. D. Watson and F. H. C. Crick published the double-helical structure of DNA, made up of two complementary DNA strands with strict base pairing: A with T, and C with G [48]. The structure can be represented as a right-handed helical ladder with the sugar-phosphate backbone as side rails and the base pairs as rungs (Figure 11a). Each helical turn consists of 10.5 bases and is 3.4 nm long, and the diameter of the helix is 2 nm wide. Of note, the paired DNA strands are antiparallel, meaning that they run in opposite directions, namely from 5' to 3' and 3' to 5', depending on the orientation of the respective sugar ring positions. The bases are paired and stabilized by forming hydrogen bonds where an A-T pair forms two and G-C forms three hydrogen bonds, resulting in higher stability of the G-C pair (Figure 11b).

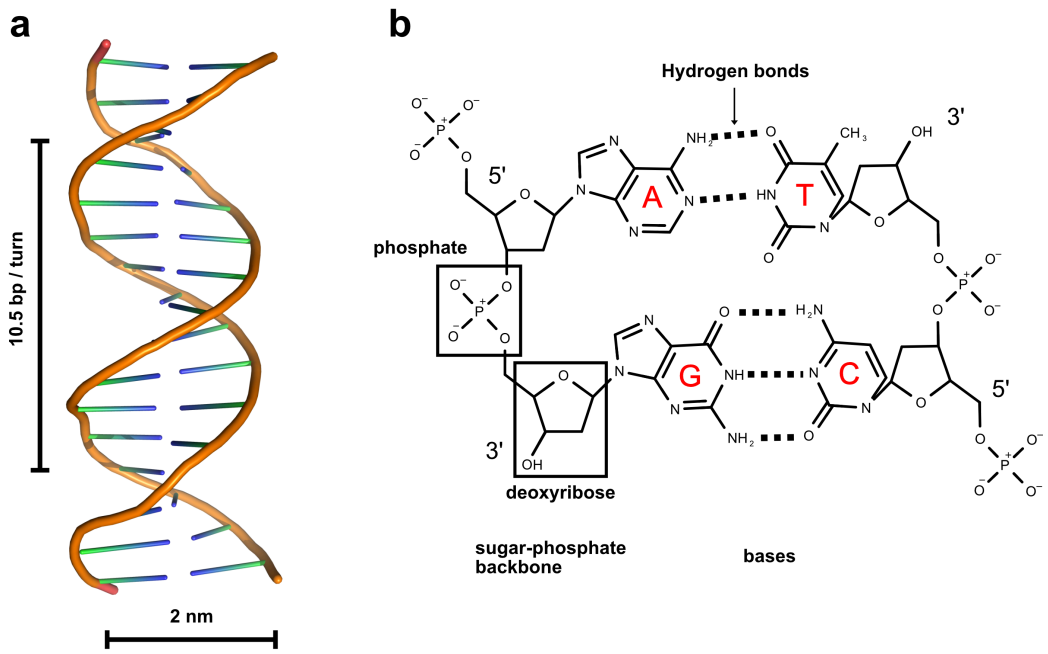

Figure 11: Double helix and building blocks of DNA. a) DNA double helix was rendered with PyMol using PDB ID 3BSE [49]. b) Chemical structures of the sugar-phosphate backbone and the Watson-Crick base pairs, adenine (A) and tyrosine (T), and guanine (G) and cytosine (C). Hydrogen bonds are illustrated as dashed lines.

1.4.2 Basics of DNA nanotechnology and DNA origami

In 1982, N. Seeman proposed that DNA can not only serve as a storage medium for the genetic code but also as a building material to create novel molecular shapes in two and three dimensions [50, 51]. The strict base pairing rules of DNA enable a rational design of sequences that assemble into desired shapes.

A scaffolded approach called DNA-Origami was introduced by Paul Rothemund in 2006 (Figure 12a) [52]. DNA-Origami uses a large scaffold strand (~7000 bases) that is folded in a certain way with the help of ~200 short oligonucleotides, called staple strands. The scaffold DNA is a circular single-stranded vector isolated from a M13mp18 phage. The staple strand sequences are designed in a way that they hybridize to certain regions of the scaffold and thereby self-assemble into the desired shape. Typically, a temperature gradient is applied in magnesium containing buffer for the scaffold and staple strands to self-anneal. The technique has been further extended to create more complex and three-dimensional structures [53] up to the gigadalton-scale [54]. In addition, software tools like CaDNAno have been created enabling researchers to efficiently design their structures based on DNA-Origami [55].

Since the specific position of each staple strand is known, they can also be employed to precisely arrange modifications with defined spacings (Figure 12b). Therefore, DNA-origami structures have been established as a reference standard to calibrate the resolution and quantification of various fluorescence microscope techniques in 2D and 3D [56-58]. More specifically, a rectangular origami structure from the original publication in 2006 has been established as a breadboard to add modifications with precise positions in two dimensions. These structures are especially suitable to calculate the imaging resolution and test new methods based on DNA-PAINT because docking strands can readily be introduced by extending a staple strand and minimal distances can be generated with as little as five nanometers [30].

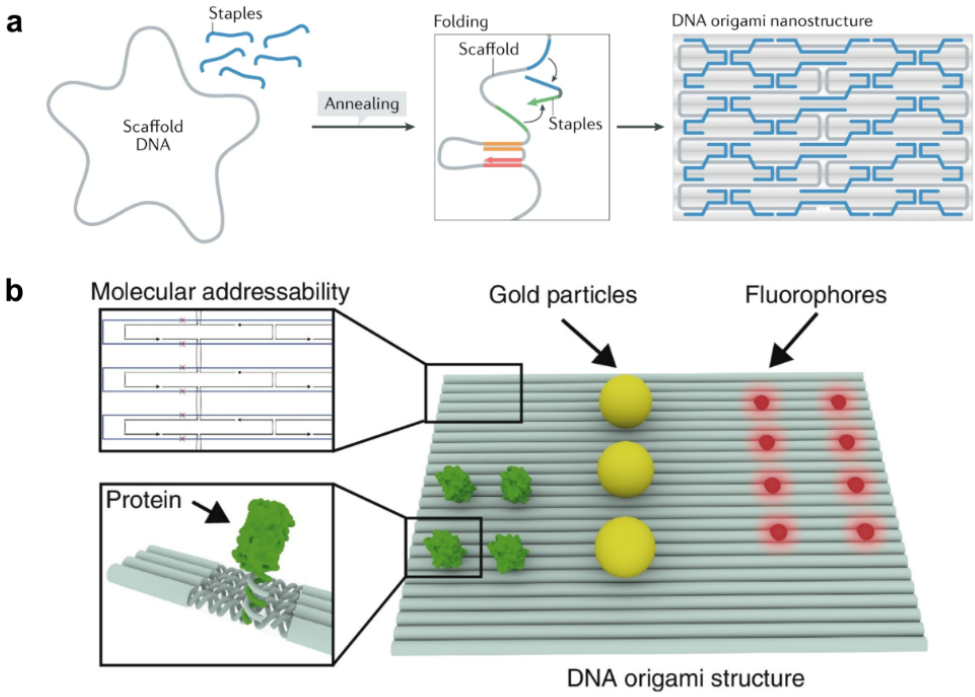

Figure 12: DNA origami for biotechnology applications. a) A long circular DNA scaffold (grey) is folded with short oligonucleotides (staples, blue). The origami folds during an annealing process where the staple strands that hybridize to the defined regions of the scaffold strand, ultimately generating a folded origami structure. Reprinted from Springer Nature, copyright 2021 [59] b) Modifications (e.g. proteins, fluorophores) can be incorporated by modifying the staples strands. The position of the staple strands is given by the origami design; thus, modifications can be added with molecular precision. Reprinted from Elsevier, copyright 2016 [60].

1.5 Labeling approaches for DNA-PAINT super-resolution microscopy

1.5.1 Labeling for fluorescence microscopy

An elementary part of fluorescence microscopy is labeling. It is required to introduce a probe (e. g. fluorophore, fluorescent protein, or DNA) to the molecule of interest. Depending on the imaging modality or sample type, various labeling strategies are available.

One labeling approach is to introduce a fluorescent protein via genetic modification or plasmid transfection. Green fluorescent protein (GFP) is the first discovered fluorescent protein and was isolated from the jellyfish *Aequorea Victoria*, discovered in 1978 [61]. It absorbs light in the blue range and fluoresces green light. Many mutations of GFP have been generated that either improve the photophysical properties, e. g. enhanced GFP (EGFP), or change their spectral properties such as the yellow or cyan fluorescent protein [62]. Besides fluorescent proteins, self-labeling fusion protein tags were developed including SNAP and HaloTag. These tags are non-fluorescent enzymes that react with small ligand molecules, O6-benzylguanine with SNAP and a chloroalkane with HaloTag [63-65]. Organic fluorophores can be attached to these ligands and used as an alternative to fluorescent proteins. Using cell-permeable dye molecules, self-labeling tags enable the use of small and bright organic fluorophores for live cell imaging. Fluorescent proteins and enzymatic self-labeling tags are well-suited for live cell imaging because the tagged proteins are directly produced inside the cell. Mostly, fusion proteins are introduced as a transgene by transfecting cells with a plasmid. However, transgene systems lead to heterogeneous expression levels that may not faithfully represent the function and localization of the fusion protein at a physiological expression level [66]. Alternatively, genome editing methods including Zinc Finger Nuclease (ZFN), Transcription activator-like effector nuclease (TALEN), and CRISPR-Cas9 have been developed to insert a protein tag directly into the gene of interest leading to endogenous expression of the fusion protein [67, 68].

Another approach to label proteins in fluorescence microscopy includes binders that bind specifically and with high affinity to the protein of interest. There are two different approaches to labeling proteins with binder: a direct and indirect approach. The direct approach uses a fluorophore-coupled primary antibody or another affinity binder that binds the protein of

interest. In contrast, the indirect approach employs an unlabeled primary binder first (e.g. primary antibody) which is, in a second staining step, detected by a secondary binder (e.g. secondary antibody). The indirect approach is popular because it includes a signal amplification step and often expensive primary binders can be applied without chemical modifications. In most cases, the specimen needs to be fixed before labeling. This is achieved by chemical fixation using cell-penetrating reagents such as formaldehyde or glutaraldehyde that can rapidly cross-link cellular biomolecules to preserve their structure. Alternatively, organic solvents and alcohols (e. g. methanol, acetone) are used for fixation by precipitating biomolecules.

1.5.2 Binder property requirements for super-resolution microscopy

An ideal binder for super-resolution microscopy requires certain characteristics that are discussed in the following paragraphs.

Affinity

For fluorescence microscopy imaging, a binder is required to bind in a stable fashion to the target molecules, ensuring a stable signal during image acquisition. Affinity is a measure of the binding strength of a ligand to its proteins and is quantified by the dissociation constant (K_D). The ligand-protein interaction is non-covalent and based on intermolecular forces including hydrogen bonds, hydrophobic, electrostatic, or Van-der-Waals forces.

The ligand-protein binding can be described by a two-state process, with the ligand concentration $[L]$, protein concentration $[P]$, and concentration of the ligand-protein complex $[LP]$ referring to the molar concentrations, respectively.

$$[L] + [P] \underset{k_{off}}{\overset{k_{on}}{\rightleftarrows}} [LP]$$

The K_D has a molar unit (M) and corresponds to the ligand concentration at which half of the proteins are occupied. Thus, the lower the concentration the higher the affinity and the tighter the binding to its protein. The dissociation constant is usually determined by measuring the ligand association (k_{on}) and dissociation rates (k_{off}).

$$K_D = \frac{[L][P]}{[LP]} = \frac{k_{off}}{k_{on}}$$

Specificity

Specificity is another crucial characteristic of binders in fluorescence microscopy. It is the ability of a binder to distinguish a certain target epitope from other (similar) epitopes. High specificity is especially important for applications in which other biomolecules are present as potential interaction partners. These applications include medical applications, biochemical methods (e.g. immunoprecipitation), and biological imaging in cells, tissues, or whole organisms. High specificity will result in low off-target binding and low background signal. To increase specificity, the binder concentration needs to be titrated, and adding competitor molecules such as BSA or animal serum in larger excess to the binder can block weak off-target interactions and surface adherence [69, 70]. When highly negative charged nucleic acid-based binders are used, anionic competitor molecules can be added to avoid non-specific electrostatic interactions due to the negative charges [71, 72].

Size

Besides high affinity and specificity, the size of the binder is to be considered. For diffraction-limited microscopy with a spatial resolution of 200 nm, the binder size is not limiting the achievable protein detection precision. If resolutions below 30 nm can be obtained, the size of the binder starts to be a limiting factor because it adds a linkage error to the target protein. This error results from the displacement of the target protein and the probe attached to the binder. In case of the common indirect labeling approach using primary and secondary antibodies, the linkage error is in the range of 20 – 30 nm. When imaging at molecular resolution in the range of 5 nm, the binder becomes a limiting factor since it must be as small as 2-5 nm [73]. Moreover, the size affects the accessibility of the binder to its target in the cell. Large binder sizes can thus lead to staining artifacts and lower labeling efficiencies [71].

Functionalization

To detect the binder with fluorescence microcopy, a probe (e. g. fluorophore, DNA) needs to be chemically attached to it. For quantitative analyses, the probe/binder ratio is ideally stoichiometrically, for instance, one binder is attached to a single fluorophore. The applicability

and usability also depend on how easy and precise a probe can be attached to the binder. Common coupling strategies will be presented in section 1.5.4.

1.5.3 Binder categories: Chances and limitations in super-resolution microscopy

This section will introduce commonly used and promising binder categories for super-resolution microscopy.

Antibodies

Antibodies, also called immunoglobulins (Ig), play an essential role in the immune system by recognizing unique molecules (antigens) of invading pathogens. They are large proteins (~150 kDa, ~10 nm) and are well recognized by their typical Y-shape. In the body, B cells produce antibodies as B cell receptors that are later secreted into the bloodstream. The structure of an intact murine IgG2a antibody was published by Harris et al. and is represented in Figure 13 [74]. Antibodies are composed of two identical light- and heavy chains that are connected by disulfide bonds. The heavy chain comprises one variable domain (V_H), a constant domain (C_{H1}), followed by a hinge region, and two more constant domains (C_{H2}, C_{H3}). The light chains are composed of one variable domain (V_L) and a constant domain (C_L). Functionally, an antibody is partitioned into two Fab (Fragment antigen-binding) regions and Fc (fragment crystallizable) region, the trunk of the Y. The Fab region is responsible for the antigen binding and contains the entire light chains and the V_H and C_{H1} regions of the heavy chains. The variable domains mediate the interaction with the antigen. Each of the variable regions contains three loops, referred to as complementary determining regions (CDRs). The CDRs define the binding affinity and specificity of the antibody to the antigen. The Fc region (C_{H2} and C_{H3}) functions as an 'adaptor' for multiple cell receptors (Fc receptor) that trigger further immune responses such as lysis of the antibody-bound pathogen.

In their application, antibodies can be classified into two categories: Monoclonal and polyclonal antibodies. Polyclonal antibodies are a heterogeneous mixture produced by different B cell clones, and therefore bind to different epitopes of the same antigen. Monoclonal antibodies originate from the same B cell clone and recognize the same epitope of an antigen.

In fluorescence microscopy, antibodies are the most used and available labeling probes. In 2015, the Cell Atlas (as part of the Human Protein Atlas) was published in which 13993 antibodies were used to map the subcellular localization of more than 12003 proteins by single-cell imaging [75, 76].

Monoclonal antibodies are preferred as primary antibody source because their availability, and well characterized affinity and specificity. Since polyclonal antibodies bind several epitopes of an antigen, they can provide a stronger signal and are less affected by inaccessibility or damage of a certain epitope by fixation for example. Polyclonal antibodies are commonly used as secondary antibodies to obtain a strong signal amplification of the bound primary antibodies.

With improved super-resolution methods molecular resolution below 20 nm can be achieved. Given the size of a single antibody of ~10 nm, an indirect staining approach using primary and secondary labels will lead to a significant displacement of the fluorescent probe to the actual target protein. Moreover, antibodies being large proteins comprise many reactive amino acids (lysines and cysteines) that make it more challenging to attach fluorophore or DNA strands in a site-specific and quantitative manner. Nevertheless, the indirect immunostaining approach provides a strong signal amplification which is beneficial for samples with high background fluorescence. Alternatively, a primary antibody alone can be coupled to a fluorescent probe. Furthermore, a single Fab fragment can be produced from an antibody to obtain a small (~50 kDa), monovalent binder. The digestion of an antibody with the enzyme papain cleaves the disulfide bonds of the hinge regions connecting Fab and Fc fragments resulting into two separated Fab and one Fc region [77].

Single domain camelid antibodies (Nanobodies)

Fully functional antibodies consisting of heavy chains and lacking light chains were discovered in the serum of *Camelidae* such as llamas and alpacas [78]. These heavy-chain only antibodies are composed of one single variable domain (V_{HH}) and two constant domains (CH_2, CH_3). A cloned and isolated V_{HH}, also referred to as nanobody or single-domain antibody, is stable and provide full antigen-binding capacities. They have a unique structure comprising three CDR regions of where CDR1 and CDR3 loops are longer than those from conventional antibodies, leading to similar binding affinities [79]. Due to their small size of (12 – 15 kDa) and nano- to picomolar affinities, nanobodies have suitable characteristics as a labeling probe for super-resolution microscopy. In comparison to conventional antibodies, nanobodies are (to date)

limited by their availability for many different targets. The development of new nanobodies requires animal immunization which is expensive and time-consuming. Furthermore, nanobodies are stable and can simply be expressed in bacteria. They can also be easily modified with a labeling tag such as an ectopic cysteine or sortase tag to facilitate site-specific functionalization with a fluorophore or DNA [80, 81].

Nanobodies have been applied for various super-resolution methods. In particular, nanobody binding to genetically encoded tags including GFP and RFP [82]. Ries et al. used a nanobody to label tubulin expressing YFP. They measured a considerably smaller microtubule diameter (FWHM ~27 nm) using nanobody labeling compared to indirect immunostaining with primary and secondary antibodies (FWHM ~45 nm), demonstrating the linkage error due to the large size of antibodies [83]. Furthermore, nanobodies were developed against small peptide tags (~12 amino acids) including BC2 tag and ALFA tag that further reduce the linkage error and are less prone to interfere with the function of the target protein [84, 85]. The structure of the nanobody (NbALFA) binding to the ALFA tag peptide is depicted in Figure 13b.

Secondary IgG binding nanobodies have been developed as a smaller alternative to polyclonal secondary IgG [86, 87]. Moreover, host-species independent multiplexing can be conducted by separately pre-mixing the nanobodies with the primary antibody and saturating their binding sites [86]. The assembled immunocomplexes are then pooled and incubated with the cell for immunostaining. Therefore, secondary nanobodies provide a flexible and simple approach for multiplexing using primary antibodies while reducing the labeling size to increase the localization accuracy.

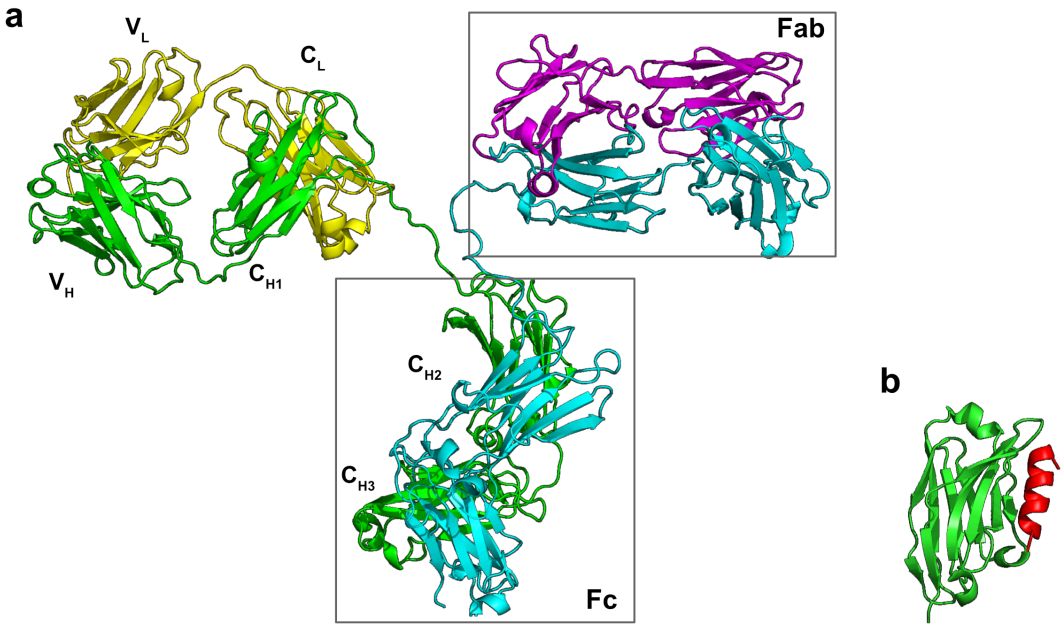

Figure 13: a) Crystal structure of an anti-canine lymphoma IgG2a monoclonal antibody (Mab231) [74]. Heavy chains are shown in green and cyan. Light chains in magenta and yellow. b) Nanobody (NbALFA, green) bound to ALFA-tag peptide (red) [85]. Structures were rendered with PyMOL using PDB ID 1IGT (IgG2s) and 6I2G (NbALFA).

Aptamers and SOMAmers

Aptamers are oligonucleotides or peptides that are selected from a library to bind specific target molecules. They are selected *in vitro* from a large sequence pool in a process called selective systematic evolution of ligands by exponential enrichment (SELEX). The first RNA aptamers were selected in 1990 against the protein T4 DNA polymerase [88, 89]. In brief, SELEX comprises three fundamental steps (Figure 14a): 1) A large sequence pool in the range of 10^{15} different sequences is incubated with the target molecule. 2) Target-bound sequences are partitioned from non-binding sequences 3) Bound sequences are recovered and amplified by PCR, followed by sequencing. This selection process is repeated until a sequence reaches the desired affinity [90].

Compared to antibodies, aptamers have the advantage of higher stability, low-cost synthesis, and better batch-to-batch consistency. In addition, they provide better flexibility for site-specific chemical modifications which can readily be introduced during synthesis. Furthermore, the SELEX process is entirely performed in vitro and only takes 2-8 weeks [91].

These characteristics in combination with their small size (15 – 80 bases), make them especially suitable as binders for super-resolution microscopy.

The chemical diversity of aptamers has been expanded by incorporating chemically modified bases into the sequence library. The company SomaLogic has successfully applied this approach by replacing dT bases with dU containing hydrophobic modifications on the C5 position (Figure 14b) [92]. These modifications include hydrophobic groups such as benzyl or naphthyl to mimic the binding properties of amino acids that are particularly frequent in antigen-binding sites of antibodies [93]. Selected aptamers display high affinities mainly due to their slow off-rate, for which they were named slow off-rate modified aptamers (SOMAmers). The SELEX process used for SOMAmers selection has enabled the generation of high-affinity aptamers against targets for which selection with standard bases had previously failed. SomaLogic has reported SOMAmer reagents against more than 3000 targets [94]. An exemplary structure of a SOMAmer binding to the human interleukin 6 protein is depicted in Figure 14c.

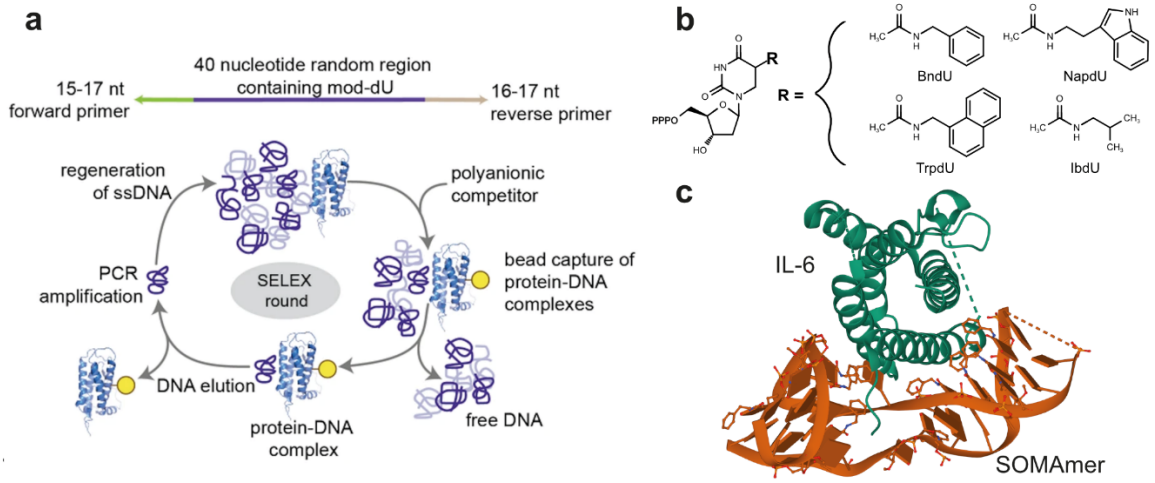

Figure 14: Selection and structure of SOMAmers: a) SELEX is performed with a sequence library containing for example 40 nucleotides randomly flanked by forward and reverse primers for PCR amplification. The random region incorporates modified-dU bases. First, the nucleotide library is mixed with the target protein and specific nucleotides will bind to the protein. Polyanionic competitors are added to dissociate weak electrostatic interaction of protein-DNA complexes. Next, proteins are captured on beads while unbound DNA is removed. DNA bound to the protein is eluted and amplified by PCR. The obtained sequences are further characterized or subjected to another SELEX round. Reprinted with permission from Springer Nature [95], copyright (2020). b) Nucleotide triphosphate analogues of uridine (dUTP) modified at the 5-position (R): 5-benzylaminocarbonyl-dU (BndU), 5-naphthylmethylaminocarbonyl-dU (NapdU), 5-tryptaminocarbonyl-dU (TrpdU), 5-isobutylaminocarbonyl-dU (iBudU); adapted from [92]. c) Crystal structure of human interleukin 6 in complex with a SOMAmer, the structure was obtained from RSCB PDB (ID 4NI7) and rendered with Mol* [96-98].

A few applications of aptamers in fluorescence microscopy have been reported. A SOMAmer binding to Her2 has been used for rapid tissue staining to detect Her2 overexpressing cells [72]. Furthermore, aptamers have also been applied in combination with STED super-resolution microscopy [71, 99]. In this study, the aptamers achieved denser labeling and epitope coverage compared to antibodies. However, besides the Her2 SOMAmer, aptamers have not been successfully applied to stain fixed cell or tissue samples.

Genetically encoded and self-labeling tags

Besides their major application in live-cell imaging, genetically encoded tags are widely used for super-resolution imaging. As previously mentioned in section 1.2.2, photoactivatable and photoswitchable proteins can be directly used for PALM imaging. In addition, they have been applied to the SMLM methods STORM and DNA-PAINT by using an affinity binder specifically developed against these tags [83, 100]. For instance, high-affinity nanobodies against commonly used fluorescent proteins have been developed such as GFP, RFP, and tagRFP [83, 100]. Also, enzymatic self-labeling tags like HALO and SNAP tags can be covalently coupled with a fluorophore or DNA coupled ligand [101]. Side-by-side comparisons of EGFP, SNAP and HALO tags have been performed by Ries et al. [102] and Schlichthaerle et al. [103] using dSTORM and DNA-PAINT. Both groups used a cell line genetically modified with a homozygous knock-in of EGFP, HALO, and SNAP at the nuclear pore complex protein Nup96. Using different tags combined with nanobodies and ligands, the typical arrangement of a nuclear pore complex was successfully reconstructed. In contrast, this was not possible using an antibody-based immunolabeling approach. The defined arrangement of the nuclear pore proteins was also established as a reference standard to determine the labeling efficiency. The GFP nanobody achieved a labeling efficiency of ~70% while HALO and SNAP reached ~50% [102]. Small affinity binders for small protein tags are useful since arbitrary proteins can be targeted with the same binder after cell engineering. On the downside, the creation of knock-in cell lines is time-consuming, and the multiplexing capability is limited by the number of orthogonal tags.

An overview of different labeling strategies and their respective linkage errors is depicted in Figure 15.

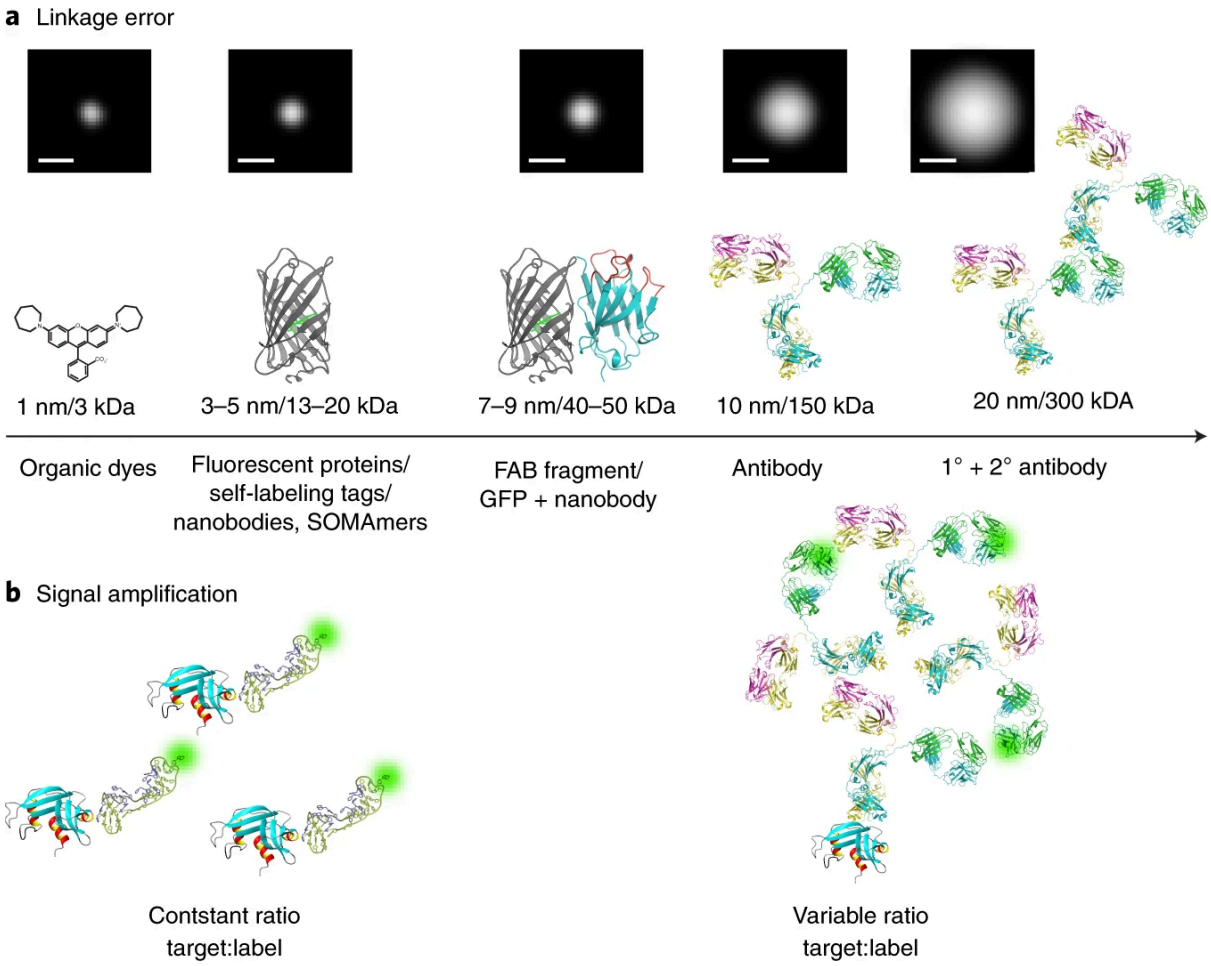

Figure 15: Linkage error and signal amplification of different labeling strategies. a) Overview of the size and molecular weight of different labeling approaches. Larger probe sizes reduce the certainty of the protein position represented by Gaussian profiles. Scale bars: 30 nm. b) Single labeled, monovalent binders like nanobodies or aptamers provide constant target-to-label ratio facilitating accurate quantification. Signal amplification between primary and secondary antibodies provides a stronger signal but prevents the quantification of target epitopes. Reprinted with permission from Springer Nature, copyright (2018) [104].

1.5.4 Protein-DNA conjugation strategies

DNA-PAINT imaging requires a short single-stranded DNA (6 nt – 11 nt) conjugated to an affinity binder. Figure 16 presents an overview of the conjugation chemistries applied in this work. Antibodies can be coupled by targeting primary amine groups (-NH_2) present on the N-termina and sidechains of the amino acid lysine with N-hydroxysuccinimide (NHS) ester as a reactive group [105]. Therefore, a DBCO-Sulfo-NHS ester as a bifunctional cross-linker is reacted with the antibody [30]. Dibenzocyclooctyne (DBCO) reacts with azide groups through a stain-promoted [3+2] azide–alkyne cycloaddition (SPAAC) that does not require copper as a catalyst [106, 107]. Thus, a DNA oligo carrying an azide modification is reacted with the DBCO group on the antibody that was previously introduced.

Besides primary amines, reduced thiols (-SH) of the amino acid cysteine react with maleimide. For example, nanobodies or Affimers can be expressed with ectopic cysteines at the N- and/or C-terminus which enable site-specific attachment of fluorophores or DNA using maleimide chemistry [80, 86, 108]. Since nanobodies carry internal disulfide bonds, they need to be carefully reduced on ice using a low concentration of the reducing agent TCEP (~5 mM). After exchanging the reduced protein to a TCEP free buffer, the binders are reacted with a maleimide-DBCO cross-linker. The subsequent DNA attachment is performed using azide modified DNA as described for the antibodies. The conjugates are then purified by anion exchange chromatography [108].

An alternative strategy to incorporate a DBCO or azide moiety into the protein is by incorporating unnatural amino acids (UAA) during protein expression [109]. In addition, labeling tags other than cysteine can be inserted, such as the sortase or ybbR tag that has been used to conjugate proteins to other biomolecules. These require a short peptide tag on the target protein that reacts with ligands modified with triple glycine (for sortase) or coenzyme A (for ybbR-tag) via catalytic enzymes [110, 111].

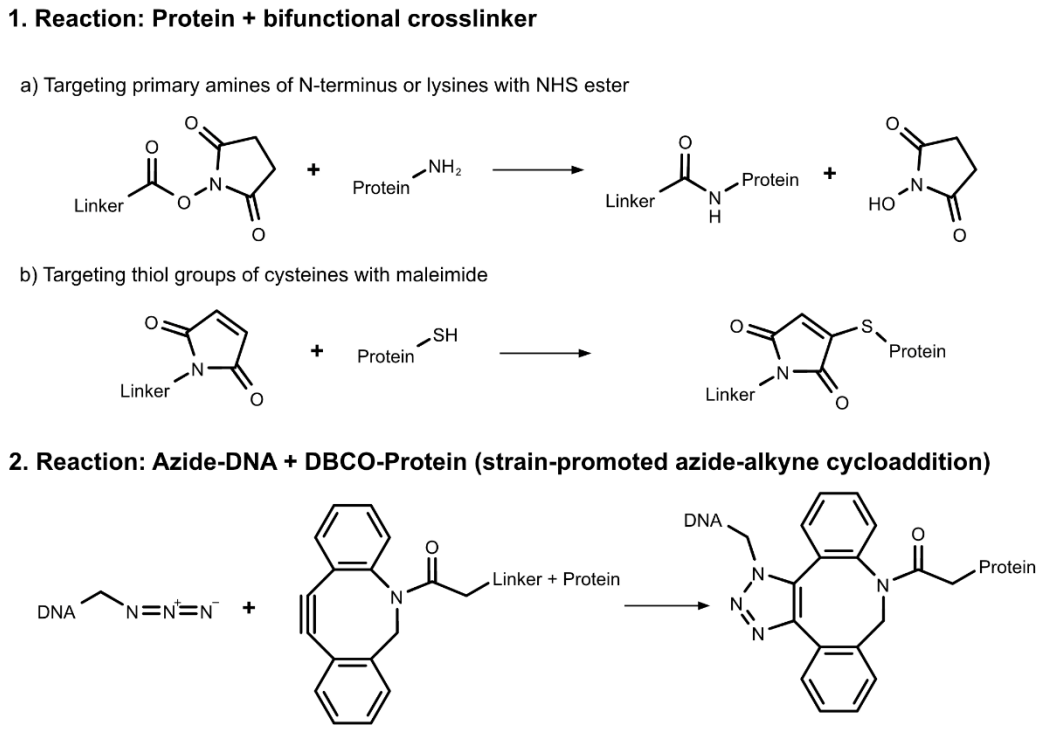

Figure 16: Protein-DNA coupling chemistries: In a first reaction the protein is coupled to a bifunctional crosslinker (e.g. DBCO-NHS ester). A protein can be targeted via primary amines present on the N-terminus or lysines with an NHS ester. Alternatively, thiol groups of the amino acid cysteine can be reacted with maleimide. In a second reaction, the DBCO functionalized protein is coupled to an azide-modified DNA oligo via strain promoted azide-alkyne cycloaddition.

1.5.5 Detecting single mRNA molecules using FISH

Fluorescence in-situ hybridization (FISH) techniques are applied to detect intracellular nucleic acids such as messenger RNA (mRNA) and DNA in fixed cells, tissues, and organisms. The general concept of FISH is to incubate fluorescently labeled oligonucleotide probes complementary to the mRNA species. Non hybridized probes are washed away, and mRNAs are then imaged with a fluorescence microscope and appear as bright single spots. Detecting single mRNA species requires a strong signal that can be achieved by either signal amplification of a bound probe or by incubating many DNA oligos conjugated to one or multiple fluorophores [112, 113]. The concept of Stellaris-FISH applies to a maximum of 48 short single labeled oligos that hybridize to the RNA transcript [113, 114]. A high number of probes leads to a low chance of false-negative detections and makes the technique less sensitive to off-target binding of a single probe, thus achieving a high signal-to-noise ratio. This approach is sensitive enough to detect single RNA transcripts in mammalian cells, tissue slices,

and model organisms including *Caenorhabditis elegans* and *Drosophila melanogaster* [113, 114].

Another method termed Oligopaint uses probes with 32 nucleotides homologous to the genome that are amplified by PCR with fluorophore-labeled primers [115]. This approach was applied for super-resolution STORM and DNA-PAINT imaging of genomic DNA and mRNA transcripts [116, 117].

2 Aims and objectives

DNA-PAINT is a powerful super-resolution technique with key advantages concerning spatial resolution, multiplexing, and quantitative imaging. However, the technique requires long image acquisition times that limit the practical applicability, particularly for biological questions, where high statistics are required. Furthermore, DNA-PAINT and super-resolution techniques, in general, are limited by the availability of small binders (~3 nm) that also provide stoichiometric labeling of the target protein for precise quantification. The overall scope of this thesis is to improve the biological applicability of DNA-PAINT by advancing labeling methods and DNA probe design. This will be achieved by 1) extending the binder portfolio with a new class of small, modified aptamer 2) implementing parallelized multiplexing with a kinetic barcoding approach, and 3) increasing the imaging speed of DNA-PAINT by accelerating the binding kinetics with improved sequence design.

Establishing modified aptamers for DNA-PAINT imaging

So far, nanobodies and Affimers have been successfully applied as small binders for DNA-PAINT imaging, but only a few examples of each category have been demonstrated. Therefore, the first aim of this thesis is to extend the binder portfolio for DNA-PAINT. As described in section 1.5.3, SOMAmers are small high-affinity binders and, since they consist of DNA, they can easily be extended with a single DNA-PAINT docking strand during synthesis. These binder properties and the large, already existing library developed by SomaLogic, make SOMAmers promising reagents to label proteins for DNA-PAINT imaging. Thus, I aim to establish a cell staining protocol that can be used to label proteins in fixed cells with SOMAmers. After achieving specific labeling, the improvement of SOMAmers compared to antibody labeling will be demonstrated with respect to resolution and quantitative imaging.

Kinetic barcoding for parallelized multiplexing

The use of DNA sequence barcodes instead of fluorophores enables a high multiplexing capability decoupled from the spectral properties of dyes. Exchange-PAINT is based on using orthogonal DNA sequences that are imaged sequentially. However, the imaging time of Exchange-PAINT scales with the number of imaging rounds that can set a practical time constraint for highly multiplexed experiments. Besides the sequence identity, the hybridization

kinetics can be changed by varying the sequence length and base compositions of the docking strand sequences. Therefore, the second aim of this thesis is to establish a barcoding approach based on hybridization kinetics of the imager/docking strands to read out multiple molecule identities after a single image acquisition round. This approach will first be optimized on defined DNA origami structures. Then, the kinetic barcoding approach will be applied for multiplexed detection of single proteins and mRNA molecules.

Repetitive sequence motives to speed up DNA-PAINT imaging

Several approaches have been developed to improve the imaging speed of DNA-PAINT (see section 1.3.4). All of them are either limited by the achievable spatial resolution or the speed improvement is only applicable for a single target. The third aim of this thesis is to establish a new sequence design that further accelerates the binding kinetics and is also applicable to other sequences. With short repetitive sequence motifs, overlapping binding sites can be displayed on a single DNA strand. This is a promising approach to increase the association rate of the imager strand to the docking strand which will accelerate DNA-PAINT imaging. I aim to establish speed-optimized six-color imaging on DNA Origami structures and demonstrate its applicability in a multiplexed experiment in fixed cells.

3 Publications

3.1 Publication I: Modified aptamers enable quantitative sub-10-nm cellular DNA-PAINT imaging

Sebastian Strauss, Philipp C. Nickels, Maximilian T. Strauss, Vilma Jimenez Sabinina, Jan Ellenberg, Jeffrey D. Carter, Shashi Gupta, Nebojsa Janjic, Ralf Jungmann

Nature Methods**,** volume 15, pages 685–688 (2018)

DOI: https://doi.org/10.1038/s41592-018-0105-0

Super-resolution imaging with DNA-PAINT has two unique advantages: Sub-10-nm spatial resolution and high multiplexing capability with Exchange-PAINT. Translating these technical capabilities to cellular imaging requires small labeling probes that are available for as many targets as possible. The commonly applied indirect immunostaining approach using a primary and secondary antibody adds a substantial error to the protein localization due to their large, combined size (~30 nm). In contrast, aptamers have ideal properties for being a suitable probe for super-resolution microscopy, particularly for DNA-PAINT – they are small, stable, and easy to modify site-specifically with a fluorophore or DNA strand.

In this study, we collaborated with the company SomaLogic, which developed a proteomics platform called SOMAscan that is based on the use of slow-off-rate modified aptamers (called SOMAmers). The SELEX selection process of these aptamers includes modified bases that carry hydrophobic residues. These hydrophobic modifications are incorporated to imitate amino acids that are abundant in antigen-binding sites of antibodies, thus leading to significantly slower off rates of selected aptamers. Moreover, the enhanced chemical diversity of SOMAmers compared to DNA/RNA aptamers makes the selection process successful for a larger number of protein targets [94]. Therefore, SomaLogic has successfully selected aptamers against more than 3000 protein targets, which are currently included in the SOMAscan assay.

This large library makes it especially promising for proteomics applications and potential multiplexed imaging using Exchange-PAINT.

I established SOMAmers as a labeling reagent for standard fluorescence and DNA-PAINT super-resolution microscopy. First, I achieved specific staining of EGFR with a SOMAmer that is coupled to a Cy3 dye. The blocking conditions were optimized by adding anionic competitor molecules into the staining buffer. I observed that adding 1000-fold molar excess of dextran sulfate (6.5 – 10 kDa) and a 100-fold molar excess of Z-Block removes non-specific interaction of SOMAmer to negatively charged compartments in the cells, more specifically in the nucleus and mitochondria. After successful optimization of the labeling conditions, the SOMAmers were extended with a DNA-PAINT docking strand and used for DNA-PAINT imaging. Using a SOMAmer binding to EGFR, I could demonstrate a spatial resolution of better than 10 nm and could clearly measure distances of approximately 15 nm. I was able to demonstrate a significant improvement of the imaging resolution with SOMAmer staining compared to primary and secondary antibody labeling. Furthermore, the stochiometric 1:1 SOMAmer-docking strand labeling ratio makes these reagents more precise for quantifications when using qPAINT [38].

Next, I demonstrated the broad applicability of SOMAmers by labeling and imaging intracellular targets such as GFP-Nup107 and catalases present inside peroxisomes. Furthermore, I performed multiplexed imaging of three different protein targets close to the membrane including: EGFR, Her2, and Hsp90.

Overall, during this study, I established a protocol to use SOMAmers for labeling proteins. By applying them in DNA-PAINT microscopy, I demonstrated that the smaller size of SOMAmers can improve the spatial resolution for cellular imaging below 10 nm, which has not been demonstrated to that date. Future work will involve screening as many SOMAmers as possible to obtain a library of aptamers that can be used for super-resolution microscopy as an alternative or in addition to antibodies or other available binders.

nature methods

BRIEF COMMUNICATION

https://doi.org/10.1038/s41592-018-0105-0

Modified aptamers enable quantitative sub-10-nm cellular DNA-PAINT imaging

Sebastian Strauss[1,2], Philipp C. Nickels[1,2], Maximilian T. Strauss[1,2], Vilma Jimenez Sabinina[3], Jan Ellenberg[3], Jeffrey D. Carter[4], Shashi Gupta[4], Nebojsa Janjic[4] and Ralf Jungmann[1,2*]

Although current implementations of super-resolution microscopy are technically approaching true molecular-scale resolution, this has not translated to imaging of biological specimens, because of the large size of conventional affinity reagents. Here we introduce slow off-rate modified aptamers (SOMAmers) as small and specific labeling reagents for use with DNA points accumulation in nanoscale topography (DNA-PAINT). To demonstrate the achievable resolution, specificity, and multiplexing capability of SOMAmers, we labeled and imaged both transmembrane and intracellular targets in fixed and live cells.

Optical super-resolution techniques[1–4] make it possible to image biological processes at resolutions well below the classical diffraction limit of light and are starting to provide novel insights into previously unobservable biological phenomena[5], with recent technical developments approaching true biomolecular resolution[6–8].

DNA-PAINT[9] is a simple implementation of single-molecule localization microscopy (SMLM) that makes use of transient binding of dye-labeled DNA strands to complementary target-bound strands, thereby enabling spatial resolution better than 5 nm, as recently demonstrated with artificial DNA nanostructures[6,8].

However, this high spatial resolution does not translate to molecular-scale imaging of cellular targets because of the relatively large size of labeling probes (~150 kDa in the case of antibodies), which is one of the major limitations in high-resolution optical microscopy. Furthermore, fully stoichiometric, quantitative labeling via site-specific conjugation is not yet readily available for a large number of targets, which prevents the analysis of complex biosystems in a quantitative manner, one of the promises of quantitative biology.

The 'ideal' labeling probe therefore needs to satisfy several requirements: it should (1) be the smallest possible size for maximal labeling efficiency and minimal linkage error, (2) allow quantitative labeling (i.e., 1:1 stoichiometry for protein targeting), and (3) allow a rapid selection procedure for novel targets (or, ideally, an already available library of well-characterized binders). Although nanobodies[10] meet some of these criteria, they are not readily available for many cellular targets. Aptamers[11,12] have the potential to fulfill most of these requirements: they allow for rapid in vitro selection, are relatively small (a few tens of kilodaltons or less), and can be quantitatively labeled. However, their widespread application to fluorescence and super-resolution imaging has thus far been limited by three main factors: (1) restricted availability of specific aptamers for a wide range of targets, (2) concerns about compatibility with fixation procedures, and (3) limited ability to label intracellular targets.

We here introduce SOMAmer reagents[13,14] as small (7–30 kDa), quantitative, and versatile labeling probes for high-resolution in situ DNA-PAINT imaging. SOMAmer reagents represent a unique class of DNA aptamers that contain modified bases with hydrophobic residues, similar to the amino acid residues abundant in antibody epitopes used for high-specificity and high-affinity binding of proteins. These base modifications increase the range of protein targets for which high-affinity ligands can be selected[15].

We successfully assayed seven different SOMAmers (21–28 kDa; Supplementary Table 1) as probes for DNA-PAINT to quantify proteins in different cellular compartments: the transmembrane receptor EGFR (Fig. 1), GFP-labeled Nup107 in nuclear pores (Fig. 2), catalase proteins localizing to peroxisomes (Fig. 3), ErbB2 and HSP90 (Supplementary Fig. 1), and the lysosomal membrane protein LIMP-2 and mitochondrial HSP60 (Supplementary Fig. 2).

To initially evaluate labeling specificity, we conjugated a dye to a SOMAmer (Fig. 1a) for diffraction-limited confocal microscopy. For subsequent DNA-PAINT imaging, we extended the SOMAmer sequence with a single-stranded docking site (Fig. 1b; on either the 3′ or the 5′ end). First, we labeled EGFR in fixed A549 cells by using a Cy3-conjugated SOMAmer and evaluated the labeling specificity by confocal microscopy (Fig. 1a,c and Supplementary Figs. 3–5). We then carried out DNA-PAINT imaging in A431 cells, using the same EGFR SOMAmer with a docking-site extension instead of the fixed dye (Fig. 1b). Comparison of the diffraction-limited (Fig. 1d,e) and DNA-PAINT images (Fig. 1f) revealed subdiffraction spatial resolution and specific targeting of EGFR proteins in the plasma membrane. Zoomed-in views (Fig. 1g) of three areas underscored the high resolution achieved owing to the small size of the SOMAmer in combination with the high localization precision of DNA-PAINT. This is further exemplified by our ability to resolve EGFR molecules spaced only ~14 nm apart (Fig. 1g). To obtain an average measure of achievable resolution, we quantified the localization precision of SOMAmer-targeted proteins by overlaying the localizations of ~34,000 EGFR proteins on the basis of their center of mass. We achieved an average localization precision of ~3.2 nm (Fig. 1h), which translated to a full width at half-maximum–limited resolution of less than 8 nm (also highlighted by the clearly separable distributions in the cross-sectional histograms in Fig. 1g). Using classical primary and DNA-conjugated secondary antibody labeling and downstream DNA-PAINT imaging of EGFR, we observed an approximately twofold larger apparent size of single EGFR proteins compared with that observed with SOMAmer labeling (Supplementary Fig. 6).

[1]Department of Physics and Center for Nanoscience, Ludwig Maximilian University, Munich, Germany. [2]Max Planck Institute of Biochemistry, Martinsried, Germany. [3]Cell Biology and Biophysics Unit, European Molecular Biology Laboratory (EMBL), Heidelberg, Germany. [4]SomaLogic, Inc., Boulder, CO, USA. *e-mail: jungmann@biochem.mpg.de

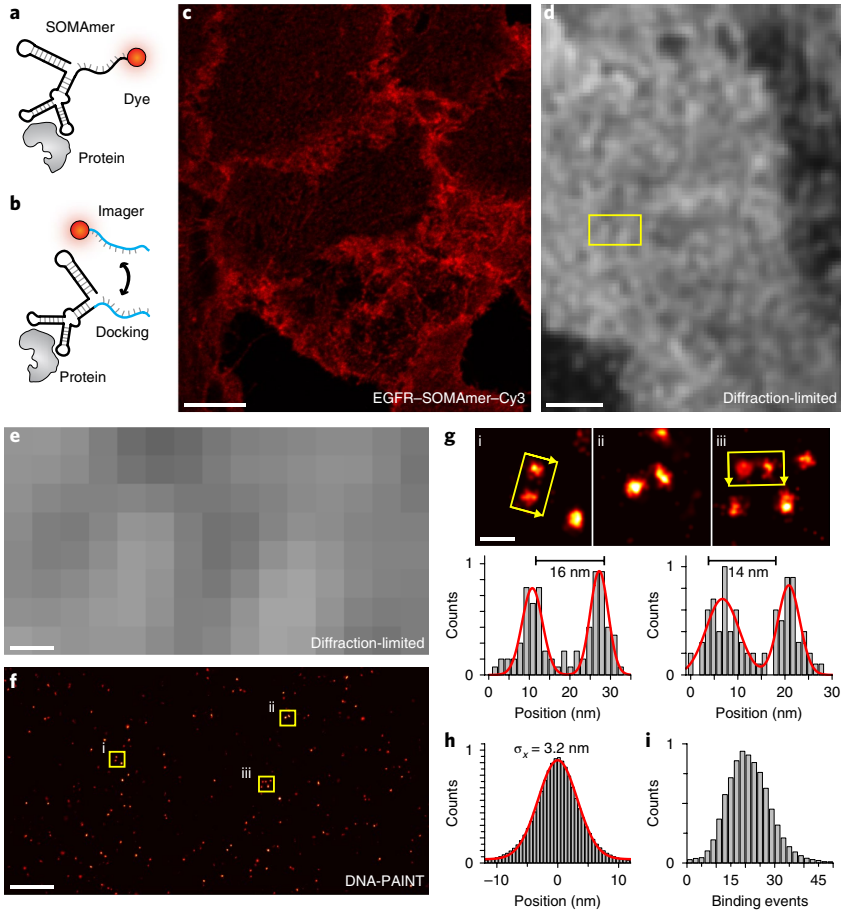

Fig. 1 | SOMAmers as labeling probes for quantitative, high-resolution DNA-PAINT imaging of membrane receptors. a, Labeling scheme using SOMAmers for diffraction-limited imaging with a fixed dye. **b**, Labeling scheme using SOMAmers for DNA-PAINT super-resolution imaging. Transient binding of a dye-labeled strand ("imager") to a complementary docking strand is enabled by single-stranded extension of the SOMAmer sequence. **c**, A SOMAmer targeting EGFR and labeled with a fixed Cy3 dye (SL1069; see scheme in **a**) allowed specific detection of EGFR in A549 cells by confocal microscopy. **d**, Diffraction-limited DNA-PAINT image of A431 cells stained with a complementary dye-labeled imager strand bound to a docking-site-modified SOMAmer (see scheme in **b**) targeting EGFR (s.d. image). **e**, Zoomed-in view of the area outlined by the yellow rectangle in **d**. **f**, Corresponding DNA-PAINT super-resolution image of the area outlined by the yellow rectangle in **d**. **g**, Top, zoomed-in views of highlighted areas i, ii, and iii in **f**. Bottom, cross-sectional histogram analysis for regions i (left) and iii (right) demonstrates high-resolution DNA-PAINT imaging of single EGFR proteins labeled with SOMAmers. **h**, Fitting of a Gaussian distribution to the center-of-mass-aligned single-molecule localizations of ~34,000 SOMAmer-labeled EGFR proteins yielded a localization precision of 3.2 nm. **i**, qPAINT analysis of single EGFR proteins yielded a unimodal distribution of binding events, confirming quantitative 1:1 labeling of EGFR proteins by SOMAmers. Scale bars, 10 µm (**c**), 2 µm (**d**), 200 nm (**e**,**f**), or 20 nm (**g**). Experiments were repeated at least three times, with similar results; representative data are shown.

As SMLM methods provide quantitative information from localization datasets[16,17], it becomes important to label target molecules in a quantitative fashion to harness the precision of such methods in biological systems. SOMAmers could deliver on this promise, as they are single-stranded nucleic acid molecules that can be easily modified during or after chemical synthesis to contain a single label.

We examined the ability of SOMAmers to serve as labeling probes for quantitative PAINT (qPAINT)[18] by labeling EGFR proteins and subsequently carrying out a qPAINT analysis on presumably single EGFRs. We quantified the same ~34,000 EGFR molecules used to determine localization precision (above) and calculated the number of binding events during the time of our image acquisition. The measure for binding events is directly linked to the number of available DNA strands per target molecule (i.e., two strands will exhibit twice as many binding events as a single site). The results revealed a unimodal distribution (Fig. 1i), thus confirming quantitative 1:1 labeling of EGFR by the SOMAmers (i.e., either one or no SOMAmer was bound). Using classical primary and DNA-conjugated secondary antibody labeling and subsequent qPAINT analysis, we observed a clear multimodal distribution of binding events, highlighting the broader distribution of binding sites in the antibody case compared with the unimodal distribution in the SOMAmer case (Supplementary Fig. 7).

Next, we turned our attention to the labeling and imaging of an intracellular target. We chose GFP-labeled Nup107 in HeLa Kyoto cells to demonstrate the widespread applicability of SOMAmers for intracellular DNA-PAINT. First, we confirmed specific labeling by GFP–Nup107 with confocal imaging, which showed good colocalization of the GFP and Cy3–SOMAmer signals (Fig. 2a). Subsequent DNA-PAINT imaging revealed super-resolved single Nup107 clusters in nuclear pore complexes (NPCs; Fig. 2b,c). Using astigmatism-based point-spread-function-shaping to obtain 3D super-localization[19], we were able to spatially separate the cytoplasmic and nuclear rings of the NPCs (Fig. 2d,e). Cross-sectional histogram analysis of both *xy*- and *xz*-projections yielded the expected distances (Fig. 2d,e).

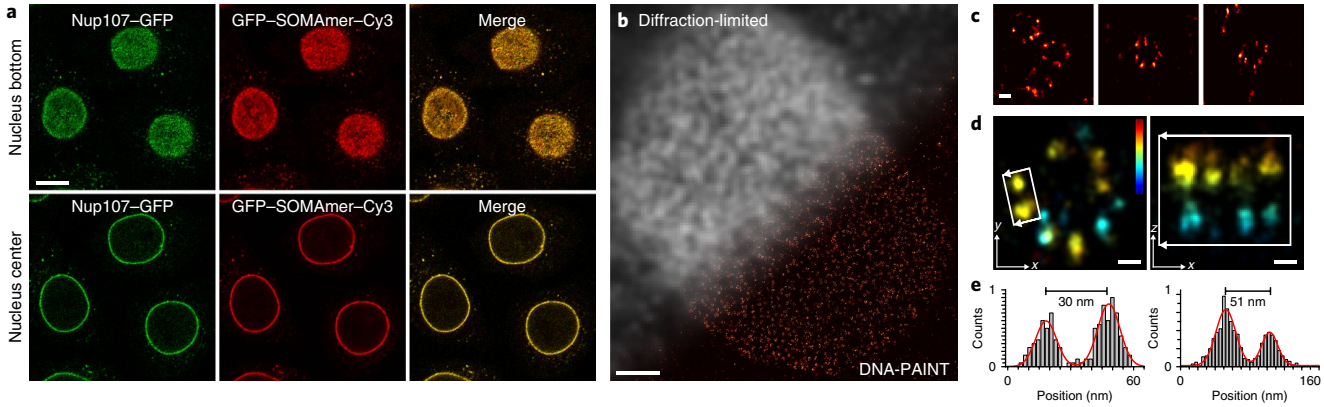

Fig. 2 | Intracellular labeling of GFP-tagged Nup107 for DNA-PAINT imaging using GFP–SOMAmers. a, Confocal images of GFP-tagged Nup107 nucleoporins labeled with Cy3-modified GFP–SOMAmers. GFP (SL1070; left, green), SOMAmer–Cy3 (center, red), and merged signal (right) at the bottom (top) and center (bottom) of the nucleus show specific binding of the SOMAmer to GFP-tagged Nup107. **b**, Diffraction-limited and corresponding DNA-PAINT super-resolution images of GFP-tagged Nup107, using a docking-strand-extended SOMAmer for GFP. **c**, Representative high-magnification views of single NPCs. **d**, *xy*-projection (left) and *xz*-projection (right) of a single NPC, showing well-resolvable clusters of Nup107 in the *xy*-projection, and nuclear and cytoplasmic rings in the *xz*-projection. Color-coding indicates height (see key; blue to red, −100 nm to 400 nm). **e**, Cross-sectional histogram analysis of outlined areas in **d** reveals a distance of ~30 nm between Nup107 clusters in *xy* (left) and ~51 nm in *z* between the nuclear and cytoplasmic rings (right). Scale bars, 10 µm (**a**), 2 µm (**b**), 50 nm (**c**), or 25 nm (**d**). Experiments were repeated at least three times, with similar results; representative data are shown.

Next, we labeled intracellular targets without relying on GFP, to further illustrate the flexibility and intracellular specificity of SOMAmers. Here we chose to label catalase proteins, which are localized to peroxisomes, and used confocal microscopy to assay the binding specificity of a dye-labeled SOMAmer for catalase. We costained peroxisomal membrane protein PMP70 with dye-labeled antibodies (Fig. 3a) in combination with fluorescein-labeled SOMAmers targeting catalase (Fig. 3b). The merged overlay image revealed colocalization of PMP70 and catalase signals, again suggesting high labeling specificity of SOMAmers (Fig. 3c). Subsequent DNA-PAINT imaging revealed resolvable single catalase molecules in peroxisomes (Fig. 3d,e). 3D DNA-PAINT micrographs furthermore revealed distinct *z* localizations of peroxisomes and catalase molecules within them (Fig. 3f–h). We then applied the multiplexing approach Exchange-PAINT[20] (Supplementary Fig. 8) to visualize antibody-stained PMP70 and SOMAmer-labeled catalase molecules, to demonstrate the capability for colabeling with antibodies and SOMAmers. For simultaneous labeling of multiple cellular targets using SOMAmer reagents, we conducted two additional Exchange-PAINT experiments: (1) simultaneous labeling and sequential imaging of HSP60 and LIMP-2 (Supplementary Fig. 2); and (2) labeling and imaging of EGFR, ErbB2, and HSP90 in single cells (Supplementary Fig. 1).

We next evaluated the effects of fixation (Supplementary Figs. 9 and 10) and anionic competitors (Supplementary Figs. 11 and 12) on the labeling specificity, as well as the possibility of direct membrane-protein staining on living cells. Aptamers in general and SOMAmers specifically are selected for native protein targets. The fixation conditions typically used for immunostaining of tissues and single cells are likely to disrupt the native structure of proteins to some extent, and thus potentially decrease or (in severe cases) prevent labeling. However, the successful SOMAmer staining demonstrated here for EGFR, Nup107–GFP, and catalase after a typical paraformaldehyde fixation suggests that SOMAmers can still specifically bind their epitopes in formaldehyde-fixed samples. Nevertheless, we expect that the fixation conditions would have to be slightly adjusted for SOMAmers targeted to other proteins in order to achieve optimal labeling specificity (see also Supplementary Table 2). Standard fixation conditions used for conventional immunostaining, such as 4% paraformaldehyde fixation, have proven to be a good starting point for this optimization process. We also note that in fixed cells, the polyanionic competitors dextran sulfate and Z-Block successfully quenched both nonspecific nuclear binding and cellular organelle binding (Supplementary Note 1).

Finally, we carried out EGFR staining without prior fixation on living cells with the EGFR SOMAmer (Supplementary Note 2 and Supplementary Fig. 13), which allowed (for the first time, to our knowledge) live-cell DNA-PAINT imaging and tracking of membrane targets in their native state (Supplementary Fig. 14 and Supplementary Video 1).

In conclusion, we introduce SOMAmers as small, efficient, quantitative, and universal labeling probes for DNA-PAINT that can make this method's high achievable resolution and quantitative imaging capability directly applicable to a diverse variety of cellular targets. SOMAmers, with their enhanced affinity and readily available library of thousands of cellular targets, are poised to replace antibodies and nanobodies as labels, thereby potentially becoming the preferred affinity reagent for super-resolution microscopy. Together with the spectrally unlimited multiplexing capabilities of Exchange-PAINT[20], SOMAmers should make it possible to eventually image tens to hundreds of cellular targets in single cells with single-molecule spatial resolution in a quantitative fashion, and furthermore allow for live labeling and imaging of membrane-bound proteins. However, we note that there is—apart from the synthesis and assaying of a large number of additional SOMAmers—a considerable challenge involved in achieving this amount of multiplexing: finding compatible fixation conditions for a large variety of targets. This could potentially be overcome by live labeling followed by subsequent fixation; however, future assays are necessary in this direction. Taken together, our findings indicate that quantitative SOMAmer labeling for DNA-PAINT (owing to the easy modification with exactly one docking site per SOMAmer) might have far-reaching implications with the potential to deliver on one of the ultimate promises of SMLM: system-wide biological studies with quantitative single-protein resolution. Possible applications could include the study of the interplay of homo- and heterodimerization of membrane receptors after different stimulation treatments on the single-protein level, which could lead to new insights into their nanoscale organization and physiological function.

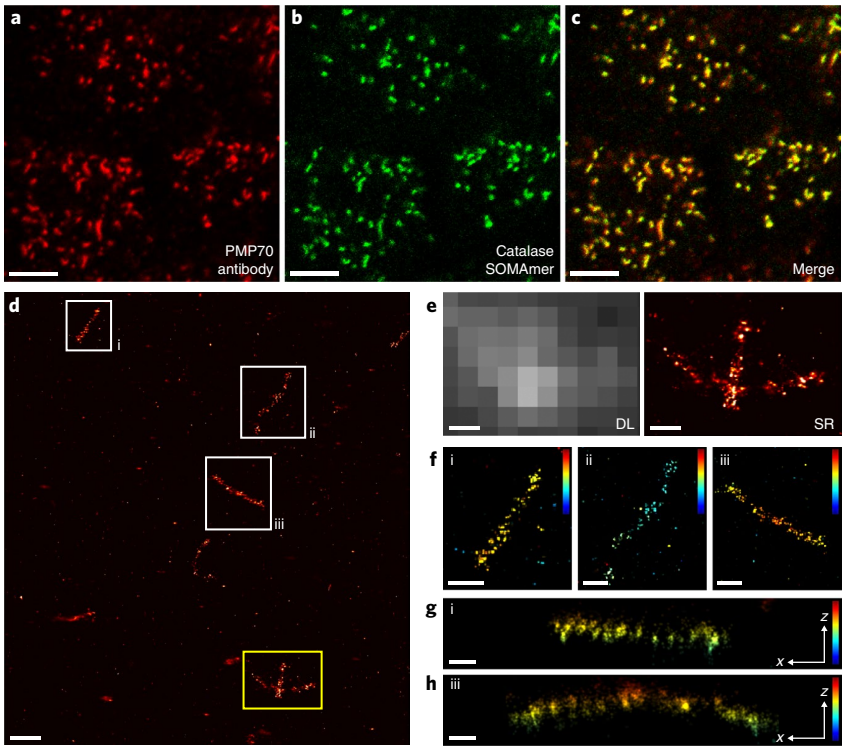

Fig. 3 | Intracellular labeling and DNA-PAINT imaging of catalase proteins in peroxisomes with SOMAmers. a, Confocal micrograph of PMP70 proteins in the peroxisomal membrane of A431 cells labeled with primary and Alexa Fluor 647–conjugated secondary antibodies. **b**, Confocal micrograph of catalase proteins labeled with fluorescein-conjugated SOMAmers. **c**, Overlay of PMP70 antibody and catalase SOMAmer (SL1071) signal, demonstrating colocalization of both proteins to peroxisomes. **d**, DNA-PAINT super-resolution image of catalase molecules in peroxisomes, obtained with docking-strand-extended SOMAmers. **e**, Comparison of diffraction-limited (DL; left) and super-resolved (SR; right) zoomed-in views of the area outlined by the yellow rectangle in **d**, with single catalase molecules in peroxisomes visible in the super-resolved image. **f**, Zoomed-in views of boxed areas i–iii in **d**. 3D localization information is color-coded, and reveals distinct *z* localizations of peroxisomes. **g**, *xz*-projection of catalase molecules in a single peroxisome from area i in **d** and **f**. **h**, *xz*-projection of catalase molecules in a single peroxisome from area iii in **d** and **f**. Scale bars, 5 µm (**a**–**c**), 500 nm (**d**), 200 nm (**e**,**f**), or 100 nm (**g**,**h**). Color scales indicate height: blue to red, −100 nm to 400 nm. Experiments were repeated at least three times, with similar results; representative data are shown.

Methods

Methods, including statements of data availability and any associated accession codes and references, are available at https://doi.org/10.1038/s41592-018-0105-0.

Received: 21 December 2017; Accepted: 12 July 2018;
Published online: 20 August 2018

References

1. Hell, S. W. & Wichmann, J. *Opt. Lett.* **19**, 780–782 (1994).
2. Betzig, E. et al. *Science* **313**, 1642–1645 (2006).
3. Hess, S. T., Girirajan, T. P. & Mason, M. D. *Biophys. J.* **91**, 4258–4272 (2006).
4. Rust, M. J., Bates, M. & Zhuang, X. *Nat. Methods* **3**, 793–795 (2006).
5. Sahl, S. J., Hell, S. W. & Jakobs, S. *Nat. Rev. Mol. Cell Biol.* **18**, 685–701 (2017).
6. Dai, M., Jungmann, R. & Yin, P. *Nat. Nanotechnol.* **11**, 798–807 (2016).
7. Balzarotti, F. et al. *Science* **355**, 606–612 (2017).
8. Schnitzbauer, J., Strauss, M. T., Schlichthaerle, T., Schueder, F. & Jungmann, R. *Nat. Protoc.* **12**, 1198–1228 (2017).
9. Jungmann, R. et al. *Nano Lett.* **10**, 4756–4761 (2010).
10. Ries, J., Kaplan, C., Platonova, E., Eghlidi, H. & Ewers, H. *Nat. Methods* **9**, 582–584 (2012).
11. Opazo, F. et al. *Nat. Methods* **9**, 938–939 (2012).
12. Gomes de Castro, M. A., Höbartner, C. & Opazo, F. *PLoS One* **12**, e0173050 (2017).
13. Gold, L. et al. *PLoS One* **5**, e15004 (2010).
14. Gupta, S. et al. *Appl. Immunohistochem. Mol. Morphol.* **19**, 273–278 (2011).
15. Rohloff, J. C. et al. *Mol. Ther. Nucleic Acids* **3**, e201 (2014).
16. Endesfelder, U. & Heilemann, M. *Nat. Methods* **11**, 235–238 (2014).
17. Culley, S. et al. *Nat. Methods* **15**, 263–266 (2018).
18. Jungmann, R. et al. *Nat. Methods* **13**, 439–442 (2016).
19. Huang, B., Wang, W., Bates, M. & Zhuang, X. *Science* **319**, 810–813 (2008).
20. Jungmann, R. et al. *Nat. Methods* **11**, 313–318 (2014).

Acknowledgements

We thank M. Spitaler and the imaging facility of the MPI of Biochemistry for confocal imaging support, and A. Auer and F. Schueder for super-resolution microscopy support. This research was funded by the German Research Foundation through the Emmy Noether Program (DFG JU 2957/1-1 to R.J.), the European Research Council through an ERC Starting Grant (MolMap; grant agreement number 680241 to R.J.), the Allen Distinguished Investigator Program through The Paul G. Allen Frontiers Group (J.E. and R.J.), the Max Planck Society (R.J.), the Max Planck Foundation (R.J.), the QBM graduate school (S.S.), and the IMPRS-LS graduate school (M.T.S.). We thank our SomaLogic colleagues in discovery, process chemistry, and analytical chemistry for their support of this project. SOMAmer reagent is a registered trademark of SomaLogic, Inc.

Author contributions

S.S. designed and performed experiments and analyzed the data. P.C.N. designed experiments. M.T.S. analyzed data and wrote software. V.J.S. and J.E. created the Nup107–GFP cell line. J.D.C., S.G., and N.J. contributed to generation of SOMAmer reagents and provided guidance on their use. R.J. conceived of and supervised the study and analyzed the data. S.S., P.C.N., and R.J. wrote the manuscript, and all authors reviewed and approved the manuscript.

Competing interests

J.D.C., S.G., and N.J. are SomaLogic, Inc., employees and stakeholders.

Additional information

Supplementary information is available for this paper at https://doi.org/10.1038/s41592-018-0105-0.

Reprints and permissions information is available at www.nature.com/reprints.

Correspondence and requests for materials should be addressed to R.J.

Publisher's note: Springer Nature remains neutral with regard to jurisdictional claims in published maps and institutional affiliations.

Methods

Materials. Cy3b-modified and thiolated DNA oligonucleotides were purchased from MWG Eurofins. 1 M Tris, pH 8.0 (AM9856); 0.5 M EDTA, pH 8.0 (AM9261); 1 M magnesium (AM9530G); 5 M sodium chloride (AM9759); ultrapure water (10977-035); sheared salmon sperm DNA (10 mg/ml; AM9680); DMEM with high glucose, GlutaMAX, and sodium pyruvate (31966-021); McCoy's 5A medium (26600-023); FBS (10500-064); 1× PBS, pH 7.2 (20012-019); 10× PBS, pH 7.4 (70011036); 0.05% trypsin–EDTA (25300-054); Leibovitz's L-15 medium (11415064); and 16% (w/v) formaldehyde solution (28906) were from Thermo Fisher Scientific. Potassium chloride (6781.1), Triton X-100 (6683.1), and EGTA (3054) were ordered from Roth. Sodium hydroxide (31627.290) was purchased from VWR. Tween-20 (P9416-50ML), glycerol (G5516-500ML), methanol (32213-2.5L), protocatechuate 3,4-dioxygenase pseudomonas (PCD; P8279), 3,4-dihydroxybenzoic acid (PCA; 37580-25G-F), (+−)-6-hydroxy-2,5,7,8-tetramethylchromane-2-carboxylic acid (Trolox; 238813-5G), PIPES (5625-37-6), dextran sulfate sodium salt from *Leuconostoc* spp. (6.5–10 kDa; D4911-10G), 0.25% trypsin–EDTA (T4049-100ML), NH_4Cl (254134-25G), BSA (A4503-10G), and human EGF (E9644-.2MG) were from Sigma-Aldrich. Sucrose (57-50-1) was obtained from Merck. A431, A549, and SK-BR-3 cells were purchased from ATCC. The HeLa Kyoto 2xZFN mEGFP–Nup107 cell line was obtained from the Ellenberg lab[21]. Tissue culture treated flasks (353136) were ordered from Falcon. Glutaraldehyde (16220) was obtained from Electron Microscopy Sciences. Eight-well chambered coverslips (0030742036) were purchased from Eppendorf, and glass-bottomed eight-well µ-slides (80827) were ordered from ibidi. 90-nm standard gold nanoparticles (G-90-10) were ordered from Cytodiagnostics. Primary monoclonal anti-EGFR (4267 S) was purchased from Cell Signaling. Secondary polyclonal anti-rabbit antibody conjugated to Alexa Fluor 647 (ab150075) and primary anti-PMP70 (ab211533) were purchased from Abcam. Secondary AffiniPure anti-mouse IgG antibody (115-005-003) was obtained from Jackson ImmunoResearch.

Buffers. The following buffers were used for sample preparation and imaging[8]:

SOMAmer staining buffer: 1× PBS, pH 7.4, 5 mM $MgCl_2$, 0.05% Tween-20, 1% BSA, 1 mM dextran sulfate, 10–100 µM Z-Block, 0.1–0.2 mg/ml sheared salmon sperm DNA
Imaging buffer: 1× PBS, pH 7.4, 500 mM NaCl, pH 8.0, 1× Trolox, 1× PCA, 1× PCD
100× Trolox: 100 mg of Trolox, 430 µl of 100% methanol, 345 µl of 1 M NaOH in 3.2 ml of H_2O
40× PCA: 154 mg of PCA, 10 ml of water, and NaOH mixed and adjusted to pH 9.0
100× PCD: 9.3 mg of PCD and 13.3 ml of buffer (100 mM Tris-HCl, pH 8.0, 50 mM KCl, 1 mM EDTA, 50% glycerol)

SOMAmer reagents. Each SOMAmer construct for SOMAmer design with docking strands is described in Supplementary Table 1.

Protein targets used for systematic evolution of ligands by exponential enrichment (SELEX). Green fluorescent protein (GFP) with a His-tag was purchased from Millipore Sigma (14-392). Catalase purified from human erythrocytes was purchased from Athens Research and Technology (16-05-030000). HSP90 with a His-tag (102036-254) and HSP60 (80059-208) were purchased from VWR. LIMP2/SR-B2 Fc chimera (1966-LM), ErbB2/Her2 Fc chimera, CF (1129-ER), and EGFR Fc chimera, CF (344-ER), were ordered from R&D Systems.

Modified aptamer discovery and synthesis. Aptamers were discovered via the SELEX method as described by Gold et al.[13]. For selections we used modified DNA libraries with a 40N random region containing either 5-(*N*-benzylcarboxamide)-2′-deoxyuridine (BndU) or 5-(*N*-(1-naphthylmethyl)carboxamide)-2′-deoxyuridine (NapdU) in place of dT. Oligonucleotides were synthesized by solid-phase synthesis with modified deoxyuridine-5-carboxamide amidite reagents as described previously[22], using phosphoramidite chemistry[23]. Each modified aptamer was cleaved and deprotected from solid support with 20% diethylamine (Sigma-Aldrich; 471216)–acetonitrile (Honeywell; CS017-56) followed by gaseous methylamine (Sigma-Aldrich; 295531) at 40 °C for 90 min, washed with 90% acetonitrile–water, and eluted with deionized water. Product was purified by HPLC with 100 mM triethylammonium bicarbonate with 5% acetonitrile (A) and 100 mM triethylammonium bicarbonate with 70% acetonitrile (B)[24] and characterized by standard methods for purity (UPLC), identity (LC/MS), quantity (UV spectrophotometry), and activity (solution binding affinity).

Z-block polyanionic competitor. Z-block was designed as a nonspecific, polyanionic competitor for SOMAmer reagent target interactions. This synthetic molecule has the same modified BndU nucleotides[2] incorporated during solid-phase synthesis by phosphoramidite chemistry[3]. After solid-phase synthesis, the product is cleaved and deprotected with t-butylamine:methanol:water (1:1:2) at 37 °C for 24 h and evaporated to dryness[25]. The reconstituted product is purified by HPLC and characterized by standard methods for purity, identity, and quantity.

Equilibrium binding constants (K_d). Equilibrium binding constants of aptamers were measured in solution at 37 °C as described by Gold et al.[13]. Briefly, heat-cooled 5′-^{32}P-radiolabeled DNA SOMAmers (heated to 90 °C for 5 min and cooled to room temperature over the course of 20–30 min) were mixed with different concentrations of target protein in binding buffer (40 mM HEPES, pH 7.5, 102 mM NaCl, 5 mM KCl, 1 mM EDTA, 0.05% Tween-20). SOMAmer–protein complexes were captured with Zorbax beads (Agilent; 899999-777) and quantified with a phosphoimager.

Cell culture. A431 and A549 cells were used for EGFR and catalase imaging. SK-BR-3 cells were used for exchange-PAINT experiments. For GFP–SOMAmer staining, we used a HeLa Kyoto 2xZFN mEGFP–Nup107 cell line. A431, A549, and HeLa cells were grown in high-glucose (4.5 g/L) DMEM supplemented with GlutaMAX, 1 mM sodium pyruvate, and 10% FBS. SK-BR-3 cells were grown in McCoy's 5A medium supplemented with 15% FBS. Cells were seeded into eight-well chambered coverslips and grown to 50–70% confluency.

SOMAmer preparation and folding. Lyophilized SOMAmer reagents were reconstituted in TE buffer (10 mM Tris, 1 mM EDTA, pH 8.0) and stored in 20 µM aliquots at −20 °C. Working aliquots were stored at 4 °C until use. SOMAmer reagents were heat-cooled in PBS at a concentration of 0.2–2 µM and used for labeling on the same day.

GFP–Nup107 SOMAmer staining. Cells were rinsed with PBS and fixed in prewarmed (to 37 °C) 2.4% paraformaldehyde in PBS for 15 min at room temperature. Then the cells were washed twice with PBS and incubated in 0.1 M NH_4Cl for 10 min. Cells were permeabilized with 0.25% Triton X-100 in PBS for 5 min and subsequently blocked with 3% BSA in PBS for 15–30 min. SOMAmer against GFP (100 nM in SOMAmer staining buffer containing 100 µM Z-Block and 1 mM dextran sulfate) was incubated with the cells for 1 h at room temperature. After incubation with the SOMAmers, the cells were washed three times with PBS supplemented with 5 mM $MgCl_2$.

EGFR (ErbB1) SOMAmer staining. Prior to fixation, A431 cells were serum-depleted overnight. Cells were rinsed with PBS and fixed in prewarmed (to 37 °C) 4% paraformaldehyde in cytoskeleton buffer[26] (500 mM NaCl, 50 mM PIPES, 15 mM $MgCl_2$, 5 mM EGTA, and 5 mM sucrose) in PBS for 30 min at room temperature. Free aldehyde groups were quenched using 0.1 M glycine and 3% BSA in PBS for 15 min. The folded SOMAmer targeting EGFR was diluted to 100 nM in SOMAmer staining buffer (1× PBS, 5 mM $MgCl_2$, 1% BSA, 0.05% Tween-20, 50 µM Z-Block, 1 mM dextran sulfate) and incubated with the cells for 1 h at room temperature. After SOMAmer incubation, the cells were washed three times with PBS supplemented with 5 mM $MgCl_2$. Post-fixation was performed with 4% paraformaldehyde and 0.1% glutaraldehyde in PBS with 5 mM $MgCl_2$ for 10 min at room temperature. Afterward, cells were washed three times with PBS and incubated in 3% BSA, 0.1 M glycine, and 5 mM $MgCl_2$ in PBS for 10 min.

EGFR immunostaining. Cells were fixed in the same way as described for EGFR SOMAmer staining. We used a monoclonal antibody targeting intracellular EGFR in blocking buffer (3% BSA, 0.05% Tween-20, 1× PBS) to stain the cells for 90 min at room temperature or overnight at 4 °C. Cells were briefly rinsed with PBS and washed three times with PBS with an incubation time of 5 min for each washing step. Secondary anti-rabbit antibody conjugated to Alexa Fluor 647 was added in blocking buffer (1:200 dilution) for 60 min at room temperature. Cells were briefly rinsed with PBS and washed three times with PBS with an incubation time of 5 min for each washing step.

PMP70 immunostaining and catalase SOMAmer staining. Cells were rinsed with PBS and fixed in prewarmed (to 37 °C) 4% paraformaldehyde in PBS for 15 min at room temperature. Then the cells were washed twice with PBS and permeabilized with 0.25% Triton X-100 in PBS for 10 min. After an additional washing step with PBS, cells were blocked with 3% BSA in PBS for 60 min. Primary anti-PMP70 was incubated in 3% BSA in PBS overnight at 4 °C. Cells were briefly rinsed with PBS and washed three times with PBS with an incubation time of 5 min for each washing step. Secondary anti-mouse antibody conjugated to Alexa Fluor 647 or P1 DNA-PAINT docking site was added in blocking buffer for 60 min at room temperature. Cells were briefly rinsed and washed three times with PBS (5 min incubation time each). Catalase SOMAmer reagent was added in staining buffer supplemented with 1 mM dextran sulfate, 10 µM Z-Block, and 0.2 mg/ml sheared salmon sperm DNA and incubated overnight at 4 °C. After SOMAmer incubation, the cells were washed three times with PBS supplemented with 5 mM $MgCl_2$.

Live-cell staining with EGFR SOMAmers. Cell medium was aspirated and the cells were briefly rinsed in phenol-red-free Leibovitz's L-15 medium. The SOMAmer live-cell labeling solution (100 nM EGFR SOMAmer reagent and 10 µM Z-Block in Leibovitz's L-15 medium) was added and incubated for 10 min at room temperature or 20 min at 4 °C. The cell-staining solution was removed and cells were washed three times with L-15 medium. Finally, cells were fixed for 30 min with 4% paraformaldehyde and 0.1% glutaraldehyde in PBS with 5 mM $MgCl_2$.

After fixation, cells were washed three times with PBS and incubated in 3% BSA and 0.1 M glycine in PBS for 10 min.

Confocal imaging. The confocal imaging was carried out on a Zeiss (Jena, Germany) LSM780 confocal laser-scanning microscope equipped with a Zeiss Plan-APO 63×/1.46-NA (numerical aperture) oil-immersion objective. GFP, Cy3, and Alexa Fluor 647 excitation was performed with 488-nm, 561-nm, and 633-nm diode lasers, respectively. The pinhole size was adjusted to 1 AU (Airy unit). Laser power was used at 4–10%, and detector gain was set to 700–900. Imaging conditions were kept constant for each experiment.

DNA-PAINT imaging. Before imaging, 90-nm gold nanoparticle fiducial markers were added and incubated for 5 min (diluted 1:5 in PBS + 5 mM $MgCl_2$). After rinsing with PBS with 5 mM $MgCl_2$, imaging buffer containing DNA-PAINT imaging strands was added. DNA-PAINT imaging was carried out on an inverted Nikon Eclipse Ti microscope (Nikon Instruments) with the Perfect Focus System, operated with an objective-type TIRF configuration with an oil-immersion objective (CFI Apo TIRF 100×/1.49-NA). Samples were excited with a 561-nm laser (200 mW nominal; Coherent Sapphire). The laser beam was passed through a cleanup filter (ZET561/10; Chroma Technology) and coupled into the microscope objective with a beam splitter (ZT561rdc; Chroma Technology). Fluorescence light was spectrally filtered with two emission filters (ET600/50 m and ET575lp; Chroma Technology) and imaged on an sCMOS (scientific complementary metal-oxide semiconductor) camera (Zyla 4.2; Andor Technologies). Imaging was performed without additional magnification in the detection path and 2 × 2 camera binning, resulting in a pixel size of 130 nm.

DNA-PAINT single-particle tracking. Cells were stained with 100 nM EGFR SOMAmer in L-15 medium and 10 µM Z-Block. After labeling, cells were washed two times with L-15. Imaging was performed with a 1 nM P1-5′ Cy3b imager. EM gain was set to 300, laser power density was set to ~0.08 kW/cm², and a 50-ms integration was used. Particle traces were analyzed with ImageTracker from the Mosaic group in ImageJ[27]. Detection settings were as follows: radius, 4; percentile, 0.8; cutoff radius, 0.0001; displacement, 1.5; link range, 2.

DNA-PAINT imaging conditions. For imaging, the following DNA-PAINT imagers were used: P1-5′-Cy3b, 5′-Cy3b-TAGATGTAT-3′; P1-3′-Cy3b, 5′-CTAGATGTAT-Cy3b-3′; P3-Cy3b, 5′-TAATGAAGA-Cy3b-3′; P5-Cy3b, 5′-CATACATTGA-Cy3b-3′; P6-Cy3b, 5′-CTTTACCTAA-Cy3b-3′. All DNA-PAINT measurements were performed in imaging buffer (1× PBS, pH 8.0, 500 mM NaCl, 1× Trolox, 1× PCA, 1× PCD).

Figure 1d–g. Imaging was performed with a 150-ms integration time for 40,000 frames with a P1-5′-Cy3b imager strand concentration of 1 nM. Laser power was set to ~1.8 kW/cm² before the back focal plane (BFP) of the objective.

Figure 2c–e. Imaging was performed with a 300-ms integration time for 60,000 frames with a P1-5′-Cy3b imager strand concentration of 0.8 nM. Laser power was set to ~0.3 kW/cm² before the BFP of the objective.

Figure 3d–h. Imaging was performed with a 250-ms integration time for 20,000 frames with a P5-Cy3b imager strand concentration of 0.6 nM. Laser power was set to ~0.8 kW/cm² before the BFP of objective

Image analysis. Super-resolution images were reconstructed with the Picasso software package as described[8,28].

Reporting Summary. Further information on research design is available in the Nature Research Reporting Summary linked to this article.

Data availability. All raw data are available upon request from the authors.

References

21. Otsuka, S. et al. *eLife* **5**, e19071 (2016).
22. Gupta, S. et al. *J. Biol. Chem.* **289**, 8706–8719 (2014).
23. Beaucage, S. L. & Caruthers, M. H. *Tetrahedr. Lett.* **22**, 1859–1862 (1981).
24. Carlson, M., Carter, J. D. & Rohloff, J. *Green Chemistry Letters and Reviews* **8**, 37–39 (2015).
25. Mullah, B., Livak, K., Andrus, A. & Kenney, P. *Nucleic Acids Res.* **26**, 1026–1031 (1998).
26. Whelan, D. R. & Bell, T. D. *Sci. Rep.* **5**, 7924 (2015).
27. Sbalzarini, I. F. & Koumoutsakos, P. *J. Struct. Biol.* **151**, 182–195 (2005).
28. Schueder, F. et al. *Nat. Commun.* **8**, 2090 (2017).

nature research

Corresponding author(s): Ralf Jungmann

Reporting Summary

Nature Research wishes to improve the reproducibility of the work that we publish. This form provides structure for consistency and transparency in reporting. For further information on Nature Research policies, see Authors & Referees and the Editorial Policy Checklist.

Statistical parameters

When statistical analyses are reported, confirm that the following items are present in the relevant location (e.g. figure legend, table legend, main text, or Methods section).

n/a	Confirmed	
☐	☒	The exact sample size (*n*) for each experimental group/condition, given as a discrete number and unit of measurement
☐	☒	An indication of whether measurements were taken from distinct samples or whether the same sample was measured repeatedly
☒	☐	The statistical test(s) used AND whether they are one- or two-sided *Only common tests should be described solely by name; describe more complex techniques in the Methods section.*
☒	☐	A description of all covariates tested
☒	☐	A description of any assumptions or corrections, such as tests of normality and adjustment for multiple comparisons
☐	☒	A full description of the statistics including central tendency (e.g. means) or other basic estimates (e.g. regression coefficient) AND variation (e.g. standard deviation) or associated estimates of uncertainty (e.g. confidence intervals)
☒	☐	For null hypothesis testing, the test statistic (e.g. *F*, *t*, *r*) with confidence intervals, effect sizes, degrees of freedom and *P* value noted *Give P values as exact values whenever suitable.*
☒	☐	For Bayesian analysis, information on the choice of priors and Markov chain Monte Carlo settings
☒	☐	For hierarchical and complex designs, identification of the appropriate level for tests and full reporting of outcomes
☒	☐	Estimates of effect sizes (e.g. Cohen's *d*, Pearson's *r*), indicating how they were calculated
☐	☒	Clearly defined error bars *State explicitly what error bars represent (e.g. SD, SE, CI)*

Our web collection on statistics for biologists may be useful.

Software and code

Policy information about availability of computer code

Data collection	Data was acquired using software supplied by instrument manufacturer (ZEISS ZEN 2011) or the open source software µmanager (Version 1.4): Journal of Biological Methods 2014 1(2):e11 doi:10.14440/jbm.2014.36
Data analysis	Open source software Fiji (distribution of ImageJ) was used to process confocal imaging data, it was described in the following publication: Nature methods 9(7): 676-682, PMID 22743772, doi:10.1038/nmeth.2019. Custom analysis software Picasso was used to process raw super-resolution data. The software is open source and was described in detail in the following publication: Nature Protocols volume 12, pages 1198–1228 (2017) doi:10.1038/nprot.2017.024.

For manuscripts utilizing custom algorithms or software that are central to the research but not yet described in published literature, software must be made available to editors/reviewers upon request. We strongly encourage code deposition in a community repository (e.g. GitHub). See the Nature Research guidelines for submitting code & software for further information.

Data

Policy information about availability of data

All manuscripts must include a data availability statement. This statement should provide the following information, where applicable:

- Accession codes, unique identifiers, or web links for publicly available datasets
- A list of figures that have associated raw data
- A description of any restrictions on data availability

All raw data are available upon request from the authors

Field-specific reporting

Please select the best fit for your research. If you are not sure, read the appropriate sections before making your selection.

☒ Life sciences ☐ Behavioural & social sciences

For a reference copy of the document with all sections, see nature.com/authors/policies/ReportingSummary-flat.pdf

Life sciences

Study design

All studies must disclose on these points even when the disclosure is negative.

Sample size	Localization precision for EGFR imaging experiments were calculated from around 30,000 labeled proteins.
Data exclusions	No data were excluded from analysis
Replication	All experiments were reliably reproduced
Randomization	No results that require randomization are presented in this study
Blinding	n/a since no allocation into groups was performed

Materials & experimental systems

Policy information about availability of materials

n/a	Involved in the study
☐	☒ Unique materials
☐	☒ Antibodies
☐	☒ Eukaryotic cell lines
☒	☐ Research animals
☒	☐ Human research participants

Unique materials

Obtaining unique materials	All unique materials are readily available from the authors or from standard commercial sources (SomaLogic)

Antibodies

Antibodies used	Primary monoclonal Anti-EGFR antibody: Cell Signaling, cat: 4267S, clone D38B1, Lot: 11, dilution 1:200 Primary antibody against extracellular region of EGFR: MA5-13319, clone 119.12, Lot: TD2556544B, dilution 1:50 Primary anti-PMP70 antibody: Abcam, ab211533, clone CL2524, dilution 1:200 Secondary polyclonal anti-rabbit antibody conjugated to Alexa Fluor 647: Abcam cat: ab150075, dilution 1:200 Secondary polyclonal AffiniPure Anti-Mouse IgG antibody: Jackson ImmunoResearch cat: 115-005-003
Validation	All antibodies were validated for IF and human species reactivity by the manufacturer according to their websites.

Eukaryotic cell lines

Policy information about cell lines

Cell line source(s)	A431, A549, and SK-BR-3 cells were purchased from ATCC. mEGFP-Nup107 HeLa Kyoto was obtained from the Ellenberg lab (Reference Otsuka, S. et al. Elife 5 (2016))

Authentication	Cell lines were not authenticated
Mycoplasma contamination	All cell lines were tested negative for mycoplasma contamination
Commonly misidentified lines (See ICLAC register)	No commonly misidentified cell lines were used

Method-specific reporting

n/a	Involved in the study
☒	☐ ChIP-seq
☒	☐ Flow cytometry
☒	☐ Magnetic resonance imaging

nature methods

SUPPLEMENTARY INFORMATION

https://doi.org/10.1038/s41592-018-0105-0

In the format provided by the authors and unedited.

Modified aptamers enable quantitative sub-10-nm cellular DNA-PAINT imaging

Sebastian Strauss[1,2], Philipp C. Nickels[1,2], Maximilian T. Strauss[1,2], Vilma Jimenez Sabinina[3], Jan Ellenberg[3], Jeffrey D. Carter[4], Shashi Gupta[4], Nebojsa Janjic[4] and Ralf Jungmann[1,2]*

[1]Department of Physics and Center for Nanoscience, Ludwig Maximilian University, Munich, Germany. [2]Max Planck Institute of Biochemistry, Martinsried, Germany. [3]Cell Biology and Biophysics Unit, European Molecular Biology Laboratory (EMBL), Heidelberg, Germany. [4]SomaLogic, Inc., Boulder, CO, USA. *e-mail: jungmann@biochem.mpg.de

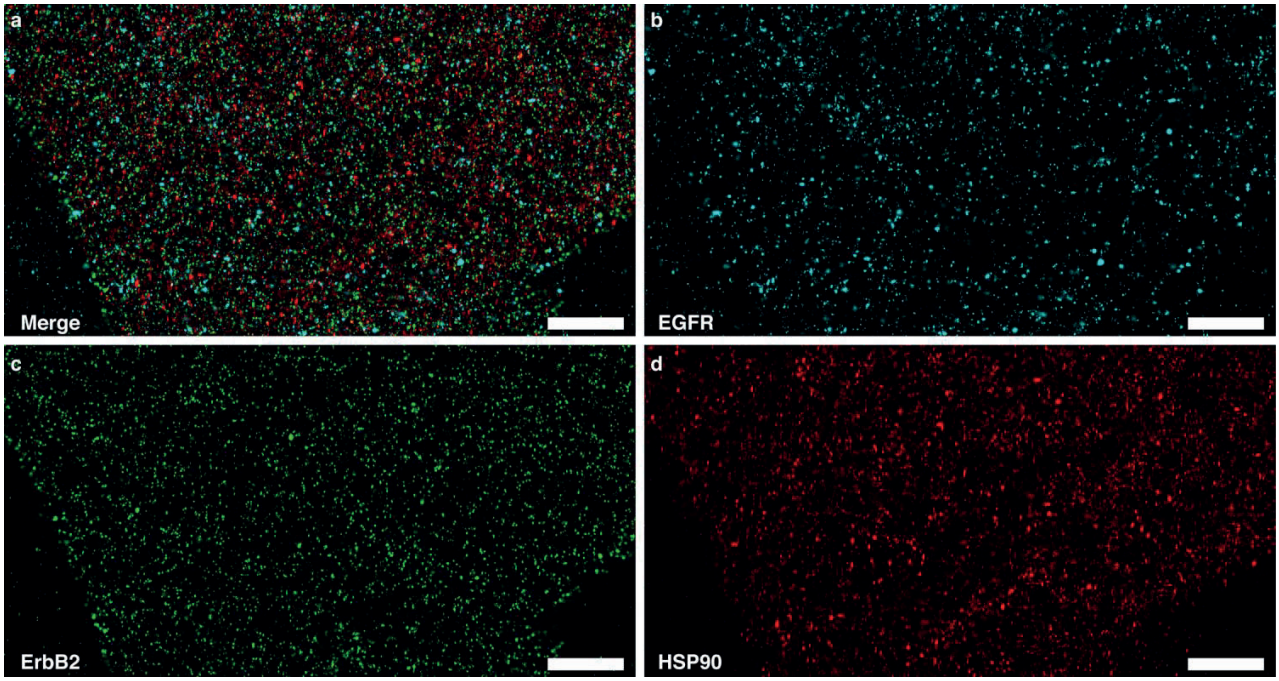

Supplementary Figure 1

Three-target Exchange-PAINT with SOMAmers in SK-BR-3 cells.

(**a**) Simultaneous labeling followed by sequential imaging using SOMAmers against EGFR (cyan), ErbB2 (green), and HSP90 (red). Merged image, all targets were acquired using Cy3b-labeled imager strands. (**b**) EGFR channel only. (**c**) ErbB2 channel only. (**d**) HSP90 channel only. Scale bars: 500 nm.

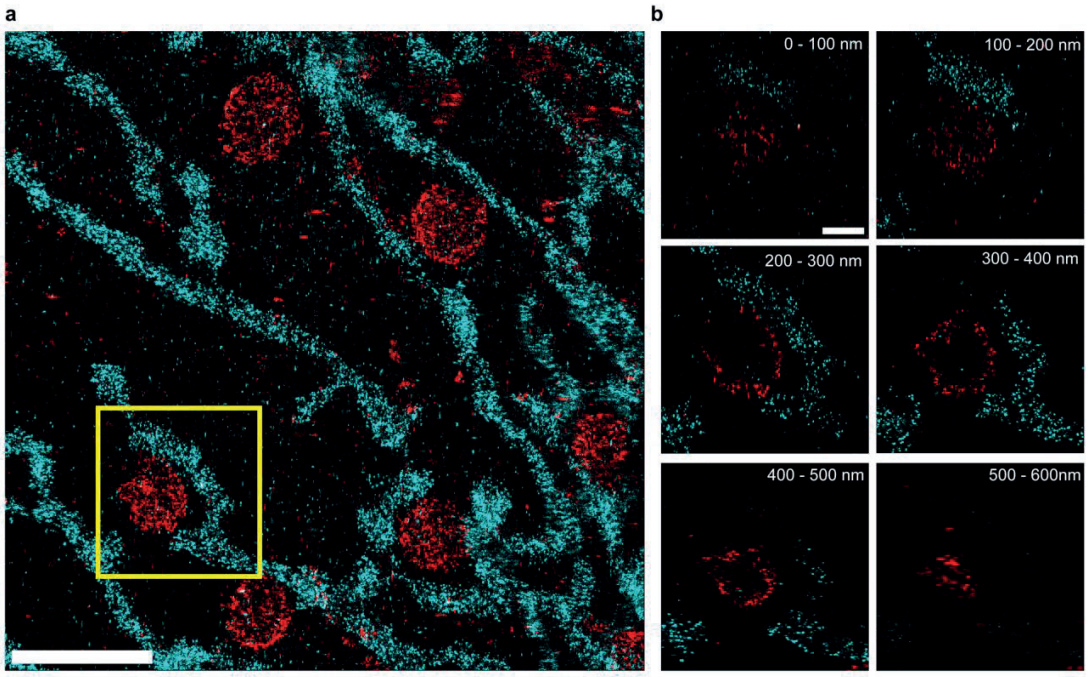

Supplementary Figure 2

Two-target 3D Exchange-PAINT with SOMAmers in SK-BR-3 cells.

(**a**) Simultaneous labeling followed by sequential imaging using SOMAmers against HSP60 (cyan) and LIMP-2 (red). All targets were acquired using Cy3b-labeled imager strands. (**b**) 100-nm z-slices of highlighted area in **a**. Scale bars: 2 µm (**a**), 500 nm (**b**).

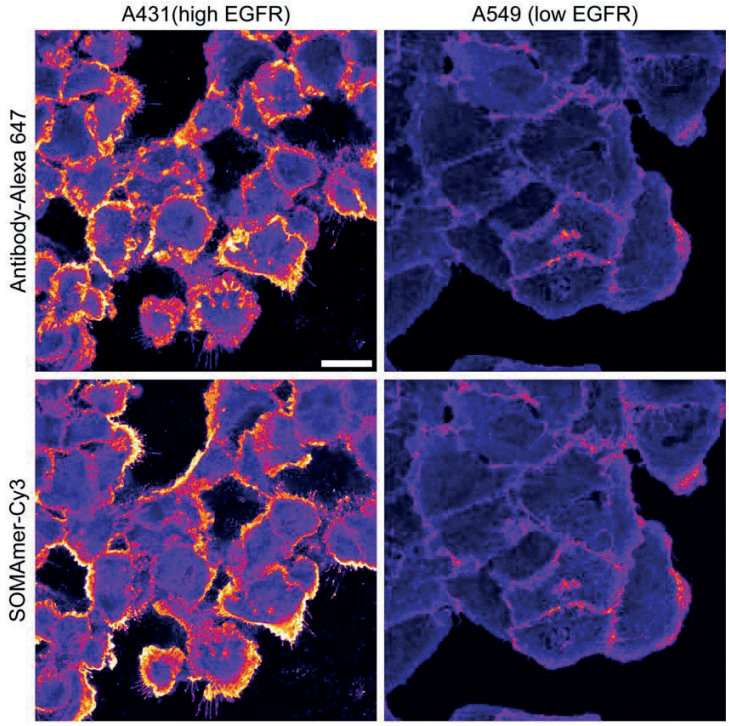

Supplementary Figure 3

Different EGFR staining intensities of A431 and A549 cells.

First, we stained the intracellular EGFR domain with primary and secondary antibodies. Next, the extracellular EGFR was stained with the Cy3 conjugated SOMAmer reagent. Confocal images were recorded at the basal membrane of the cells. Staining intensities of both antibody and SOMAmer correlated with the expression level of EGFR of A431 cells (high) and A549 cells (low), demonstrating the specific staining of EGFR. Scale bar: 20 μm.

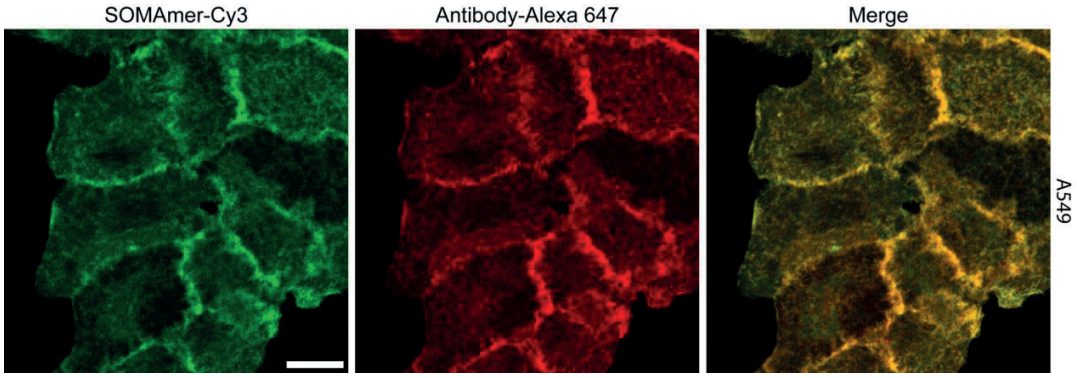

Supplementary Figure 4

EGFR SOMAmer and antibody costaining.

Z-Projections of a 5 µm thick confocal Z-Stack (10 slices in total, 0.5 µm step size per slice) through several A549 cells. **Left:** SOMAmer staining of EGFR. **Middle:** Conventional antibody staining of EGFR. **Right:** SOMAmer and antibody signal merged. The high degree of co-localization shows the specificity of the SOMAmer to EGFR. Scale bar: 15 µm.

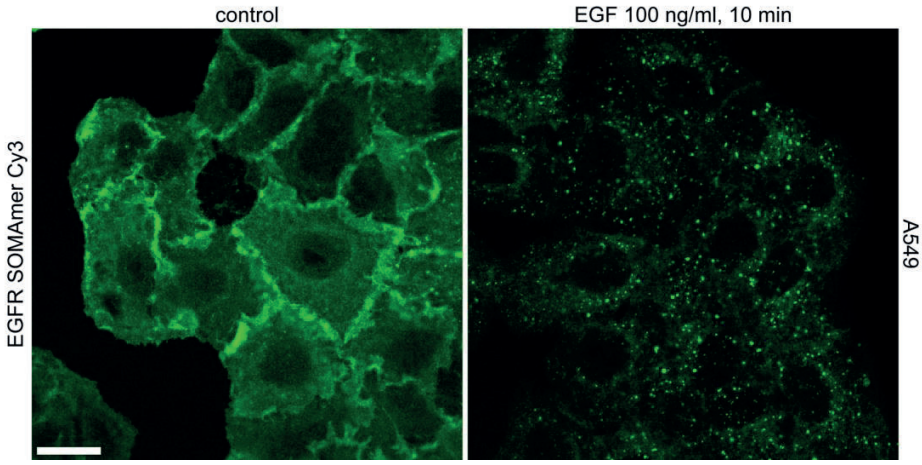

Supplementary Figure 5

EGFR SOMAmer staining before and after EGF stimulation.

Left: Untreated, serum-starved A549 cells showed a uniform EGFR staining in the plasma membrane. **Right:** After EGF stimulation of the A549 cells, distinct vesicles and highly reduced signal from the plasma membrane was observed. Scale bar: 20 µm.

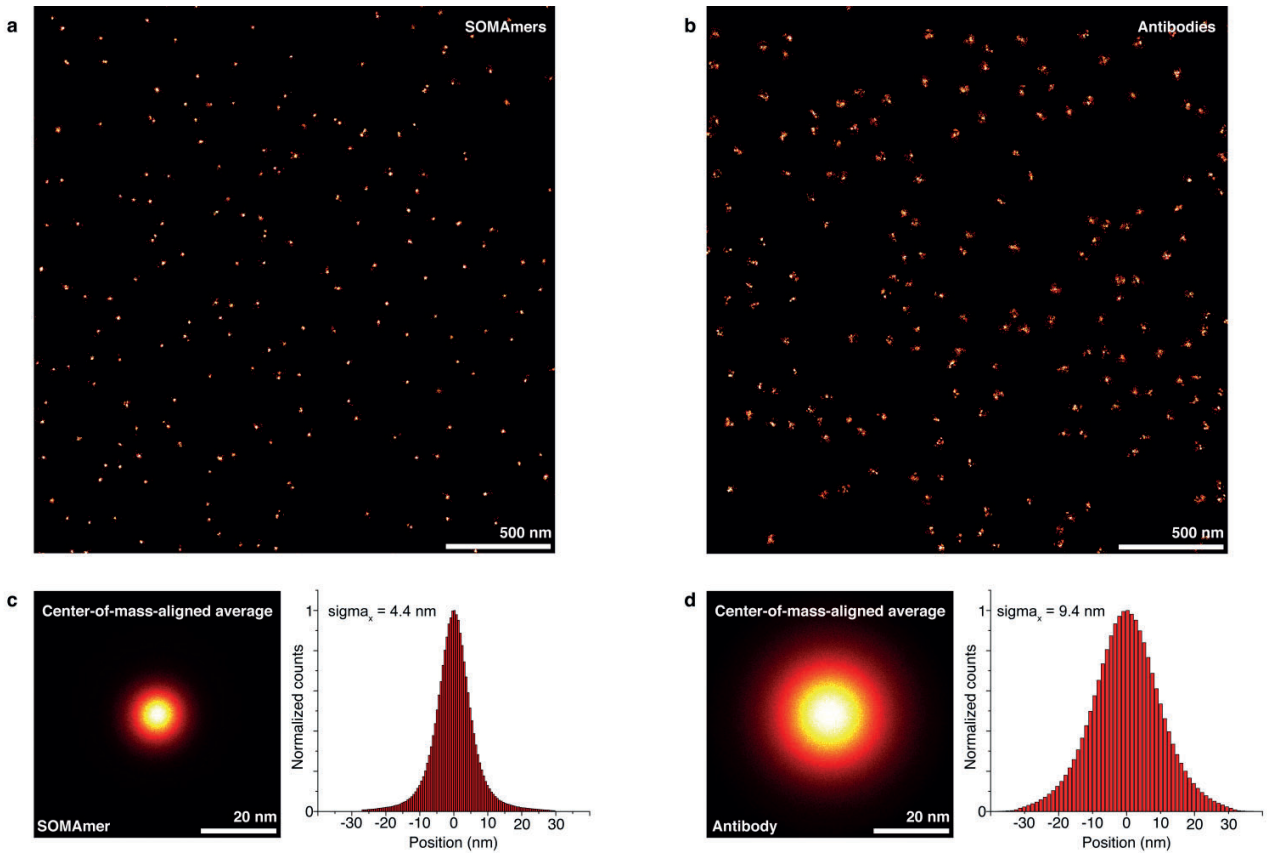

Supplementary Figure 6

EGFR SOMAmer versus antibody linkage error comparison.

(**a**) DNA-PAINT overview image of SOMAmer-stained EGFR proteins. (**b**) DNA-PAINT overview image of primary- and DNA-conjugated-secondary-stained EGFR proteins. (**c**) ~20,000 single receptor molecules labeled using SOMAmers aligned by their center of mass (left). 1D histogram of localizations yields a combined labeling and imaging precision of 4.4 nm (right). (**d**) ~30,000 single receptor molecules labeled using antibodies aligned by their center of mass (left). 1D histogram of localizations yields a combined labeling and imaging precision of 9.4 nm. The difference between SOMAmer- and antibody-based labeling stems almost exclusively from the increased linkage error of the primary/secondary antibody sandwich, as we localize single molecules in both experiments with ~4 nm precision. This demonstrates that SOMAmer labels in this case are not the precision-limiting factor when imaging single EGFR protein molecules, while antibody labeling broadens the true protein localization roughly two-fold.

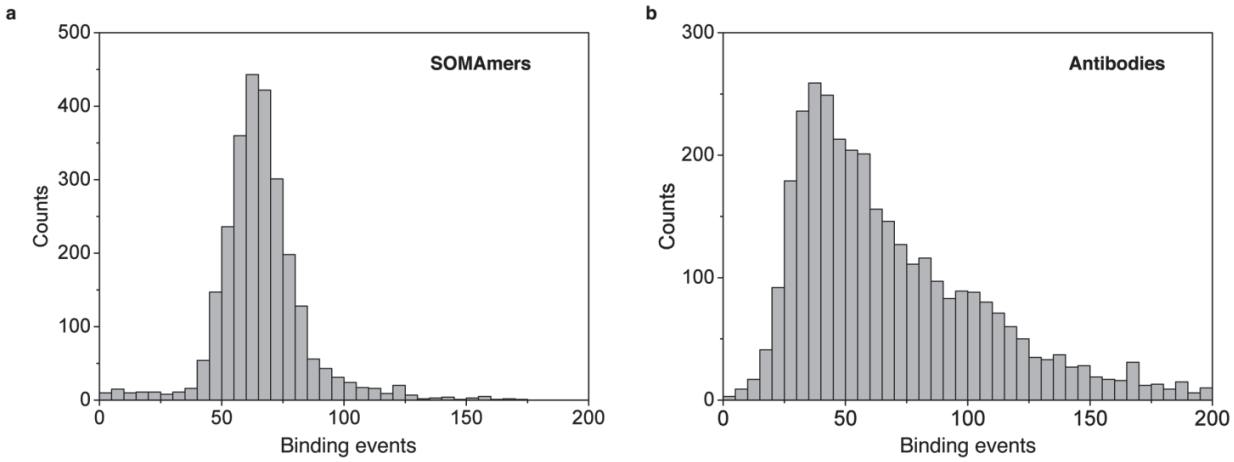

Supplementary Figure 7

EGFR SOMAmer versus antibody quantitative labeling comparison.

(**a**) qPAINT analysis of single EGFR proteins labeled with SOMAmer reagents (n = 2670) yields a unimodal distribution of binding events, confirming quantitative 1:1 labeling of EGFR proteins. (**b**) qPAINT analysis of single EGFR proteins (n = 3406) labeled with antibody reagents yields a multimodal distribution of binding events, confirming non-quantitative labeling of EGFR proteins.

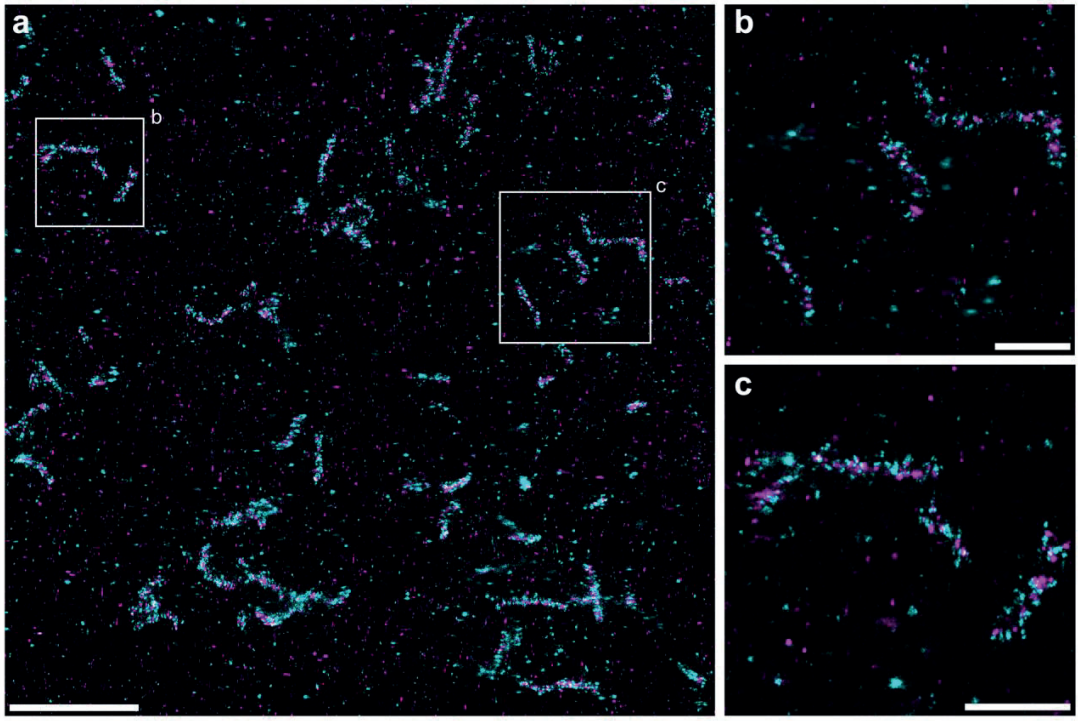

Supplementary Figure 8

3D Exchange-PAINT imaging of PMP70 and catalase in A431 cells.

(**a**) Exchange PAINT image of PMP70 (cyan) labeled with primary and secondary antibodies and catalase (magenta) targeted using a SOMAmer reagent. (**b, c**) Zoom-ins into regions highlighted in (a). Exchange-PAINT imaging shows peroxisomal membrane protein PMP70 surrounding catalase which is located inside peroxisomes Scale bars: 2 µm (**a**), 500 nm (**b-c**).

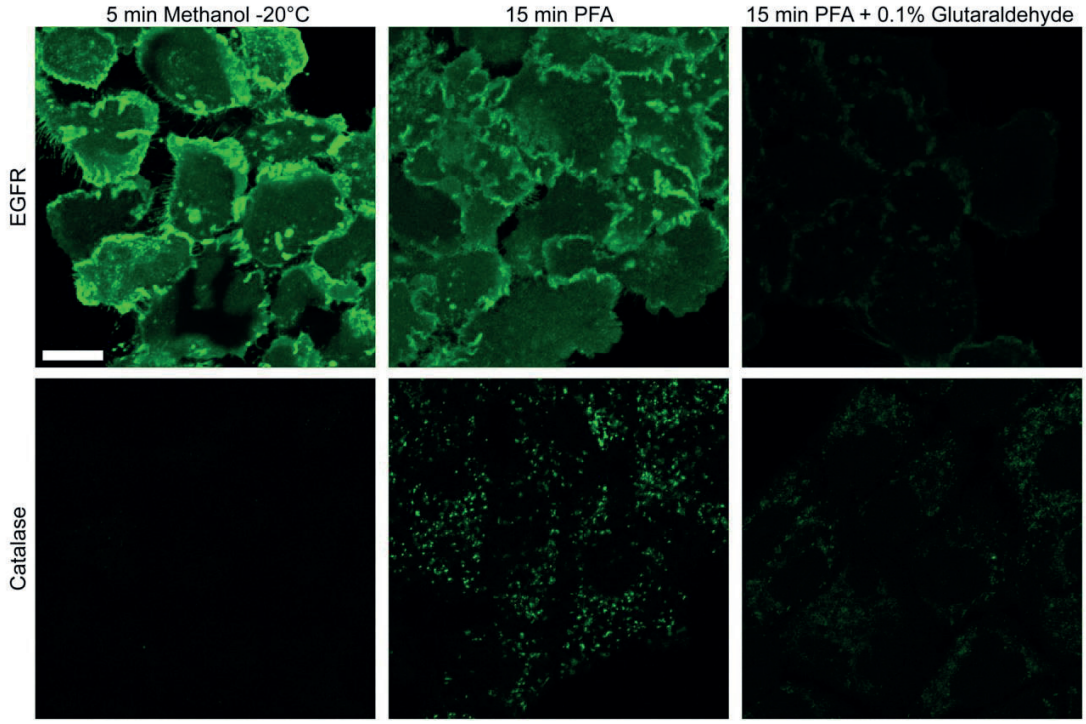

Supplementary Figure 9

Comparison of different fixation conditions for SOMAmer staining in A431 cells.

Three different fixation conditions were tested for EGFR and catalase binding SOMAmer reagents. Fixation protocols significantly affect the staining intensity. Chemical fixation with only paraformaldehyde shows positive staining of both targets whereas addition of glutaraldehyde significantly decreased the signal. Methanol fixation resulted in high SOMAmer staining intensity for EGFR, but no signal could be observed for catalase. Scale bar: 15 µm.

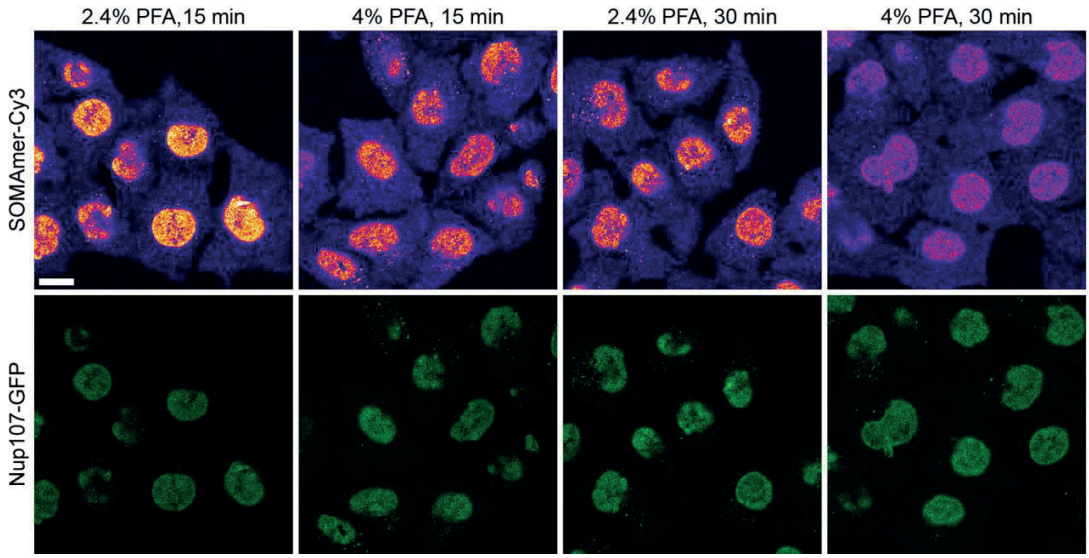

Supplementary Figure 10

Mild fixation conditions favor SOMAmer binding to GFP.

Four different paraformaldehyde (PFA) concentrations and incubation times were evaluated for GFP SOMAmer staining intensity on HeLa Kyoto 2xZFN mEGFP–Nup107 cells. We saw increased SOMAmer-Cy3 signal (top row) for short incubation time and low PFA concentration. Unchanged signal from GFP (bottom row) shows preservation of the Nup107 protein for all tested fixation conditions. Scale bar: 15 µm.

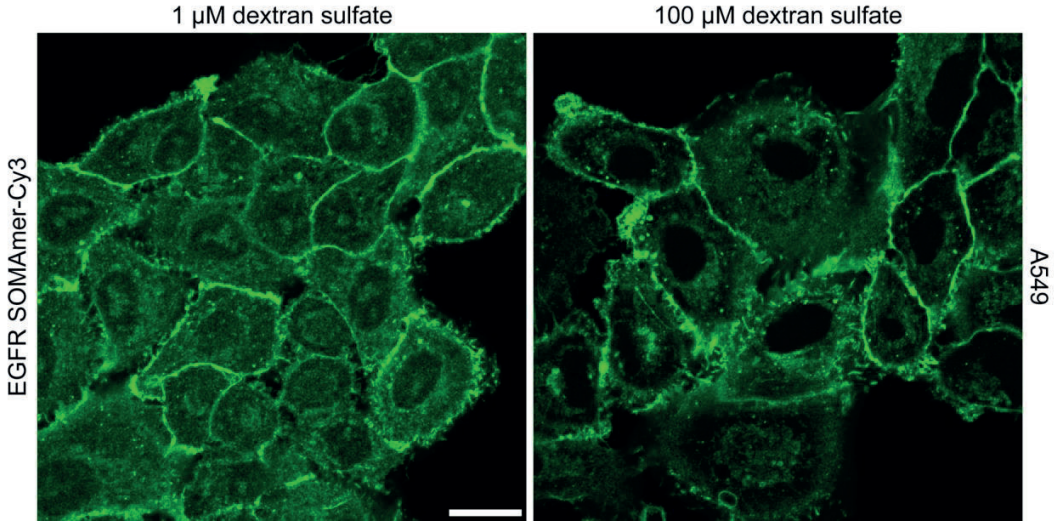

Supplementary Figure 11

Addition of low-molecular-weight dextran sulfate blocks unspecific nuclear SOMAmer binding.

Fixed A549 cells were incubated with 100 nM of EGFR SOMAmer in SOMAmer staining buffer containing 100 µM Z-Block and either 1 µM (left) or 100 µM (right) dextran sulfate. The increase of dextran sulfate concentration led to a drastic decrease of signal in the nucleus. Scale bar: 20 µm.

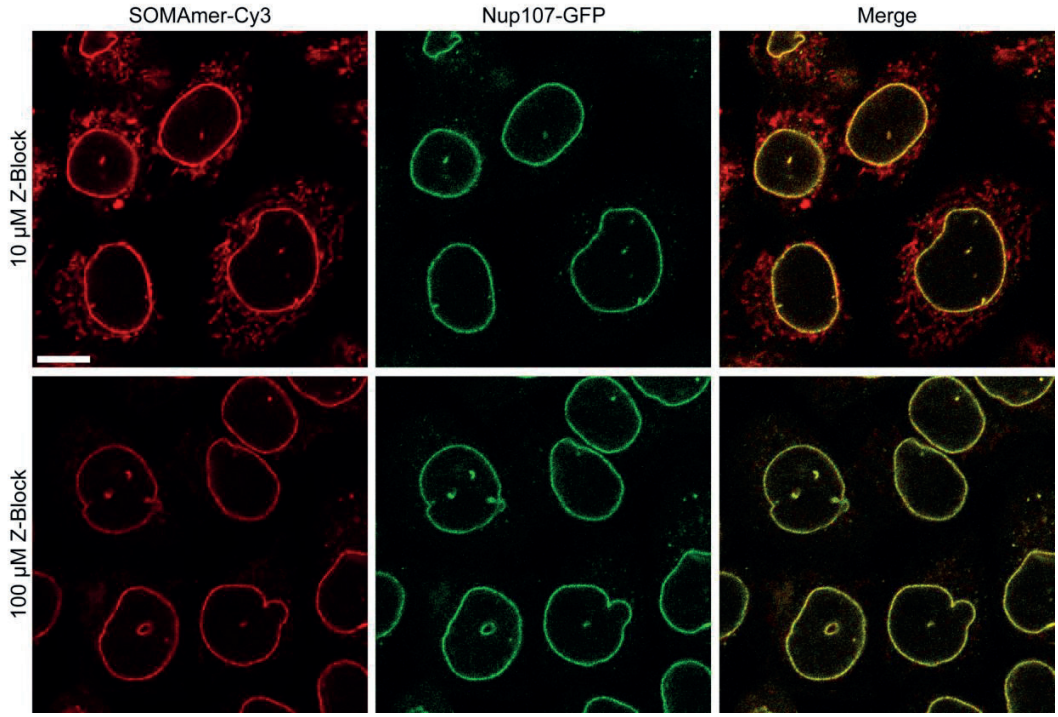

Supplementary Figure 12

Addition of Z-Block quenches unspecific binding of SOMAmer to cellular organelles.

Fixed HeLa Kyoto 2xZFN mEGFP–Nup107 cells were incubated with 100 nM of EGFR SOMAmer in SOMAmer staining buffer containing 1 mM dextran sulfate and either 10 µM (top) or 100 µM (bottom) Z-Block. The increase of Z-Block concentration led to a drastic decrease of signal from cellular organelles. Scale bar: 10 µm.

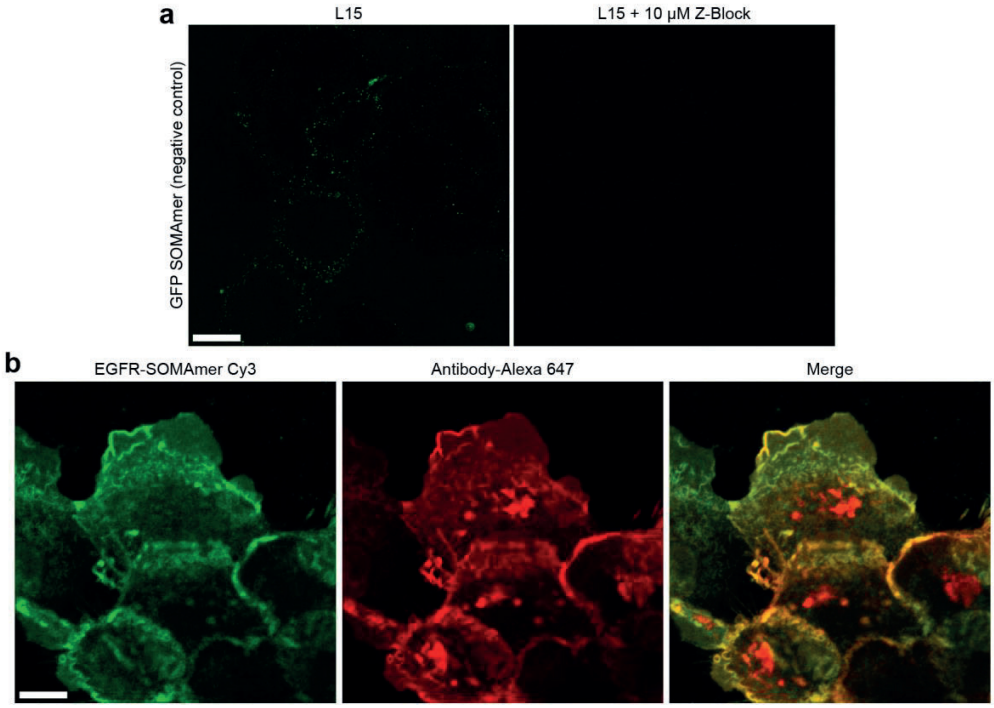

Supplementary Figure 13

EGFR SOMAmer can be used to stain living cells with little unspecific binding.

(**a**) Staining of A431 cells with the GFP SOMAmer as a negative control led to only very little unspecific signal (left), which could be effectively quenched via the addition of 10 µM Z-Block (right). (**b**) SOMAmer staining of EGFR in living A431 cells (left) in comparison to conventional antibody staining (middle). The high degree of colocalization in the merged image (right) demonstrates the specificity of the SOMAmer staining on living cells. Scale bars: 20 µm (**a**), 10 µm (**b**).

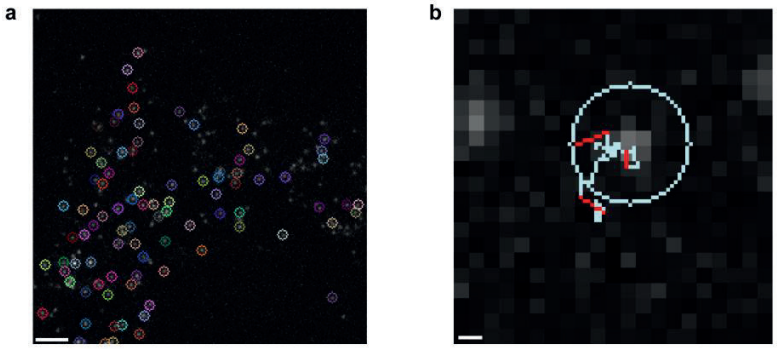

Supplementary Figure 14

Live-cell DNA-PAINT single particle trajectories.

(**a**) Exemplary frame from live-cell DNA-PAINT using EGFR-SOMAmer (Supplementary Movie 1) with spots detected for particle tracking. (**b**) Exemplary single-particle-trajectory of a DNA-PAINT imager targeting a diffusing SOMAmer-labeled EGFR protein (trajectory length ~2 s). Scale bars: 5 µm (**a**), 1 µm (**b**).

Supplementary Tables

Supplementary Table 1 | SOMAmer reagents

SOMAmer reagent	Target	Design/Modifications	Base Count	MW (kDa)	K_d (nM)
Cyanine-3-P1-SL1070	GFP	Cy3-5'-ATACATCTA-TT-SOMAmer-3'-inverted-dT	50	21.0	0.2
Cyanine-3-P1-SL1069	EGFR (ERBB1)	Cy3-5'-ATACATCTA-TT-SOMAmer-3'-inverted-dT	50	21.6	1.6
P1-SL1069	EGFR (ERBB1)	5'-ATACATCTA-TT-SOMAmer-3'-inverted-dT	50	21.1	1.4
Fl-SL1071-P5	Catalase	Fluorescein-5'-SOMAmer-TT-TCAATGTAT-3'	50	20.5	0.1
Fl-SL1072-P3	LIMP2	Fluorescein-5'-SOMAmer-TT-TCTTCATTA-3'	50	20.8	40
P1- SL1073	HSP60	5'-ATACATCTA-TT-SOMAmer-3'-inverted-dT	74	28.4	3
Fl- SL1074-P6	HSP90a/b	Fluorescein-5'-SOMAmer-TT-TTAGGTAAA-3'	50	21.0	2
Fl-SL1075-P3	ErbB2	Fluorescein-5'-SOMAmer-TT-TCTTCATTA-3'	50	17.4	10

Supplementary Table 2 | Tested SOMAmer reagents for PFA and methanol fixation protocol

Target	SOMAmer ID	PFA fixation	Methanol fixation
EGFR	P1-SL1069	+	+
EGFR	Cyanine-3-P1-SL1069	+	+
ErbB2	Fl-SL1075-P3	+	+
ErbB2	FI-SL1081-P3	-	-
ErbB2	SL1082-P3	+	+
HSP90a/b	Fl_SL1074-P6	+	+
LIMP2	Fl-SL1072-P3	+	-
HSP60	P1-SL1073	Low signal	+
HSP60	Cyanine-3-P1-SL1076	Low signal	+
Catalase	Fl-SL1071-P5	+	-
Calreticulin	Fl-SL1077-P6	-	-
LaminB	Fl-SL1078-P3	Low signal	Not tested
GTP-binding nuclear protein Ran	Fl-SL1079-P5	-	-
DnaJ homolog TIM14	Fl-SL1080-P3	-	-
GFP	Cyanine-3-P1-SL1070	+	Not tested

Supplementary Notes

Supplementary Note 1: Use of polyanionic competitors during staining

The addition of competitors during the SOMAmer staining reaction can help to reduce non-specific binding and thus improve the signal-to-noise ratio. Although SOMAmers typically have very high, antibody-like affinities to their targets, cells contain many proteins with a modest nonspecific affinity towards the SOMAmers, such as highly abundant plasma proteins that can bind DNA. Another source of non-specific SOMAmer binding is electrostatic attraction of the polyanionic aptamers to positively charged regions of some proteins, such as histones in the nucleus. Here, we used two different competitors simultaneously: The first is low molecular weight dextran sulfate (6.5–10 kDa), typically used during SOMAmer selection as kinetic challenger, which has been shown to reduce nonspecific binding in cell staining[1]. High concentrations of dextran sulfate drastically decreased off-target binding of the SOMAmers in the nucleus (**Supplementary Figure 11**). The second competitor we used is a DNA-based polyanionic competitor named Z-Block (SomaLogic). Z-Block contains the modified nucleotides (Bn-dU) as some of the SOMAmers (30-mer, [5'-AC[Bn-dU]$_2$]$_7$AC-3']) and strongly reduces intracellular off-target interactions of the SOMAmers. An increase in the Z-Block concentration led to a highly improved signal-to-noise level (**Supplementary Figure 12**). The optimum concentration of competitors was evaluated for every SOMAmer construct individually. We found that a molar excess of 1,000 times for Z-Block and 10,000 times for dextran sulfate are a good starting point to reduce unspecific binding to a minimum and to obtain the maximum signal for specific staining at the same time.

Supplementary Note 2: Live-cell staining and DNA-PAINT single-particle-tracking

We tested if it is possible to use SOMAmers to label the extracellular EGFR in living A431 cells. We observed efficient membrane staining after 20 min of incubation at 4°C with the SOMAmers diluted in L-15 cell medium supplemented with 10 µM Z-Block (**Supplementary Figure 13b**). We show successful EGFR SOMAmer labeling with downstream fixation (4% PFA, 30 min), permeabilization and immunostaining of intracellular EGFR using primary and secondary antibodies. Co-localization of SOMAmer and antibody signal shows the specificity of the EGFR SOMAmer. We tested potential non-specific binding of the SOMAmers on living cells by using the GFP-SOMAmer as a negative staining control in A431 cells (**Supplementary Figure 13a**) and observed a low amount of non-specific binding, which could be efficiently reduced by the addition of 10 µM Z-Block.

Supplementary Methods

Secondary antibody conjugation to DNA
Anti-mouse secondary antibody was conjugated to a DNA-PAINT docking site (Thiol-5'-TTATACATCTA-3') using maleimide-PEG2-succinimidyl ester[2, 3].

Supplementary Figure 1
SK-BR-3 cells were fixed in pre-warmed (to 37°C) 4% paraformaldehyde in PBS for 15 min at room temperature, then washed twice with PBS and permeabilized with 0.25% Triton-X-100 in PBS for 15 min. The folded SOMAmer reagents against EGFR, ErbB2 and HSP90 were diluted to 100 nM in SOMAmer staining buffer (1×PBS, 5 mM $MgCl_2$, 1% BSA, 0.05% Tween-20, 0.1 mg/ml sheared salmon sperm DNA, 10 µM Z-Block, 1 mM dextran sulfate) and incubated with the cells overnight at 4°C. After SOMAmer incubation, the cells were washed three times with PBS + 5 mM $MgCl_2$. Post-fixation was performed using 4% paraformaldehyde in PBS + 5 mM $MgCl_2$ for 10 min at room temperature, then washed three times with PBS + 5 mM $MgCl_2$.

Imaging conditions

Imaging round	Imager strand	Imager concentration	Frames	Integration time	Laser power density
1. ErbB2	TAATGAAGA-Cy3b	0.75 nM	23,177	250 ms	0.83 kW/cm^2
2. EGFR	Cy3b-TAGATGTAT	3 nM	23,512	250 ms	0.83 kW/cm^2
3. HSP90	CTTTACCTAA-Cy3b	0.5 nM	30,000	250 ms	0.83 kW/cm^2

A cylindrical lens was used for 3D astigmatism imaging.

Supplementary Figure 2
SK-BR-3 cells were fixed with -20°C 100% methanol for 5 min at room temperature, then, washed three times with PBS. The folded SOMAmer reagents were diluted to 100 nM in SOMAmer staining buffer (1× PBS, 5 mM $MgCl_2$, 1% BSA, 0.05% Tween-20, 0.1 mg/ml sheared salmon sperm DNA, 10 µM Z-Block, 1 mM dextran sulfate) and incubated with the cells overnight at 4°C. After SOMAmer incubation, the cells were washed three times with PBS + 5 mM $MgCl_2$. Post-fixation was performed using 4% paraformaldehyde in PBS + 5 mM $MgCl_2$ for 10 min at room temperature followed by washing three times with PBS + 5 mM $MgCl_2$.

Imaging conditions

Imaging round	Imager strand	Imager concentration	Frames	Integration time	Laser power density
1. LIMP2	TAATGAAGA-Cy3b	1.5 nM	20,000	250 ms	0.41 kW/cm^2
2. HSP60	Cy3b-TAGATGTAT	0.3 nM	40,000	250 ms	0.62 kW/cm^2

A cylindrical lens was used for 3D astigmatism imaging.

Supplementary Figures 6 and 7
Prior to fixation, A431 (Supp. Figure 6) or A549 (Supp. Figure 7) cells were serum depleted overnight and treated with 80 µM endocytosis inhibitor Dynasore (Sigma Aldrich, SML0340) for ~30 min. Cells were fixed with ice-cold 4% paraformaldehyde in PBS for 30 minutes at room temperature, then washed two times with PBS and permeabilized with 0.25% Triton-X-100 for 15 min.

SOMAmer staining: The folded SOMAmer against EGFR was diluted to 100 nM in SOMAmer staining buffer (1×PBS, 5 mM $MgCl_2$, 1% BSA, 0.05% Tween-20, 0.1 mg/ml salmon sperm DNA, 10 µM Z-Block, 1 mM dextran sulfate) and incubated with the cells overnight at 4°C. After SOMAmer incubation, the cells were washed three times with PBS + 5 mM $MgCl_2$. Post-fixation was performed using 1% paraformaldehyde and 0.1% glutaraldehyde in PBS + 5 mM $MgCl_2$ for 10 min at room temperature followed by washing three times with PBS + 5 mM $MgCl_2$.

EGFR immunostaining: Cells were blocked with 3% BSA in PBS for 60 min at room temperature. Primary antibody against the extracellular region of EGFR (Thermo Fisher, MA5-13319) was diluted (1:50) in 3% BSA in PBS and incubated with the cells overnight at 4°C. Cells were rinsed with PBS and washed three times with an incubation time of 5 min. Secondary anti-mouse antibody conjugated to a P1 docking site was diluted in 3% BSA in PBS and incubated with the cells for 1 h at room temperature. Cells were rinsed with PBS and washed three times with an incubation time of 5 min. Post-fixation was performed using 1% paraformaldehyde and 0.1% Glutaraldehyde in PBS + 5 mM $MgCl_2$ for 10 min at room temperature followed by washing three times with PBS + 5 mM $MgCl_2$.

Imaging conditions for Supplementary Figure 6:

	Imager strand	Imager concentration	Frames	Integration time	Laser power density
SOMAmer	Cy3b-TAGATGTAT	1.2 nM	50,000	150 ms	1.9 kW/cm^2
Antibody	CTAGATGTAT-Cy3b	0.25 nM	50,000	150 ms	1.9 kW/cm^2

For analysis, ~20,000 – 30,000 single EGFR proteins were selected and analyzed using Picasso's pick tool with a radius of 65 nm (adjusted to the experimental localization precision in order to fully select single receptors).

Imaging conditions for Supplementary Figure 7:

	Imager strand	Imager concentration	Frames	Integration time	Laser power density
SOMAmer	AGATGTAT-Cy3b	15 nM	40,000	100 ms	0.41 kW/cm^2
Antibody	AGATGTAT-Cy3b	2.5 nM	40,000	100 ms	0.41 kW/cm^2

For analysis, ~3,000 single EGFR proteins were selected and analyzed using Picasso's pick tool with a radius of ~90 nm (adjusted to the experimental localization precision in order to fully select single receptors).

Supplementary Figure 8

Imaging conditions:

Imaging Round	Imager strand	Imager concentration	Frames	Integration time	Laser power density
1. Catalase	CATACATTGA-Cy3b	1 nM	30,000	250 ms	0.83 kW/cm^2
2. PMP70	CTAGATGTAT-Cy3b	0.3 nM	30,000	200 ms	1.2 kW/cm^2

A cylindrical lens was used for 3D astigmatism imaging.

Supplementary References

1. Gupta, S. et al. *Appl Immunohisto M M* **19**, 273-278 (2011).
2. Agasti, S.S. et al. *Chem Sci* **8**, 3080-3091 (2017).
3. Schnitzbauer, J., Strauss, M.T., Schlichthaerle, T., Schueder, F. & Jungmann, R. *Nat Protoc* **12**, 1198-1228 (2017).

3.2 Publication II: 124-Color Super-resolution Imaging by Engineering DNA-PAINT Blinking Kinetics

Orsolya K. Wade*, Johannes B. Woehrstein*, Philipp C. Nickels*, **Sebastian Strauss***, Florian Stehr, Johannes Stein, Florian Schueder, Maximilian T. Strauss, Mahipal Ganji, Joerg Schnitzbauer, Heinrich Grabmayr, Peng Yin, Petra Schwille, and Ralf Jungmann

(* equal contribution)

Nano Letters, volume 19, issue 4, pages 2641-2646 (2019)

DOI: https://doi.org/10.1021/acs.nanolett.9b00508

To understand the interplay and complexity of biological systems, it is crucial to observe as many molecules as possible within the same specimen. As opposed to traditional fluorescence techniques, the number of 'colors' that can be achieved in DNA-based imaging techniques is encoded in the DNA sequence rather than the spectral separation of fluorophores. Therefore, using Exchange-PAINT, the number of channels that can be multiplexed is theoretically only limited by the number of available orthogonal DNA-PAINT docking strand sequences [33]. However, despite the labeling of all targets of interest performed simultaneously, the read-out is performed sequentially. This implicates that the imaging time scales linearly with the number of rounds to be measured, making the duration of an experiment the practical limit for multiplexing capabilities.

In this study, we tackled this constraint and present an approach that enables us to read out multiple colors after a single image acquisition. By manipulating the hybridization kinetics of docking and imager strands, we aimed to program distinct kinetic fingerprints as barcodes to distinguish multiple targets after image acquisition. To achieve this, we manipulated two hybridization kinetic features: Binding frequency and binding time. By using docking sites of different length (e. g. 8 vs 10 nt), the binding time (or bright time) can be varied. The frequency is modulated by different number of binding sites per dockings site (e. g. 1 vs. 3). We successfully demonstrated the distinction of different kinetic fingerprints on DNA origami structures that are decorated with docking sites of different length and concatenations. Different

kinetic barcodes could also be resolved, when spaced only ~40 nm apart on DNA origami structures. Furthermore, we applied kinetic barcoding in cellular imaging in two showcases – protein and mRNA imaging. First, we labeled the proteins CHC and PMP70 using secondary antibodies conjugated to docking sites with different lengths (8 nt vs 9 nt). The proteins were distinguished after one image acquisition based on the difference in the mean bright time values. Next, we performed RNA-FISH on housekeeping genes GAPDH and TFRC. Both mRNAs were targeted by 20 probes that were either extended with one or three docking sites. Counting the number of binding events on each RNA resulted in two separated Gaussian distributions after calculating and plotting the binding frequency. In a final experiment, we used kinetic barcoding to demonstrate highly multiplexed imaging of more than 100 targets. To achieve this, we combined five distinct frequency levels with three different sequences that were labeled with spectrally distinct fluorophores ATTO 488, Cy3B, and ATTO 655. Five frequency levels and three colors result in 125 possible combinations of which the triple zero is excluded (ultimately 124 combinations). This was experimentally achieved by incorporating 0, 3, 9, 22, or 44 binding sites of three different sequences into distinct DNA origami structures.

In conclusion, kinetic barcoding provides a solution to read out multiple channels. The method is one step forward towards high-throughput super-resolution imaging using a simple microscope setup. However, the applicability of this technique is limited by the fact that the targets must be spatially separated to identify their unique kinetic barcode. We can predict future applications of this method for the imaging of mRNA and membrane proteins since they usually appear as distinct spots.

NANO LETTERS

Letter

Cite This: *Nano Lett.* 2019, 19, 2641−2646

pubs.acs.org/NanoLett

124-Color Super-resolution Imaging by Engineering DNA-PAINT Blinking Kinetics

Orsolya K. Wade,[†,‡,⊥] Johannes B. Woehrstein,[†,‡,⊥] Philipp C. Nickels,[†,‡,⊥] Sebastian Strauss,[†,‡,⊥] Florian Stehr,[‡] Johannes Stein,[‡] Florian Schueder,[†,‡] Maximilian T. Strauss,[†,‡] Mahipal Ganji,[†,‡] Joerg Schnitzbauer,[†,‡] Heinrich Grabmayr,[†,‡] Peng Yin,[§,∥] Petra Schwille,[‡] and Ralf Jungmann*[,†,‡]

[†]Department of Physics and Center for Nanoscience, Ludwig Maximilian University, 80539 Munich, Germany

[‡]Max Planck Institute of Biochemistry, 82152 Martinsried, Germany

[§]Wyss Institute for Biologically Inspired Engineering, Harvard University, Boston, Massachusetts 02138, United States

[∥]Department of Systems Biology, Harvard Medical School, Boston, Massachusetts 02115, United States

Supporting Information

ABSTRACT: Optical super-resolution techniques reach unprecedented spatial resolution down to a few nanometers. However, efficient multiplexing strategies for the simultaneous detection of hundreds of molecular species are still elusive. Here, we introduce an entirely new approach to multiplexed super-resolution microscopy by designing the blinking behavior of targets with engineered binding frequency and duration in DNA-PAINT. We assay this kinetic barcoding approach *in silico* and *in vitro* using DNA origami structures, show the applicability for multiplexed RNA and protein detection in cells, and finally experimentally demonstrate 124-plex super-resolution imaging within minutes.

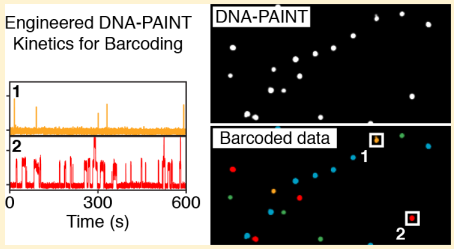

KEYWORDS: *Super-resolution microscopy, DNA nanotechnology, DNA-PAINT, barcoding, multiplexing*

The development of optical super-resolution techniques allows researchers to unravel molecular properties of biological systems with thus far unprecedented detail.[1−4] While recent technical advancements propel the achievable spatial resolution to the true molecular scale of only a few nanometers,[5−7] current implementations are still limited when it comes to imaging many molecular species simultaneously in single cells and beyond. This so-called multiplexing is traditionally achieved using spectrally distinct, fixed labels (e.g., dye-coupled antibodies or nucleic acid probes) on target molecules of interest such as proteins, DNA, or RNA. While spectral multiplexing approaches are relatively straightforward to implement, the amount of "plex" is inherently limited by the number of distinguishable spectral labels in the detectable emission spectrum, which is in most instances three or four.[8] However, in order to fully understand the detailed molecular workings of the complex cellular machinery, one ideally would need to be able to look at hundreds if not thousands of unique components and their molecular interplay.

Some efforts to extend spectral multiplexing capabilities include multiparameter and combinatorial detection,[9,10] multispectral acquisition,[11] and spectrally resolved detection.[12,13] While these approaches increase the number of detectable targets, they are ultimately still limited by the spectral properties of fluorescent molecules used to label target structures.

To overcome the limitation inherent in spectral separation for multiplexed detection, several approaches have recently been devised that employ sequential labeling and imaging of targets using spectrally indistinct probes[14−17] (i.e., the same dye molecule). Some of these implementations rely on simultaneous labeling of target molecules with orthogonal DNA-barcoded affinity reagents (e.g., antibodies) followed by sequential imaging using dye-labeled complementary oligos (e.g., Exchange-PAINT[14] or Universal DNA Exchange[17,18]). Others use sequential labeling, imaging, and quenching based on dye-conjugated antibodies, e.g., STORM.[15,16] While both implementations differ slightly in the combined time for labeling and imaging of each target, the overall experimental time eventually scales linearly with the number of targets to be acquired. This fact ultimately sets a practical limit to the amount of multiplexing achievable. While it might be reasonable to obtain tens of targets with sequential multiplexing, it will become prohibitively time-intensive (and eventually impossible) for hundreds or even thousands of targets. Thus, current multiplexing approaches are inherently limited in terms of the achievable coding depth, overall acquisition time, and ease-of-use.

To overcome this limitation, we here propose an entirely orthogonal approach to achieve multiplexed detection in single-molecule-based super-resolution experiments that allows hundreds or more targets to be imaged simultaneously. Instead

Received: February 4, 2019
Revised: February 20, 2019
Published: March 13, 2019

DOI: 10.1021/acs.nanolett.9b00508
Nano Lett. 2019, 19, 2641−2646

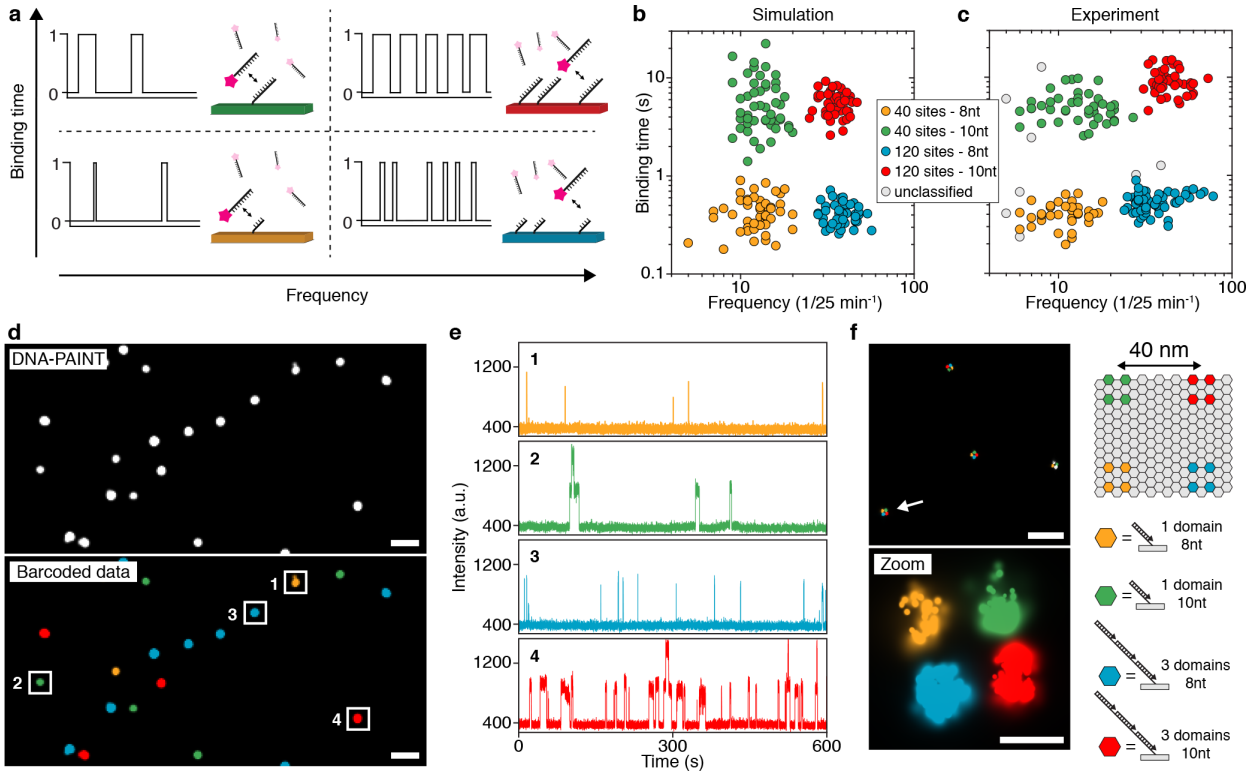

Figure 1. Simultaneous multiplexed super-resolution imaging by engineering blinking kinetics. (a) Engineering blinking kinetics in DNA-PAINT allows the creation of "barcodes" for simultaneous multiplexing, using only a single imager strand species. Frequency can be encoded by designing a certain number of binding sites per target, e.g., a single binding site, leading to a defined blinking frequency. Tripling the number of binding sites triples the blinking frequency (left to right). Similarly, binding duration can be engineered by adjusting the length of the docking strand on a specific target: an 8 nt docking sequence will lead to a "short" binding duration, while a 10 nt docking sequence will result in longer binding (bottom to top). (b) Simulations of four kinetically different structures (40 and 120 binding sites and 8 and 10 nt lengths) show four clearly distinguishable populations corresponding to the engineered frequency and duration levels (see Supplementary Figure 1 for details on cluster detection). (c) Experimental results from DNA origami structures imaged using a single imager strand species show four distinguishable populations in good agreement with *in silico* data from c (see Supplementary Figure 5 for details on cluster detection). (d) Exemplary overview DNA-PAINT image of the four DNA origami structures (top). Same data set, now color-coded according to identified clusters in c (bottom). (e) Exemplary intensity versus time traces from highlighted regions in d representing each of the four unique DNA origami species. (f) Engineering frequency and duration on DNA origami below the diffraction limit. Each corner of the structure is designed to exhibit a unique kinetic fingerprint. Scale bars: 1 μm (d), 500 nm (f, top), 40 nm (f, bottom). For details regarding simulation parameters and cluster identification, see Methods in Supporting Information.

of relying on spectral information or sequential imaging, we engineer targets to blink autonomously with precisely adjustable kinetic signatures (i.e., frequency and duration of blinks), essentially providing a distinct kinetic barcode for hundreds of unique molecular species.

In order to implement and demonstrate the concept of engineered blinking kinetics for simultaneous multiplexed super-resolution imaging, we chose DNA-PAINT[7,19] as imaging modality. In DNA-PAINT, short dye-labeled oligonucleotides bind transiently to complementary, target-bound DNA molecules, thus creating an apparent blinking at the target site, which in turn is used for stochastic super-resolution microscopy. Due to the versatile programmability of DNA probes, the binding kinetics such as blinking frequency and duration can be tuned precisely and used downstream as "barcodes" for multiplexed detection.

The concept of engineering binding kinetics with DNA-PAINT is schematically shown in Figure 1a. In order to tune the blinking frequency of targets, we label one species with a single DNA-PAINT binding site and an orthogonal species with three binding sites. Assuming a constant influx of imager strands, the blinking frequency will scale linearly with the number of binding sites (e.g., resulting in a blinking frequency of two for the single binding site and a frequency of six for three sites; see Figure 1a). Similarly, we can modulate the blinking duration for a given target molecule by adjusting the length of the docking strand (e.g., 8 nt long docking strands will result in relatively short binding events, while 10 nt long docking sites will result in longer events; see Figure 1a). As binding frequency and duration are independent of each other in DNA-PAINT, these parameters can be combined to perform combinatorial barcoding with just a single imager strand species, thus enabling simultaneous multiplexed imaging.

In order to screen for the optimal conditions to design distinguishable binding kinetics in terms of frequency and duration, we first performed *in silico* DNA-PAINT experiments. Tuning parameters such as binding time, imager strand concentration, number of binding sites, duration of image acquisition, and others (see online methods for details), we

DOI: 10.1021/acs.nanolett.9b00508
Nano Lett. 2019, 19, 2641−2646

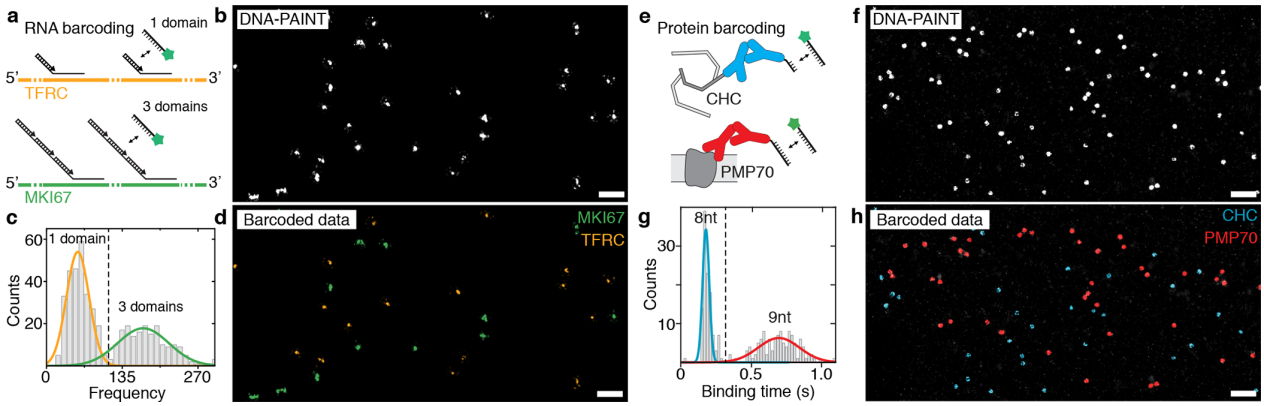

Figure 2. Engineered binding kinetics allow simultaneous multiplexed super-resolution imaging of RNA and proteins in cells. (a) Scheme showing the implementation of frequency barcoding for smRNA-FISH. Two distinct RNA species (TFRC and MKI67) are labeled with FISH probes featuring 40 binding sites for DNA-PAINT or 120 binding sites, respectively. (b) Resulting DNA-PAINT data after image acquisition shows TFRC and MKI67 mRNA molecules as single spots, which are not yet distinguishable. (c) Plotting the blinking frequency for all detected single mRNA molecules shows a clearly distinguishable distribution of a low and a high frequency, corresponding to the FISH probe set for TFRC (yellow) and MKI67 (green), respectively. (d) Distinct frequencies are used to assign a pseudocolor for each RNA species. (e) Scheme showing the implementation of duration barcoding for protein detection. Two distinct protein species are labeled with DNA-conjugated antibodies featuring an 8 and 9 nt binding site for DNA-PAINT imaging. (f) Resulting DNA-PAINT data after image acquisition shows CHC and PMP70 proteins as clusters, which are not yet distinguishable. (g) Plotting the binding duration for selected protein locations shows a clearly distinguishable distribution of short and long binding species, corresponding to the two proteins. (h) Distinct durations are used to assign a pseudocolor for each protein species. Scale bars: 1 μm.

were able to engineer four distinguishable blinking regimes (two blinking frequencies based on 40 and 120 binding sites and two blinking durations based on 400 ms and 5 s) that can now be used for combinatorial barcoding with a single imager strand species only, allowing four-target super-resolution imaging in a relatively short duration of 25 min (Figure 1b and Supplementary Figure 1).

Next, to experimentally validate the *in silico* results, we turned to DNA origami[20] structures to implement the engineered frequency and duration levels, as these structures are exquisitely programmable for super-resolution microscopy.[21] We designed four structures carrying 40 and 120 binding sites either with 8 or 10 nt extensions of the same sequence and imaged them simultaneously using a single imager strand species (see also Supplementary Figure 2, Supplementary Tables 2−5, and Supplementary Note 1). In the resulting raw DNA-PAINT data, we performed kinetic analysis for each structure following an initial filtering step (Supplementary Figures 3 and 4) and plotted the obtained binding time and frequency in a 2D plot in the same manner as for the *in silico* data. Next, we subjected the 2D data set to a clustering analysis (hdbscan;[22] for details, see Methods in the Supporting Information), which resulted in four cluster species, in good agreement with the *in silico* data (Figure 1c and Supplementary Figure 5). This cluster identity now allows us to transform the raw DNA-PAINT image data (Figure 1d, top) to a barcoded pseudocolor image, where each DNA origami structure is assigned to one of the four cluster species (Figure 1d, bottom and Supplementary Figure 6). Examining the intensity versus time traces of four structures that were each assigned to one of the clusters indeed shows the distinct and expected kinetic fingerprints (Figure 1e).

To demonstrate that the kinetic barcoding approach allows satisfactory super-resolution performance, we designed a DNA origami structure with four different "binding spots", at the four corners of the structure, each with four or 12 binding sites of either 8 or 10 nt length. Again, we performed DNA-PAINT using a single imager strand species and were able to visualize all four corners of the structure, separated by 40 nm. The blinking kinetics of the binding spots were then used to assign each to its correct corner (Figure 1f), demonstrating the application of blinking kinetics for super-resolution microscopy (Supplementary Figures 7 and 8).

Next, we designed two experiments to demonstrate the general applicability of our simultaneous multiplexing approach *in situ* in two biologically relevant settings. First, we implemented two-color frequency barcoding for two distinct mRNA species using a combination of DNA-PAINT implemented on a Spinning Disk Confocal microscope[23] and smRNA-FISH[14,24] (Figure 2a−d). We labeled TFRC and MKI67 mRNA species using two sets of FISH probes displaying 40 and 120 binding sites, respectively (see Figure 2a for probe design and Supplementary Tables 6 and 7 for probe sequences). After image acquisition, the RNA species appear as super-resolved spots in the resulting DNA-PAINT image (Figure 2b, see Methods in the Supporting Information for acquisition details). We then performed kinetic analysis on the individual RNA molecules and obtained a distribution of two populations corresponding to two distinct blinking frequencies, as designed (Figure 2c). Similar to the *in vitro* case (Figure 1), we assigned a pseudocolor to each of the blinking frequencies and rerendered a barcoded data set (Figure 2d), where we are now able to clearly distinguish TFRC from MKI67 mRNA molecules.

To demonstrate that binding duration can be used in a similar fashion to barcode biomolecules in cells, we next used DNA-conjugated antibodies targeting the clathrin heavy chain (CHC) and a peroxisomal membrane protein (PMP70) inside HeLa cells, where each secondary antibody species carries a DNA-PAINT binding site of different length (Figure 2e and Supplementary Table 8). Similar to the mRNA experiments, we performed image acquisition and analysis and obtained a

DOI: 10.1021/acs.nanolett.9b00508
Nano Lett. 2019, 19, 2641−2646

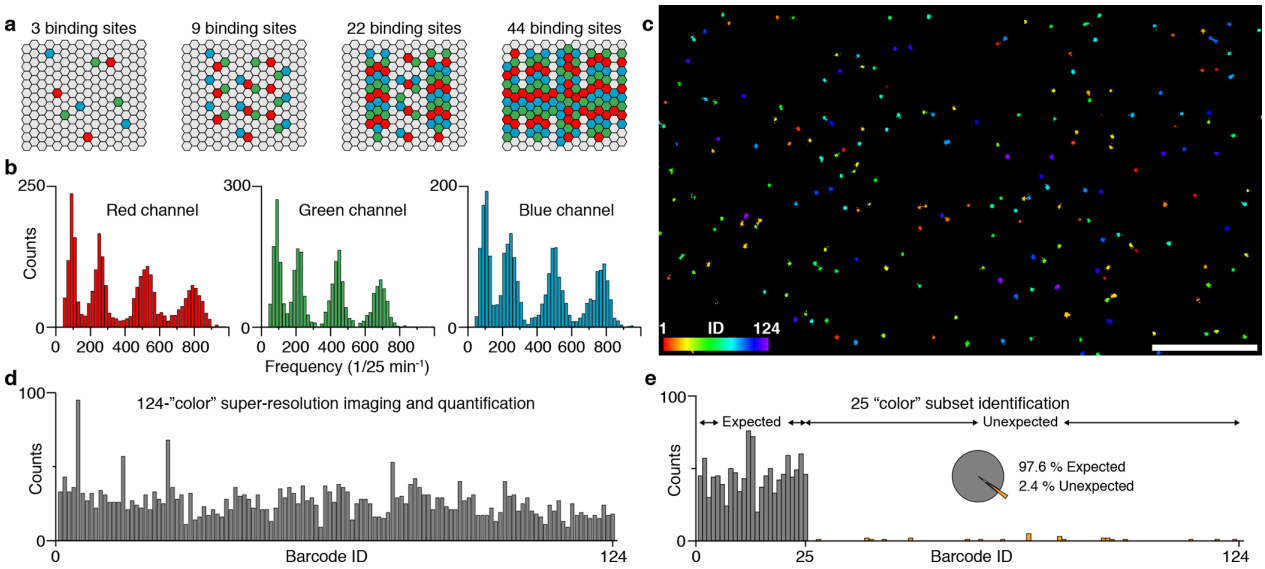

Figure 3. Frequency-based 124-plex super-resolution imaging. (a) DNA origami structures are extended with three unique sequences (red, green, or blue) with 0, 3, 9, 22, or 44 copies, respectively. Using combinatorial labeling, this yields a total of $5^3 - 1 = 124$ unique target structures, achieved by distinguishing five frequency levels and using three spectral colors (i.e., three imager strand species). (b) Binding frequency distribution for all 124 DNA origami structures show four clearly distinguishable frequency levels corresponding to 3, 9, 22, and 44 binding sites for each spectral color (red, green, and blue), respectively. Based on these distributions, a unique barcode ID from a pool of 124 can be assigned to each structure. (c) DNA-PAINT super-resolution image of all 124 DNA origami structures, color-coded according to the assigned binding frequency and spectral color. (d) Quantification of the 124-plex experiment shows that all 124 structures could be identified. In total, 3289 structures were quantified, from which 243 were discarded due to ambiguous frequencies (i.e., overlap of distributions in b). (e) Twenty-five out of 124 structures were imaged in one sample in order to assess identification performance. In total, 1165 structures were quantified, from which 28 were categorized as false-positives (i.e., unexpected) resulting in an accuracy of 97.6%. The ratio between lowest expected and highest unexpected is 20 to 7. Scale bar: 5 μm.

DNA-PAINT data set (Figure 2f). This was then transformed using kinetic analysis (Figure 2g) into a pseudocolored, barcoded image, where we were able to clearly distinguish areas of CHC and PMP70 based on the blinking duration (Figure 2h).

The proof-of-concept experiments for DNA origami, RNA, and protein barcoding underline the general applicability of the kinetic barcoding concept *in vitro* and *in situ*. However, to fully demonstrate the power of kinetic barcoding, we turned our attention to the question of how much simultaneous multiplexing can be achieved within a relatively short period of time. By combining four distinguishable binding frequencies with three spectral colors, we should be able to achieve simultaneous, 124-plex super-resolution imaging within a few minutes acquisition time. To demonstrate that this is indeed feasible, we designed and constructed 124 unique DNA origami structures carrying 0, 3, 9, 22, or 44 copies of three orthogonal binding sites each, respectively (Figure 3a and Supplementary Tables 9 and 10). After folding and purification (Supplementary Figure 9), we pooled all 124 distinct DNA origami structures into a single sample and performed 3-color DNA-PAINT imaging using Atto655-, Cy3B-, or Atto488-labeled orthogonal imager strands (Supplementary Table 11). As before, we performed kinetic analysis on each of the structures and plotted the distribution of binding frequencies for each spectral color separately (Figure 3b). We were able to clearly distinguish four distinct frequency populations in each of the three spectral colors. Using these levels, we assigned a unique barcode ID to each of the origami structures in the sample based on color and frequency and were able to render a full 124 pseudocolor super-resolution data set (Figure 3c, see also Methods in the Supporting Information for identification).

Next, we quantified all DNA origami in the data set and were able to verify that indeed all 124 unique structures could be identified (Figure 3d). Finally, in order to assay the performance in terms of false positive identification of our multiplexing approach, we performed a similar experiment as described above, but now using only a subset of 25 out of the total 124 DNA origami structures (Figure 3e). The resulting quantitative analysis yielded a remarkable accuracy of 97.6%, underlining the robustness of our multiplexing approach based on engineered binding kinetics. We note, however, that this high number of multiplexing and robustness might not be achievable in a straightforward fashion in a cellular setting, e.g., for mRNA barcoding using smRNA-FISH as shown in the examples above, due to the increased complexity in the intracellular environment and suboptimal or target-dependent labeling efficiencies.

In conclusion, we introduced an entirely new barcoding approach for multiplexed detection based on precisely engineering blinking kinetics in stochastic super-resolution microscopy: kinetic barcoding. We demonstrated the implementation using DNA-PAINT both *in vitro* and *in situ*, currently reaching 124-plex within minutes. Zooming out, we envision that kinetic barcoding could be applied to ask Systems Biology questions in single cells with super-resolution by simultaneously imaging hundreds of DNA, RNA, and protein targets reaching transcriptomics- and proteomics-style experiments with a simple localization microscopy approach: "Localizomics". Finally, one could envision its extension to even more multiplexing by implementing readouts such as

DOI: 10.1021/acs.nanolett.9b00508
Nano Lett. 2019, 19, 2641−2646

molecular brightness of imager strands, fluorescence lifetime, and more.[25]

■ ASSOCIATED CONTENT

Supporting Information

The Supporting Information is available free of charge on the ACS Publications website at DOI: 10.1021/acs.nanolett.9b00508.

Materials and methods alongside detailed information about the optical setups, DNA origami self-assembly, RNA-FISH probe design and antibodies, sample preparation and data processing, sequences for DNA origami folding, DNA-PAINT docking and imager sequences, and RNA-FISH probes (PDF)

■ AUTHOR INFORMATION

Corresponding Author

*E-mail: jungmann@biochem.mpg.de. Phone: +49 89 8578 3410.

ORCID

Johannes Stein: 0000-0002-1335-1120
Peng Yin: 0000-0002-2769-6357
Petra Schwille: 0000-0002-6106-4847
Ralf Jungmann: 0000-0003-4607-3312

Author Contributions

⊥These authors contributed equally to this work. O.K.W. designed and performed experiments and analyzed data. J.B.W. designed and performed experiments and analyzed data. P.C.N. designed and performed DNA origami experiments and analyzed the data. S.S. designed and performed smRNA-FISH and protein barcoding experiments. F.St. and J.S. performed DNA origami and *in silico* experiments, developed data analysis methods and analyzed data. F.Sc. designed and performed smRNA-FISH experiments, performed DNA origami experiments and analyzed data. M.T.S. developed software and analyzed data. M.G. designed and performed smRNA-FISH experiments and wrote the manuscript. J.S. developed software and analyzed data. H.G. developed software and performed DNA origami experiments. P.Y. supervised the initial phase of the study. P.S. developed data analysis strategies and supervised the study. R.J. conceived and supervised the study, analyzed the data, and wrote the manuscript. All authors reviewed and approved the manuscript.

Funding

This research was funded by the German Research Foundation through the Emmy Noether Program (DFG JU 2957/1−1) and the SFB1032 (Project A11), the European Research Council through an ERC Starting Grant (MolMap, Grant agreement number 680241), the Allen Distinguished Investigator Program through the Paul G. Allen Frontiers Group, the Max Planck Society, and the Max Planck Foundation. P.Y. acknowledges support by the NSF (CCF-1317291) and the NIH (1-U01-MH106011 and R01EB018659).

Notes

The authors declare the following competing financial interest(s): J.B.W, R.J., and P.Y. filed a provisional patent based on this work. R.J. and P.Y. are co-founders of Ultivue, Inc.

■ ACKNOWLEDGMENTS

We thank Martin Spitaler and the imaging facility of the MPI of Biochemistry for confocal imaging support. We thank Alexander Auer for microscopy support and help with data acquisition. We thank Julian Bauer and Patrick Schueler for experimental support. We thank Mingjie Dai for help with data processing. We thank William M. Shih for fruitful discussions. O.K.W., S.S., F.St., and J.S. acknowledge support by the QBM graduate school. M.T.S. acknowledges support by the IMPRS-LS graduate school. M.G. acknowledges funding from the European Union's Horizon 2020 research and innovation programme under the Marie Skłodowska-Curie grant agreement no 796606.

■ REFERENCES

(1) Hell, S. W.; Sahl, S. J.; Bates, M.; Zhuang, X. W.; Heintzmann, R.; Booth, M. J.; Bewersdorf, J.; Shtengel, G.; Hess, H.; Tinnefeld, P.; Honigmann, A.; Jakobs, S.; Testa, I.; Cognet, L.; Lounis, B.; Ewers, H.; Davis, S. J.; Eggeling, C.; Klenerman, D.; Willig, K. I.; Vicidomini, G.; Castello, M.; Diaspro, A.; Cordes, T. The 2015 super-resolution microscopy roadmap. *J. Phys. D: Appl. Phys.* **2015**, *48* (44), 443001.

(2) Kanchanawong, P.; Shtengel, G.; Pasapera, A. M.; Ramko, E. B.; Davidson, M. W.; Hess, H. F.; Waterman, C. M. Nanoscale architecture of integrin-based cell adhesions. *Nature* **2010**, *468* (7323), 580−4.

(3) Xu, K.; Zhong, G.; Zhuang, X. Actin, spectrin, and associated proteins form a periodic cytoskeletal structure in axons. *Science* **2013**, *339* (6118), 452−6.

(4) Sahl, S. J.; Hell, S. W.; Jakobs, S. Fluorescence nanoscopy in cell biology. *Nat. Rev. Mol. Cell Biol.* **2017**, *18* (11), 685−701.

(5) Dai, M. J.; Jungmann, R.; Yin, P. Optical imaging of individual biomolecules in densely packed clusters. *Nat. Nanotechnol.* **2016**, *11* (9), 798−807.

(6) Balzarotti, F.; Eilers, Y.; Gwosch, K. C.; Gynna, A. H.; Westphal, V.; Stefani, F. D.; Elf, J.; Hell, S. W. Nanometer resolution imaging and tracking of fluorescent molecules with minimal photon fluxes. *Science* **2017**, *355* (6325), 606−612.

(7) Schnitzbauer, J.; Strauss, M. T.; Schlichthaerle, T.; Schueder, F.; Jungmann, R. Super-resolution microscopy with DNA-PAINT. *Nat. Protoc.* **2017**, *12*, 1198−1228.

(8) Dempsey, G. T.; Vaughan, J. C.; Chen, K. H.; Bates, M.; Zhuang, X. Evaluation of fluorophores for optimal performance in localization-based super-resolution imaging. *Nat. Methods* **2011**, *8* (12), 1027−36.

(9) Lubeck, E.; Cai, L. Single-cell systems biology by super-resolution imaging and combinatorial labeling. *Nat. Methods* **2012**, *9* (7), 743−8.

(10) Bates, M.; Dempsey, G. T.; Chen, K. H.; Zhuang, X. Multicolor super-resolution fluorescence imaging via multi-parameter fluorophore detection. *ChemPhysChem* **2012**, *13* (1), 99−107.

(11) Valm, A. M.; Cohen, S.; Legant, W. R.; Melunis, J.; Hershberg, U.; Wait, E.; Cohen, A. R.; Davidson, M. W.; Betzig, E.; Lippincott-Schwartz, J. Applying systems-level spectral imaging and analysis to reveal the organelle interactome. *Nature* **2017**, *546* (7656), 162−167.

(12) Zhang, Z.; Kenny, S. J.; Hauser, M.; Li, W.; Xu, K. Ultrahigh-throughput single-molecule spectroscopy and spectrally resolved super-resolution microscopy. *Nat. Methods* **2015**, *12* (10), 935−8.

(13) Bongiovanni, M. N.; Godet, J.; Horrocks, M. H.; Tosatto, L.; Carr, A. R.; Wirthensohn, D. C.; Ranasinghe, R. T.; Lee, J. E.; Ponjavic, A.; Fritz, J. V.; Dobson, C. M.; Klenerman, D.; Lee, S. F. Multi-dimensional super-resolution imaging enables surface hydrophobicity mapping. *Nat. Commun.* **2016**, *7*, 13544.

(14) Jungmann, R.; Avendano, M. S.; Woehrstein, J. B.; Dai, M. J.; Shih, W. M.; Yin, P. Multiplexed 3D cellular super-resolution imaging with DNA-PAINT and Exchange-PAINT. *Nat. Methods* **2014**, *11* (3), 313−U292.

DOI: 10.1021/acs.nanolett.9b00508
Nano Lett. 2019, 19, 2641−2646

(15) Tam, J.; Cordier, G. A.; Borbely, J. S.; Sandoval Alvarez, A.; Lakadamyali, M. Cross-talk-free multi-color STORM imaging using a single fluorophore. *PLoS One* **2014**, *9* (7), No. e101772.
(16) Valley, C. C.; Liu, S.; Lidke, D. S.; Lidke, K. A. Sequential superresolution imaging of multiple targets using a single fluorophore. *PLoS One* **2015**, *10* (4), No. e0123941.
(17) Schueder, F.; Strauss, M. T.; Hoerl, D.; Schnitzbauer, J.; Schlichthaerle, T.; Strauss, S.; Yin, P.; Harz, H.; Leonhardt, H.; Jungmann, R. Universal Super-Resolution Multiplexing by DNA Exchange. *Angew. Chem., Int. Ed.* **2017**, *56* (14), 4052−4055.
(18) Wang, Y.; Woehrstein, J. B.; Donoghue, N.; Dai, M.; Avendano, M. S.; Schackmann, R. C. J.; Zoeller, J. J.; Wang, S. S. H.; Tillberg, P. W.; Park, D.; Lapan, S. W.; Boyden, E. S.; Brugge, J. S.; Kaeser, P. S.; Church, G. M.; Agasti, S. S.; Jungmann, R.; Yin, P. Rapid Sequential in Situ Multiplexing with DNA Exchange Imaging in Neuronal Cells and Tissues. *Nano Lett.* **2017**, *17* (10), 6131−6139.
(19) Jungmann, R.; Steinhauer, C.; Scheible, M.; Kuzyk, A.; Tinnefeld, P.; Simmel, F. C. Single-Molecule Kinetics and Super-Resolution Microscopy by Fluorescence Imaging of Transient Binding on DNA Origami. *Nano Lett.* **2010**, *10* (11), 4756−4761.
(20) Rothemund, P. W. K. Folding DNA to create nanoscale shapes and patterns. *Nature* **2006**, *440* (7082), 297−302.
(21) Schlichthaerle, T.; Strauss, M. T.; Schueder, F.; Woehrstein, J. B.; Jungmann, R. DNA nanotechnology and fluorescence applications. *Curr. Opin. Biotechnol.* **2016**, *39*, 41−47.
(22) Campello, R. J. G. B.; Moulavi, D.; Sander, J. In *Density-Based Clustering Based on Hierarchical Density Estimates*; Springer Berlin Heidelberg: Berlin, Heidelberg, 2013; pp 160−172.
(23) Schueder, F.; Lara-Gutierrez, J.; Beliveau, B. J.; Saka, S. K.; Sasaki, H. M.; Woehrstein, J. B.; Strauss, M. T.; Grabmayr, H.; Yin, P.; Jungmann, R. Multiplexed 3D super-resolution imaging of whole cells using spinning disk confocal microscopy and DNA-PAINT. *Nat. Commun.* **2017**, *8* (1), 2090.
(24) Raj, A.; van den Bogaard, P.; Rifkin, S. A.; van Oudenaarden, A.; Tyagi, S. Imaging individual mRNA molecules using multiple singly labeled probes. *Nat. Methods* **2008**, *5* (10), 877−879.
(25) Johnson-Buck, A.; Shih, W. M. Single-Molecule Clocks Controlled by Serial Chemical Reactions. *Nano Lett.* **2017**, *17* (12), 7940−7944.

DOI: 10.1021/acs.nanolett.9b00508
Nano Lett. 2019, 19, 2641−2646

124-color super-resolution imaging by engineering DNA-PAINT blinking kinetics

Orsolya K. Wade[1,2,5], Johannes B. Woehrstein[1,2,5], Philipp C. Nickels[1,2,5], Sebastian Strauss[1,2,5], Florian Stehr[2], Johannes Stein[2], Florian Schueder[1,2], Maximilian T. Strauss[1,2], Mahipal Ganji[1,2], Joerg Schnitzbauer[1,2], Heinrich Grabmayr[1,2], Peng Yin[3,4], Petra Schwille[2] & Ralf Jungmann[1,2]

[1]Department of Physics and Center for Nanoscience, Ludwig Maximilian University, 80539 Munich, Germany, [2]Max Planck Institute of Biochemistry, 82152 Martinsried near Munich, Germany, [3]Wyss Institute for Biologically Inspired Engineering, Harvard University, Boston, Massachusetts, USA, [4]Department of Systems Biology, Harvard Medical School, Boston, Massachusetts, USA. [5]These authors contributed equally to this work.

Supplementary Methods	
Supplementary Figure 1	**Cluster detection in simulated data**
Supplementary Figure 2	**DNA origami designs for binding duration and frequency modulation**
Supplementary Figure 3	**Filtering DNA origami data prior to clustering**
Supplementary Figure 4	**DNA-PAINT images of DNA origami before and after filtering**
Supplementary Figure 5	**Cluster detection in DNA origami data**
Supplementary Figure 6	**DNA origami data before and after cluster identification**
Supplementary Figure 7	**Clustering results for four-corner DNA origami**
Supplementary Figure 8	**Four-corner DNA origami structures before and after cluster identification**
Supplementary Figure 9	**Agarose gels of the 124 individual DNA origami structures**
Supplementary Table 1	**DNA-PAINT imager strands**
Supplementary Table 2	**Core staple strands for rectangular DNA origami**
Supplementary Table 3	**Biotinylated staple strands**
Supplementary Table 4	**Modified staple strands for DNA origami**
Supplementary Table 5	**List of DNA-PAINT handles**
Supplementary Table 6	**RNA-FISH probe set targeting MKI67 mRNA variant 2**
Supplementary Table 7	**RNA-FISH probe set targeting TFRC mRNA variant 4**
Supplementary Table 8	**Docking sites conjugated to secondary antibodies**
Supplementary Table 9	**Staple strands used for 124 color DNA origami structures**
Supplementary Table 10	**Barcode IDs and combinations of frequencies to achieve 124 colors**
Supplementary Note 1	**Design of rectangular DNA origami**
Supplementary Note 2	**RNA-FISH probe design**
Supplementary Note 3	**Sequences of MKI67 mRNA variant 2 used for probe design, 11427 bp**
Supplementary Note 4	**Sequences of TFRC mRNA variant 4 used for probe design, 4695 bp**
Supplementary References	

Supplementary Methods

Materials

Unmodified, dye-labeled, and biotinylated DNA oligonucleotides were purchased from MWG Eurofins or Integrated DNA Technologies. DNA scaffold strands were purchased from Tilibit (p7249, identical to M13mp18). Streptavidin was purchased from Thermo Fisher (cat: S-888). BSA-Biotin was obtained from Sigma-Aldrich (cat: A8549). Glass slides were ordered from Thermo Fisher (cat: 10756991) and coverslips were purchased from Marienfeld (cat: 0107032). Freeze 'N Squeeze columns were ordered from Bio-Rad (cat: 732-6165). PEG-8000 was purchased from Merck (cat: 6510-1KG). Tris 1M pH 8.0 (cat: AM9856), EDTA 0.5M pH 8.0 (cat: AM9261), Magnesium 1M (cat: AM9530G) and Sodium Chloride 5M (cat: AM9759) were ordered from Ambion. Ultrapure water (cat: 10977-035) was purchased from Thermo Fisher Scientific. Potassium chloride (cat: 6781.1) was ordered from Roth. Sodium hydroxide (cat: 31627.290) was purchased from VWR. Tween-20 (cat: P9416-50ML), Glycerol (cat: G5516-500ML) and Methanol (cat: 32213-2.5L) were ordered from Sigma-Aldrich. Protocatechuate 3,4-Dioxygenase Pseudomonas (PCD) (cat: P8279), 3,4-Dihydroxybenzoic acid (PCA) (cat: 37580-25G-F) and (+-)-6-Hydroxy-2,5,7,8-tetra-methylchromane-2-carboxylic acid (Trolox) (cat: 238813-5G) were purchased from Sigma-Aldrich. SYBR Safe DNA gel stain was purchased from Invitrogen (cat: SS33102). HeLa cells were purchased from the Leibniz Institute DSMZ (cat: ACC-57). A549 cells were purchased from ATCC. Dulbecco's Modified Eagle medium (DMEM) with high glucose, GlutaMAX™ and sodium pyruvate (cat: 31966-021), Fetal Bovine Serum (FBS) (cat: 10500-064), 1× Phosphate Buffered Saline (PBS) pH 7.2 (cat: 20012-019), 10× PBS pH 7.4 (cat: 70011036), and 0.05% Trypsin–EDTA (cat: 25300-054) were purchased from Thermo Fisher Scientific. 16% (w/v) Paraformaldehyde (cat: 28906) was purchased from Thermo Fisher Scientific. Glutaraldehyde (cat: 16220) was obtained from Electron Microscopy Sciences. Bovine Serum Albumin (cat: A4503-10G) was ordered from Sigma-Aldrich. Penicillin-Streptomycin (cat: 15140-122) was ordered from Thermo Fisher Scientific. Triton X-100 (cat: 6683.1) was purchased from Roth. Glass-bottomed 8-well µ-slides (cat: 80827) were obtained from ibidi. Primary polyclonal goat anti-CHC antibody (cat: sc-6579) was purchased from Santa Cruz Biotechnology. Primary monoclonal mouse anti-PMP70 antibody (cat: SAB4200181) was purchased from Sigma-Aldrich. Secondary polyclonal antibodies (cat: 705-005-147 and 715-005-150) were purchased from Jackson ImmunoResearch. Dextran sulfate 50% solution was purchased from Merck (cat: S4030). Sheared Salmon Sperm DNA (cat: AM9680), 10× PBS (cat: AM9624), 20× SSC (cat: AM9763), Hi-Di Formamide (cat: 4440753), yeast tRNA (cat: 15401011), and UltraPure BSA (cat: AM2616) was purchased from Thermo Fisher Scientific. Ribonucleoside Vanadyl Complex (VRC) (cat: S1402S) and RNase Inhibitor, Murine (cat: M0314S) were purchased from New England Biolabs.

Buffers

Origami buffers. Four buffers were used for DNA origami sample preparation and imaging: Folding Buffer (10 mM Tris, 10 mM EDTA, 12.5 mM $MgCl_2$, pH 8); Buffer A (10 mM Tris-HCl pH 7.5, 100 mM NaCl, 0.05 % Tween 20, pH 7.5); Buffer B (5 mM Tris-HCl pH 8, 10 mM $MgCl_2$, 1 mM EDTA, 0.05 % Tween 20, pH 8); Origami imaging buffer (same as B, but supplemented with 1× PCA, 1× PCD, and 1× Trolox). 100× Trolox: 100 mg Trolox, 430 µL 100 % Methanol, 345 µL 1M NaOH in 3.2 ml H_2O. 40× PCA: 154 mg PCA, 10 ml water and NaOH were mixed and pH was adjusted 9.0. 100× PCD: 9.3 mg PCD, 13.3 ml of buffer (100 mM Tris-HCl pH 8, 50 mM KCl, 1 mM EDTA, 50 % Glycerol). 2× PEG-Buffer was used for PEG precipitation (15 % PEG-8000, 500 mM NaCl in 1× TE buffer, pH 8.0). RNA-FISH buffers: Wash buffer: 10% formamide in 2× SSC; Hybridization buffer: 12.5 nM of working probe solution in 2xSSC, 10% formamide, 10% dextran sulfate, 0.1 mg/ml yeast tRNA, 0.1 mg/ml sheared salmon sperm DNA, 2 mM VRC, 0.10 mg/ml UltraPure BSA, RNase Inhibitor, Murine ~10U/µl. Blocking buffer for Immunofluorescence: 3% BSA, 0.1% Triton X-100 in PBS. Cell imaging buffer: (1× PBS pH 8, 500 mM NaCl, 1× PCA, 1× PCD, 1× Trolox).

Stochastic binding simulations

DNA-PAINT blinking traces were simulated using the stochastic reaction simulation tool COPASI[1]. Simulations were carried out as described earlier[2]. In brief, we simulated structures displaying 40 binding sites of 8 nt length, or 40 sites of 10 nt length and structures displaying 120 sites of 8 nt or 120 sites of 10 nt length. All simulation parameters were experimentally obtained. For 8 nt and 10 nt binding sites, a mean binding duration of 0.4 s and 5 s was determined, respectively. With our current imaging buffer constitution, an association rate of $2.9 \cdot 10^6 (\mathrm{Ms})^{-1}$ was used. Imager concentration was set to 80 pM, and the integration time to 30 ms with 1500 s total acquisition time. For each DNA origami design, 50 structures were simulated separately. The data from the four simulations were pooled, and clustered using the HDBSCAN algorithm, with 'min_cluster_size' set to 15, and 'min_samples' set to 1. (**Supplementary Figure 1**).

DNA origami design, assembly and purification

DNA origami structures were designed using the design module of Picasso[3]. Folding of structures was performed using the following components: p7249 M13 single-stranded DNA scaffold (0.01 µM), core staples (0.5 µM), biotin staples (0.5 µM), modified staples (each 0.5 µM), 1× folding buffer in a total of 20 µl for each sample. Annealing was done by cooling the mixture from 65 ºC to 25 ºC in 2 hours in a thermocycler. Structures were purified either using PEG-precipitation[4] (40 versus 120 binding sites and 4 corner origami), or by running the samples on a 1.5% agarose gel (1.5% agarose, 0.5× TA buffer, 12.5 mM $MgCl_2$, 1× SYBR Safe), cutting out bands containing the folded structures and purifying them using Freeze 'N Squeeze Columns (spun for 5 min at 1,000 ×g) (124 color imaging) (**Supplementary Figure 9**).

Cell culture

HeLa cells were used for CHC and PMP70 imaging. For RNA-FISH experiments A-549 cells were used. All cells were grown in high glucose (4.5 g/l) DMEM supplemented with GlutaMAX™, 1 mM sodium pyruvate and 10% FBS. Cells were seeded into 8-well-chambered cover glasses and grown to approximately 70% confluency.

Design of RNA- Fluorescence in situ Hybridization probes

RNA-FISH probes were designed against the mRNA sequence of the longest transcript variant of each gene (**Supplementary Notes 3** and **4**). FASTA sequences were taken from the NCBI Genome Browser. We used the Stellaris® Probe Designer version 4.2 with a masking level of 5 to get 40 probe strands for each target. These probes were then elongated on the 3'-end with DNA-PAINT handle sequences for DNA-PAINT imaging (**Supplementary Note 2**).

Hybridization of RNA-FISH probes

Cell media was aspirated and cells were rinsed with 1× PBS. Cells were fixed with 4% formaldehyde in 1× PBS for 10 min at room temperature, then washed two times with 1× PBS and 4 mM VRC. Permeabilization was carried out with 70% (v/v) ethanol for 6 hours at 4 ºC. Before hybridization, cells were incubated in wash buffer supplemented with 4 mM VRC for 10 minutes at room temperature. Hybridization: 300 µl of the hybridization solution containing 12.5 nM of probes was added to the cells. Hybridization was carried out in a sealed chamber at 37 ºC for 16 hours. Washing: Chambers were rinsed once then washed twice for 30 min each at 37 ºC in wash buffer.

Antibody conjugation

Antibodies were conjugated to DNA-PAINT docking sites via maleimide-PEG2-succinimidyl ester chemistry[3, 5] (see **Supplementary Table 8** for handle sequences).

CHC and PMP70 Immunostaining

Cell medium was aspirated and cells were fixed with 3% paraformaldehyde, 0.1% glutaraldehyde, and 0.3% Triton X-100 in PBS for 10 min at room temperature, then washed three times with PBS. Free aldehyde groups were reduced using 1 mg/ml sodium borohydride in PBS for 7 min, followed by three washing steps with PBS for 5 min. Cells were blocked and permeabilized with blocking buffer for 90 min. Cells were stained with primary antibodies, anti-CHC goat and anti-PMP70 mouse (both diluted 1:100), in blocking buffer overnight at 4 ºC. Cells were washed three times with PBS for 5 min. Cells were incubated with DNA-conjugated secondary antibodies (anti-goat-P12-8 nt and anti-mouse-P13-9 nt (**Supplementary Table 8**) diluted in blocking buffer (1:200) for 1 hour at room temperature before finally washing the cells three times in PBS for 5 min.

Super-resolution microscope setups

Custom TIRF Setup. Fluorescence imaging was carried out on an inverted Nikon Eclipse Ti microscope (Nikon Instruments) with the Perfect Focus System, applying an objective-type TIRF configuration with an oil-immersion objective (Apo SR TIRF 100×, NA 1.49, Oil). Two lasers were used for excitation: 561 nm (200 mW, Coherent Sapphire) or 640 nm (150 mW, Toptica iBeam smart). The laser beam was passed through cleanup filters (ZET561/10 or ZET642/20, Chroma Technology) and coupled into the microscope objective using a beam splitter (ZT561rdc or ZT647rdc, Chroma Technology). Fluorescence light was spectrally filtered with an emission filter (ET600/50m and ET575lp or ET705/72m and ET665lp, Chroma Technology) and imaged on an electron-multiplying charge-coupled device (EMCCD) camera (Andor iXon Ultra 897) or sCMOS camera (Andor Zyla 4.2) without further magnification, resulting in an effective pixel size of 160 nm (EMCCD) or 130 nm (sCMOS after 2×2 binning). Our custom TIRF setup was used for Figures 1d and 2f (EMCCD). Spinning Disk Confocal Setup: DNA-PAINT imaging of RNA-FISH samples was performed using an Andor Dragonfly Spinning Disk Confocal system (Andor) based on an inverted Nikon Eclipse Ti2 microscope (Nikon Instruments) with the Perfect Focus System, using an oil immersion objective (Plan Apo 100×, NA 1.45, Oil). For excitation, a 561 nm laser (2 W, MPB) was used. The laser beam was passed through a beam conditioning unit (Andor Borealis) for reshaping the beam from a Gaussian profile to a flat top profile. Next, the beam was coupled into the Andor Dragonfly spinning disk unit, passed through the multi-pinhole disk with a pinhole size of 40 µm and from there coupled into the objective lens. Excitation and emission light was spectrally split using a beam splitter (CR-DFLY-DMQD-01). Fluorescence light was spectrally filtered with an emission filter (TR-DFLY-F600-050) and imaged on an sCMOS camera (Andor Zyla 4.2 PLUS) without further magnification, resulting in an effective pixel size of 130 nm (sCMOS after 2×2 binning). The field of view was 1024 × 1024 pixels which is equivalent to 133.12 µm × 133.12 µm when taking the pixel size into account. The disk speed was set to 6000 rpm and an excitation field stop of 13.3mm × 13.3mm was applied. The Spinning Disk Confocal setup was used to acquire the image in **Figure 2b**.

Imaging conditions

Figure 1d. Imaging was carried out using an imager strand concentration of 75 pM (P3-Cy3B). 50,000 frames were acquired using the EMCCD camera at 30 ms integration time with the EM gain set to 300, the pre-amp gain set to 3, and the readout bandwidth set to 17 MHz. Laser power (@561 nm) was set to 2.5 mW (measured before the back focal plane (BFP) of the objective).

Figure 1f. Images were acquired with an imager strand concentration of 2 nM (P3-Cy3B imager). 150,000 frames were acquired using the EMCCD camera at 30 ms integration time with the EM gain set to 300, the pre-amp gain set to 3, and the readout bandwidth set to 17 MHz. Laser power (@561 nm) was set to 500 mW (measured at the back focal plane (BFP) of the objective).

Figure 2b. DNA-PAINT microscopy was carried out using 10 nM of P3-Cy3B in imaging buffer. 40,000 frames were acquired using the EMCCD camera at 200 ms integration time and a readout bandwidth of 540 MHz. Laser power (@560 nm) was set to 500 mW resulting in a power of 18.3 mW at the sample plane. This can be translated to an intensity of 103.27 W/cm^2 at the sample plane.

Figure 2f. DNA-PAINT imaging of protein samples was carried out using the following imager strands: P12-Cy3B (250 pM) and P13-Cy3B (50 pM) in imaging buffer. 80,000 frames were acquired using the EMCCD camera at 30 ms integration time with the EM gain set to 300, the pre-amp gain set to 3, and the readout mode to 17 MHz. Laser power (@561 nm) was set to 8 mW (measured before the back focal plane (BFP) of the objective).

Figure 3c. Imaging was carried out using the following imager strands: P1-Atto655 (20 nM), P2-Cy3B (20 nM) and P3- Atto488 (20 nM), in Buffer B. 15,000 frames were acquired using the EMCCD camera at 100 ms integration time with the EM gain set to 300, the pre-amp gain set to 3, and the readout mode to 17 MHz. Laser power was set to ~25 mW (@488 nm), ~30 mW (@561 nm), and ~30 mW (@642 nm, all measured before the back focal plane (BFP) of the objective).

For all imager strand sequences see **Supplementary Table 1**.

Image analysis

Raw fluorescence data was subjected to spot-finding and subsequent super-resolution reconstruction using the 'Picasso' software package[3].

Analysis of DNA origami data

Automated structure selection: After super-resolution reconstruction, structures were automatically selected using Picasso's 'Pick similar' function with the following settings: Pick radius: 320 nm; Standard deviation: 2.

Filtering: After automated selection, picked 'spots' were further processed in order to remove unspecific binding events from specific ones originating from DNA origami locations. To achieve this, we implemented a multi-step filtering procedure. First, in order to remove non-repetitive binding events (e.g. imager strands non-specifically adsorbing to the surface), we fitted the mean frame value of binding events (from all picked spots) throughout the whole image acquisition. The rationale behind this step is that repetitive, correct picks (i.e. containing DNA origami structures) will yield a mean frame value of roughly half the number of total frames in the acquisition (gaussian distributed), while non-repetitive events will in most cases not last throughout the whole image acquisition time frame, leading to a mean frame value that is outside this distribution. We chose the mean of the distribution and set a cut-off value at +/- two times the standard deviation for filtering. Next, to also filter out structures with a non-repetitive blinking behavior, but with most events occurring around the mean frame value, we plotted the standard deviation of the mean frame values and used a cut-off value of 2000, and all data below this threshold were disregarded. (see **Supplementary Figures 3** and **4** for results).

Cluster Analysis: After filtering, the data was analyzed using an HDBSCAN[6] clustering algorithm. 'Min_cluster_size' was set to 15, and 'min_samples' was set to 1, in the case of the four origami species (**Supplementary Figure 5 and 6**), and to 20 and 3, respectively, in the case of the 4-corner origami structures (**Supplementary Figures 7** and **8**).

Barcode Identification of 124 origami structures: First, all structures from all three acquisition rounds were aligned. Every structure exhibits a distinct kinetic blinking information in each of the three channels. This information was extracted for each spectral channel. The distribution of the number of binding events in each channel shows four separated clusters (see **Figure 3b**). After assigning every picked structure to one of the clusters in each channel, barcodes were identified.

Analysis of RNA-FISH data

Single mRNA species were manually selected using Picasso's pick tool with a pick diameter of 520 nm. Kinetic information was extracted as for the DNA origami case. Localizations were linked allowing a gap size of 2 frames between localizations to obtain a list of single binding events. The total number of binding events calculated from each structure was plotted to obtain a histogram of binding frequencies.

Analysis of protein data

Approximately 200 protein clusters were manually selected using Picasso's pick tool with a pick diameter of 240 nm. Kinetic information was extracted as for the DNA origami case. Localizations were linked allowing a gap size of 15 frames between localizations to obtain a list of single binding events. A mean binding time (i.e. blinking duration) was calculated from all events per pick.

Supplementary Figures

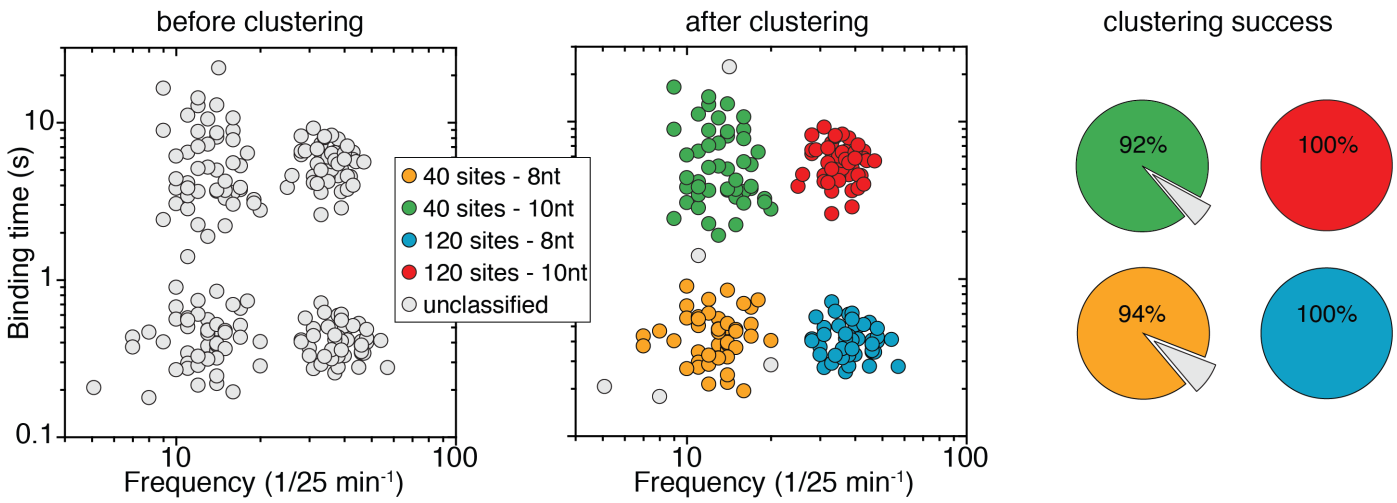

Supplementary Figure 1 | Cluster detection in simulated data. Data points from four individual stochastic binding simulations (for details see Online Methods) were clustered using HDBSCAN[6]. Data points plotted according to binding time and blinking frequency before clustering (**left**), and data plotted after clustering (**middle**). Individual colors were assigned to each of the resulting four populations. As each population was simulated individually, by comparing the results of the clustering algorithm to the original data, we were able to acquire the success rate of the clustering algorithm we used. The clustering resulted in a positive assignment rate of more than 92% in the case of all four populations (**right**).

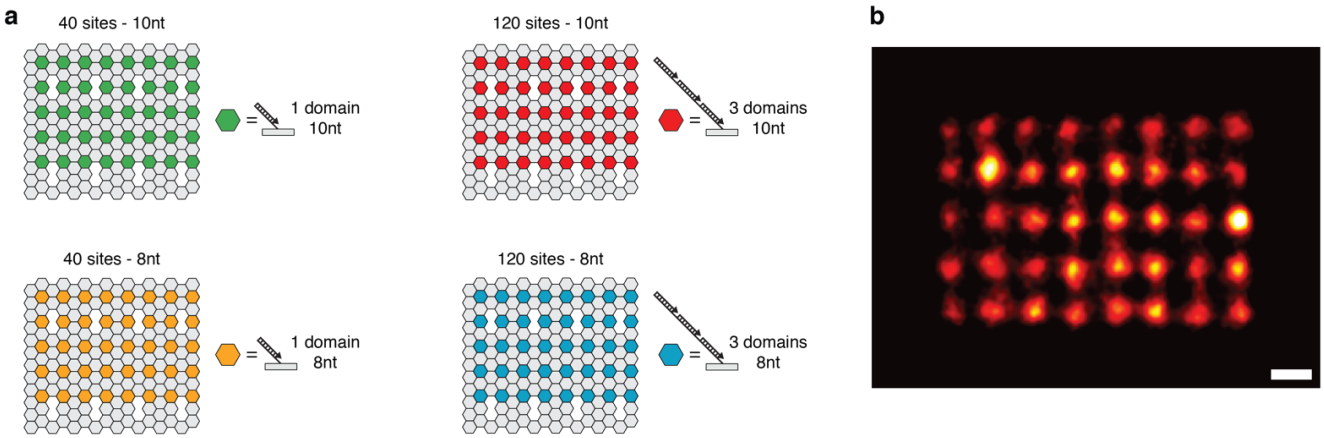

Supplementary Figure 2 | DNA origami designs for binding duration and frequency modulation. (**a**) Four DNA origami structures with different numbers and lengths of DNA-PAINT docking sites. Structures represented with green contain 40 binding domains of 10 nucleotide length each, while structures represented with yellow contain 40 binding sites, each 8 nucleotides long. Red and blue DNA origami structures were also modified at 40 positions, with each modification consisting of three sequential binding domains, resulting in a total of 120 binding sites on each structure. Red structures have 10 nucleotide long binding domains, while blue structures have 8 nucleotide long binding domains. (**b**) Super-resolved sum image of DNA origami clearly reveals the correct formation of the structures by showing all 40 binding sites, spaced 10 nm apart. Scale bar: 10 nm.

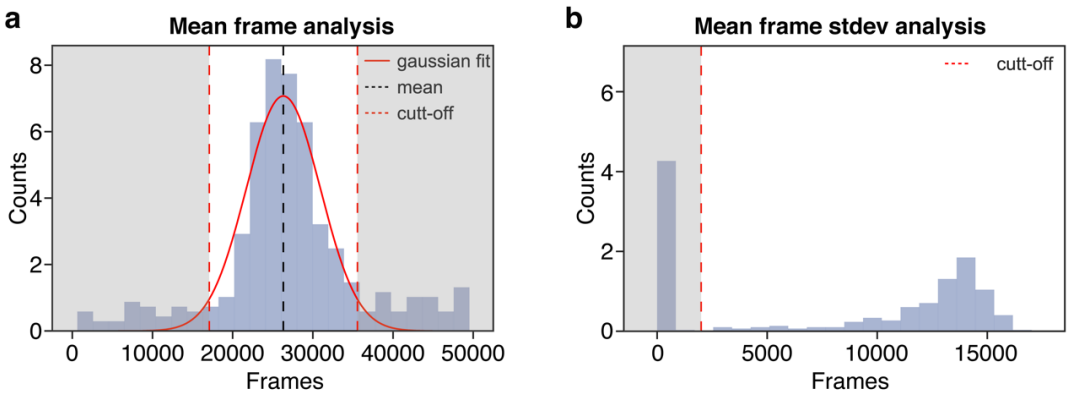

Supplementary Figure 3 | Filtering DNA origami data prior to clustering. (**a**) Resulting mean frame analysis (see Online Methods for description). Picks are rejected (gray) based on the following metric: More than 2× standard deviation of the mean. (**b**) For filtering of structures that show non-repetitive binding, however whose bindings are clustered around the mean frame, we plotted the standard deviation of the mean frame. Using a cut-off value of 2000 (red dashed line) all data below this threshold were disregarded (gray).

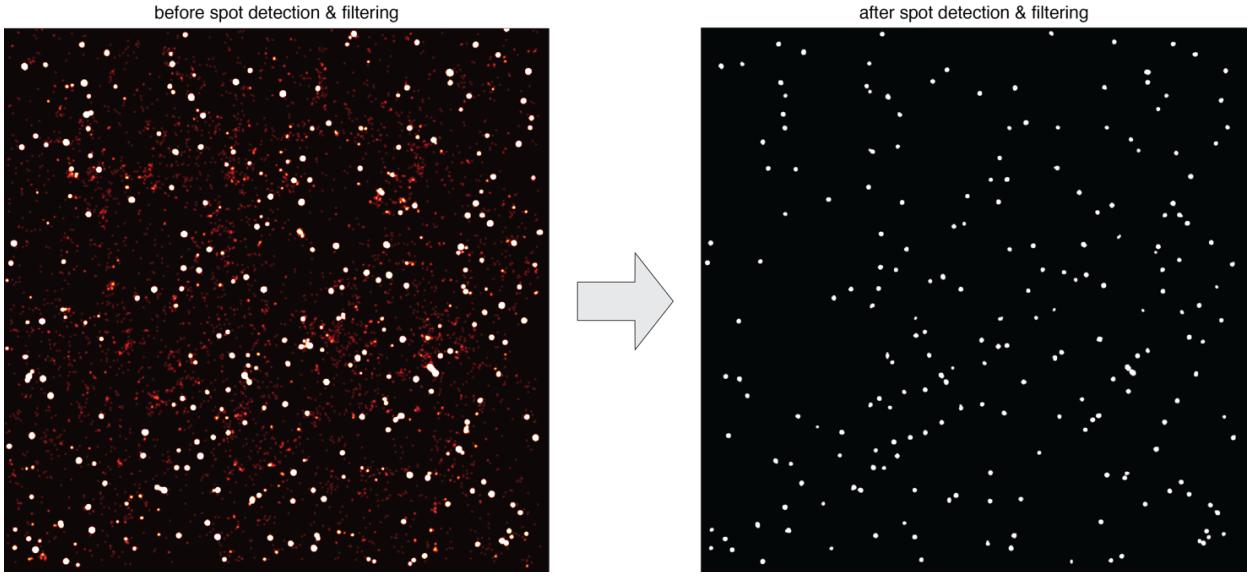

Supplementary Figure 4 | DNA-PAINT images of DNA origami before and after filtering. All initially identified localizations were rendered using Picasso Render, which was subsequently used for spot detection and picking of structures. (**left**). We rendered the same dataset after we ran all localizations from the picked spots through our filtering system (**Supplementary Figure 3** and Online Methods). Background noise and unspecific blinking events are filtered out, and no longer appear in the newly rendered image (**right**). Image size: 40.96 µm.

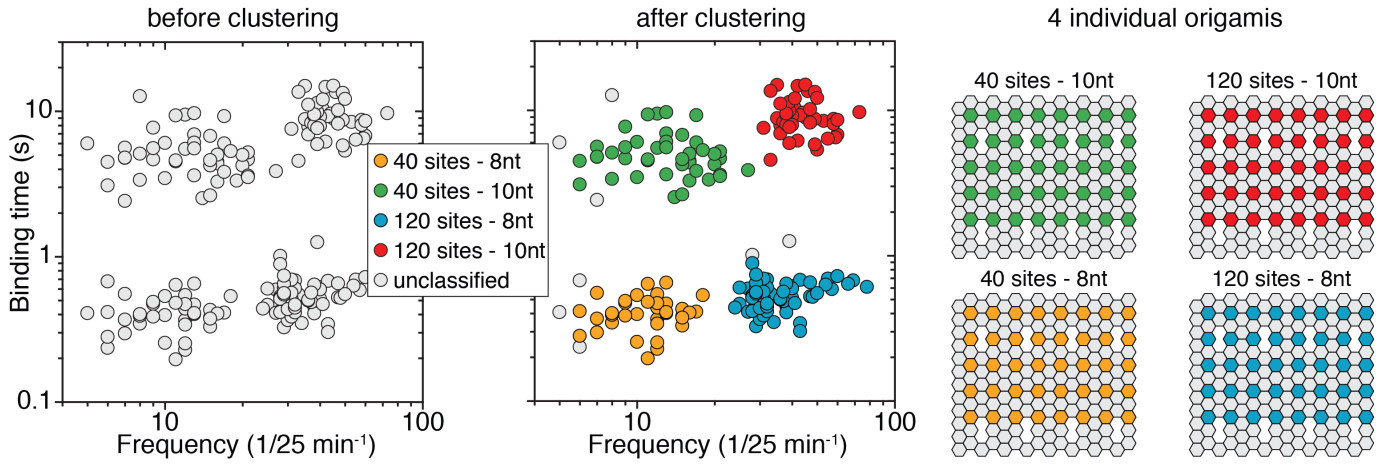

Supplementary Figure 5 | Cluster detection in DNA origami data. Data from measurements of four different DNA origami samples displaying 40 binding sites of 8 nt and 10 nt, and 120 binding sites of 8 nt and 10 nt long binding sites were acquired and plotted according to their blinking frequency and blinking duration (**left**). Clustering the data using the HDBSCAN[6] algorithm resulted in four populations, to which we assigned distinct colors (green, yellow, red and blue). Using the assigned colors, we re-plotted each data point, in the color it was assigned. Grey dots indicate structures that could not be assigned to any of the four populations (**center**). Green: 40 domains, 10 nt; Yellow: 40 domains, 8 nt; Red: 120 domains, 10 nt, Blue: 120 domains 8nt (**right**).

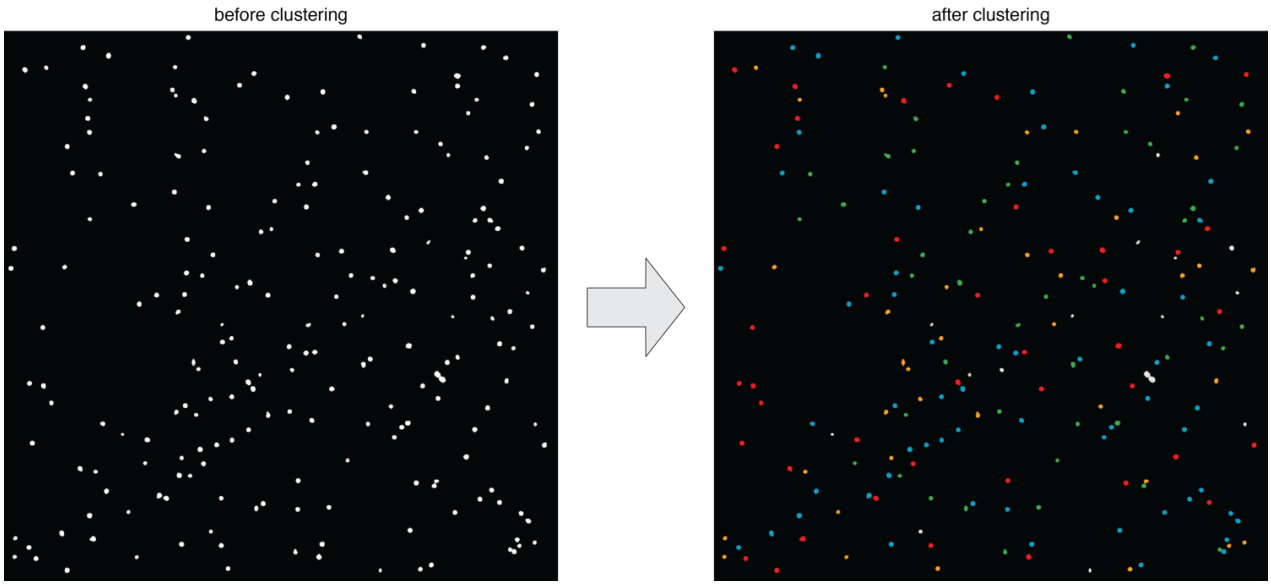

Supplementary Figure 6 | DNA origami data before and after cluster identification. After spot detection and filtering, all DNA origami structures (seen as white spots in the left image) were clustered according to their blinking behavior (**Supplementary Figure 5**) (**left**). We then re-rendered the image assigning a pseudo-color for each spot, according to the population it belonged to - green, yellow, red or blue (**right**). Image size: 40.96 µm.

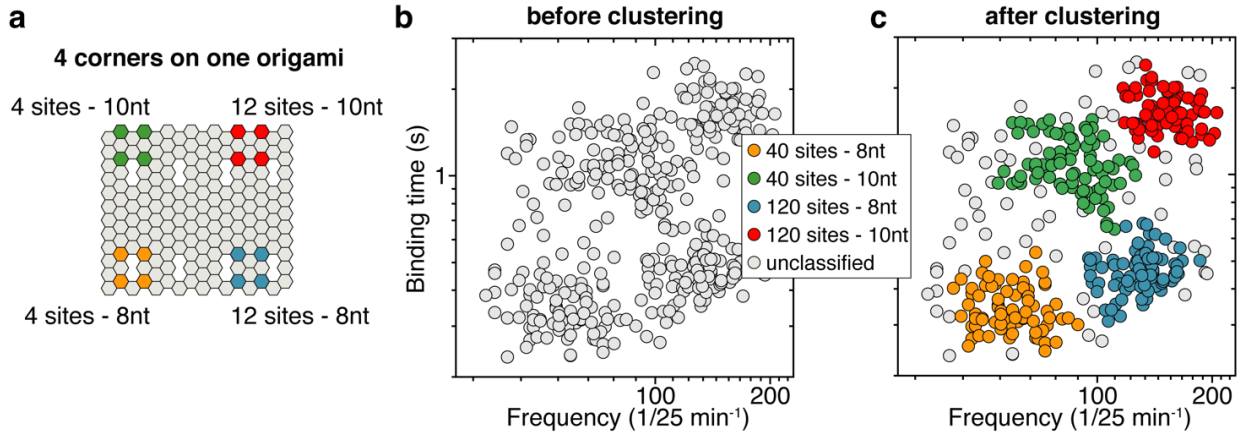

Supplementary Figure 7 | Clustering results for four-corner DNA origami. (**a**) We designed a DNA origami structure that contained all four previously used binding site designs, one in each corner. Four DNA origami staples were modified at each corner, resulting in the following designs: 4 single domains with a 10 nt binding site, (green), 4 single domains with an 8 nt binding site, 4 staples with 4×3 (12) domains with 10nt binding sites (red), and 4 staples with 4×3 (12) domains with 8 nt binding sites (blue). (**b**) These origami structures were imaged using DNA-PAINT, and the binding times and binding frequencies were plotted, after filtering, as in the case of the four separate origami species. (**c**) We then clustered the data using HDBSCAN and re-plotted them, marking the points with the color of the cluster they were assigned to. Grey dots were not assigned to any cluster.

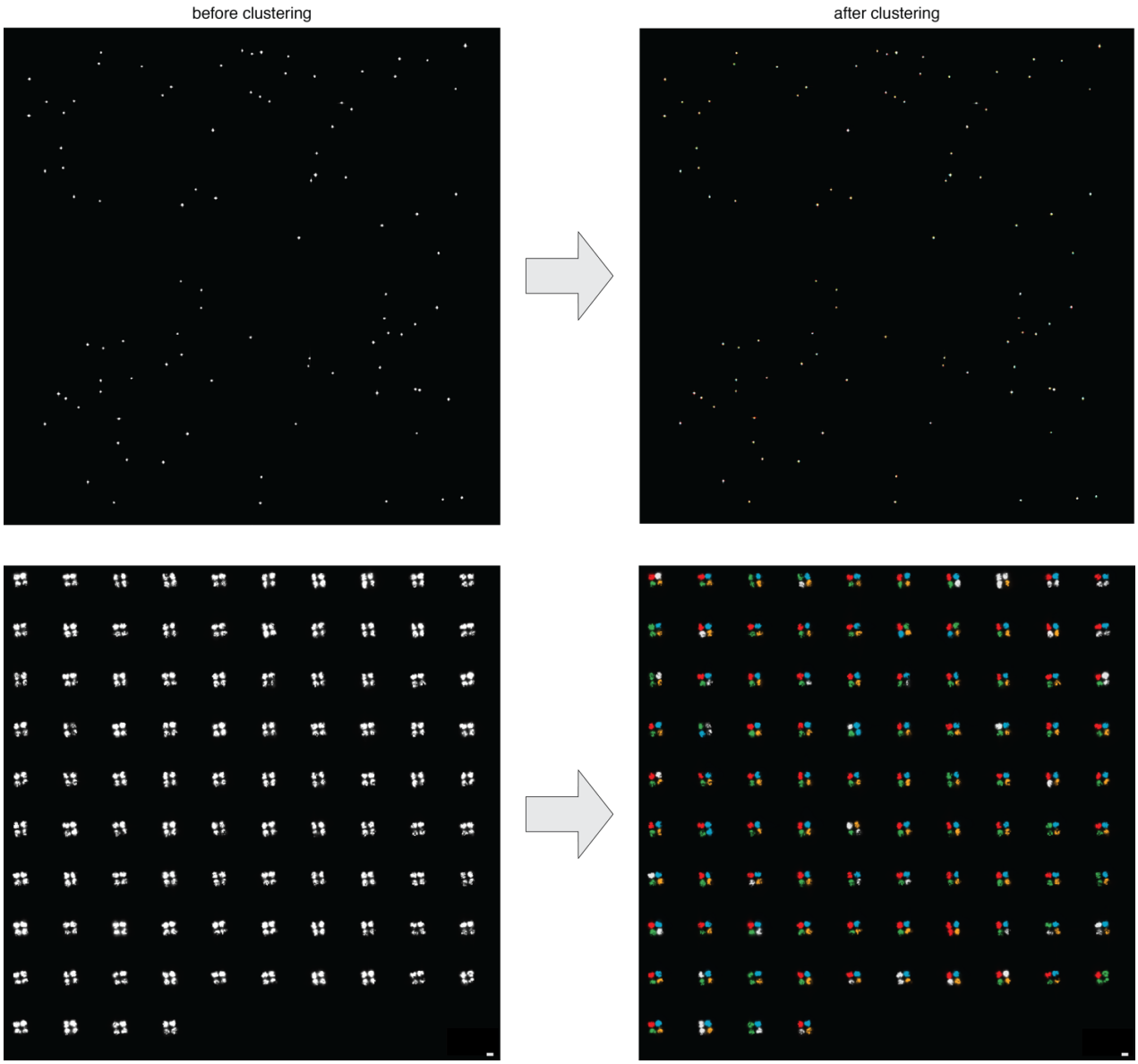

Supplementary Figure 8 | Four-corner DNA origami structures before and after cluster identification. Images of four corner DNA origami structures on coverslip before and after clustering of the four corners of each structure (**top**). A higher magnification image of picked origami structures rendered in ordered succession, before and after clustering (**bottom**). Each corner was then picked individually, and all localizations were run through the HDBSCAN algorithm. Results of the clustering algorithm can be seen on the bottom right image, with the identified corners shown in color. As expected we were able to assign the four corners to the four different kinetic populations according to their blinking behavior, even with the lower number of binding sites. Scale bars: 40 nm.

Supplementary Figure 9 | Agarose gels of the 124 individual DNA origami structures. Fluorescent scan of the agarose gels of the 124 individual frequency barcodes (1.5% agarose, 1×TAE buffer + 10mM $MgCl_2$, 1× SybrSafe stain). All individual monomer bands (monomer band for barcode ID = 1 is indicated by red arrow) were physically extracted from the gel and the structures purified using Freeze'N'Squeeze spin columns. L: Ladder, Sc: Scaffold strands.

Supplementary Tables

Supplementary Table 1 | DNA-PAINT imager strands

Name	Sequence	Dye on 3′-end
P1	5′-CTAGATGTAT-3′	Atto655
P2	5′-TATGTAGATC-3′	Cy3B
P3	5′-GTAATGAAGA-3′	Atto488 or Cy3B
P12	5′-GCTCTAACTA-3′	Cy3B
P13	5′-CCTTCTCTAT-3′	Cy3B

Supplementary Table 2 | Core staple strands for rectangular DNA origami

Position	Name	Sequence
A1	21[32]23[31]BLK	TTTTCACTCAAAGGGCGAAAAACCATCACC
B1	23[32]22[48]BLK	CAAATCAAGTTTTTTGGGGTCGAAACGTGGA
C1	21[56]23[63]BLK	AGCTGATTGCCCTTCAGAGTCCACTATTAAAGGGTGCCGT
D1	23[64]22[80]BLK	AAAGCACTAAATCGGAACCCTAATCCAGTT
E1	21[96]23[95]BLK	AGCAAGCGTAGGGTTGAGTGTTGTAGGGAGCC
F1	23[96]22[112]BLK	CCCGATTTAGAGCTTGACGGGGAAAAAGAATA
G1	21[120]23[127]BLK	CCCAGCAGGCGAAAAATCCCTTATAAATCAAGCCGGCG
H1	21[160]22[144]BLK	TCAATATCGAACCTCAAATATCAATTCCGAAA
I1	23[128]23[159]BLK	AACGTGGCGAGAAAGGAAGGGAAACCAGTAA
J1	23[160]22[176]BLK	TAAAAGGGACATTCTGGCCAACAAAGCATC
K1	21[184]23[191]BLK	TCAACAGTTGAAAGGAGCAAATGAAAAATCTAGAGATAGA
L1	23[192]22[208]BLK	ACCCTTCTGACCTGAAAGCGTAAGACGCTGAG
M1	21[224]23[223]BLK	CTTTAGGGCCTGCAACAGTGCCAATACGTG
N1	23[224]22[240]BLK	GCACAGACAATATTTTTGAATGGGGTCAGTA
O1	21[248]23[255]BLK	AGATTAGAGCCGTCAAAAAACAGAGGTGAGGCCTATTAGT
P1	23[256]22[272]BLK	CTTTAATGCGCGAACTGATAGCCCCACCAG
A2	19[32]21[31]BLK	GTCGACTTCGGCCAACGCGCGGGGTTTTTC
B2	22[47]20[48]BLK	CTCCAACGCAGTGAGACGGGCAACCAGCTGCA
D2	22[79]20[80]BLK	TGGAACAACCGCCTGGCCCTGAGGCCCGCT
E2	19[96]21[95]BLK	CTGTGTGATTGCGTTGCGCTCACTAGAGTTGC
F2	22[111]20[112]BLK	GCCCGAGAGTCCACGCTGGTTTGCAGCTAACT
H2	19[160]20[144]BLK	GCAATTCACATATTCCTGATTATCAAAGTGTA
I2	22[143]21[159]BLK	TCGGCAAATCCTGTTTGATGGTGGACCCTCAA
J2	22[175]20[176]BLK	ACCTTGCTTGGTCAGTTGGCAAAGAGCGGA
L2	22[207]20[208]BLK	AGCCAGCAATTGAGGAAGGTTATCATCATTTT

M2	19[224]21[223]BLK	CTACCATAGTTTGAGTAACATTTAAAATAT
N2	22[239]20[240]BLK	TTAACACCAGCACTAACAACTAATCGTTATTA
P2	22[271]20[272]BLK	CAGAAGATTAGATAATACATTTGTCGACAA
A3	17[32]19[31]BLK	TGCATCTTTCCCAGTCACGACGGCCTGCAG
B3	20[47]18[48]BLK	TTAATGAACTAGAGGATCCCCGGGGGGTAACG
D3	20[79]18[80]BLK	TTCCAGTCGTAATCATGGTCATAAAAGGGG
E3	17[96]19[95]BLK	GCTTTCCGATTACGCCAGCTGGCGGCTGTTTC
F3	20[111]18[112]BLK	CACATTAAAATTGTTATCCGCTCATGCGGGCC
H3	17[160]18[144]BLK	AGAAAACAAAGAAGATGATGAAACAGGCTGCG
I3	20[143]19[159]BLK	AAGCCTGGTACGAGCCGGAAGCATAGATGATG
J3	20[175]18[176]BLK	ATTATCATTCAATATAATCCTGACAATTAC
L3	20[207]18[208]BLK	GCGGAACATCTGAATAATGGAAGGTACAAAAT
M3	17[224]19[223]BLK	CATAAATCTTTGAATACCAAGTGTTAGAAC
N3	20[239]18[240]BLK	ATTTTAAAATCAAAATTATTTGCACGGATTCG
P3	20[271]18[272]BLK	CTCGTATTAGAAATTGCGTAGATACAGTAC
A4	15[32]17[31]BLK	TAATCAGCGGATTGACCGTAATCGTAACCG
B4	18[47]16[48]BLK	CCAGGGTTGCCAGTTTGAGGGGACCCGTGGGA
C4	15[64]18[64]BLK	GTATAAGCCAACCCGTCGGATTCTGACGACAGTATCGGCCGCAAGGCG
D4	18[79]16[80]BLK	GATGTGCTTCAGGAAGATCGCACAATGTGA
E4	15[96]17[95]BLK	ATATTTTGGCTTTCATCAACATTATCCAGCCA
F4	18[111]16[112]BLK	TCTTCGCTGCACCGCTTCTGGTGCGGCCTTCC
G4	15[128]18[128]BLK	TAAATCAAAATAATTCGCGTCTCGGAAACCAGGCAAAGGGAAGG
H4	15[160]16[144]BLK	ATCGCAAGTATGTAAATGCTGATGATAGGAAC
I4	18[143]17[159]BLK	CAACTGTTGCGCCATTCGCCATTCAAACATCA
J4	18[175]16[176]BLK	CTGAGCAAAAATTAATTACATTTTGGGTTA
K4	15[192]18[192]BLK	TCAAATATAACCTCCGGCTTAGGTAACAATTTCATTTGAAGGCGAATT
L4	18[207]16[208]BLK	CGCGCAGATTACCTTTTTTAATGGGAGAGACT
M4	15[224]17[223]BLK	CCTAAATCAAAATCATAGGTCTAAACAGTA
N4	18[239]16[240]BLK	CCTGATTGCAATATATGTGAGTGATCAATAGT
O4	15[256]18[256]BLK	GTGATAAAAAGACGCTGAGAAGAGATAACCTTGCTTCTGTTCGGGAGA
P4	18[271]16[272]BLK	CTTTTACAAAATCGTCGCTATTAGCGATAG
A5	13[32]15[31]BLK	AACGCAAAATCGATGAACGGTACCGGTTGA
B5	16[47]14[48]BLK	ACAAACGGAAAAGCCCCAAAAACACTGGAGCA
C5	13[64]15[63]BLK	TATATTTTGTCATTGCCTGAGAGTGGAAGATT
D5	16[79]14[80]BLK	GCGAGTAAAAATATTTAAATTGTTACAAAG
E5	13[96]15[95]BLK	TAGGTAAACTATTTTTGAGAGATCAAACGTTA
F5	16[111]14[112]BLK	TGTAGCCATTAAAATTCGCATTAAATGCCGGA
G5	13[128]15[127]BLK	GAGACAGCTAGCTGATAAATTAATTTTTGT

12

H5	13[160]14[144]BLK	GTAATAAGTTAGGCAGAGGCATTTATGATATT
I5	16[143]15[159]BLK	GCCATCAAGCTCATTTTTTAACCACAAATCCA
J5	16[175]14[176]BLK	TATAACTAACAAAGAACGCGAGAACGCCAA
K5	13[192]15[191]BLK	GTAAAGTAATCGCCATATTTAACAAAACTTTT
L5	16[207]14[208]BLK	ACCTTTTTATTTTAGTTAATTTCATAGGGCTT
M5	13[224]15[223]BLK	ACAACATGCCAACGCTCAACAGTCTTCTGA
N5	16[239]14[240]BLK	GAATTTATTTAATGGTTTGAAATATTCTTACC
O5	13[256]15[255]BLK	GTTTATCAATATGCGTTATACAAACCGACCGT
P5	16[271]14[272]BLK	CTTAGATTTAAGGCGTTAAATAAAGCCTGT
A6	11[32]13[31]BLK	AACAGTTTTGTACCAAAAACATTTTATTTC
B6	14[47]12[48]BLK	AACAAGAGGGATAAAAATTTTTAGCATAAAGC
C6	11[64]13[63]BLK	GATTTAGTCAATAAAGCCTCAGAGAACCCTCA
D6	14[79]12[80]BLK	GCTATCAGAAATGCAATGCCTGAATTAGCA
E6	11[96]13[95]BLK	AATGGTCAACAGGCAAGGCAAAGAGTAATGTG
F6	14[111]12[112]BLK	GAGGGTAGGATTCAAAAGGGTGAGACATCCAA
G6	11[128]13[127]BLK	TTTGGGGATAGTAGTAGCATTAAAAGGCCG
H6	11[160]12[144]BLK	CCAATAGCTCATCGTAGGAATCATGGCATCAA
I6	14[143]13[159]BLK	CAACCGTTTCAAATCACCATCAATTCGAGCCA
J6	14[175]12[176]BLK	CATGTAATAGAATATAAAGTACCAAGCCGT
K6	11[192]13[191]BLK	TATCCGGTCTCATCGAGAACAAGCGACAAAAG
L6	14[207]12[208]BLK	AATTGAGAATTCTGTCCAGACGACTAAACCAA
M6	11[224]13[223]BLK	GCGAACCTCCAAGAACGGGTATGACAATAA
N6	14[239]12[240]BLK	AGTATAAAGTTCAGCTAATGCAGATGTCTTTC
O6	11[256]13[255]BLK	GCCTTAAACCAATCAATAATCGGCACGCGCCT
P6	14[271]12[272]BLK	TTAGTATCACAATAGATAAGTCCACGAGCA
A7	9[32]11[31]BLK	TTTACCCCAACATGTTTTAAATTTCCATAT
B7	12[47]10[48]BLK	TAAATCGGGATTCCCAATTCTGCGATATAATG
C7	9[64]11[63]BLK	CGGATTGCAGAGCTTAATTGCTGAAACGAGTA
D7	12[79]10[80]BLK	AAATTAAGTTGACCATTAGATACTTTTGCG
E7	9[96]11[95]BLK	CGAAAGACTTTGATAAGAGGTCATATTTCGCA
F7	12[111]10[112]BLK	TAAATCATATAACCTGTTTAGCTAACCTTTAA
G7	9[128]11[127]BLK	GCTTCAATCAGGATTAGAGAGTTATTTTCA
H7	9[160]10[144]BLK	AGAGAGAAAAAAATGAAAATAGCAAGCAAACT
I7	12[143]11[159]BLK	TTCTACTACGCGAGCTGAAAAGGTTACCGCGC
J7	12[175]10[176]BLK	TTTTATTTAAGCAAATCAGATATTTTTTGT
K7	9[192]11[191]BLK	TTAGACGGCCAAATAAGAAACGATAGAAGGCT
L7	12[207]10[208]BLK	GTACCGCAATTCTAAGAACGCGAGTATTATTT
M7	9[224]11[223]BLK	AAAGTCACAAAATAAACAGCCAGCGTTTTA

13

N7	12[239]10[240]BLK	CTTATCATTCCCGACTTGCGGGAGCCTAATTT
O7	9[256]11[255]BLK	GAGAGATAGAGCGTCTTTCCAGAGGTTTTGAA
P7	12[271]10[272]BLK	TGTAGAAATCAAGATTAGTTGCTCTTACCA
A8	7[32]9[31]BLK	TTTAGGACAAATGCTTTAAACAATCAGGTC
B8	10[47]8[48]BLK	CTGTAGCTTGACTATTATAGTCAGTTCATTGA
C8	7[56]9[63]BLK	ATGCAGATACATAACGGGAATCGTCATAAATAAAGCAAAG
D8	10[79]8[80]BLK	GATGGCTTATCAAAAAGATTAAGAGCGTCC
E8	7[96]9[95]BLK	TAAGAGCAAATGTTTAGACTGGATAGGAAGCC
F8	10[111]8[112]BLK	TTGCTCCTTTCAAATATCGCGTTTGAGGGGGT
G8	7[120]9[127]BLK	CGTTTACCAGACGACAAAGAAGTTTTGCCATAATTCGA
H8	7[160]8[144]BLK	TTATTACGAAGAACTGGCATGATTGCGAGAGG
I8	10[143]9[159]BLK	CCAACAGGAGCGAACCAGACCGGAGCCTTTAC
J8	10[175]8[176]BLK	TTAACGTCTAACATAAAAACAGGTAACGGA
K8	7[184]9[191]BLK	CGTAGAAAATACATACCGAGGAAACGCAATAAGAAGCGCA
L8	10[207]8[208]BLK	ATCCCAATGAGAATTAACTGAACAGTTACCAG
M8	7[224]9[223]BLK	AACGCAAAGATAGCCGAACAAACCCTGAAC
N8	10[239]8[240]BLK	GCCAGTTAGAGGGTAATTGAGCGCTTTAAGAA
O8	7[248]9[255]BLK	GTTTATTTTGTCACAATCTTACCGAAGCCCTTTAATATCA
P8	10[271]8[272]BLK	ACGCTAACACCCACAAGAATTGAAAATAGC
A9	5[32]7[31]BLK	CATCAAGTAAAACGAACTAACGAGTTGAGA
B9	8[47]6[48]BLK	ATCCCCCTATACCACATTCAACTAGAAAAATC
D9	8[79]6[80]BLK	AATACTGCCCAAAAGGAATTACGTGGCTCA
E9	5[96]7[95]BLK	TCATTCAGATGCGATTTTAAGAACAGGCATAG
F9	8[111]6[112]BLK	AATAGTAAACACTATCATAACCCTCATTGTGA
H9	5[160]6[144]BLK	GCAAGGCCTCACCAGTAGCACCATGGGCTTGA
I9	8[143]7[159]BLK	CTTTTGCAGATAAAAACCAAAATAAAGACTCC
J9	8[175]6[176]BLK	ATACCCAACAGTATGTTAGCAAATTAGAGC
L9	8[207]6[208]BLK	AAGGAAACATAAAGGTGGCAACATTATCACCG
M9	5[224]7[223]BLK	TCAAGTTTCATTAAAGGTGAATATAAAAGA
N9	8[239]6[240]BLK	AAGTAAGCAGACACCACGGAATAATATTGACG
P9	8[271]6[272]BLK	AATAGCTATCAATAGAAAATTCAACATTCA
A10	3[32]5[31]BLK	AATACGTTTGAAAGAGGACAGACTGACCTT
B10	6[47]4[48]BLK	TACGTTAAAGTAATCTTGACAAGAACCGAACT
D10	6[79]4[80]BLK	TTATACCACCAAATCAACGTAACGAACGAG
E10	3[96]5[95]BLK	ACACTCATCCATGTTACTTAGCCGAAAGCTGC
F10	6[111]4[112]BLK	ATTACCTTTGAATAAGGCTTGCCCAAATCCGC
H10	3[160]4[144]BLK	TTGACAGGCCACCACCAGAGCCGCGATTTGTA
I10	6[143]5[159]BLK	GATGGTTTGAACGAGTAGTAAATTTACCATTA

14

J10	6[175]4[176]BLK	CAGCAAAAGGAAACGTCACCAATGAGCCGC
L10	6[207]4[208]BLK	TCACCGACGCACCGTAATCAGTAGCAGAACCG
M10	3[224]5[223]BLK	TTAAAGCCAGAGCCGCCACCCTCGACAGAA
N10	6[239]4[240]BLK	GAAATTATTGCCTTTAGCGTCAGACCGGAACC
P10	6[271]4[272]BLK	ACCGATTGTCGGCATTTTCGGTCATAATCA
A11	1[32]3[31]BLK	AGGCTCCAGAGGCTTTGAGGACACGGGTAA
B11	4[47]2[48]BLK	GACCAACTAATGCCACTACGAAGGGGGTAGCA
C11	1[64]4[64]BLK	TTTATCAGGACAGCATCGGAACGACACCAACCTAAAACGAGGTCAATC
D11	4[79]2[80]BLK	GCGCAGACAAGAGGCAAAAGAATCCCTCAG
E11	1[96]3[95]BLK	AAACAGCTTTTTGCGGGATCGTCAACACTAAA
F11	4[111]2[112]BLK	GACCTGCTCTTTGACCCCCAGCGAGGGAGTTA
G11	1[128]4[128]BLK	TGACAACTCGCTGAGGCTTGCATTATACCAAGCGCGATGATAAA
H11	1[160]2[144]BLK	TTAGGATTGGCTGAGACTCCTCAATAACCGAT
I11	4[143]3[159]BLK	TCATCGCCAACAAAGTACAACGGACGCCAGCA
J11	4[175]2[176]BLK	CACCAGAAAGGTTGAGGCAGGTCATGAAAG
K11	1[192]4[192]BLK	GCGGATAACCTATTATTCTGAAACAGACGATTGGCCTTGAAGAGCCAC
L11	4[207]2[208]BLK	CCACCCTCTATTCACAAACAAATACCTGCCTA
M11	1[224]3[223]BLK	GTATAGCAAACAGTTAATGCCCAATCCTCA
N11	4[239]2[240]BLK	GCCTCCCTCAGAATGGAAAGCGCAGTAACAGT
O11	1[256]4[256]BLK	CAGGAGGTGGGGTCAGTGCCTTGAGTCTCTGAATTTACCGGGAACCAG
P11	4[271]2[272]BLK	AAATCACCTTCCAGTAAGCGTCAGTAATAA
A12	0[47]1[31]BLK	AGAAAGGAACAACTAAAGGAATTCAAAAAAA
B12	2[47]0[48]BLK	ACGGCTACAAAAGGAGCCTTTAATGTGAGAAT
C12	0[79]1[63]BLK	ACAACTTTCAACAGTTTCAGCGGATGTATCGG
D12	2[79]0[80]BLK	CAGCGAAACTTGCTTTCGAGGTGTTGCTAA
E12	0[111]1[95]BLK	TAAATGAATTTTCTGTATGGGATTAATTTCTT
F12	2[111]0[112]BLK	AAGGCCGCTGATACCGATAGTTGCGACGTTAG
G12	0[143]1[127]BLK	TCTAAAGTTTTGTCGTCTTTCCAGCCGACAA
H12	0[175]0[144]BLK	TCCACAGACAGCCCTCATAGTTAGCGTAACGA
I12	2[143]1[159]BLK	ATATTCGGAACCATCGCCCACGCAGAGAAGGA
J12	2[175]0[176]BLK	TATTAAGAAGCGGGGTTTTGCTCGTAGCAT
K12	0[207]1[191]BLK	TCACCAGTACAAACTACAACGCCTAGTACCAG
L12	2[207]0[208]BLK	TTTCGGAAGTGCCGTCGAGAGGGTGAGTTTCG
M12	0[239]1[223]BLK	AGGAACCCATGTACCGTAACACTTGATATAA
N12	2[239]0[240]BLK	GCCCGTATCCGGAATAGGTGTATCAGCCCAAT
O12	0[271]1[255]BLK	CCACCCTCATTTTCAGGGATAGCAACCGTACT
P12	2[271]0[272]BLK	GTTTTAACTTAGTACCGCCACCCAGAGCCA

15

Supplementary Table 3 | Biotinylated staple strands

No	Pos	Name	Sequence	Modification
1	C02	18[63]20[56]BIOTIN	ATTAAGTTTACCGAGCTCGAATTCGGGAAACCTGTCGTGC	5'-BT
2	C09	4[63]6[56]BIOTIN	ATAAGGGAACCGGATATTCATTACGTCAGGACGTTGGGAA	5'-BT
3	G02	18[127]20[120]BIOTIN	GCGATCGGCAATTCCACACAACAGGTGCCTAATGAGTG	5'-BT
4	G09	4[127]6[120]BIOTIN	TTGTGTCGTGACGAGAAACACCAAATTTCAACTTTAAT	5'-BT
5	K02	18[191]20[184]BIOTIN	ATTCATTTTTGTTTGGATTATACTAAGAAACCACCAGAAG	5'-BT
6	K09	4[191]6[184]BIOTIN	CACCCTCAGAAACCATCGATAGCATTGAGCCATTTGGGAA	5'-BT
7	O02	18[255]20[248]BIOTIN	AACAATAACGTAAAACAGAAATAAAAATCCTTTGCCCGAA	5'-BT
8	O09	4[255]6[248]BIOTIN	AGCCACCACTGTAGCGCGTTTTCAAGGGAGGGAAGGTAAA	5'-BT

Supplementary Table 4 | Modified staple strands for DNA origami. The underlined 3'-end sequence (same for all the modified staples) is specific for the structures with 40 domains of 8nt length. Supplementary Table 5 contains the sequences modifications corresponding to the other three DNA origami species used in the experiments.

No	Pos	Name	Sequence
1	A1	P3(40,8)_1_B3	TTAATGAACTAGAGGATCCCCGGGGGGTAACG **TTTCTTCATT**
2	A2	P3(40,8)_1_B5	ACAAACGGAAAAGCCCCAAAAACACTGGAGCATTTCTTCATT
3	A3	P3(40,8)_1_B7	TAAATCGGGATTCCCAATTCTGCGATATAATGTTTCTTCATT
4	A4	P3(40,8)_1_B9	ATCCCCCTATACCACATTCAACTAGAAAAATCTTTCTTCATT
5	A5	P3(40,8)_1_B11	GACCAACTAATGCCACTACGAAGGGGGTAGCATTTCTTCATT
6	A6	P3(40,8)_1_D3	TTCCAGTCGTAATCATGGTCATAAAAGGGGTTTCTTCATT
7	A7	P3(40,8)_1_D5	GCGAGTAAAAATATTTAAATTGTTACAAAGTTTCTTCATT
8	A8	P3(40,8)_1_D7	AAATTAAGTTGACCATTAGATACTTTTGCGTTTCTTCATT
9	A9	P3(40,8)_1_D9	AATACTGCCCAAAAGGAATTACGTGGCTCATTTCTTCATT
10	A10	P3(40,8)_1_D11	GCGCAGACAAGAGGCAAAAGAATCCCTCAGTTTCTTCATT
11	A11	P3(40,8)_1_F3	CACATTAAAATTGTTATCCGCTCATGCGGGCCTTTCTTCATT
12	A12	P3(40,8)_1_F5	TGTAGCCATTAAAATTCGCATTAAATGCCGGATTTCTTCATT
13	B1	P3(40,8)_1_F7	TAAATCATATAACCTGTTTAGCTAACCTTTAATTTCTTCATT
14	B2	P3(40,8)_1_F9	AATAGTAAACACTATCATAACCCTCATTGTGATTTCTTCATT
15	B3	P3(40,8)_1_F11	GACCTGCTCTTTGACCCCCAGCGAGGGAGTTATTTCTTCATT
16	B4	P3(40,8)_1_H3	AGAAAACAAAGAAGATGATGAAACAGGCTGCGTTTCTTCATT
17	B5	P3(40,8)_1_H5	GTAATAAGTTAGGCAGAGGCATTTATGATATTTTTCTTCATT
18	B6	P3(40,8)_1_H7	AGAGAGAAAAAAATGAAAATAGCAAGCAAACTTTTCTTCATT
19	B7	P3(40,8)_1_H9	GCAAGGCCTCACCAGTAGCACCATGGGCTTGATTTCTTCATT
20	B8	P3(40,8)_1_H11	TTAGGATTGGCTGAGACTCCTCAATAACCGATTTTCTTCATT
21	B9	P3(40,8)_2_B3	ATTATCATTCAATATAATCCTGACAATTACTTTCTTCATT
22	B10	P3(40,8)_2_B5	TATAACTAACAAAGAACGCGAGAACGCCAATTTCTTCATT
23	B11	P3(40,8)_2_B7	TTTTATTTAAGCAAATCAGATATTTTTTGTTTTCTTCATT
24	B12	P3(40,8)_2_B9	ATACCCAACAGTATGTTAGCAAATTAGAGCTTTCTTCATT

25	C1	P3(40,8)_2_B11	CACCAGAAAGGTTGAGGCAGGTCATGAAAGTTTCTTCATT
26	C2	P3(40,8)_2_D3	GCGGAACATCTGAATAATGGAAGGTACAAAATTTTCTTCATT
27	C3	P3(40,8)_2_D5	ACCTTTTTATTTTAGTTAATTTCATAGGGCTTTTTCTTCATT
28	C4	P3(40,8)_2_D7	GTACCGCAATTCTAAGAACGCGAGTATTATTTTTTCTTCATT
29	C5	P3(40,8)_2_D9	AAGGAAACATAAAGGTGGCAACATTATCACCGTTTCTTCATT
30	C6	P3(40,8)_2_D11	CCACCCTCTATTCACAAACAAATACCTGCCTATTTCTTCATT
31	C7	P3(40,8)_2_F3	ATTTTAAAATCAAAATTATTTGCACGGATTCGTTTCTTCATT
32	C8	P3(40,8)_2_F5	GAATTTATTTAATGGTTTGAAATATTCTTACCTTTCTTCATT
33	C9	P3(40,8)_2_F7	CTTATCATTCCCGACTTGCGGGAGCCTAATTTTTTCTTCATT
34	C10	P3(40,8)_2_F9	AAGTAAGCAGACACCACGGAATAATATTGACGTTTCTTCATT
35	C11	P3(40,8)_2_F11	GCCTCCCTCAGAATGGAAAGCGCAGTAACAGTTTTCTTCATT
36	C12	P3(40,8)_2_H3	CTCGTATTAGAAATTGCGTAGATACAGTACTTTCTTCATT
37	D1	P3(40,8)_2_H5	CTTAGATTTAAGGCGTTAAATAAAGCCTGTTTTCTTCATT
38	D2	P3(40,8)_2_H7	TGTAGAAATCAAGATTAGTTGCTCTTACCATTTCTTCATT
39	D3	P3(40,8)_2_H9	AATAGCTATCAATAGAAAATTCAACATTCATTTCTTCATT
40	D4	P3(40,8)_2_H11	AAATCACCTTCCAGTAAGCGTCAGTAATAATTTCTTCATT

Supplementary Table 5 | List of DNA-PAINT handles

Name	Sequence added to 3′ ends of core staples
P3-40-8nt	5′-TT-TCTTCATT-3′
P3-40-10nt	5′-TT-TCTTCATTAC-3′
P3-120-8nt	5′-TT-TCTTCATT-TT-TCTTCATT-TT-TCTTCATT-3′
P3-120-10nt	5′-TT-TCTTCATTAC-TT-TCTTCATTAC-TT-TCTTCATTAC-3′

Supplementary Table 6 | RNA-FISH probe set targeting MKI67 mRNA variant 2

No.	Name	Sequence
1	MKI67_P3Plus_120_1	gccagaagcaaatttacaactc-TT-TCTTCATTAGCG TT-TCTTCATTA-TT-TCTTCATTA
2	MKI67_P3Plus_120_2	cagtaagttgagtataatccgtTTTCTTCATTAGCGTTTCTTCATTATTTCTTCATTA
3	MKI67_P3Plus_120_3	tttgcaatgttgttttgacacaTTTCTTCATTAGCGTTTCTTCATTATTTCTTCATTA
4	MKI67_P3Plus_120_4	aattatgtaatattgcctcctgTTTCTTCATTAGCGTTTCTTCATTATTTCTTCATTA
5	MKI67_P3Plus_120_5	aataacagacccatttacttgtTTTCTTCATTAGCGTTTCTTCATTATTTCTTCATTA
6	MKI67_P3Plus_120_6	tagttattacatctccatgtttTTTCTTCATTAGCGTTTCTTCATTATTTCTTCATTA
7	MKI67_P3Plus_120_7	gactttcattttcatacctgaaTTTCTTCATTAGCGTTTCTTCATTATTTCTTCATTA
8	MKI67_P3Plus_120_8	gagaagctagatcttgagacacTTTCTTCATTAGCGTTTCTTCATTATTTCTTCATTA
9	MKI67_P3Plus_120_9	tattaggaggcaagttttcatcTTTCTTCATTAGCGTTTCTTCATTATTTCTTCATTA
10	MKI67_P3Plus_120_10	cattaccagagactttcttttgTTTCTTCATTAGCGTTTCTTCATTATTTCTTCATTA
11	MKI67_P3Plus_120_11	tgatagacactctctttgaaggTTTCTTCATTAGCGTTTCTTCATTATTTCTTCATTA
12	MKI67_P3Plus_120_12	ttgcaacaatcagatttgcttcTTTCTTCATTAGCGTTTCTTCATTATTTCTTCATTA

13	MKI67_P3Plus_120_13	taaattgactgtgaacttcgccTTTCTTCATTAGCGTTTCTTCATTATTTCTTCATTA
14	MKI67_P3Plus_120_14	tacttttttcagtatgagctttcTTTCTTCATTAGCGTTTCTTCATTATTTCTTCATTA
15	MKI67_P3Plus_120_15	aatgaagttgttgagcactctgTTTCTTCATTAGCGTTTCTTCATTATTTCTTCATTA
16	MKI67_P3Plus_120_16	gaaagatcttccttaaagtccaTTTCTTCATTAGCGTTTCTTCATTATTTCTTCATTA
17	MKI67_P3Plus_120_17	gtcttgaacatttcagctattcTTTCTTCATTAGCGTTTCTTCATTATTTCTTCATTA
18	MKI67_P3Plus_120_18	agaacacatttcctccaaaactTTTCTTCATTAGCGTTTCTTCATTATTTCTTCATTA
19	MKI67_P3Plus_120_19	gtttccattttctctaatacacTTTCTTCATTAGCGTTTCTTCATTATTTCTTCATTA
20	MKI67_P3Plus_120_20	cagagaagtcattttgtaggtgTTTCTTCATTAGCGTTTCTTCATTATTTCTTCATTA
21	MKI67_P3Plus_120_21	tgtatattcctgaactctgtagTTTCTTCATTAGCGTTTCTTCATTATTTCTTCATTA
22	MKI67_P3Plus_120_22	tattggttctggttgtaatgacTTTCTTCATTAGCGTTTCTTCATTATTTCTTCATTA
23	MKI67_P3Plus_120_23	tattttggtagttttctcatcaTTTCTTCATTAGCGTTTCTTCATTATTTCTTCATTA
24	MKI67_P3Plus_120_24	aagaattcttcctctacatctgTTTCTTCATTAGCGTTTCTTCATTATTTCTTCATTA
25	MKI67_P3Plus_120_25	gagttcccataaatgctttaatTTTCTTCATTAGCGTTTCTTCATTATTTCTTCATTA
26	MKI67_P3Plus_120_26	cgaagaattcttcttctacgtcTTTCTTCATTAGCGTTTCTTCATTATTTCTTCATTA
27	MKI67_P3Plus_120_27	aatgcgtagatgtttttctcacTTTCTTCATTAGCGTTTCTTCATTATTTCTTCATTA
28	MKI67_P3Plus_120_28	cagttttatcgttagtcattgaTTTCTTCATTAGCGTTTCTTCATTATTTCTTCATTA
29	MKI67_P3Plus_120_29	agactccataaatgctttcatgTTTCTTCATTAGCGTTTCTTCATTATTTCTTCATTA
30	MKI67_P3Plus_120_30	gtagtttttcgttagtcattgTTTCTTCATTAGCGTTTCTTCATTATTTCTTCATTA
31	MKI67_P3Plus_120_31	tgtctggaaaagctctctgaagTTTCTTCATTAGCGTTTCTTCATTATTTCTTCATTA
32	MKI67_P3Plus_120_32	aaatgtgttgatgtctttctctTTTCTTCATTAGCGTTTCTTCATTATTTCTTCATTA
33	MKI67_P3Plus_120_33	gatacttctgtgattttgtcatTTTCTTCATTAGCGTTTCTTCATTATTTCTTCATTA
34	MKI67_P3Plus_120_34	ctattttggtagttttctcatgTTTCTTCATTAGCGTTTCTTCATTATTTCTTCATTA
35	MKI67_P3Plus_120_35	tattttggtagttttctcatcaTTTCTTCATTAGCGTTTCTTCATTATTTCTTCATTA
36	MKI67_P3Plus_120_36	ctgagtgctaaaaattcttcctTTTCTTCATTAGCGTTTCTTCATTATTTCTTCATTA
37	MKI67_P3Plus_120_37	tgtctggaagagttctttgaagTTTCTTCATTAGCGTTTCTTCATTATTTCTTCATTA
38	MKI67_P3Plus_120_38	ttttgtcatcagtcattgattcTTTCTTCATTAGCGTTTCTTCATTATTTCTTCATTA
39	MKI67_P3Plus_120_39	ttaaacgctttgatgctcttacTTTCTTCATTAGCGTTTCTTCATTATTTCTTCATTA
40	MKI67_P3Plus_120_40	acgttgcttcaatactttgatgTTTCTTCATTAGCGTTTCTTCATTATTTCTTCATTA

Supplementary Table 7 | RNA-FISH probe set targeting TFRC mRNA variant 4

No.	Name	Sequence
1	TFRC-P3+_P1+_40-1	cttatcaactatgatcaccgagTTTCTTCATTAGCGTTTTATACATCTACGG
2	TFRC-P3+_P1+_40-2	cagatgagcatgtccaaagaatTTTCTTCATTAGCGTTTTATACATCTACGG
3	TFRC-P3+_P1+_40-3	tgattgaaggaagggaatccagTTTCTTCATTAGCGTTTTATACATCTACGG
4	TFRC-P3+_P1+_40-4	actacaacatagtgatctggttTTTCTTCATTAGCGTTTTATACATCTACGG
5	TFRC-P3+_P1+_40-5	agaccatatctgagaacatctgTTTCTTCATTAGCGTTTTATACATCTACGG
6	TFRC-P3+_P1+_40-6	cactccaactggcaaagataatTTTCTTCATTAGCGTTTTATACATCTACGG
7	TFRC-P3+_P1+_40-7	cctttaaatgcagggacgaaagTTTCTTCATTAGCGTTTTATACATCTACGG
8	TFRC-P3+_P1+_40-8	attcaacatcatgggttagtttTTTCTTCATTAGCGTTTTATACATCTACGG
9	TFRC-P3+_P1+_40-9	cacaaatgaaagcagttggctgTTTCTTCATTAGCGTTTTATACATCTACGG
10	TFRC-P3+_P1+_40-10	aatacagccactgtaaactcagTTTCTTCATTAGCGTTTTATACATCTACGG
11	TFRC-P3+_P1+_40-11	ttattttgtttacgcagtttcaTTTCTTCATTAGCGTTTTATACATCTACGG

12	TFRC-P3+_P1+_40-12	taaaactcattgtcaatgtcccTTTCTTCATTAGCGTTTTATACATCTACGG
13	TFRC-P3+_P1+_40-13	taccaagatgatgggatggaatTTTCTTCATTAGCGTTTTATACATCTACGG
14	TFRC-P3+_P1+_40-14	tatctaccctgtattaaaagctTTTCTTCATTAGCGTTTTATACATCTACGG
15	TFRC-P3+_P1+_40-15	attccatcatggacatttttaTTTCTTCATTAGCGTTTTATACATCTACGG
16	TFRC-P3+_P1+_40-16	acaacaacaggaaagaggcagtTTTCTTCATTAGCGTTTTATACATCTACGG
17	TFRC-P3+_P1+_40-17	aactggtttctgacattttcatTTTCTTCATTAGCGTTTTATACATCTACGG
18	TFRC-P3+_P1+_40-18	aggattcagagagatcattcacTTTCTTCATTAGCGTTTTATACATCTACGG
19	TFRC-P3+_P1+_40-19	atggaaaggcttagatctcattTTTCTTCATTAGCGTTTTATACATCTACGG
20	TFRC-P3+_P1+_40-20	gaatgaggaaaccagctacattTTTCTTCATTAGCGTTTTATACATCTACGG
21	TFRC-P3+_P1+_40-21	tttggcagcatattattctttaTTTCTTCATTAGCGTTTTATACATCTACGG
22	TFRC-P3+_P1+_40-22	cttagcaacccctaattaaattTTTCTTCATTAGCGTTTTATACATCTACGG
23	TFRC-P3+_P1+_40-23	tcactgcatttaggaaaaccagTTTCTTCATTAGCGTTTTATACATCTACGG
24	TFRC-P3+_P1+_40-24	gcctttaagtgacattgatttaTTTCTTCATTAGCGTTTTATACATCTACGG
25	TFRC-P3+_P1+_40-25	accttggataaactgagctataTTTCTTCATTAGCGTTTTATACATCTACGG
26	TFRC-P3+_P1+_40-26	tacagacactgtggtaggtaaaTTTCTTCATTAGCGTTTTATACATCTACGG
27	TFRC-P3+_P1+_40-27	gaaacactgttcccgataattaTTTCTTCATTAGCGTTTTATACATCTACGG
28	TFRC-P3+_P1+_40-28	gttgggatacatgttagatactTTTCTTCATTAGCGTTTTATACATCTACGG
29	TFRC-P3+_P1+_40-29	attaagtagaggacctggagaaTTTCTTCATTAGCGTTTTATACATCTACGG
30	TFRC-P3+_P1+_40-30	ttaaaacttgtccgcactaagtTTTCTTCATTAGCGTTTTATACATCTACGG
31	TFRC-P3+_P1+_40-31	ctctgctttaagtcaaaaggtcTTTCTTCATTAGCGTTTTATACATCTACGG
32	TFRC-P3+_P1+_40-32	ttaattgatcaccacgaatgggTTTCTTCATTAGCGTTTTATACATCTACGG
33	TFRC-P3+_P1+_40-33	cagctgatcatcacgtttataaTTTCTTCATTAGCGTTTTATACATCTACGG
34	TFRC-P3+_P1+_40-34	cacattcaagtgaggctgtaaaTTTCTTCATTAGCGTTTTATACATCTACGG
35	TFRC-P3+_P1+_40-35	atttaagtacgtgtgcgtaacaTTTCTTCATTAGCGTTTTATACATCTACGG
36	TFRC-P3+_P1+_40-36	ttatacgatgaacatgccacatTTTCTTCATTAGCGTTTTATACATCTACGG
37	TFRC-P3+_P1+_40-37	aagtaactcaaccctaactgtaTTTCTTCATTAGCGTTTTATACATCTACGG
38	TFRC-P3+_P1+_40-38	tgtcactagtctgatatttcatTTTCTTCATTAGCGTTTTATACATCTACGG
39	TFRC-P3+_P1+_40-39	atctccttaacgagaagacatcTTTCTTCATTAGCGTTTTATACATCTACGG
40	TFRC-P3+_P1+_40-40	ctaacacagtaaaggtcatgcaTTTCTTCATTAGCGTTTTATACATCTACGG

Supplementary Table 8 | Docking sites conjugated to secondary antibodies

Antibody	Docking site	Docking site sequence
Secondary-Goat	P12-8	5′-TT-TAGTTAGA-3′
Secondary-Mouse	P13-9	5′-TT-ATAGAGAGG-3′

Supplementary Table 9 | Staple strands used for 124 color DNA origami structures. All staple strands are included, except for biotinylated staples (empty rows). Core staple strands were extended with either P1, P2 or P3 handle sequences.

Plate Position	Oligo Name	Sequence
A1	21[32]23[31]BLK	TTTTCACTCAAAGGGCGAAAAACCATCACC
A2	19[32]21[31]P2	GTCGACTTCGGCCAACGCGCGGGGTTTTTC TTATCTACATA

A3	17[32]19[31]P3	TGCATCTTTCCCAGTCACGACGGCCTGCAG TTTCTTCATTA
A4	15[32]17[31]P1	TAATCAGCGGATTGACCGTAATCGTAACCG TTATACATCTA
A5	13[32]15[31]P2	AACGCAAAATCGATGAACGGTACCGGTTGA TTATCTACATA
A6	11[32]13[31]P3	AACAGTTTTGTACCAAAAACATTTTATTTC TTTCTTCATTA
A7	9[32]11[31]P1	TTTACCCCAACATGTTTTAAATTTCCATAT TTATACATCTA
A8	7[32]9[31]P2	TTTAGGACAAATGCTTTAAACAATCAGGTC TTATCTACATA
A9	5[32]7[31]P1	CATCAAGTAAAACGAACTAACGAGTTGAGA TTATACATCTA
A10	3[32]5[31]P3	AATACGTTTGAAAGAGGACAGACTGACCTT TTTCTTCATTA
A11	1[32]3[31]BLK	AGGCTCCAGAGGCTTTGAGGACACGGGTAA
A12	0[47]1[31]BLK	AGAAAGGAACAACTAAAGGAATTCAAAAAAA
B1	23[32]22[48]BLK	CAAATCAAGTTTTTTGGGGTCGAAACGTGGA
B2	22[47]20[48]P3	CTCCAACGCAGTGAGACGGGCAACCAGCTGCA TTTCTTCATTA
B3	20[47]18[48]P1	TTAATGAACTAGAGGATCCCCGGGGGGTAACG TTATACATCTA
B4	18[47]16[48]P2	CCAGGGTTGCCAGTTTGAGGGGACCCGTGGGA TTATCTACATA
B5	16[47]14[48]P3	ACAAACGGAAAAGCCCCAAAAACACTGGAGCA TTTCTTCATTA
B6	14[47]12[48]P1	AACAAGAGGGATAAAAATTTTTAGCATAAAGC TTATACATCTA
B7	12[47]10[48]P2	TAAATCGGGATTCCCAATTCTGCGATATAATG TTATCTACATA
B8	10[47]8[48]P3	CTGTAGCTTGACTATTATAGTCAGTTCATTGA TTTCTTCATTA
B9	8[47]6[48]P1	ATCCCCCTATACCACATTCAACTAGAAAAATC TTATACATCTA
B10	6[47]4[48]P2	TACGTTAAAGTAATCTTGACAAGAACCGAACT TTATCTACATA
B11	4[47]2[48]P1	GACCAACTAATGCCACTACGAAGGGGGTAGCA TTATACATCTA
B12	2[47]0[48]BLK	ACGGCTACAAAAGGAGCCTTTAATGTGAGAAT
C1	21[56]23[63]BLK	AGCTGATTGCCCTTCAGAGTCCACTATTAAAGGGTGCCGT
C2		
C3		
C4	15[64]18[64]BLK	GTATAAGCCAACCCGTCGGATTCTGACGACAGTATCGGCCGCAAGGCG
C5	13[64]15[63]P2	TATATTTTGTCATTGCCTGAGAGTGGAAGATT TTATCTACATA
C6	11[64]13[63]P3	GATTTAGTCAATAAAGCCTCAGAGAACCCTCA TTTCTTCATTA
C7	9[64]11[63]P1	CGGATTGCAGAGCTTAATTGCTGAAACGAGTA TTATACATCTA
C8	7[56]9[63]BLK	ATGCAGATACATAACGGGAATCGTCATAAATAAAGCAAAG
C9		
C10		
C11	1[64]4[64]BLK	TTTATCAGGACAGCATCGGAACGACACCAACCTAAAACGAGGTCAATC
C12	0[79]1[63]BLK	ACAACTTTCAACAGTTTCAGCGGATGTATCGG
D1	23[64]22[80]BLK	AAAGCACTAAATCGGAACCCTAATCCAGTT
D2	22[79]20[80]P3	TGGAACAACCGCCTGGCCCTGAGGCCCGCT TTTCTTCATTA
D3	20[79]18[80]P1	TTCCAGTCGTAATCATGGTCATAAAAGGGG TTATACATCTA
D4	18[79]16[80]P2	GATGTGCTTCAGGAAGATCGCACAATGTGA TTATCTACATA
D5	16[79]14[80]P3	GCGAGTAAAAATATTTAAATTGTTACAAAG TTTCTTCATTA
D6	14[79]12[80]P1	GCTATCAGAAATGCAATGCCTGAATTAGCA TTATACATCTA
D7	12[79]10[80]P2	AAATTAAGTTGACCATTAGATACTTTTGCG TTATCTACATA

20

D8	10[79]8[80]P3	GATGGCTTATCAAAAAGATTAAGAGCGTCC TTTCTTCATTA
D9	8[79]6[80]P1	AATACTGCCCAAAAGGAATTACGTGGCTCA TTATACATCTA
D10	6[79]4[80]P2	TTATACCACCAAATCAACGTAACGAACGAG TTATCTACATA
D11	4[79]2[80]P3	GCGCAGACAAGAGGCAAAAGAATCCCTCAG TTTCTTCATTA
D12	2[79]0[80]BLK	CAGCGAAACTTGCTTTCGAGGTGTTGCTAA
E1	21[96]23[95]BLK	AGCAAGCGTAGGGTTGAGTGTTGTAGGGAGCC
E2	19[96]21[95]P2	CTGTGTGATTGCGTTGCGCTCACTAGAGTTGC TTATCTACATA
E3	17[96]19[95]P3	GCTTTCCGATTACGCCAGCTGGCGGCTGTTTC TTTCTTCATTA
E4	15[96]17[95]P1	ATATTTTGGCTTTCATCAACATTATCCAGCCA TTATACATCTA
E5	13[96]15[95]P2	TAGGTAAACTATTTTTGAGAGATCAAACGTTA TTATCTACATA
E6	11[96]13[95]P3	AATGGTCAACAGGCAAGGCAAAGAGTAATGTG TTTCTTCATTA
E7	9[96]11[95]P1	CGAAAGACTTTGATAAGAGGTCATATTTCGCA TTATACATCTA
E8	7[96]9[95]P2	TAAGAGCAAATGTTTAGACTGGATAGGAAGCC TTATCTACATA
E9	5[96]7[95]P3	TCATTCAGATGCGATTTTAAGAACAGGCATAG TTTCTTCATTA
E10	3[96]5[95]P1	ACACTCATCCATGTTACTTAGCCGAAAGCTGC TTATACATCTA
E11	1[96]3[95]P2	AAACAGCTTTTTGCGGGATCGTCAACACTAAA TTATCTACATA
E12	0[111]1[95]BLK	TAAATGAATTTTCTGTATGGGATTAATTTCTT
F1	23[96]22[112]BLK	CCCGATTTAGAGCTTGACGGGGAAAAAGAATA
F2	22[111]20[112]P3	GCCCGAGAGTCCACGCTGGTTTGCAGCTAACT TTTCTTCATTA
F3	20[111]18[112]P1	CACATTAAAATTGTTATCCGCTCATGCGGGCC TTATACATCTA
F4	18[111]16[112]P2	TCTTCGCTGCACCGCTTCTGGTGCGGCCTTCC TTATCTACATA
F5	16[111]14[112]P3	TGTAGCCATTAAAATTCGCATTAAATGCCGGA TTTCTTCATTA
F6	14[111]12[112]P1	GAGGGTAGGATTCAAAAGGGTGAGACATCCAA TTATACATCTA
F7	12[111]10[112]P2	TAAATCATATAACCTGTTTAGCTAACCTTTAA TTATCTACATA
F8	10[111]8[112]P3	TTGCTCCTTTCAAATATCGCGTTTGAGGGGGT TTTCTTCATTA
F9	8[111]6[112]P1	AATAGTAAACACTATCATAACCCTCATTGTGA TTATACATCTA
F10	6[111]4[112]P2	ATTACCTTTGAATAAGGCTTGCCCAAATCCGC TTATCTACATA
F11	4[111]2[112]P3	GACCTGCTCTTTGACCCCCAGCGAGGGAGTTA TTTCTTCATTA
F12	2[111]0[112]BLK	AAGGCCGCTGATACCGATAGTTGCGACGTTAG
G1	21[120]23[127]BLK	CCCAGCAGGCGAAAAATCCCTTATAAATCAAGCCGGCG
G2		
G3		
G4	15[128]18[128]BLK	TAAATCAAAATAATTCGCGTCTCGGAAACCAGGCAAAGGGAAGG
G5	13[128]15[127]P2	GAGACAGCTAGCTGATAAATTAATTTTTGT TTATCTACATA
G6	11[128]13[127]P3	TTTGGGGATAGTAGTAGCATTAAAAGGCCG TTTCTTCATTA
G7	9[128]11[127]P1	GCTTCAATCAGGATTAGAGAGTTATTTTCA TTATACATCTA
G8	7[120]9[127]BLK	CGTTTACCAGACGACAAAGAAGTTTTGCCATAATTCGA
G9		
G10		
G11	1[128]4[128]BLK	TGACAACTCGCTGAGGCTTGCATTATACCAAGCGCGATGATAAA
G12	0[143]1[127]BLK	TCTAAAGTTTTGTCGTCTTTCCAGCCGACAA

21

H1	21[160]22[144]P3	TCAATATCGAACCTCAAATATCAATTCCGAAA TTTCTTCATTA
H2	19[160]20[144]P3	GCAATTCACATATTCCTGATTATCAAAGTGTA TTTCTTCATTA
H3	17[160]18[144]P2	AGAAAACAAAGAAGATGATGAAACAGGCTGCG TTATCTACATA
H4	15[160]16[144]P3	ATCGCAAGTATGTAAATGCTGATGATAGGAAC TTTCTTCATTA
H5	13[160]14[144]P3	GTAATAAGTTAGGCAGAGGCATTTATGATATT TTTCTTCATTA
H6	11[160]12[144]P2	CCAATAGCTCATCGTAGGAATCATGGCATCAA TTATCTACATA
H7	9[160]10[144]P3	AGAGAGAAAAAAAATGAAAATAGCAAGCAAACT TTTCTTCATTA
H8	7[160]8[144]P3	TTATTACGAAGAACTGGCATGATTGCGAGAGG TTTCTTCATTA
H9	5[160]6[144]P2	GCAAGGCCTCACCAGTAGCACCATGGGCTTGA TTATCTACATA
H10	3[160]4[144]P3	TTGACAGGCCACCACCAGAGCCGCGATTTGTA TTTCTTCATTA
H11	1[160]2[144]P3	TTAGGATTGGCTGAGACTCCTCAATAACCGAT TTTCTTCATTA
H12	0[175]0[144]BLK	TCCACAGACAGCCCTCATAGTTAGCGTAACGA
A1	23[128]23[159]BLK	AACGTGGCGAGAAAGGAAGGGAAACCAGTAA
A2	22[143]21[159]P1	TCGGCAAATCCTGTTTGATGGTGGACCCTCAA TTATACATCTA
A3	20[143]19[159]P2	AAGCCTGGTACGAGCCGGAAGCATAGATGATG TTATCTACATA
A4	18[143]17[159]P1	CAACTGTTGCGCCATTCGCCATTCAAACATCA TTATACATCTA
A5	16[143]15[159]P1	GCCATCAAGCTCATTTTTTAACCACAAATCCA TTATACATCTA
A6	14[143]13[159]P2	CAACCGTTTCAAATCACCATCAATTCGAGCCA TTATCTACATA
A7	12[143]11[159]P1	TTCTACTACGCGAGCTGAAAAGGTTACCGCGC TTATACATCTA
A8	10[143]9[159]P1	CCAACAGGAGCGAACCAGACCGGAGCCTTTAC TTATACATCTA
A9	8[143]7[159]P2	CTTTTGCAGATAAAAACCAAAATAAAGACTCC TTATCTACATA
A10	6[143]5[159]P1	GATGGTTTGAACGAGTAGTAAATTTACCATTA TTATACATCTA
A11	4[143]3[159]P1	TCATCGCCAACAAAGTACAACGGACGCCAGCA TTATACATCTA
A12	2[143]1[159]P2	ATATTCGGAACCATCGCCCACGCAGAGAAGGA TTATCTACATA
B1	23[160]22[176]BLK	TAAAAGGGACATTCTGGCCAACAAAGCATC
B2	22[175]20[176]P3	ACCTTGCTTGGTCAGTTGGCAAAGAGCGGA TTTCTTCATTA
B3	20[175]18[176]P1	ATTATCATTCAATATAATCCTGACAATTAC TTATACATCTA
B4	18[175]16[176]P2	CTGAGCAAAAATTAATTACATTTTGGGTTA TTATCTACATA
B5	16[175]14[176]P3	TATAACTAACAAAGAACGCGAGAACGCCAA TTTCTTCATTA
B6	14[175]12[176]P1	CATGTAATAGAATATAAAGTACCAAGCCGT TTATACATCTA
B7	12[175]10[176]P2	TTTTATTTAAGCAAATCAGATATTTTTTGT TTATCTACATA
B8	10[175]8[176]P3	TTAACGTCTAACATAAAAACAGGTAACGGA TTTCTTCATTA
B9	8[175]6[176]P1	ATACCCAACAGTATGTTAGCAAATTAGAGC TTATACATCTA
B10	6[175]4[176]P2	CAGCAAAAGGAAACGTCACCAATGAGCCGC TTATCTACATA
B11	4[175]2[176]P3	CACCAGAAAGGTTGAGGCAGGTCATGAAAG TTTCTTCATTA
B12	2[175]0[176]BLK	TATTAAGAAGCGGGGTTTTGCTCGTAGCAT
C1	21[184]23[191]BLK	TCAACAGTTGAAAGGAGCAAATGAAAAATCTAGAGATAGA
C2		
C3		
C4	15[192]18[192]BLK	TCAAATATAACCTCCGGCTTAGGTAACAATTTCATTTGAAGGCGAATT
C5	13[192]15[191]P1	GTAAAGTAATCGCCATATTTAACAAAACTTTT TTATACATCTA

22

C6	11[192]13[191]P2	TATCCGGTCTCATCGAGAACAAGCGACAAAAG TTATCTACATA
C7	9[192]11[191]P1	TTAGACGGCCAAATAAGAAACGATAGAAGGCT TTATACATCTA
C8	7[184]9[191]BLK	CGTAGAAAATACATACCGAGGAAACGCAATAAGAAGCGCA
C9		
C10		
C11	1[192]4[192]BLK	GCGGATAACCTATTATTCTGAAACAGACGATTGGCCTTGAAGAGCCAC
C12	0[207]1[191]BLK	TCACCAGTACAAACTACAACGCCTAGTACCAG
D1	23[192]22[208]BLK	ACCCTTCTGACCTGAAAGCGTAAGACGCTGAG
D2	22[207]20[208]P2	AGCCAGCAATTGAGGAAGGTTATCATCATTTT TTATCTACATA
D3	20[207]18[208]P3	GCGGAACATCTGAATAATGGAAGGTACAAAAT TTTCTTCATTA
D4	18[207]16[208]P1	CGCGCAGATTACCTTTTTTAATGGGAGAGACT TTATACATCTA
D5	16[207]14[208]P2	ACCTTTTTATTTTAGTTAATTTCATAGGGCTT TTATCTACATA
D6	14[207]12[208]P3	AATTGAGAATTCTGTCCAGACGACTAAACCAA TTTCTTCATTA
D7	12[207]10[208]P1	GTACCGCAATTCTAAGAACGCGAGTATTATTT TTATACATCTA
D8	10[207]8[208]P2	ATCCCAATGAGAATTAACTGAACAGTTACCAG TTATCTACATA
D9	8[207]6[208]P3	AAGGAAACATAAAGGTGGCAACATTATCACCG TTTCTTCATTA
D10	6[207]4[208]P1	TCACCGACGCACCGTAATCAGTAGCAGAACCG TTATACATCTA
D11	4[207]2[208]P2	CCACCCTCTATTCACAAACAAATACCTGCCTA TTATCTACATA
D12	2[207]0[208]BLK	TTTCGGAAGTGCCGTCGAGAGGGTGAGTTTCG
E1	21[224]23[223]BLK	CTTTAGGGCCTGCAACAGTGCCAATACGTG
E2	19[224]21[223]P1	CTACCATAGTTTGAGTAACATTTAAAATAT TTATACATCTA
E3	17[224]19[223]P2	CATAAATCTTTGAATACCAAGTGTTAGAAC TTATCTACATA
E4	15[224]17[223]P3	CCTAAATCAAAATCATAGGTCTAAACAGTA TTTCTTCATTA
E5	13[224]15[223]P1	ACAACATGCCAACGCTCAACAGTCTTCTGA TTATACATCTA
E6	11[224]13[223]P2	GCGAACCTCCAAGAACGGGTATGACAATAA TTATCTACATA
E7	9[224]11[223]P3	AAAGTCACAAAATAAACAGCCAGCGTTTTA TTTCTTCATTA
E8	7[224]9[223]P1	AACGCAAAGATAGCCGAACAAACCCTGAAC TTATACATCTA
E9	5[224]7[223]P2	TCAAGTTTCATTAAAGGTGAATATAAAAGA TTATCTACATA
E10	3[224]5[223]P3	TTAAAGCCAGAGCCGCCACCCTCGACAGAA TTTCTTCATTA
E11	1[224]3[223]P1	GTATAGCAAACAGTTAATGCCCAATCCTCA TTATACATCTA
E12	0[239]1[223]BLK	AGGAACCCATGTACCGTAACACTTGATATAA
F1	23[224]22[240]BLK	GCACAGACAATATTTTTGAATGGGGTCAGTA
F2	22[239]20[240]P2	TTAACACCAGCACTAACAACTAATCGTTATTA TTATCTACATA
F3	20[239]18[240]P3	ATTTTAAAATCAAAATTATTTGCACGGATTCG TTTCTTCATTA
F4	18[239]16[240]P1	CCTGATTGCAATATATGTGAGTGATCAATAGT TTATACATCTA
F5	16[239]14[240]P2	GAATTTATTTAATGGTTTGAAATATTCTTACC TTATCTACATA
F6	14[239]12[240]P3	AGTATAAAGTTCAGCTAATGCAGATGTCTTTC TTTCTTCATTA
F7	12[239]10[240]P1	CTTATCATTCCCGACTTGCGGGAGCCTAATTT TTATACATCTA
F8	10[239]8[240]P2	GCCAGTTAGAGGGTAATTGAGCGCTTTAAGAA TTATCTACATA
F9	8[239]6[240]P3	AAGTAAGCAGACACCACGGAATAATATTGACG TTTCTTCATTA
F10	6[239]4[240]P1	GAAATTATTGCCTTTAGCGTCAGACCGGAACC TTATACATCTA

23

F11	4[239]2[240]P2	GCCTCCCTCAGAATGGAAAGCGCAGTAACAGT TTATCTACATA
F12	2[239]0[240]BLK	GCCCGTATCCGGAATAGGTGTATCAGCCCAAT
G1	21[248]23[255]BLK	AGATTAGAGCCGTCAAAAAACAGAGGTGAGGCCTATTAGT
G2		
G3		
G4	15[256]18[256]BLK	GTGATAAAAAGACGCTGAGAAGAGATAACCTTGCTTCTGTTCGGGAGA
G5	13[256]15[255]P1	GTTTATCAATATGCGTTATACAAACCGACCGT TTATACATCTA
G6	11[256]13[255]P2	GCCTTAAACCAATCAATAATCGGCACGCGCCT TTATCTACATA
G7	9[256]11[255]P3	GAGAGATAGAGCGTCTTTCCAGAGGTTTTGAA TTTCTTCATTA
G8	7[248]9[255]BLK	GTTTATTTTGTCACAATCTTACCGAAGCCCTTTAATATCA
G9		
G10		
G11	1[256]4[256]BLK	CAGGAGGTGGGGTCAGTGCCTTGAGTCTCTGAATTTACCGGGAACCAG
G12	0[271]1[255]BLK	CCACCCTCATTTTCAGGGATAGCAACCGTACT
H1	23[256]22[272]BLK	CTTTAATGCGCGAACTGATAGCCCCACCAG
H2	22[271]20[272]BLK	CAGAAGATTAGATAATACATTTGTCGACAA
H3	20[271]18[272]P3	CTCGTATTAGAAATTGCGTAGATACAGTAC TTTCTTCATTA
H4	18[271]16[272]P1	CTTTTACAAAATCGTCGCTATTAGCGATAG TTATACATCTA
H5	16[271]14[272]P2	CTTAGATTTAAGGCGTTAAATAAAGCCTGT TTATCTACATA
H6	14[271]12[272]P3	TTAGTATCACAATAGATAAGTCCACGAGCA TTTCTTCATTA
H7	12[271]10[272]P1	TGTAGAAATCAAGATTAGTTGCTCTTACCA TTATACATCTA
H8	10[271]8[272]P2	ACGCTAACACCCACAAGAATTGAAAATAGC TTATCTACATA
H9	8[271]6[272]P3	AATAGCTATCAATAGAAAATTCAACATTCA TTTCTTCATTA
H10	6[271]4[272]P1	ACCGATTGTCGGCATTTTCGGTCATAATCA TTATACATCTA
H11	4[271]2[272]P2	AAATCACCTTCCAGTAAGCGTCAGTAATAA TTATCTACATA
H12	2[271]0[272]BLK	GTTTTAACTTAGTACCGCCACCCAGAGCCA

Supplementary Table 10 | Barcode IDs and combinations of frequencies to achieve 124 colors

Barcode ID	Red (P1 handle)	Green (P2 handle)	Blue (P3 handle)
0	0	0	0
1	0	0	3
2	0	0	9
3	0	0	22
4	0	0	44
5	0	3	0
6	0	3	3
7	0	3	9
8	0	3	22
9	0	3	44
10	0	9	0
11	0	9	3
12	0	9	9
13	0	9	22
14	0	9	44
15	0	22	0
16	0	22	3
17	0	22	9

18	0	22	22
19	0	22	44
20	0	44	0
21	0	44	3
22	0	44	9
23	0	44	22
24	0	44	44
25	3	0	0
26	3	0	3
27	3	0	9
28	3	0	22
29	3	0	44
30	3	3	0
31	3	3	3
32	3	3	9
33	3	3	22
34	3	3	44
35	3	9	0
36	3	9	3
37	3	9	9
38	3	9	22
39	3	9	44
40	3	22	0
41	3	22	3
42	3	22	9
43	3	22	22
44	3	22	44
45	3	44	0
46	3	44	3
47	3	44	9
48	3	44	22
49	3	44	44
50	9	0	0
51	9	0	3
52	9	0	9
53	9	0	22
54	9	0	44
55	9	3	0
56	9	3	3
57	9	3	9
58	9	3	22
59	9	3	44
60	9	9	0
61	9	9	3
62	9	9	9
63	9	9	22
64	9	9	44
65	9	22	0
66	9	22	3
67	9	22	9
68	9	22	22
69	9	22	44
70	9	44	0
71	9	44	3
72	9	44	9
73	9	44	22
74	9	44	44
75	22	0	0
76	22	0	3
77	22	0	9
78	22	0	22
79	22	0	44
80	22	3	0
81	22	3	3
82	22	3	9
83	22	3	22
84	22	3	44

25

85	22	9	0
86	22	9	3
87	22	9	9
88	22	9	22
89	22	9	44
90	22	22	0
91	22	22	3
92	22	22	9
93	22	22	22
94	22	22	44
95	22	44	0
96	22	44	3
97	22	44	9
98	22	44	22
99	22	44	44
100	44	0	0
101	44	0	3
102	44	0	9
103	44	0	22
104	44	0	44
105	44	3	0
106	44	3	3
107	44	3	9
108	44	3	22
109	44	3	44
110	44	9	0
111	44	9	3
112	44	9	9
113	44	9	22
114	44	9	44
115	44	22	0
116	44	22	3
117	44	22	9
118	44	22	22
119	44	22	44
120	44	44	0
121	44	44	3
122	44	44	9
123	44	44	22
124	44	44	44

Supplementary Note 1: Design of rectangular DNA origami

The DNA origami we used for the 40 and 120 binding site experiments was based on the original flat, rectangular structure[7]. For both the 40 and 120 binding sites, the same core staples were used, and the same 40 staples were modified in the case of all four species. All DNA-PAINT handle extensions added to the staple strands can be found in **Supplementary Tables 3** and **4**. We used the same basic structure for the 124 barcoded origami species as well.

Supplementary Note 2: RNA-FISH probe design

To the 3'-end of the probe's complementary region we added either a P3+ meta-stable handle sequence (in the case of MKI67) or a P3+ and a P1+ meta-stable handle sequence (in the case of TFRC)[8]. By hybridizing meta-stable imager strands to these handles we were able to identify favorable planes in the cell and could also use the acquired diffraction limited signals as an initial control to overlay with the subsequently acquired DNA-PAINT data.

Name	**Sequence**
MKI67_P3Plus_120_1	probe-TT-TCTTCATTAGCG-TT-TCTTCATTA-TT-TCTTCATTA
TFRC-P3+_P1+_40-1	probe-TT-TCTTCATTAGCG-TT-TT-ATACATCTACGG

In the case of MKI67 probes, the complementary region to the mRNA is in small letters, followed by a P3+ meta-stable handle (12 bp) and two P3 transient DNA-PAINT handle sequences (9bp) at the 3' end. The TFRC probes are elongated on

the 3’ end with a P3+ meta-stable handle (12 bp) and a P1+ meta-stable handle (12bp). The handle sequences are separated from each other by thymine (T) spacers. (See **Supplementary Table 5** and **6** for all probes).

Supplementary Note 3: Sequence of MKI67 mRNA variant 2 used for probe design, 11427 bp

TACCGGGCGGAGGTGAGCGCGGCGCCGGCTCCTCCTGCGGCGGACTTTGGGTGCGACTTGACGAGCGGTGGTTCGACAAGTGGCCTTGCGGGCCGGATCGTCCCAGTGGAAG
AGTTGTAAATTTGCTTCTGGCCTTCCCCTACGGATTATACCTGGCCTTCCCCTACGGATTATACTCAACTTACTGTTTAGAAAATGTGGCCCACGAGACGCCTGGTTACTAT
CAAAAGGAGCGGGGTCGACGGTCCCCACTTTCCCCTGAGCCTCAGCACCTGCTTGTTTGGAAGGGGTATTGAATGTGACATCCGTATCCAGCTTCCTGTTGTGTCAAAACAA
CATTGCAAAATTGAAATCCATGAGCAGGAGGCAATATTACATAATTTCAGTTCCACAAATCCAACACAAGTAAATGGGTCTGTTATTGATGAGCCTGTACGGCTAAAACATG
GAGATGTAATAACTATTATTGATCGTTCCTTCAGGTATGAAAATGAAAGTCTTCAGAATGGAAGGAAGTCAACTGAATTTCCAAGAAAAATACGTGAACAGGAGCCAGCACG
TCGTGTCTCAAGATCTAGCTTCTCTTCTGACCCTGATGAGAGTGAGGGAATACCTTTGAAAAGAAGGCGTGTGTCCTTTGGTGGGCACCTAAGACCTGAACTATTTGATGAA
AACTTGCCTCCTAATACGCCTCTCAAAAGGGGAGAAGCCCCAACCAAAAGAAAGTCTCTGGTAATGCACACTCCACCTGTCCTGAAGAAAATCATCAAGGAACAGCCTCAAC
CATCAGGAAAACAAGAGTCAGGTTCAGAAATCCATGTGGAAGTGAAGGCACAAAGCTTGGTTATAAGCCCTCCAGCTCCTAGTCCTAGGAAAACTCCAGTTGCCAGTGATCA
ACGCCGTAGGTCCTGCAAAACAGCCCCTGCTTCCAGCAGCAAATCTCAGACAGAGGTTCCTAAGAGAGGAGGGAGAAAGAGTGGCAACCTGCCTTCAAAGAGAGTGTCTATC
AGCCGAAGTCAACATGATATTTTACAGATGATATGTTCCAAAAGAAGAAGTGGTGCTTCGGAAGCAAATCTGATTGTTGCAAAATCATGGGCAGATGTAGTAAAACTTGGTG
CAAAACAAACACAAACTAAAGTCATAAAACATGGTCCTCAAAGGTCAATGAACAAAAGGCAAAGAAGACCTGCTACTCCAAAGAAGCCTGTGGGCGAAGTTCACAGTCAATT
TAGTACAGGCCACGCAAACTCTCCTTGTACCATAATAATAGGGAAAGCTCATACTGAAAAAGTACATGTGCCTGCTCGACCCTACAGAGTGCTCAACAACTTCATTTCCAAC
CAAAAAATGGACTTTAAGGAAGATCTTTCAGGAATAGCTGAAATGTTCAAGACCCCAGTGAAGGAGCAACCGCAGTTGACAAGCACATGTCACATCGCTATTTCAAATTCAG
AGAATTTGCTTGGAAAACAGTTTCAAGGAACTGATTCAGGAGAAGAACCTCTGCTCCCCACCTCAGAGAGTTTTGGAGGAAATGTGTTCTTCAGTGCACAGAATGCAGCAAA
ACAGCCATCTGATAAATGCTCTGCAAGCCCTCCCTTAAGACGGCAGTGTATTAGAGAAAATGGAAACGTAGCAAAAACGCCCAGGAACACCTACAAAATGACTTCTCTGGAG
ACAAAAACTTCAGATACTGAGACAGAGCCTTCAAAAACAGTATCCACTGCAAACAGGTCAGGAAGGTCTACAGAGTTCAGGAATATACAGAAGCTACCTGTGGAAAGTAAGA
GTGAAGAAACAAATACAGAAATTGTTGAGTGCATCCTAAAAAGAGGTCAGAAGGCAACACTACTACAACAAAGGAGAGAAGGAGAGATGAAGGAAATAGAAAGACCTTTTGA
GACATATAAGGAAAATATTGAATTAAAAGAAAACGATGAAAAGATGAAAGCAATGAAGAGATCAAGAACTTGGGGGCAGAAATGTGCACCAATGTCTGACCTGACAGACCTC
AAGAGCTTGCCTGATACAGAACTCATGAAAGACACGGCACGTGGCCAGAATCTCCTCCAAACCCAAGATCATGCCAAGGCACCAAAGAGTGAGAAAGGCAAAATCACTAAAA
TGCCCTGCCAGTCATTACAACCAGAACCAATAAACACCCCAACACACACAAAACAACAGTTGAAGGCATCCCTGGGGAAAGTAGGTGTGAAAGAAGAGCTCCTAGCAGTCGG
CAAGTTCACACGGACGTCAGGGGAGACCACGCACACGCACAGAGAGCCAGCAGGAGATGGCAAGAGCATCAGAACGTTTAAGGAGTCTCCAAAGCAGATCCTGGACCCAGCA
GCCCGTGTAACTGGAATGAAGAAGTGGCCAAGAACGCCTAAGGAAGAGGCCCAGTCACTAGAAGACCTGGCTGGCTTCAAAGAGCTCTTCCAGACACCAGGTCCCTCTGAGG
AATCAATGACTGATGAGAAAACTACCAAAATAGCCTGCAAATCTCCACCACCAGAATCAGTGGACACTCCAACAAGCACAAAGCAATGGCCTAAGAGAAGTCTCAGGAAAGC
AGATGTAGAGGAAGAATTCTTAGCACTCAGGAAACTAACACCATCAGCAGGGAAAGCCATGCTTACGCCCAAACCAGCAGGAGGTGATGAGAAAGACATTAAAGCATTTATG
GGAACTCCAGTGCAGAAACTGGACCTGGCAGGAACTTTACCTGGCAGCAAAAGACAGCTACAGACTCCTAAGGAAAAGGCCCAGGCTCTAGAAGACCTGGCTGGCTTTAAAG
AGCTCTTCCAGACTCCTGGTCACACCGAGGAATTAGTGGCTGCTGGTAAAACCACTAAAATACCCTGCGACTCTCCACAGTCAGACCCAGTGGACACCCCAACAAGCACAAA
GCAACGACCCAAGAGAAGTATCAGGAAAGCAGATGTAGAGGGAGAACTCTTAGCGTGCAGGAATCTAATGCCATCAGCAGGCAAAGCCATGCACACGCCTAAACCATCAGTA
GGTGAAGAGAAAGACATCATCATATTTGTGGGAACTCCAGTGCAGAAACTGGACCTGACAGAGAACTTAACCGGCAGCAAGAGACGGCCACAAACTCCTAAGGAAGAGGCCC
AGGCTCTGGAAGACCTGACTGGCTTTAAAGAGCTCTTCCAGACCCCTGGTCATACTGAAGAAGCAGTGGCTGCTGGCAAAACTACTAAAATGCCCTGCGAATCTTCTCCACC
AGAATCAGCAGACACCCCAACAAGCACAAGAAGGCAGCCCAAGACACCTTTGGAGAAAAGGGACGTACAGAAGGAGCTCTCAGCCCTGAAGAAGCTCACACAGACATCAGGG
GAAACCACACACACAGATAAAGTACCAGGAGGTGAGGATAAAAGCATCAACGCGTTTAGGGAAACTGCAAAACAGAAACTGGACCCAGCAGCAAGTGTAACTGGTAGCAAGA
GGCACCCAAAAACTAAGGAAAAGGCCCAACCCCTAGAAGACCTGGCTGGCTTGAAAGAGCTCTTCCAGACACCAGTATGCACTGACAAGCCCACGACTCACGAGAAAACTAC
CAAAATAGCCTGCAGATCACAACCAGACCCAGTGGACACACCAACAAGCTCCAAGCCACAGTCCAAGAGAAGTCTCAGGAAAGTGGACGTAGAAGAAGAATTCTTCGCACTC
AGGAAACGAACACCATCAGCAGGCAAAGCCATGCACACACCCAAACCAGCAGTAAGTGGTGAGAAAAACATCTACGCATTTATGGGAACTCCAGTGCAGAAACTGGACCTGA
CAGAGAACTTAACTGGCAGCAAGAGACGGCTACAAACTCCTAAGGAAAAGGCCCAGGCTCTAGAAGACCTGGCTGGCTTTAAAGAGCTCTTCCAGACACGAGGTCACACTGA
GGAATCAATGACTAACGATAAAACTGCCAAAGTAGCCTGCAAATCTTCACAACCAGACCCAGACAAAAACCCAGCAAGCTCCAAGCGACGGCTCAAGACATCCCTGGGGAAA
GTGGGCGTGAAAGAAGAGCTCCTAGCAGTTGGCAAGCTCACACAGACATCAGGAGAGACTACACACACACACACAGAGCCAACAGGAGATGGTAAGAGCATGAAAGCATTTA
TGGAGTCTCCAAAGCAGATCTTAGACTCAGCAGCAAGTCTAACTGGCAGCAAGAGGCAGCTGAGAACTCCTAAGGGAAAGTCTGAAGTCCCTGAAGACCTGGCCGGCTTCAT
CGAGCTCTTCCAGACACCAAGTCACACTAAGGAATCAATGACTAACGAAAAAACTACCAAAGTATCCTACAGAGCTTCACAGCCAGACCTAGTGGACACCCCAACAAGCTCC
AAGCCACAGCCCAAGAGAAGTCTCAGGAAAGCAGACACTGAAGAAGAATTTTTAGCATTTAGGAAACAAACGCCATCAGCAGGCAAAGCCATGCACACACCCAAACCAGCAG
TAGGTGAAGAGAAAGACATCAACACGTTTTTGGGAACTCCAGTGCAGAAACTGGACCAGCCAGGAAATTTACCTGGCAGCAATAGACGGCTACAAACTCGTAAGGAAAAGGC
CCAGGCTCTAGAAGAACTGACTGGCTTCAGAGAGCTTTTCCAGACACCATGCACTGATAACCCCACGACTGATGAGAAAACTACCAAAAAAATACTCTGCAAATCTCCGCAA
TCAGACCCAGCGGACACCCCAACAAACACAAAGCAACGGCCCAAGAGAAGCCTCAAGAAAGCAGACGTAGAGGAAGAATTTTTAGCATTCAGGAAACTAACACCATCAGCAG
GCAAAGCCATGCACACGCCTAAAGCAGCAGTAGGTGAAGAGAAAGACATCAACACATTTGTGGGGACTCCAGTGGAGAAACTGGACCTGCTAGGAAATTTACCTGGCAGCAA
GAGACGGCCACAAACTCCTAAAGAAAAGGCCAAGGCTCTAGAAGATCTGGCTGGCTTCAAAGAGCTCTTCCAGACACCAGGTCACACTGAGGAATCAATGACCGATGACAAA
ATCACAGAAGTATCCTGCAAATCTCCACAACCAGACCCAGTCAAAACCCCAACAAGCTCCAAGCAACGACTCAAGATATCCTTGGGGAAAGTAGGTGTGAAAGAAGAGGTCC
TACCAGTCGGCAAGCTCACACAGACGTCAGGGAAGACCACACAGACACACAGAGAGACAGCAGGAGATGGAAAGAGCATCAAAGCGTTTAAGGAATCTGCAAAGCAGATGCT
GGACCCAGCAAACTATGGAACTGGGATGGAGAGGTGGCCAAGAACACCTAAGGAAGAGGCCCAATCACTAGAAGACCTGGCCGGCTTCAAAGAGCTCTTCCAGACACCAGAC
CACACTGAGGAATCAACAACTGATGACAAAACTACCAAAATAGCCTGCAAATCTCCACCACCAGAATCAATGGACACTCCAACAAGCACAAGGAGGCGGCCCAAAACACCTT
TGGGGAAAAGGGATATAGTGGAAGAGCTCTCAGCCCTGAAGCAGCTCACACAGACCACACACACAGACAAAGTACCAGGAGATGAGGATAAAGGCATCAACGTGTTCAGGGA
AACTGCAAAACAGAAACTGGACCCAGCAGCAAGTGTAACTGGTAGCAAGAGGCAGCCAAGAACTCCTAAGGGAAAAGCCCAACCCCTAGAAGACTTGGCTGGCTTGAAAGAG
CTCTTCCAGACACCAATATGCACTGACAAGCCCACGACTCATGAGAAAACTACCAAAATAGCCTGCAGATCTCCACAACCAGACCCAGTGGGTACCCCAACAATCTTCAAGC
CACAGTCCAAGAGAAGTCTCAGGAAAGCAGACGTAGAGGAAGAATCCTTAGCACTCAGGAAACGAACACCATCAGTAGGGAAAGCTATGGACACACCCAAACCAGCAGGAGG
TGATGAGAAAGACATGAAAGCATTTATGGGAACTCCAGTGCAGAAATTGGACCTGCCAGGAAATTTACCTGGCAGCAAAAGATGGCCACAAACTCCTAAGGAAAAGGCCCAG
GCTCTAGAAGACCTGGCTGGCTTCAAAGAGCTCTTCCAGACACCAGGCACTGACAAGCCCACGACTGATGAGAAAACTACCAAAATAGCCTGCAAATCTCCACAACCAGACC
CAGTGGACACCCCAGCAAGCACAAAGCAACGGCCCAAGAGAAACCTCAGGAAAGCAGACGTAGAGGAAGAATTTTTAGCACTCAGGAAACGAACACCATCAGCAGGCAAAGC
CATGGACACACCAAAACCAGCAGTAAGTGATGAGAAAAATATCAACACATTTGTGGAAACTCCAGTGCAGAAACTGGACCTGCTAGGAAATTTACCTGGCAGCAAGAGACAG
CCACAGACTCCTAAGGAAAAGGCTGAGGCTCTAGAGGACCTGGTTGGCTTCAAAGAACTCTTCCAGACACCAGGTCACACTGAGGAATCAATGACTGATGACAAAATCACAG
AAGTATCCTGTAAATCTCCACAGCCAGAGTCATTCAAAACCTCAAGAAGCTCCAAGCAAAGGCTCAAGATACCCCTGGTGAAAGTGGACATGAAAGAAGAGCCCCTAGCAGT
CAGCAAGCTCACACGGACATCAGGGGAGACTACGCAAACACACACAGAGCCAACAGGAGATAGTAAGAGCATCAAAGCGTTTAAGGAGTCTCCAAAGCAGATCCTGGACCCA
GCAGCAAGTGTAACTGGTAGCAGGAGGCAGCTGAGAACTCGTAAGGAAAAGGCCCGTGCTCTAGAAGACCTGGTTGACTTCAAAGAGCTCTTCTCAGCACCAGGTCACACTG
AAGAGTCAATGACTATTGACAAAAACACAAAAATTCCCTGCAAATCTCCCCCACCAGAACTAACAGACACTGCCACGAGCACAAAGAGATGCCCCAAGACACGTCCCAGGAA
AGAAGTAAAAGAGGAGCTCTCAGCAGTTGAGAGGCTCACGCAAACATCAGGGCAAAGCACACACACACACAAAGAACCAGCAAGCGGTGATGAGGGCATCAAAGTATTGAAG
CAACGTGCAAAGAAGAAACCAAACCCAGTAGAAGAGGAACCCAGCAGGAGAAGGCCAAGAGCACCTAAGGAAAAGGCCCAACCCCTGGAAGACCTGGCCGGCTTCACAGAGC
TCTCTGAAACATCAGGTCACACTCAGGAATCACTGACTGCTGGCAAAGCCACTAAAATACCCTGCGAATCTCCCCCACTAGAAGTGGTAGACACCACAGCAAGCACAAAGAG
GCATCTCAGGACACGTGTGCAGAAGGTACAAGTAAAAGAAGAGCCTTCAGCAGTCAAGTTCACACAAACATCAGGGGAAACCACGGATGCAGACAAAGAACCAGCAGGTGAA
GATAAAGGCATCAAAGCATTGAAGGAATCTGCAAAACAGACACCGGCTCCAGCAGCAAGTGTAACTGGCAGCAGGAGACGGCCAAGAGCACCCAGGGAAAGTGCCCAAGCCA
TAGAAGACCTAGCTGGCTTCAAAGACCCAGCAGCAGGTCACACTGAAGAATCAATGACTGATGACAAAACCACTAAAATACCCTGCAAATCATCACCAGAACTAGAAGACAC
CGCAACAAGCTCAAAGAGACGGCCCAGGACACGTGCCCAGAAAGTAGAAGTGAAGGAGGAGCTGTTAGCAGTTGGCAAGCTCACACAAACCTCAGGGGAGACCACGCACACC
GACAAAGAGCCGGTAGGTGAGGGCAAAGGCACGAAAGCATTTAAGCAACCTGCAAAGCGGAAGCTGGACGCAGAAGATGTAATTGGCAGCAGGAGACAGCCAAGAGCACCTA

27

AGGAAAAGGCCCAACCCCTGGAAGATCTGGCCAGCTTCCAAGAGCTCTCTCAAACACCAGGCCACACTGAGGAACTGGCAAATGGTGCTGCTGATAGCTTTACAAGCGCTCC
AAAGCAAACACCTGACAGTGGAAAACCTCTAAAAATATCCAGAAGAGTTCTTCGGGCCCCTAAAGTAGAACCCGTGGGAGACGTGGTAAGCACCAGAGACCCTGTAAAATCA
CAAAGCAAAAGCAACACTTCCCTGCCCCCACTGCCCTTCAAGAGGGGAGGTGGCAAAGATGGAAGCGTCACGGGAACCAAGAGGCTGCGCTGCATGCCAGCACCAGAGGAAA
TTGTGGAGGAGCTGCCAGCCAGCAAGAAGCAGAGGGTTGCTCCCAGGGCAAGAGGCAAATCATCCGAACCCGTGGTCATCATGAAGAGAAGTTTGAGGACTTCTGCAAAAAG
AATTGAACCTGCGGAAGAGCTGAACAGCAACGACATGAAAACCAACAAAGAGGAACACAAATTACAAGACTCGGTCCCTGAAAATAAGGGAATATCCCTGCGCTCCAGACGC
CAAAATAAGACTGAGGCAGAACAGCAAATAACTGAGGTCTTTGTATTAGCAGAAAGAATAGAAATAAACAGAAATGAAAAGAAGCCCATGAAGACCTCCCCAGAGATGGACA
TTCAGAATCCAGATGATGGAGCCCGGAAACCCATACCTAGAGACAAAGTCACTGAGAACAAAAGGTGCTTGAGGTCTGCTAGACAGAATGAGAGCTCCCAGCCTAAGGTGGC
AGAGGAGAGCGGAGGGCAGAAGAGTGCGAAGGTTCTCATGCAGAATCAGAAAGGGAAAGGAGAAGCAGGAAATTCAGACTCCATGTGCCTGAGATCAAGAAAGACAAAAAGC
CAGCCTGCAGCAAGCACTTTGGAGAGCAAATCTGTGCAGAGAGTAACGCGGAGTGTCAAGAGGTGTGCAGAAAATCCAAAGAAGGCTGAGGACAATGTGTGTGTCAAGAAAA
TAAGAACCAGAAGTCATAGGGACAGTGAAGATATTTGACAGAAAAATCGAACTGGGAAAAATATAATAAAGTTAGTTTTGTGATAAGTTCTAGTGCAGTTTTTGTCATAAAT
TACAAGTGAATTCTGTAAGTAAGGCTGTCAGTCTGCTTAAGGGAAGAAAACTTTGGATTTGCTGGGTCTGAATCGGCTTCATAAACTCCACTGGGAGCACTGCTGGGCTCCT
GGACTGAGAATAGTTGAACACCGGGGGCTTTGTGAAGGAGTCTGGGCCAAGGTTTGCCCTCAGCTTTGCAGAATGAAGCCTTGAGGTCTGTCACCACCCACAGCCACCCTAC
AGCAGCCTTAACTGTGACACTTGCCACACTGTGTCGTCGTTTGTTTGCCTATGTCCTCCAGGGCACGGTGGCAGGAACAACTATCCTCGTCTGTCCCAACACTGAGCAGGCA
CTCGGTAAACACGAATGAATGGATGAGCGCACGGATGAATGGAGCTTACAAGATCTGTCTTTCCAATGGCCGGGGGCATTTGGTCCCCAAATTAAGGCTATTGGACATCTGC
ACAGGACAGTCCTATTTTTGATGTCCTTTCCTTTCTGAAAATAAAGTTTTGTGCTTTGGAGAATGACTCGTGAGCACATCTTTAGGGACCAAGAGTGACTTTCTGTAAGGAG
TGACTCGTGGCTTGCCTTGGTCTCTTGGGAATACTTTTCTAACTAGGGTTGCTCTCACCTGAGACATTCTCCACCCGCGGAATCTCAGGGTCCCAGGCTGTGGGCCATCACG
ACCTCAAACTGGCTCCTAATCTCCAGCTTTCCTGTCATTGAAAGCTTCGGAAGTTTACTGGCTCTGCTCCCGCCTGTTTTCTTTCTGACTCTATCTGGCAGCCCGATGCCAC
CCAGTACAGGAAGTGACACCAGTACTCTGTAAAGCATCATCATCCTTGGAGAGACTGAGCACTCAGCACCTTCAGCCACGATTTCAGGATCGCTTCCTTGTGAGCCGCTGCC
TCCGAAATCTCCTTTGAAGCCCAGACATCTTTCTCCAGCTTCAGACTTGTAGATATAACTCGTTCATCTTCATTTACTTTCCACTTTGCCCCCTGTCCTCTCTGTGTTCCCC
AAATCAGAGAATAGCCCGCCATCCCCCAGGTCACCTGTCTGGATTCCTCCCCATTCACCCACCTTGCCAGGTGCAGGTGAGGATGGTGCACCAGACAGGGTAGCTGTCCCCC
AAAATGTGCCCTGTGCGGGCAGTGCCCTGTCTCCACGTTTGTTTCCCCAGTGTCTGGCGGGGAGCCAGGTGACATCATAAATACTTGCTGAATGAATGCAGAAATCAGCGGT
ACTGACTTGTACTATATTGGCTGCCATGATAGGGTTCTCACAGCGTCATCCATGATCGTAAGGGAGAATGACATTCTGCTTGAGGGAGGGAATAGAAAGGGGCAGGGAGGGG
ACATCTGAGGGCTTCACAGGGCTGCAAAGGGTACAGGGATTGCACCAGGGCAGAACAGGGGAGGGTGTTCAAGGAAGAGTGGCTCTTAGCAGAGGCACTTTGGAAGGTGTGA
GGCATAAATGCTTCCTTCTACGTAGGCCAACCTCAAAACTTTCAGTAGGAATGTTGCTATGATCAAGTTGTTCTAACACTTTAGACTTAGTAGTAATTATGAACCTCACATA
GAAAAATTTCATCCAGCCATATGCCTGTGGAGTGGAATATTCTGTTTAGTAGAAAAATCCTTTAGAGTTCAGCTCTAACCAGAAATCTTGCTGAAGTATGTCAGCACCTTTT
CTCACCCTGGTAAGTACAGTATTTCAAGAGCACGCTAAGGGTGGTTTTCATTTTACAGGGCTGTTGATGATGGGTTAAAAATGTTCATTTAAGGGCTACCCCCGTGTTTAAT
AGATGAACACCACTTCTACACAACCCTCCTTGGTACTGGGGGAGGGAGAGATCTGACAAATACTGCCCATTCCCCTAGGCTGACTGGATTTGAGAACAAATACCCACCCATT
TCCACCATGGTATGGTAACTTCTCTGAGCTTCAGTTTCCAAGTGAATTTCCATGTAATAGGACATTCCCATTAAATACAAGCTGTTTTTACTTTTTCGCCTCCCAGGGCCTG
TGGGATCTGGTCCCCCAGCCTCTCTTGGGCTTTCTTACACTAACTCTGTACCTACCATCTCCTGCCTCCCTTAGGCAGGCACCTCCAACCACCACACACTCCCTGCTGTTTT
CCCTGCCTGGAACTTTCCCTCCTGCCCCACCAAGATCATTTCATCCAGTCCTGAGCTCAGCTTAAGGGAGGCTTCTTGCCTGTGGGTTCCCTCACCCCCATGCCTGTCCTCC
AGGCTGGGGCAGGTTCTTAGTTTGCCTGGAATTGTTCTGTACCTCTTTGTAGCACGTAGTGTTGTGGAAACTAAGCCACTAATTGAGTTTCTGGCTCCCCTCCTGGGGTTGT
AAGTTTTGTTCATTCATGAGGGCCGACTGCATTTCCTGGTTACTCTATCCCAGTGACCAGCCACAGGAGATGTCCAATAAAGTATGTGATGAAATGGTCTTAAAAAAAAAAA
AAA

Supplementary Note 4: Sequence of TFRC mRNA variant 4 used for probe design, 4695 bp

ACGCACAGCCCCCCTGGGGGCCGGGGGCGGGGCCAGGCTATAAACCGCCGGTTAGGGGCCGCCATCCCCTCAGAGCGTCGGGATATCGGGTGGCGGCTCGGGACGGAGGACG
CGCTAGTGTTCTTCTGTGTGGCAGTTCAGAATGATGGATCAAGCTAGATCAGCATTCTCTAACTTGGCTGCTGAATGAAAATTCATATGTCCCTCGTGAGGCTGGATCTCAA
AAAGATGAAAATCTTGCGTTGTATGTTGAAAATCAATTTCGTGAATTTAAACTCAGCAAAGTCTGGCGTGATCAACATTTTGTTAAGATTCAGGTCAAAGACAGCGCTCAAA
ACTCGGTGATCATAGTTGATAAGAACGGTAGACTTGTTTACCTGGTGGAGAATCCTGGGGGTTATGTGGCGTATAGTAAGGCTGCAACAGTTACTGGTAAACTGGTCCATGC
TAATTTTGGTACTAAAAAAGATTTTGAGGATTTATACACTCCTGTGAATGGATCTATAGTGATTGTCAGAGCAGGGAAAATCACCTTTGCAGAAAAGGTTGCAAATGCTGAA
AGCTTAAATGCAATTGGTGTGTTGATATACATGGACCAGACTAAATTTCCCATTGTTAACGCAGAACTTTCATTCTTTGGACATGCTCATCTGGGGACAGGTGACCCTTACA
CACCTGGATTCCCTTCCTTCAATCACACTCAGTTTCCACCATCTCGGTCATCAGGATTGCCTAATATACCTGTCCAGACAATCTCCAGAGCTGCTGCAGAAAAGCTGTTTGG
GAATATGGAAGGAGACTGTCCCTCTGACTGGAAAACAGACTCTACATGTAGGATGGTAACCTCAGAAAGCAAGAATGTGAAGCTCACTGTGAGCAATGTGCTGAAAGAGATA
AAAATTCTTAACATCTTTGGAGTTATTAAAGGCTTTGTAGAACCAGATCACTATGTTGTAGTTGGGGCCCAGAGAGATGCATGGGGCCCTGGAGCTGCAAAATCCGGTGTAG
GCACAGCTCTCCTATTGAAACTTGCCCAGATGTTCTCAGATATGGTCTTAAAAGATGGGTTTCAGCCCAGCAGAAGCATTATCTTTGCCAGTTGGAGTGCTGGAGACTTTGG
ATCGGTTGGTGCCACTGAATGGCTAGAGGGATACCTTTCGTCCCTGCATTTAAAGGCTTTCACTTATATTAATCTGGATAAAGCGGTTCTTGGTACCAGCAACTTCAAGGTT
TCTGCCAGCCCACTGTTGTATACGCTTATTGAGAAAACAATGCAAAATGTGAAGCATCCGGTTACTGGGCAATTTCTATATCAGGACAGCAACTGGGCCAGCAAAGTTGAGA
AACTCACTTTAGACAATGCTGCTTTCCCTTTCCTTGCATATTCTGGAATCCCAGCAGTTTCTTTCTGTTTTTGCGAGGACACAGATTATCCTTATTTGGGTACCACCATGGA
CACCTATAAGGAACTGATTGAGAGGATTCCTGAGTTGAACAAAGTGGCACGAGCAGCTGCAGAGGTCGCTGGTCAGTTCGTGATTAAACTAACCCATGATGTTGAATTGAAC
CTGGACTATGAGAGGTACAACAGCCAACTGCTTTCATTTGTGAGGGATCTGAACCAATACAGAGCAGACATAAAGGAAATGGGCCTGAGTTTACAGTGGCTGTATTCTGCTC
GTGGAGACTTCTTCCGTGCTACTTCCAGACTAACAACAGATTTCGGGAATGCTGAGAAAACAGACAGATTTGTCATGAAGAAACTCAATGATCGTGTCATGAGAGTGGAGTA
TCACTTCCTCTCTCCCTACGTATCTCCAAAAGAGTCTCCTTTCCGACATGTCTTCTGGGGCTCCGGCTCTCACACGCTGCCAGCTTTACTGGAGAACTTGAAACTGCGTAAA
CAAAATAACGGTGCTTTTAATGAAACGCTGTTCAGAAACCAGTTGGCTCTAGCTACTTGGACTATTCAGGGAGCTGCAAATGCCCTCTCTGGTGACGTTTGGGACATTGACA
ATGAGTTTTAAATGTGATACCCATAGCTTCCATGAGAACAGCAGGGTAGTCTGGTTTCTAGACTTGTGCTGATCGTGCTAAATTTTCAGTAGGGCTACAAAACCTGATGTTA
AAATTCCATCCCATCATCTTGGTACTACTAGATGTCTTTAGGCAGCAGCTTTTAATACAGGGTAGATAACCTGTACTTCAAGTTAAAGTGAATAACCACTTAAAAAATGTCC
ATGATGGAATATTCCCCTATCTCTAGAATTTTAAGTGCTTTGTAATGGGAACTGCCTCTTTCCTGTTGTTGTTAATGAAAATGTCAGAAACCAGTTATGTGAATGATCTCTC
TGAATCCTAAGGGCTGGTCTCTGCTGAAGGTTGTAAGTGGTCGCTTACTTTGAGTGATCCTCCAACTTCATTTGATGCTAAATAGGAGATACCAGGTTGAAAGACCTTCTCC
AAATGAGATCTAAGCCTTTCCATAAGGAATGTAGCTGGTTTCCTCATTCCTGAAAGAAACAGTTAACTTTCAGAAGAGATGGGCTTGTTTTCTTGCCAATGAGGTCTGAAAT
GGAGGTCCTTCTGCTGGATAAAATGAGGTTCAACTGTTGATTGCAGGAATAAGGCCTTAATATGTTAACCTCAGTGTCATTTATGAAAAGAGGGGACCAGAAGCCAAAGACT
TAGTATATTTTCTTTTCCTCTGTCCCTTCCCCCATAAGCCTCCATTTAGTTCTTTGTTATTTTTGTTTCTTCCAAAGCACATTGAAAGAGAACCAGTTTCAGGTGTTTAGTT
GCAGACTCAGTTTGTCAGACTTTAAAGAATAATATGCTGCCAAATTTTGGCCAAAGTGTTAATCTTAGGGGAGAGCTTTCTGTCCTTTTGGCACTGAGATATTTATTGTTTA
TTTATCAGTGACAGAGTTCACTATAAATGGTGTTTTTTTAATAGAATATAATTATCGGAAGCAGTGCCTTCCATAATTATGACAGTTATACTGTCGGTTTTTTTTAAATAAA
AGCAGCATCTGCTAATAAAACCCAACAGATACTGGAAGTTTTGCATTTATGGTCAACACTTAAGGGTTTTAGAAAACAGCCGTCAGCCAAATGTAATTGAATAAAGTTGAAG
CTAAGATTTAGAGATGAATTAAATTTAATTAGGGGTTGCTAAGAAGCGAGCACTGACCAGATAAGAATGCTGGTTTTCCTAAATGCAGTGAATTGTGACCAAGTTATAAATC
AATGTCACTTAAAGGCTGTGGTAGTACTCCTGCAAAATTTTATAGCTCAGTTTATCCAAGGTGTAACTCTAATTCCCATTTTGCAAAATTTCCAGTACCTTTGTCACAATCC
TAACACATTATCGGGAGCAGTGTCTTCCATAATGTATAAAGAACAAGGTAGTTTTTACCTACCACAGTGTCTGTATCGGAGACAGTGATCTCCATATGTTACACTAAGGGTG
TAAGTAATTATCGGGAACAGTGTTTCCCATAATTTTCTTCATGCAATGACATCTTCAAAGCTTGAAGATCGTTAGTATCTAACATGTATCCCAACTCCTATAATTCCCTATC
TTTTAGTTTTAGTTGCAGAAACATTTTGTGGTCATTAAGCATTGGGTGGGTAAATTCAACCACTGTAAAATGAAATTACTACAAAATTTGAAATTTAGCTTGGGTTTTTGTT
ACCTTTATGGTTTCTCCAGGTCCTCTACTTAATGAGATAGTAGCATACATTTATAATGTTTGCTATTGACAAGTCATTTTAACTTTATCACATTATTTGCATGTTACCTCCT
ATAAACTTAGTGCGGACAAGTTTTAATCCAGAATTGACCTTTTGACTTAAAGCAGAGGGACTTTGTATAGAAGGTTTGGGGGCTGTGGGGAAGGAGAGTCCCCTGAAGGTCT
GACACGTCTGCCTACCCATTCGTGGTGATCAATTAAATGTAGGTATGAATAAGTTCGAAGCTCCGTGAGTGAACCATCATTATAAACGTGATGATCAGCTGTTTGTCATAGG
GCAGTTGGAAACGGCCTCCTAGGGAAAAGTTCATAGGGTCTCTTCAGGTTCTTAGTGTCACTTACCTAGATTTACAGCCTCACTTGAATGTGTCACTACTCACAGTCTCTTT
AATCTTCAGTTTTATCTTTAATCTCCTCTTTTATCTTGGACTGACATTTAGCGTAGCTAAGTGAAAAGGTCATAGCTGAGATTCCTGGTTCGGGTGTTACGCACACGTACTT
AAATGAAAGCATGTGGCATGTTCATCGTATAACACAATATGAATACAGGGCATGCATTTTGCAGCAGTGAGTCTCTTCAGAAAACCCTTTTCTACAGTTAGGGTTGAGTTAC
TTCCTATCAAGCCAGTACGTGCTAACAGGCTCAATATTCCTGAATGAAATATCAGACTAGTGACAAGCTCCTGGTCTTGAGATGTCTTCTCGTTAAGGAGATGGGCCTTTTG

GAGGTAAAGGATAAAATGAATGAGTTCTGTCATGATTCACTATTCTAGAACTTGCATGACCTTTACTGTGTTAGCTCTTTGAATGTTCTTGAAATTTTAGACTTTCTTTGTA
AACAAATGATATGTCCTTATCATTGTATAAAAGCTGTTATGTGCAACAGTGTGGAGATTCCTTGTCTGATTTAATAAAATACTTAAACACTGAAAAAAAAAAA

Supplementary References

1. Hoops, S.; Sahle, S.; Gauges, R.; Lee, C.; Pahle, J.; Simus, N.; Singhal, M.; Xu, L.; Mendes, P.; Kummer, U., COPASI--a COmplex PAthway SImulator. *Bioinformatics* **2006,** *22* (24), 3067-74.
2. Jungmann, R.; Avendano, M. S.; Dai, M.; Woehrstein, J. B.; Agasti, S. S.; Feiger, Z.; Rodal, A.; Yin, P., Quantitative super-resolution imaging with qPAINT. *Nat Methods* **2016,** *13* (5), 439-42.
3. Schnitzbauer, J.; Strauss, M. T.; Schlichthaerle, T.; Schueder, F.; Jungmann, R., Super-resolution microscopy with DNA-PAINT. *Nat Protoc* **2017,** *12*, 1198-1228.
4. Stahl, E.; Martin, T. G.; Praetorius, F.; Dietz, H., Facile and scalable preparation of pure and dense DNA origami solutions. *Angew Chem Int Ed Engl* **2014,** *53* (47), 12735-40.
5. Agasti, S. S.; Wang, Y.; Schueder, F.; Sukumar, A.; Jungmann, R.; Yin, P., DNA-barcoded labeling probes for highly multiplexed Exchange-PAINT imaging. *Chem Sci* **2017,** *8* (4), 3080-3091.
6. Campello, R. J. G. B.; Moulavi, D.; Sander, J. In *Density-Based Clustering Based on Hierarchical Density Estimates*, Berlin, Heidelberg, Springer Berlin Heidelberg: Berlin, Heidelberg, 2013; pp 160-172.
7. Rothemund, P. W. K., Folding DNA to create nanoscale shapes and patterns. *Nature* **2006,** *440* (7082), 297-302.
8. Schueder, F.; Strauss, M. T.; Hoerl, D.; Schnitzbauer, J.; Schlichthaerle, T.; Strauss, S.; Yin, P.; Harz, H.; Leonhardt, H.; Jungmann, R., Universal Super-Resolution Multiplexing by DNA Exchange. *Angew Chem Int Ed Engl* **2017,** *56* (14), 4052-4055.

3.3 Publication III: Up to 100-fold speed-up and multiplexing in optimized DNA-PAINT

Sebastian Strauss, Ralf Jungmann

Nature Methods, volume 17, pages 789–791 (2020).

DOI: https://doi.org/10.1038/s41592-020-0869-x

The slow speed of DNA-PAINT is limiting its suitability for biological and high content applications and as discussed in section (1.3.4) several approaches have been established with the aim to increase the imaging speed of DNA-PAINT. This includes reducing the background fluorescence in FRET-PAINT [40-42] or enhancing the association rate of the imager and docking site by optimized sequence design and optimized buffer conditions [44]. While these techniques were successful to speed-up DNA-PAINT, they are still limited in either the achievable spatial resolution or multiplexing capabilities.

In this publication, I improved the docking site sequence design by introducing short DNA motifs that comprise overlapping binding sites. For example, a short motif TCC can be concatenated multiple times resulting in TCCTCCTCCTCCTCCTCC(T) which is 19 nucleotides long but contains five binding sites for the complementary imager strand AGGAGGA. I applied this design for six different motifs that are based on a two-letter code to avoid hairpin formation with extended length. Using DNA origami structures, I was able to demonstrate that the binding frequency scales linearly with the number of (overlapping) binding sites on one docking strand. I then measured these binding frequencies on 20-nm-grid structures, using single binding sites. For the 10xR2 sequence, I measured an apparent association rate of ~10^8 M^{-1} s^{-1}, which is approximately a hundred-fold increase compared to a standard P1 sequence. Furthermore, I demonstrated that there is no detrimental effect stemming from the extended docking site for spatial resolution or specific protein staining in cells. In fact, I was able to resolve 5 nm distances on DNA origami structure using a 5xR1 sequence. Using a site-specifically couple GFP nanobody, I successfully imaged the nuclear pore complex (Nup96) with high labeling efficiency and spatial resolution. To demonstrate the feasibility of

multiplexed speed-optimized imaging, I imaged 20-nm-grids decorated with six different speed-sequences. In each round, I resolved 20-nm distances with an image acquisition time of only five minutes per round. Finally, I performed a 4-plex multiplexing experiment in cells, targeting 4 different receptor tyrosine kinases. In SKOV3 EGFR-tagRFP Her-GFP cells we labeled GFP, and RFP with specific nanobodies, and c-Met and Erbb3 with a combination of primary antibody and secondary nanobody. With a localization precision of approximately 5 nm for each target, I was able to resolve homo- and heterodimerization of these receptors and measured distances between receptors of 16 and 24 nm respectively.

In conclusion, using short concatenated sequence motifs with overlapping binding sites, I could further speed up DNA-PAINT imaging and make it applicable for up to six-target multiplexing. The improved binding frequencies of imager strands are not only useful for faster imaging but also enable the use of lower imager concentrations resulting in reduced background fluorescence and an increased signal-to-noise ratio.

nature methods

BRIEF COMMUNICATION

https://doi.org/10.1038/s41592-020-0869-x

Up to 100-fold speed-up and multiplexing in optimized DNA-PAINT

Sebastian Strauss[1,2] and Ralf Jungmann[1,2] ✉

DNA-PAINT's imaging speed has recently been significantly enhanced by optimized sequence design and buffer conditions. However, this implementation has not reached an ultimate speed limit and is only applicable to imaging of single targets. To further improve acquisition speed, we introduce concatenated, periodic DNA sequence motifs, yielding up to 100-fold-faster sampling in comparison to traditional DNA-PAINT. We extend this approach to six orthogonal sequence motifs, now enabling speed-optimized multiplexed imaging.

Super-resolution imaging has enabled the visualization of biological structures below the diffraction limit of light[1–3]. DNA-PAINT is an easy-to-implement super-resolution technique providing better than 5-nm spatial resolution, as previously demonstrated on DNA nanostructures[4]. Furthermore, we have recently combined DNA-PAINT with small labeling probes to translate this high spatial resolution to cellular imaging on the level of single proteins[5,6]. In addition, DNA-barcoded labeling probes in combination with sequential readout enable spectrally unlimited multiplexing in Exchange-PAINT[7]. However, in practice, the biological applicability of DNA-PAINT is restricted owing to rather slow imaging, often resulting in acquisition times of up to hours[8]. The imaging speed is limited by the intrinsic hybridization kinetics of the respective docking and imager strand sequence pair. Recently, this issue has been addressed by rational sequence design[9] and careful buffer optimization, resulting in DNA-PAINT image acquisition that is an order of magnitude faster[10]. Further improvement has been achieved by preloading DNA-PAINT imager strands with Argonaute proteins[11]. While these advancements in image acquisition speed have paved the way toward high-throughput studies using DNA-PAINT, a tenfold improvement might not be the ultimate speed limit. Furthermore, while sequence optimization alone yielded a respectable fivefold speed increase for the best performing sequence, it lacks multiplexing capability, as orthogonal sequences with similar hybridization properties are not available.

Here we introduce a new concept to further increase imaging speed in DNA-PAINT, by using the fact that the frequency of imagers binding to their docking strands scales linearly with the number of available binding sites, a fact that has been central to quantitative imaging in qPAINT[12]. An intuitive way to achieve multiple docking sequences per target would be to simply change a single complementary sequence (Fig. 1a) to a concatenated version (for example, five repeats; Fig. 1b, top). However, while this seems logical, it comes at the disadvantage of also increasing the length of the docking strand, for example, from 7 nucleotides for one site to 35 nucleotides for five concatenated sites. This might lead not only to a potential reduction in spatial resolution but also possibly to increased nonspecific binding to cellular components. To address both issues, we here opted for a more compact sequence design featuring a repetitive sequence motif, for example, $(TCC)_n$, which can be concatenated to provide overlapping binding sites (Fig. 1b, bottom). This allows us to theoretically design five docking site repeats, by only increasing the strand length to 19 nucleotides, rather than 35 nucleotides. To test our approach, we designed two DNA origami 20-nm grids[13] carrying 1× and 5× versions of our overlapping sequence design (called R1) targeted with Cy3B-labeled imager strands. DNA-PAINT imaging of both structures showed improved sampling for the 5× versions, and subsequent qPAINT analysis yielded an approximately fivefold increase in the mean number of binding events (551 versus 99) for origami structures carrying 5×R1 sequences (Fig. 1c,d and Extended Data Fig. 1). We furthermore quantitatively assessed the number of detected binding events for up to ten repeats for single binding sites on DNA origami, finding a linear increase in binding events with the number of repeats (Fig. 1e and Supplementary Fig. 1).

We then turned our attention to introducing multiplexing capabilities to speed-optimized DNA-PAINT by designing five additional orthogonal sequence motifs, which could again be concatenated to form overlapping binding sites (Fig. 2a). These were based on a motif containing either three bases—R2, $(ACC)_n$; R5, $(CTT)_n$; R6, $(AAC)_n$—or two bases—R3, $(CT)_n$; R4, $(AC)_n$—while maintaining a two-letter code sequence (that is, AC or TC only) to avoid transient hairpin formation of the docking site[9,10]. We assayed the hybridization kinetics of these sequences using DNA origami with single docking sites (Extended Data Figs. 2 and 3, and Supplementary Figs. 2 and 3). As for the R1 sequence described above, concatenation of the R2 to R6 sequences also resulted in a linear increase in binding frequency. Using six 20-nm-grid structures carrying R1–R6 docking sites, we could show that imager strands only bind specifically to their corresponding docking sites, thus providing quantitative proof of their respective orthogonality (Extended Data Fig. 4 and Supplementary Fig. 4). To benchmark the achievable Exchange-PAINT imaging speed, we used the same origami structures and were able to clearly resolve 20-nm distances with sufficient sampling after 5 min for each round, resulting in a total raw image acquisition time of just 30 min for the six-plex super-resolution experiment (Fig. 2b,c and Extended Data Fig. 5). We note that we did not observe a considerable effect of photo-induced depletion of docking sites[14] owing to the shorter overall binding times for the sequences and the use of an oxygen scavenger and triplet-state quencher system[15] (PCA, PCD and trolox; Methods).

Despite the extended length of the concatenated docking strands, we were able to maintain DNA-PAINT's sub-5-nm spatial resolution capability, as substantiated by imaging 5-nm features on 'MPI' logos designed on DNA origami (Fig. 2d and Extended Data Fig. 6). Because of the relatively low imager concentration of 200 pM, we achieved a high signal-to-noise ratio, enabling 5-nm resolution

[1]Faculty of Physics and Center for Nanoscience, Ludwig Maximilian University, Munich, Germany. [2]Max Planck Institute of Biochemistry, Martinsried, Germany. ✉e-mail: jungmann@biochem.mpg.de

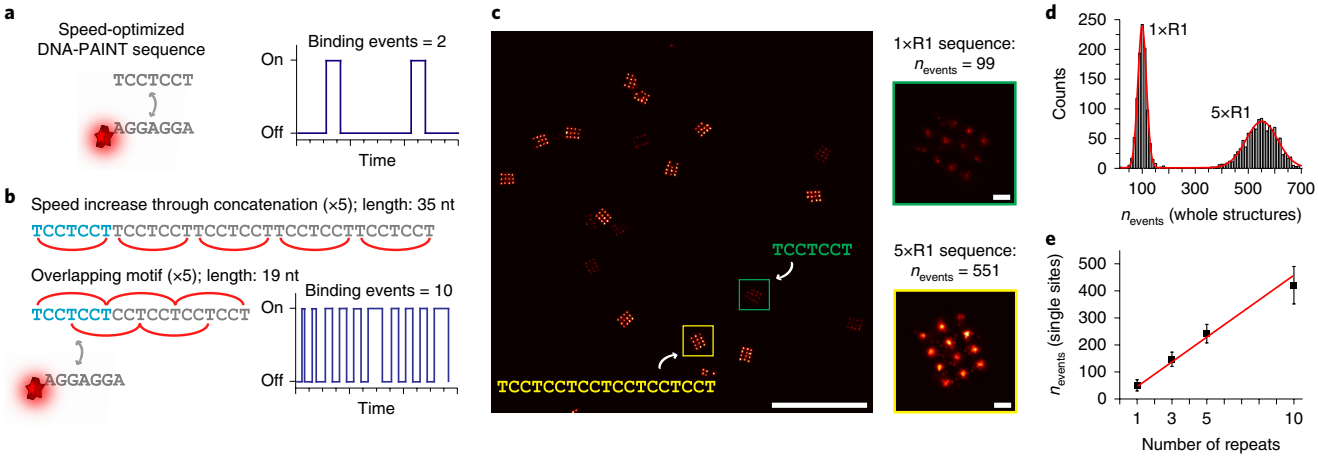

Fig. 1 | Faster DNA-PAINT through overlapping sequence motifs. a, A single speed-optimized DNA-PAINT sequence exhibits a certain number of binding events (for example, two per unit time). **b**, Top, concatenation leads to a linear increase in binding frequency and thus imaging speed. Bottom, using periodic sequence motifs enables overlapping binding sites, thus allowing shorter docking sequences. **c**, Proof of concept using two 20-nm DNA origami grids carrying 1×R1 and 5×R1 sequence extensions, showing an increase in the number of binding events (insets, magnified views of the areas highlighted in the overview; $n = 2{,}226$). **d**, Analysis of binding events for the whole DNA origami structures from **c** showing an increase in the number of events for the 5×R1 sequence motif ($n = 2{,}226$). **e**, Comparison of the number of binding events for single docking strands featuring 1×, 3×, 5× and 10× binding motifs shows a linear increase in the number of binding events ($n = 3{,}805$). Center lines depict the mean value of the Gaussian fit, and error bars depict the s.d. of the fit. Scale bars: 500 nm (**c**, overview), 20 nm (**c**, insets). Each experiment was repeated three times independently with similar results.

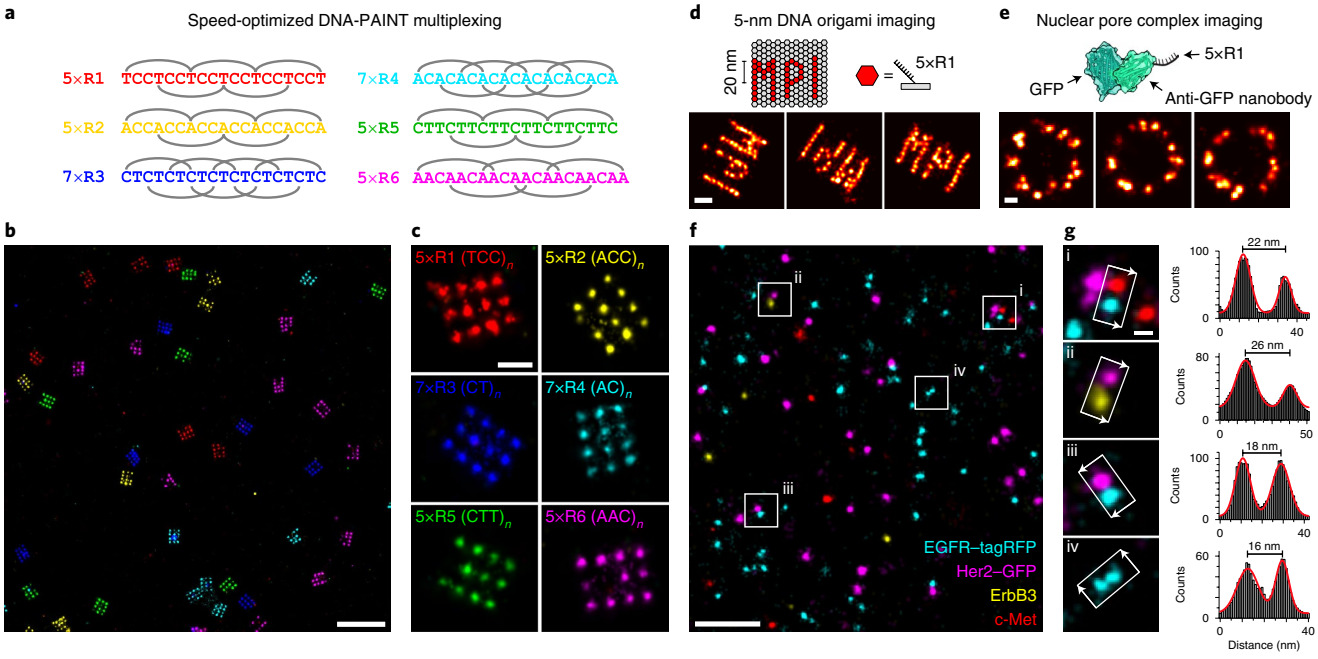

Fig. 2 | Multiplexing with concatenated speed-optimized motifs. a, Design of six orthogonal binding motifs enables speed-optimized multiplexing in Exchange-PAINT experiments. **b**, Proof-of-concept experiments using 20-nm-grid DNA origami with six orthogonal sequence motifs resolved in 5 min per round. **c**, Example structures from the experiment depicted in **b**. **d**, Imaging of 5-nm features on 'MPI' origami structures carrying 5×R1 binding sites. **e**, EGFP–Nup96 proteins labeled with nanobodies that were site-specifically coupled to 5×R1 docking sites. **f**, Cellular proof-of-concept study using four orthogonal overlapping sequence motifs targeting cell-surface receptors (EGFR, Her2, ErbB3 and c-Met) using a combination of DNA-conjugated primary nanobodies (against EGFR–tagRFP and Her2–GFP) and secondary nanobodies against primary antibodies (ErbB3 and c-Met). **g**, Four-plex Exchange-PAINT with improved docking site sequences enables single-protein resolution, revealing presumably homo- and heterodimers of RTKs, highlighted by c-Met–EGFR (i), Her2–ErbB3 (ii) and EGFR–Her2 (iii) heterodimers and EGFR homodimers (iv) with distance measures between 16 and 26 nm using a cross-sectional histogram analysis. Scale bars: 200 nm (**b**), 40 nm (**c**), 20 nm (**d**,**e**,**g**) and 200 nm (**f**). Each experiment was repeated three times independently with similar results.

with a camera integration time of only 100 ms (as compared to the 350 ms used in previous works[4]). Next, we applied our new approach to cellular imaging. We site-specifically coupled the 5×R1 sequence to an anti-GFP nanobody[16,17] and visualized the nuclear pore complex protein Nup96 in U2OS cells expressing Nup96–mEGFP (refs. [18,19]). We achieved highly specific and efficient labeling at sub-10-nm spatial resolution (Fig. 2e and Extended Data Fig. 7). We furthermore demonstrated two-plex Exchange-PAINT imaging using a combination of primary and secondary antibodies for tubulin and vimentin (Extended Data Fig. 8), showing specific labeling of cytoskeletal structures.

Finally, we performed four-plex Exchange-PAINT using four of the new sequences to demonstrate cellular imaging with single-protein resolution by targeting the receptor tyrosine kinases (RTKs) EGFR, Her2, ErbB3 and c-Met. To accomplish this, we used a commercially available double-knock-in cell line (SKOV-3 cells expressing Her2–GFP and EGFR–tagRFP) and DNA-conjugated nanobodies against both fluorescent proteins[20]. In addition, we used a combination of primary antibodies and DNA-conjugated secondary nanobodies[17] to label c-Met and ErbB3 in these cells (Fig. 2f and Extended Data Fig. 9). We obtained single-protein resolution with calculated localization precisions[21] of approximately 5 nm (Supplementary Table 10) for all four receptors and visualized homo- and heterodimerization of these RTKs with measured distances between 16–22 nm (Fig. 2g).

In conclusion, we have introduced a new concept to design docking sites with tunable hybridization kinetics and demonstrated up to 100-fold-faster imaging as compared to classical DNA-PAINT. At the same time, we introduced up to six-plex Exchange-PAINT imaging using speed-optimized docking sites. Besides faster DNA-PAINT, the new sequences enable imaging at lower imager concentration, leading to reduced background and thus increased signal-to-noise ratio. We note that the considerable increase in sampling frequency will potentially prove crucial in biological applications in tissues or imaging of nuclear targets further away from the coverslip, where high signal-to-noise ratio is essential. A further promising application is to use changes of kinetic hybridization properties for multiplexing with kinetic barcoding as previously reported[22]. For instance, the R3 sequence motif provides clearly distinguishable bright (τ_B) and dark (τ_D) times, thus enabling efficient kinetic barcoding, for example, on the level of single target proteins, which was thus far not achievable[22] (Extended Data Fig. 10). We note that our approach could be combined with preloading of imager strands using DNA-binding proteins[11] and fluorogenic probes[23] to potentially further increase imaging speed. Finally, the improved sampling frequency as compared to traditional DNA-PAINT could now enable single-protein-sensitive, high-resolution studies of a multitude of cell-surface receptor proteins and other biomedical applications with sample statistics thus far out of reach.

Online content

Any methods, additional references, Nature Research reporting summaries, source data, extended data, supplementary information, acknowledgements, peer review information; details of author contributions and competing interests; and statements of data and code availability are available at https://doi.org/10.1038/s41592-020-0869-x.

Received: 20 February 2020; Accepted: 18 May 2020;
Published online: 29 June 2020

References

1. Hell, S. W. & Wichmann, J. Breaking the diffraction resolution limit by stimulated emission: stimulated-emission-depletion fluorescence microscopy. *Opt. Lett.* **19**, 780–782 (1994).
2. Betzig, E. et al. Imaging intracellular fluorescent proteins at nanometer resolution. *Science* **313**, 1642–1645 (2006).
3. Rust, M. J., Bates, M. & Zhuang, X. Sub-diffraction-limit imaging by stochastic optical reconstruction microscopy (STORM). *Nat. Methods* **3**, 793–795 (2006).
4. Schnitzbauer, J., Strauss, M. T., Schlichthaerle, T., Schueder, F. & Jungmann, R. Super-resolution microscopy with DNA-PAINT. *Nat. Protoc.* **12**, 1198–1228 (2017).
5. Strauss, S. et al. Modified aptamers enable quantitative sub-10-nm cellular DNA-PAINT imaging. *Nat. Methods* **15**, 685–688 (2018).
6. Schlichthaerle, T. et al. Site-specific labeling of affimers for DNA-PAINT microscopy. *Angew. Chem. Int. Ed. Engl.* **57**, 11060–11063 (2018).
7. Jungmann, R. et al. Multiplexed 3D cellular super-resolution imaging with DNA-PAINT and Exchange-PAINT. *Nat. Methods* **11**, 313–318 (2014).
8. Dai, M., Jungmann, R. & Yin, P. Optical imaging of individual biomolecules in densely packed clusters. *Nat. Nanotechnol.* **11**, 798–807 (2016).
9. Schickinger, M., Zacharias, M. & Dietz, H. Tethered multifluorophore motion reveals equilibrium transition kinetics of single DNA double helices. *Proc. Natl Acad. Sci. USA* **115**, E7512–E7521 (2018).
10. Schueder, F. et al. An order of magnitude faster DNA-PAINT imaging by optimized sequence design and buffer conditions. *Nat. Methods* **16**, 1101–1104 (2019).
11. Filius, M. et al. High-speed super-resolution imaging using protein-assisted DNA-PAINT. *Nano Lett.* **20**, 2264–2270 (2020).
12. Jungmann, R. et al. Quantitative super-resolution imaging with qPAINT. *Nat. Methods* **13**, 439–442 (2016).
13. Rothemund, P. W. Folding DNA to create nanoscale shapes and patterns. *Nature* **440**, 297–302 (2006).
14. Blumhardt, P. et al. Photo-induced depletion of binding sites in DNA-PAINT microscopy. *Molecules* **23**, 3165 (2018).
15. Aitken, C. E., Marshall, R. A. & Puglisi, J. D. An oxygen scavenging system for improvement of dye stability in single-molecule fluorescence experiments. *Biophysical J.* **94**, 1826–1835 (2008).
16. Schlichthaerle, T. et al. Direct visualization of single nuclear pore complex proteins using genetically-encoded probes for DNA-PAINT. *Angew. Chem. Int. Ed. Engl.* **58**, 13004–13008 (2019).
17. Pleiner, T. et al. Nanobodies: site-specific labeling for super-resolution imaging, rapid epitope-mapping and native protein complex isolation. *eLife* **4**, e11349 (2015).
18. Thevathasan, J. V. et al. Nuclear pores as versatile reference standards for quantitative superresolution microscopy. *Nat. Methods* **16**, 1045–1053 (2019).
19. Gwosch, K. C. et al. MINFLUX nanoscopy delivers 3D multicolor nanometer resolution in cells. *Nat. Methods* **17**, 217–224 (2020).
20. Sograte-Idrissi, S. et al. Nanobody detection of standard fluorescent proteins enables multi-target DNA-PAINT with high resolution and minimal displacement errors. *Cells* **8**, 48 (2019).
21. Endesfelder, U., Malkusch, S., Fricke, F. & Heilemann, M. A simple method to estimate the average localization precision of a single-molecule localization microscopy experiment. *Histochem. Cell Biol.* **141**, 629–638 (2014).
22. Wade, O. K. et al. 124-color super-resolution imaging by engineering DNA-PAINT blinking kinetics. *Nano Lett.* **19**, 2641–2646 (2019).
23. Chung, K. K. et al. Fluorogenic probe for fast 3D whole-cell DNA-PAINT. Preprint at *bioRxiv* https://doi.org/10.1101/2020.04.29.066886 (2020).

Methods

Materials. Unmodified DNA oligonucleotides were purchased from MWG Eurofins and Metabion. DNA oligonucleotides modified with C3-azide, Cy3B and ATTO 655 were ordered from Metabion and MWG Eurofins. M13mp18 scaffold was obtained from Tilibit. Magnesium (1 M; AM9530G), sodium chloride (5 M; AM9759), ultrapure water (10977-035), Tris (1 M, pH 8; AM9855G), EDTA (0.5 M, pH 8.0; AM9260G) and 10× PBS (70011051) were purchased from Thermo Fisher Scientific. BSA (A4503-10G) was ordered from Sigma-Aldrich. Triton X-100 (6683.1), sodium borohydride (>97%; 4051.1), ammonium chloride (K298.1) and potassium chloride (6781.1) were purchased from Carl Roth. Sodium hydroxide (31627.290) was purchased from VWR. Paraformaldehyde (15710) and glutaraldehyde (16220) were obtained from Electron Microscopy Sciences. Tween-20 (P9416-50ML), glycerol (65516-500ml), methanol (32213-2.5L), protocatechuate 3,4-dioxygenase pseudomonas (PCD; P8279), 3,4-dihydroxybenzoic acid (PCA; 37580-25G-F) and (±)-6-hydroxy-2,5,7,8-tetra-methylchromane-2-carboxylic acid (trolox; 238813-5G) were ordered from Sigma-Aldrich. Streptavidin (S-888) was purchased from Thermo Fisher. Biotin-labeled BSA (A8549) was obtained from Sigma-Aldrich. Coverslips (0107032) and glass slides (10756991) were purchased from Marienfeld and Thermo Fisher Scientific. Double-sided tape (665D) was ordered from Scotch. Two-component silica twinsil speed 22 (1300 1002) was purchased from Picodent. FBS (10500-064), 1× PBS (pH 7.2; 20012-019) and 0.05% trypsin–EDTA (25300-054) were purchased from Thermo Fisher Scientific. Ninety-nanometer gold nanoparticles (G-90-100) were ordered from Cytodiagnostics.

Buffers. The following buffers were used for sample preparation and imaging:

- Buffer A: 10 mM Tris pH 8, 100 mM NaCl and 0.05% Tween-20
- Buffer B: 10 mM $MgCl_2$, 5 mM Tris-HCl pH 8, 1 mM EDTA and 0.05% Tween-20, pH 8
- Buffer C (imaging buffer): 1× PBS, 1 mM EDTA and 500 mM NaCl, pH 7.4; optionally supplemented with 1× trolox, 1× PCA and 1× PCD
- Blocking buffer: 1× PBS pH 7.4, 1 mM EDTA, 3% BSA and 0.02% Tween-20

Trolox, PCA and PCD. 100× trolox was made by adding 100 mg trolox to 430 µl of 100% methanol and 345 µl of 1 M NaOH in 3.2 ml water. 40× PCA was made by mixing 154 mg PCA in 10 ml water and NaOH and adjusting the pH to 9.0. 100× PCD was made by adding 9.3 mg PCD to 13.3 ml of buffer (100 mM Tris-HCl pH 8, 50 mM KCl, 1 mM EDTA, 50% glycerol).

DNA origami self-assembly. All DNA origami structures were designed with the Picasso design tool[4]. Self-assembly of DNA origami was accomplished in a one-pot reaction mix with a total volume of 40 µl, consisting of 10 nM scaffold strand (for sequences, see Supplementary Data 1), 100 nM folding staples (Supplementary Data 2–4), 500 nM biotinylated staples (Supplementary Table 3) and 1 µM staple strands with docking site extensions (for respective sequences, see Supplementary Tables 4 and 5, and Supplementary Data 2–4) in folding buffer (5 mM Tris pH 8, 1 mM EDTA, 12.5 mM $MgCl_2$). The reaction mix was then subjected to a thermal annealing ramp using a thermocycler. The reaction mix was first incubated at 80 °C for 5 min, cooled using a temperature gradient from 60 to 4 °C in steps of 1 °C per 3.21 min and finally held at 4 °C.

DNA origami purification. DNA origami structures were purified via ultrafiltration using Amicon Ultra Centrifugal Filters with a 50-kDa molecular weight cutoff (MWCO; Merck Millipore, UFC505096) as previously described[24]. In brief, folded origami was brought to 500 µl with FoB5 buffer (5 mM Tris, 1 mM EDTA, 5 mM NaCl, 5 mM $MgCl_2$, pH 8) and spun for 6 min at 5,000*g*. This process was repeated twice. Purified DNA origami structures were recovered into a new tube by centrifugation for 5 min at 5,000*g*.

DNA origami sample preparation. For sample preparation, a piece of coverslip and a glass slide were sandwiched together with two strips of double-sided tape to form a flow chamber with an inner volume of ~20 µl. First, 20 µl of biotin-labeled BSA (1 mg ml^{-1}; dissolved in buffer A) was flushed into the chamber and incubated for 2 min. The chamber was then washed with 40 µl of buffer A. A volume of 20 µl of streptavidin (0.1 mg ml^{-1}; dissolved in buffer A) was then flushed into the chamber and allowed to bind for 2 min. After washing with 20 µl of buffer A and subsequently with 20 µl of buffer B, 20 µl of biotin-labeled DNA structures (~200 pM) in buffer B was flushed into the chamber and incubated for 2 min. The chamber was washed with 40 µl of buffer B. Finally, 20 µl of the imager solution in imaging buffer (Supplementary Table 8) was flushed into the chamber, which was subsequently sealed with two-component silica before imaging. For multiplexing experiments, a bottomless six-channel slide (ibidi, 80608) was attached to a coverslip. The same sample preparation was performed as described above with adjusted volumes of 120 µl for each washing and incubation step. In between imaging rounds, the sample was washed 4–5 times with 120 µl PBS until no residual signal from the previous imager solution was detected (total washing time of approximately 3–5 min). Then, the next imager solution was introduced.

Antibody–DNA conjugation. Antibodies were conjugated to DNA-PAINT docking sites (Supplementary Table 7) via DBCO-sulfo-NHS ester chemistry as previously reported[4]. In brief, antibodies were reacted with 20-fold excess of a bifunctional DBCO-sulfo-NHS ester (Jena Biosciences, CLK-A124-10). Unreacted linker was removed using Zeba Spin Desalting columns (0.5 ml, 40,000 MWCO; Thermo Fisher Scientific, 89882). Azide-functionalized DNA was added to the DBCO-antibodies at a tenfold molar excess and reacted overnight at 4 °C. Afterward, the buffer was exchanged to PBS using Amicon centrifugal filters (100,000 MWCO).

Nanobody–DNA conjugation. Nanobodies against GFP, tagRFP, and rabbit and mouse IgG were purchased from Nanotag with a single ectopic cysteine at the C terminus for site-specific and quantitative conjugation. Conjugation to DNA-PAINT docking sites (Supplementary Table 7) was performed similarly to the previously described method[20]. First, buffer was exchanged to 1× PBS + 5 mM EDTA, pH 7.0, using Amicon centrifugal filters (10,000 MWCO) and free cysteines were reacted with 20-fold molar excess of bifunctional maleimide-DBCO linker (Sigma-Aldrich, 760668) for 2–3 h on ice. Unreacted linker was removed by buffer exchange to PBS using Amicon centrifugal filters. Azide-functionalized DNA was added at 5–10 molar excess to the DBCO-nanobody and reacted overnight at 4 °C. Unconjugated nanobody and free azide-DNA were removed by anion exchange using an ÄKTA Pure liquid chromatography system equipped with a Resource Q 1-ml column.

Cell culture. U2OS-CRISPR-Nup96-mEGFP cells (a gift from the Ries and Ellenberg laboratories) and SKOV3 GFP-Her2 tagRFP-EGFR cells (purchased from Sigma-Aldrich, CLL1143-1VL) were cultured in McCoy's 5A medium (Thermo Fisher Scientific, 16600082) supplemented with 10% FBS. For imaging, cells were seeded 1–2 d before fixation in glass-bottomed eight-well µ-slides (ibidi, 80827).

Cell fixation. All fixatives were preheated to 37 °C before addition to the cells.

Microtubules and vimentin. U2OS-CRISPR-Nup96-mEGFP cells were first pre-extracted with 0.3% glutaraldehyde and 0.25% Triton X-100 for 90 s, followed by fixation with 3% glutaraldehyde for 10 min. Afterward, samples were rinsed twice with PBS and free aldehyde groups were reduced with 0.1% $NaBH_4$ for 5 min. After rinsing four times with PBS, cells were blocked and permeabilized in blocking buffer with 0.25% Triton X-100 for 2 h. Cells were incubated with primary antibodies against vimentin and α-tubulin overnight at 4 °C. After washing away unbound primary antibodies four times with PBS, secondary antibodies conjugated to DNA-PAINT docking sites were diluted in blocking buffer and incubated with the cells for 1 h at room temperature. Finally, unbound antibodies were removed by washing three times with PBS for 5 min.

Nup96–EGFP imaging. U2OS-CRISPR-Nup96-mEGFP cells were fixed with 2.4% paraformaldehyde in PBS for 30 min at room temperature. After fixation, cells were washed three times with PBS and incubated with 0.1 M NH_4Cl in PBS for 5 min. Then, cells were permeabilized with 0.25% Triton X-100 for 5 min and afterward blocked in blocking buffer for 1 h. Cells were incubated with anti-GFP nanobodies at a concentration of approximately 50 nM in blocking buffer supplemented with 0.05 mg ml^{-1} sheared salmon sperm DNA overnight at 4 °C. Unbound nanobodies were removed by washing three times with PBS for 5 min.

Receptor tyrosine kinases. SKOV3 GFP-Her2 tagRFP-EGFR cells were fixed with 4% paraformaldehyde. After fixation, cells were washed three times with PBS and incubated with 0.1 M NH_4Cl in PBS for 5 min. Then, cells were permeabilized with 0.25% Triton X-100 for 15 min and afterward blocked in blocking buffer for 1 h. Nanobodies and primary antibodies (Supplementary Table 6) were diluted in blocking buffer supplemented with 0.05 mg ml^{-1} sheared salmon sperm DNA and incubated with the cells overnight at 4 °C. Unbound nanobodies and antibodies were removed by washing three times with PBS for 5 min.

Microscope setup. Fluorescence imaging was carried out on an inverted microscope (Nikon Instruments, Eclipse Ti2) with the Perfect Focus System, applying an objective-type TIRF configuration equipped with an oil-immersion objective (Nikon Instruments, Apo SR TIRF ×100, NA 1.49, Oil). 561-nm and 642-nm lasers (MPB Communications, 2 W, DPSS system) were used for excitation. The laser beams were passed through cleanup filters (Chroma Technology, ZET561/10 and ZET 640/10) and coupled into the microscope objective using a beam splitter (Chroma Technology, ZT561rdc and ZT640rdc). Fluorescence was spectrally filtered with an emission filter (Chroma Technology, ET600/50m and ET700/75m) and imaged on an sCMOS camera (Andor, Zyla 4.2 Plus) without further magnification, resulting in an effective pixel size of 130 nm (after 2 × 2 binning). Images were acquired by choosing a region of interest with a size of 512 × 512 pixels. More detailed imaging conditions for the respective experiments are shown in Supplementary Table 8.

Image analysis. Raw fluorescence data were subjected to super-resolution reconstruction using the Picasso software package[4] (latest version available at

https://github.com/jungmannlab/picasso). Drift correction was performed with a redundant cross-correlation and gold particles as fiducials. Gold particles were also used to align multiple rounds for Exchange-PAINT experiments. For quantification of binding kinetics, localizations were linked allowing a gap size of three frames and a maximum distance of 130 nm. Origami structures were automatically selected using Picasso's 'pick similar' function. The kinetic information of the detected selections was extracted with the 'save pick properties' command. Further quantification such as histogram analysis and fitting was performed with Origin Pro (version 2019b). Kinetic barcoding analysis (Extended Data Fig. 10) was performed as previously described[22]. The data were segmented using the HDBSCAN clustering algorithm[25] with input parameter 'Min_cluster size' set to 10.

Reporting Summary. Further information on research design is available in the Nature Research Reporting Summary linked to this article.

Data availability

All raw data are available upon reasonable request from the authors.

References

24. Wagenbauer, K. F. et al. How we make DNA origami. *ChemBioChem* **18**, 1873–1885 (2017).
25. McInnes, L., Healy, J. & Astels, S. hdbscan: hierarchical density based clustering. *J. Open Source Softw.* **2**, 205 (2017).

Acknowledgements

This work has been supported in part by the German Research Foundation through the Emmy Noether Program (DFG JU 2957/1-1), the SFB1032 (project A11), the European Research Council through an ERC Starting Grant (MolMap; grant agreement number 680241), the Allen Distinguished Investigator Program through the Paul G. Allen Frontiers Group, the Danish National Research Foundation (Centre for Cellular Signal Patterns, DNRF135), the Max Planck Foundation and the Max Planck Society. We thank the Ries and Ellenberg groups at EMBL for the kind gift of the cell line expressing Nup96–mEGFP. We thank T. Schlichthaerle, M. Ganji and F. Schueder for fruitful discussions. S.S. acknowledges support by the QBM Graduate School.

Author contributions

S.S. conceived and performed experiments, analyzed data and contributed to the writing of the manuscript. R.J. conceived and supervised the study, interpreted data and wrote the manuscript. Both authors reviewed and approved the manuscript.

Competing interests

The authors declare no competing interests.

Additional information

Extended data is available for this paper at https://doi.org/10.1038/s41592-020-0869-x.

Supplementary information is available for this paper at https://doi.org/10.1038/s41592-020-0869-x.

Correspondence and requests for materials should be addressed to R.J.

Peer review information Rita Strack was the primary editor on this article and managed its editorial process and peer review in collaboration with the rest of the editorial team.

Reprints and permissions information is available at www.nature.com/reprints.

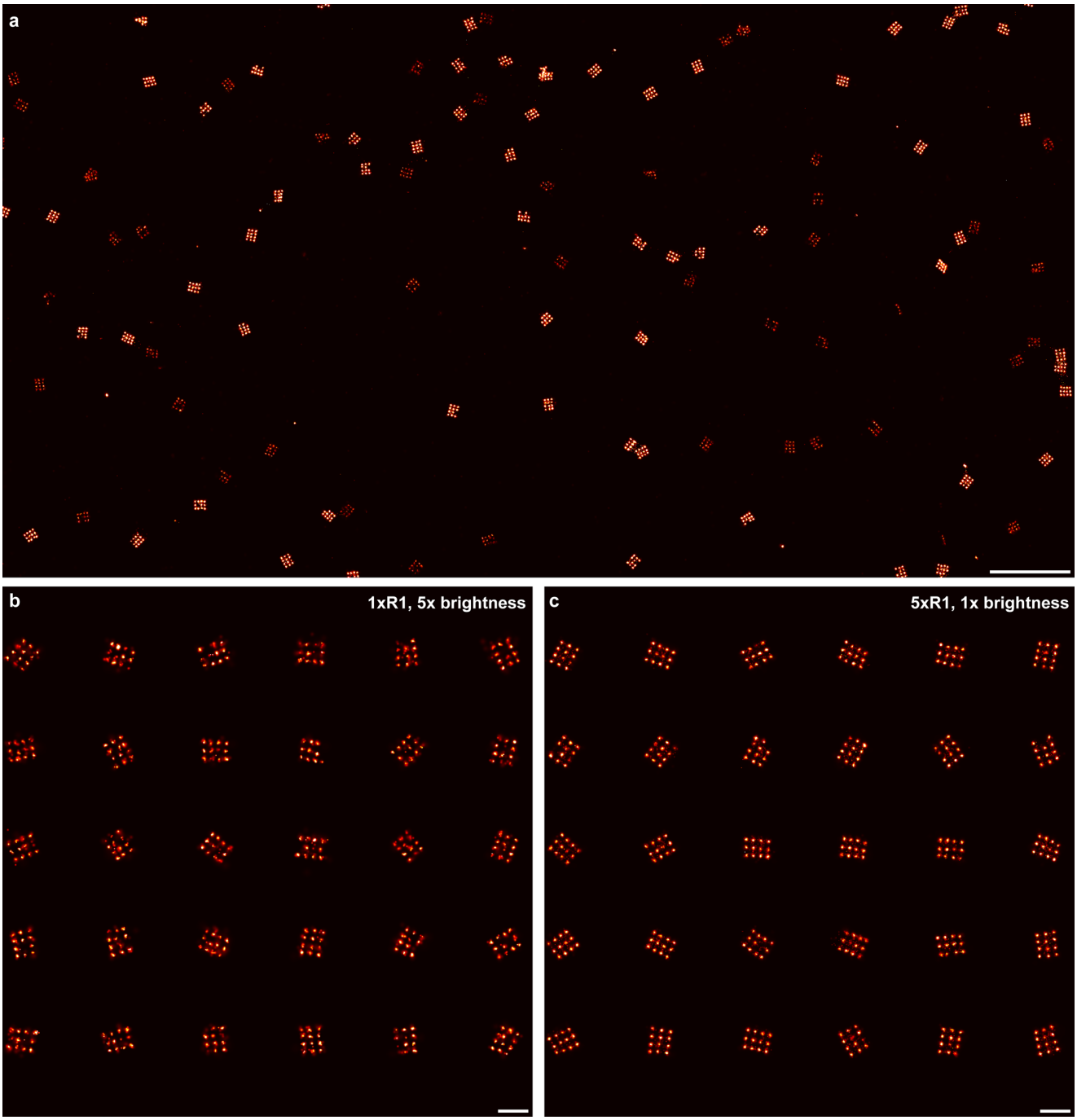

Extended Data Fig. 1 | Imaging of 20-nm grids with 1xR1 and 5xR1 docking sites. 20-nm grids with 1×R1 and 5×R1 docking sites were measured in the same sample. The data represents linked localizations, hence the brightness scales linearly with the number of binding events. **a**, Overview image. (**b** and **c**) 25 selected structures of 1× and 5×R1 DNA origami, respectively. 1×R1 structures show comparable signal intensity to 5×R1 after 5-fold increase of brightness level. Scale bars, 500 nm (**a**), 100 nm (**b**, **c**). (Integration time: 100 ms, 40 000 frames, 500 pM R1 Cy3B, Excitation intensity: 125 W/cm^2). The experiment was repeated two times independently with similar results.

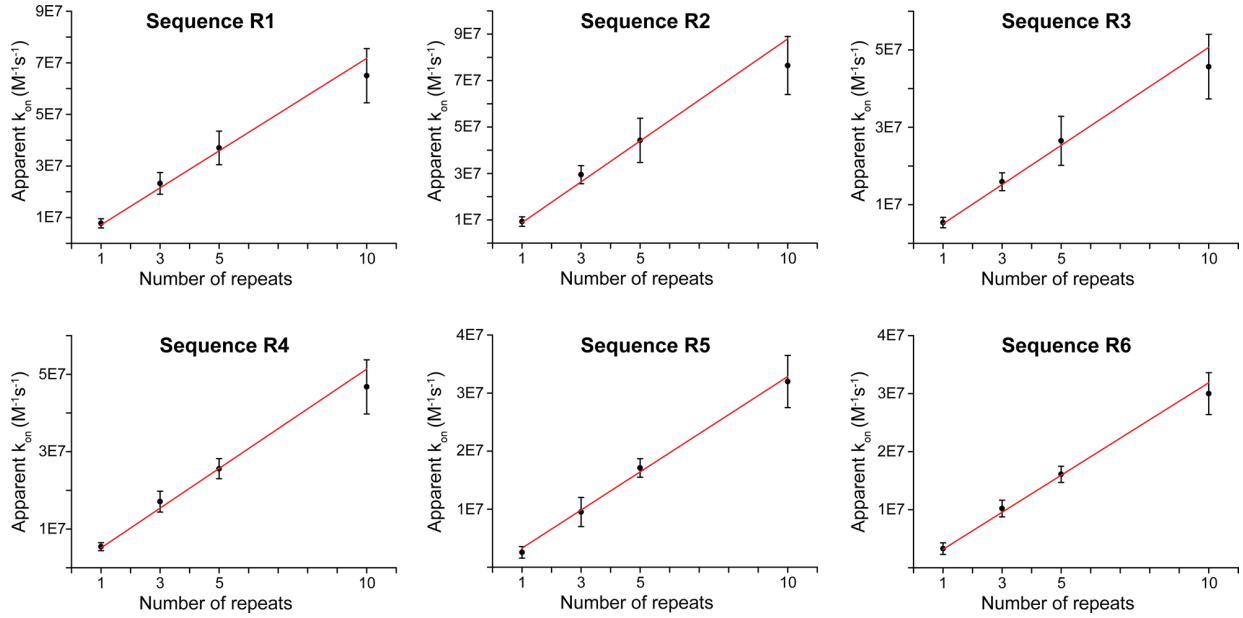

Extended Data Fig. 2 | Linear increase of k_{on} with number of repeats for 6 different sequence motifs. Apparent k_{on} values were calculated by fitting the average dark times obtained from single binding sites on DNA origami with a Gaussian function and subsequently calculating $k_{on} = 1/(\tau_d \cdot c)$, where c denotes the imager strand concentration. Error bars indicate standard deviation of Gaussian fits. All overlapping binding site motifs show a linear dependency until 5x repeats. Some 10x binding motifs exhibit a lower-than-expected k_{on}, which could be explained by decreased accessibility due to the increased sequence length (and thus flexibility). Mean k_{on} values are additionally denoted in Supplementary Table 1. We note that each graph consists of data gathered from three separate experiments per sequence, containing repeat pairs of 1x and 3×, 1x and 5×, and 3x and 10×, respectively (see Supplementary Fig. 2). Furthermore, higher motif repeats were performed with reduced imager strand concentration to avoid multiple binding events. Plotting apparent k_{on} values allows us to faithfully compare sequence repeats (see Supplementary Tables 8 and 9 for details about image acquisition parameters and number of analyzed origami structures).

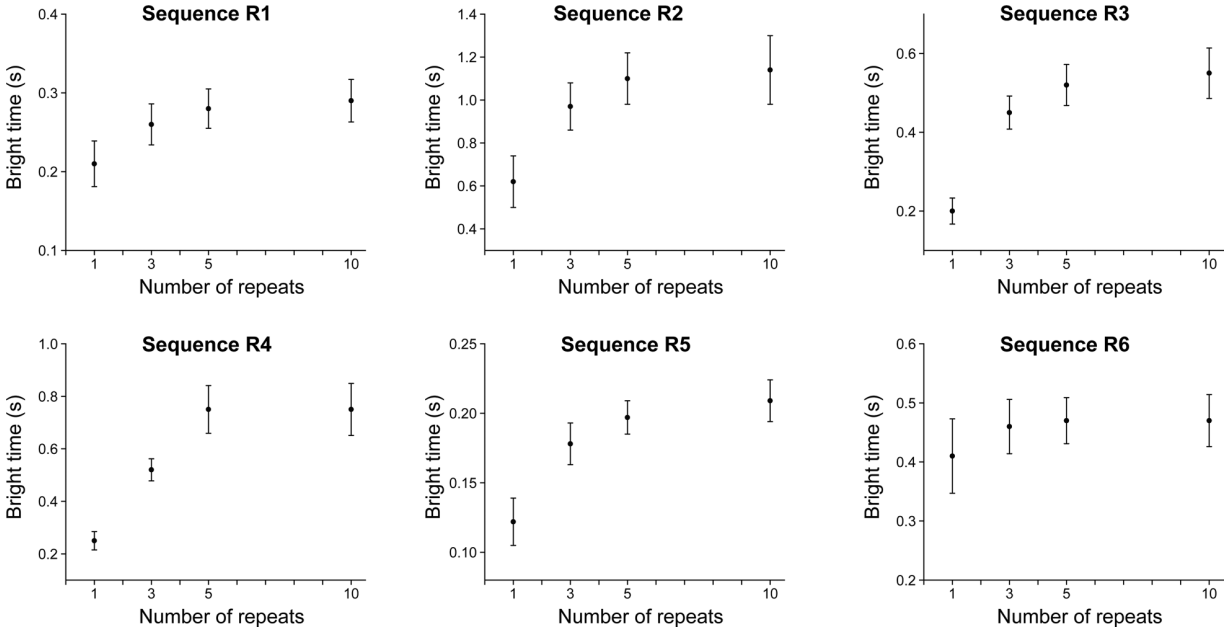

Extended Data Fig. 3 | Mean bright time values depending on the number of repeats. Analysis was performed with the same data sets presented in Extended Data Fig. 2 and Supplementary Fig. 2. Each data point shows the average of the calculated mean bright time (τ_B) values of each origami structure. Error bars indicate standard deviation. Bright times increase with increasing number of repeats (at various degrees depending on the sequence). Increasing times can particularly be observed from 1 to 3 repeats, whereas it is similar/equal from 5 to 10 repeats, indicating a potential stabilization of DNA hybridization due to extended overhangs of the docking site sequences.

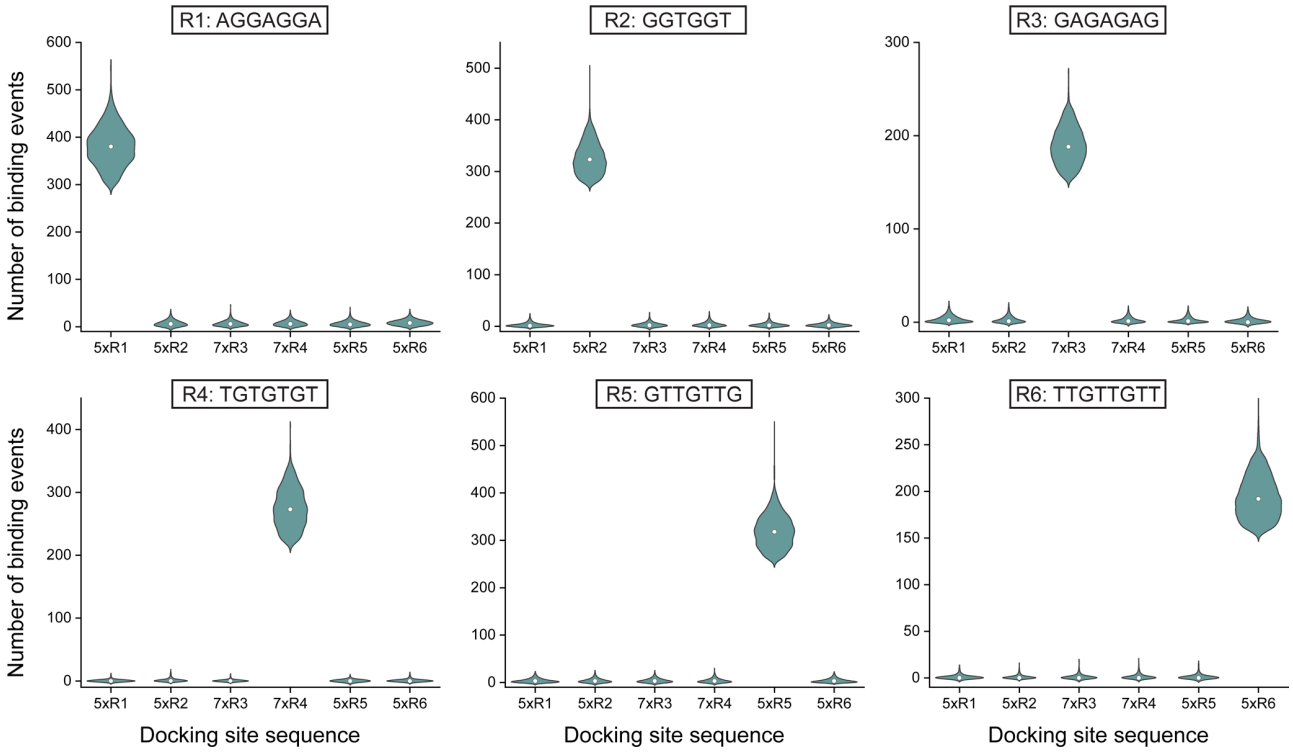

Extended Data Fig. 4 | Quantification of sequence orthogonality. To evaluate the orthogonality of the designed docking sites, the number of binding events of the respective imager sequences (labeled in each graph) in the DNA origami Exchange-PAINT experiment from Supplementary Fig. 4 is quantified for all six structures in the same sample. The violin plots show the distribution of the calculated mean number of binding events detected per structure. The white circle in the violin plots depicts the median number of binding events. A significant number of binding events was exclusively detected for imagers binding to their corresponding docking sites, highlighting exquisite sequence orthogonality, making the sequences applicable for multiplexing experiments. (Number of analyzed origami structures: 5×R1: n = 3515; 5×R2: n = 2436; 7×R3: n = 2619; 7×R4: n = 2502; 5×R5: n = 2962; 5×R6: n = 3381).

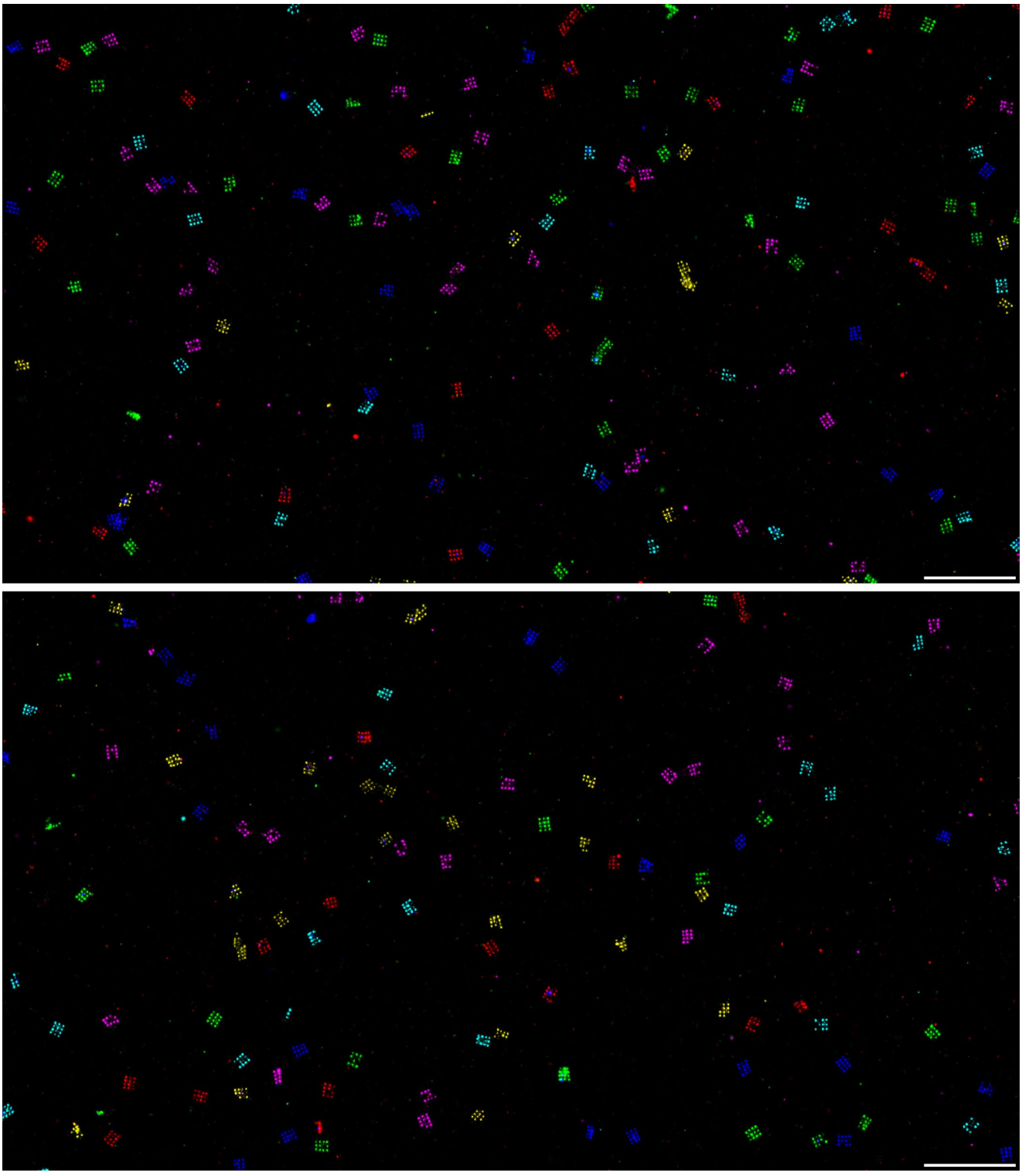

Extended Data Fig. 5 | 6-color Exchange-PAINT in 30 minutes image acquisition time. 6 different 20-nm-grid origami structures carrying 6 orthogonal concatenated docking sites were measured sequentially with an imaging time of no longer than 5 minutes per round. Each channel shows clearly resolved and sampled 20-nm-grids and NeNa values below 4 nm (see Supplementary Table 10) in two exemplary field of views. Scale bar: 500 nm. (Integration time: 50 ms, 5 500 frames, Imager concentrations: R1_6nt (5 nM), R2_6nt (2 nM), R3_2 (5 nM), R4_6nt (5 nM), R5 (10 nM), R6_6nt (10 nM), Excitation intensity: 650 W/cm^2). The experiment was repeated three times independently with similar results.

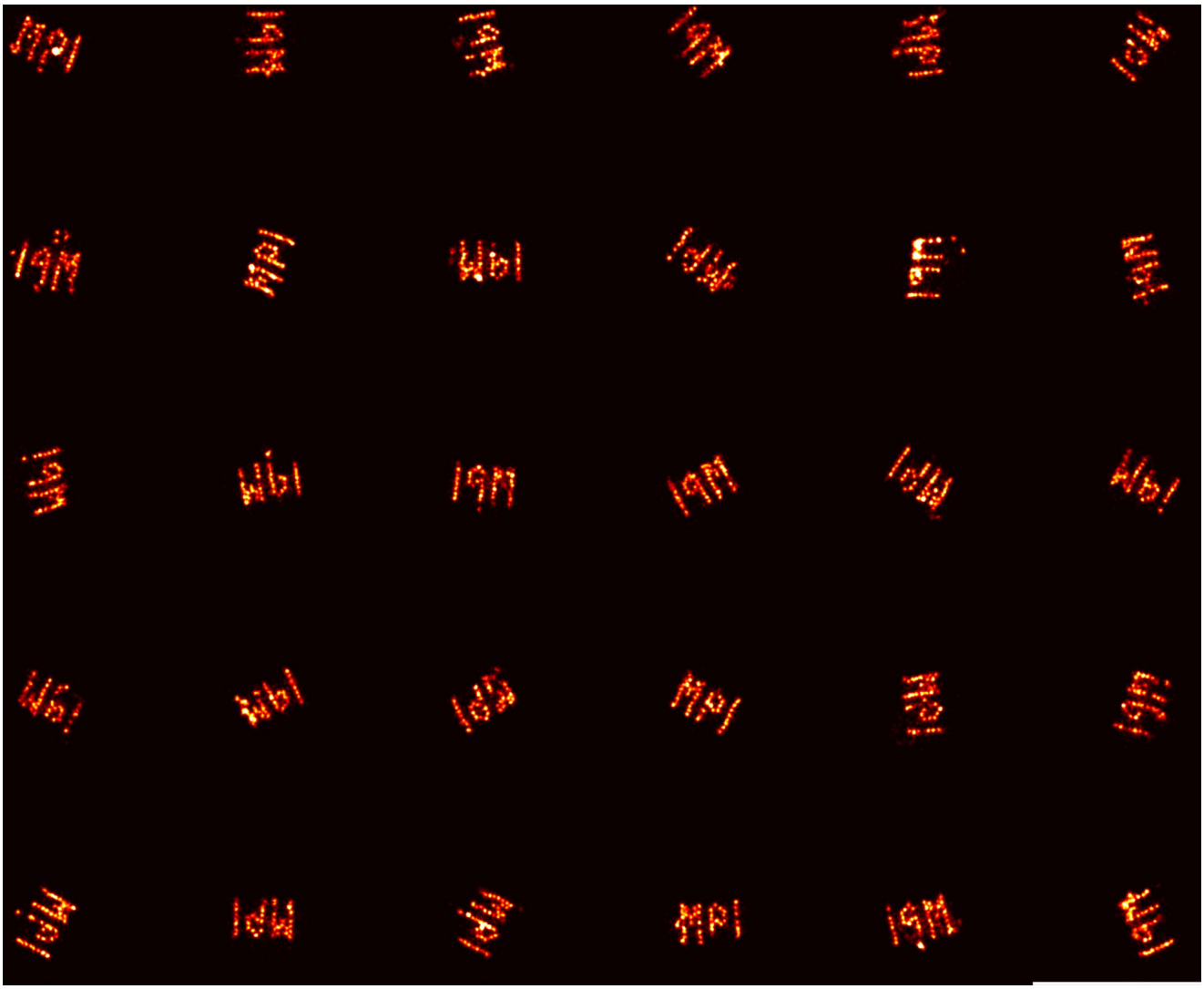

Extended Data Fig. 6 | Sub-5-nm resolution imaging with 5xR1 sequence. Array of 30 selected DNA origami structures showing an MPI logo with neighboring docking sites designed to be spaced in 5 nm distances. Extended length of the 5×R1 docking site does not negatively affect the resolution capability as 5-nm-distances can be clearly resolved. Scale bar: 200 nm. (integration time: 100 ms, 40 000 frames, 200 pM R1-Cy3B, Excitation intensity: 650 W/cm^2). The experiment was repeated three times independently with similar results.

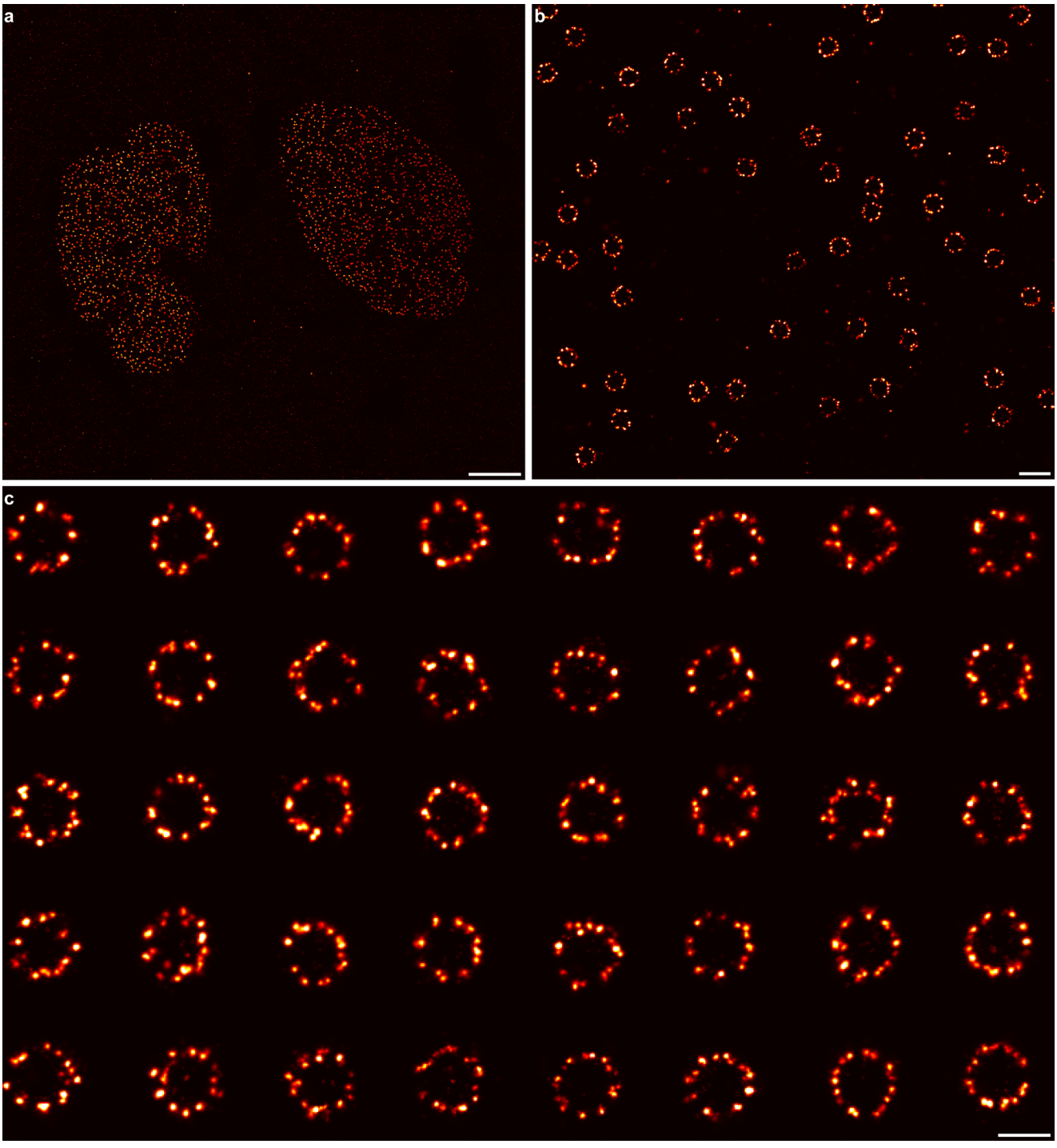

Extended Data Fig. 7 | Nuclear pore complex imaging using 5xR1 sequence with a GFP nanobody. a, Overview image showing specific staining of NPCs at the nuclear envelope. **b**, Zoom-in area shows distinct NPC structures. **c**, Zoom-in of 40 picked NPCs with clearly resolved single Nup96 proteins. Scale bars, 5 µm (**a**), 200 nm (**b**), 100 nm (**c**). (Integration time: 100 ms, 40 000 frames, 250 pM R1 Cy3B, Excitation intensity: 180 W/cm^2). The experiment was repeated three times independently with similar results.

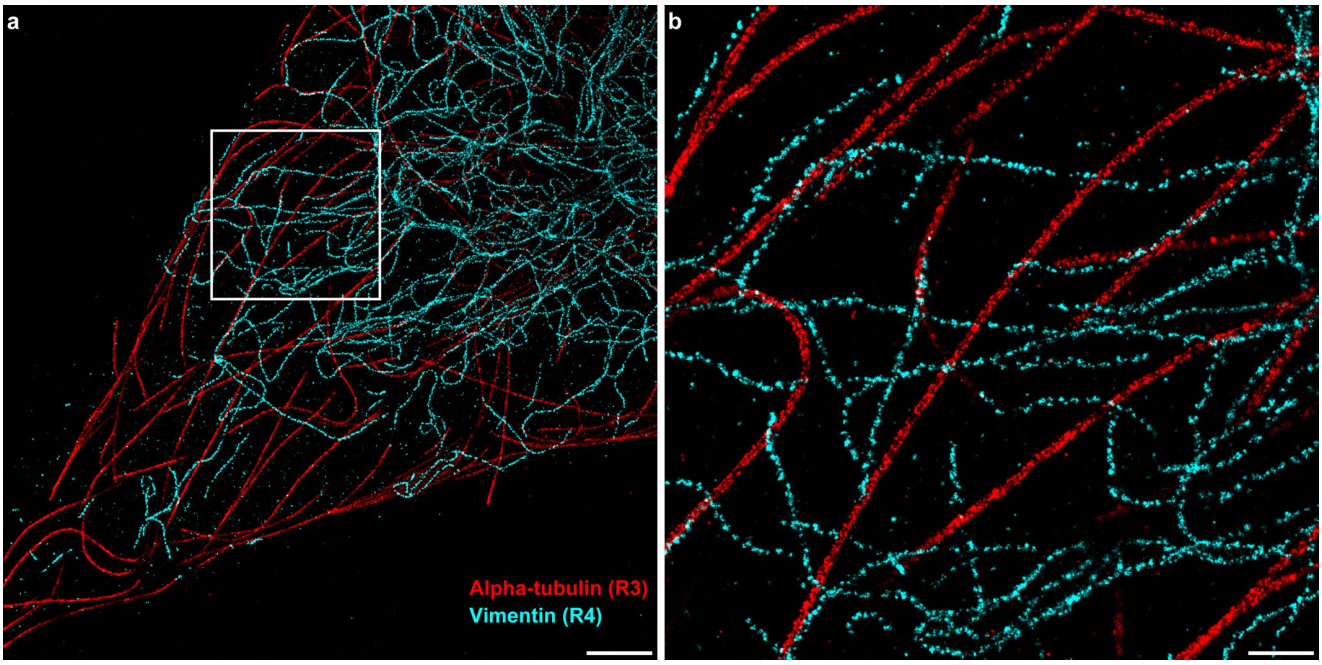

Extended Data Fig. 8 | Two-round Exchange-PAINT alpha-tubulin and vimentin imaging. Alpha-tubulin and vimentin were labeled with primary and secondary antibodies. **a**, Overview image shows specific labeling of vimentin and microtubules. **b**, Zoom-in to the region highlighted in **a**. Scale bars, 2 µm (**a**), 500 nm (**b**). (Integration time: 100 ms, 20 000 frames, R3/4 50 pM, Excitation intensity: 200 W/cm^2). The experiment was repeated two times independently with similar results.

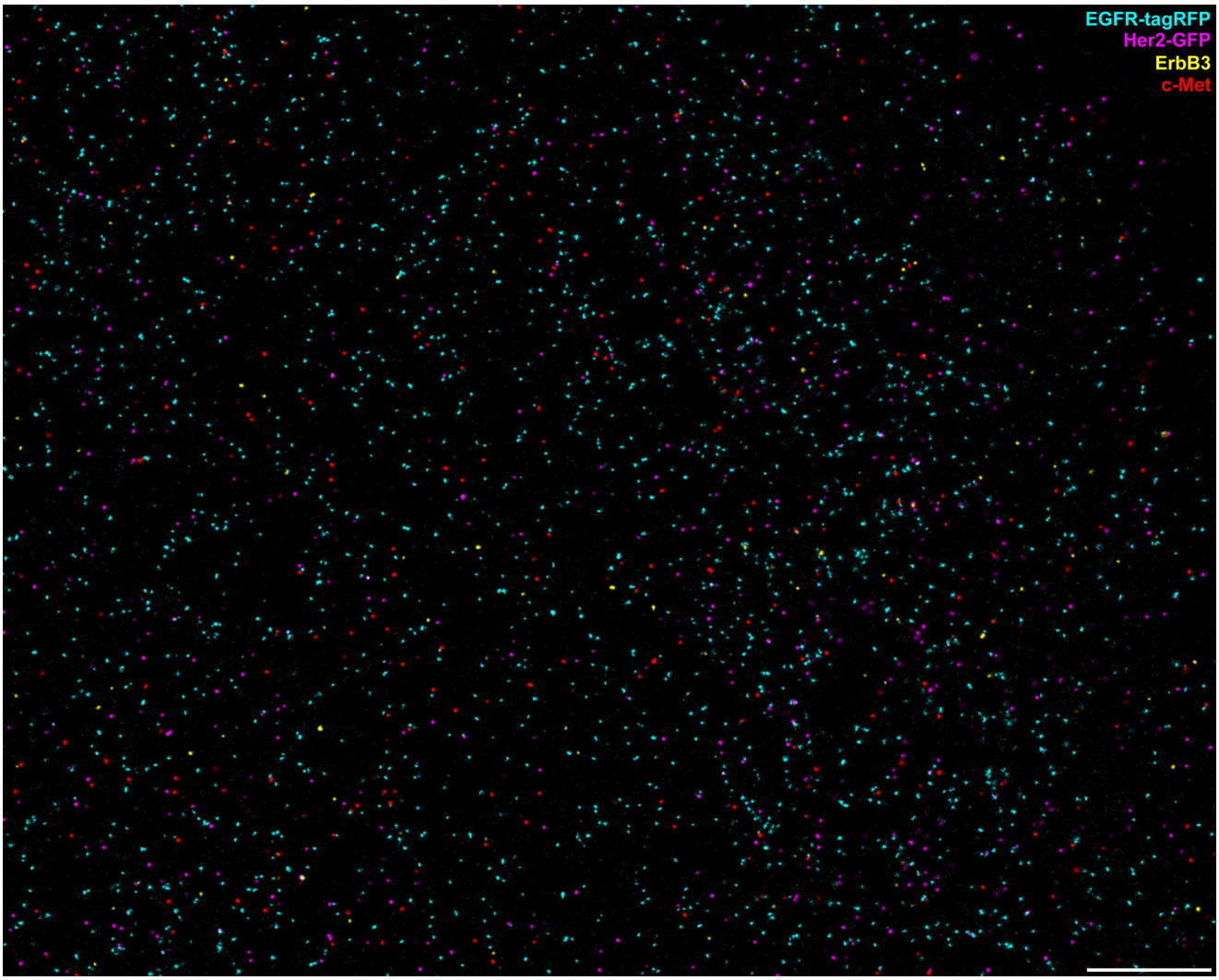

Extended Data Fig. 9 | 4-color overview image of receptor tyrosine kinases. Large FOV display from the data shown in Fig. 2f and g. Receptors in SKOV3 GFP-Her2 tagRFP-EGFR cells were labeled using DNA-conjugated nanobodies as shown in Supplementary Table 6 and 7. Data is represented as linked localizations. Each channel reveals distinct single molecules on the cell surface. Scale bar: 1 µm. Image acquisition parameters are shown in Supplementary Table 8. The experiment was repeated three times independently with similar results.

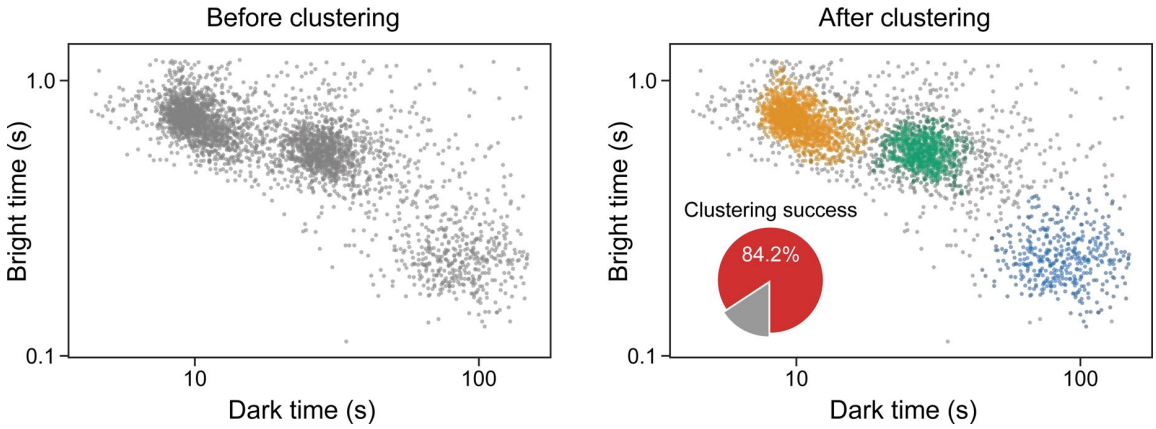

Extended Data Fig. 10 | Improved kinetic properties for barcoding. Concatenation of binding sequences leads to an increased bright time and a decreased dark time which can be used for barcoding based on these kinetic parameters. Potential barcoding capability was demonstrated on single 1×, 3× and 10× R3 binding sites, because the R3 sequence shows distinct separation of bright and dark time values (Extended Data Figs. 2 and 3, Supplementary Fig. 2). The barcoding capability was tested by using a HDBSCAN clustering algorithm. 84.2% of the 3492 analyzed binding sites were classified as either 1×R3 (blue), 3×R3 (green) or 10×R3 (orange). (Integration time: 100 ms, 20 000 frames, 3 nM R3 Cy3B, Excitation intensity: 25 W/cm^2, all structures measured in the same sample).

nature research

Corresponding author(s): Ralf Jungmann

Last updated by author(s): May 13, 2020

Reporting Summary

Nature Research wishes to improve the reproducibility of the work that we publish. This form provides structure for consistency and transparency in reporting. For further information on Nature Research policies, see Authors & Referees and the Editorial Policy Checklist.

Statistics

For all statistical analyses, confirm that the following items are present in the figure legend, table legend, main text, or Methods section.

n/a	Confirmed	
☐	☒	The exact sample size (*n*) for each experimental group/condition, given as a discrete number and unit of measurement
☐	☒	A statement on whether measurements were taken from distinct samples or whether the same sample was measured repeatedly
☒	☐	The statistical test(s) used AND whether they are one- or two-sided *Only common tests should be described solely by name; describe more complex techniques in the Methods section.*
☒	☐	A description of all covariates tested
☒	☐	A description of any assumptions or corrections, such as tests of normality and adjustment for multiple comparisons
☐	☒	A full description of the statistical parameters including central tendency (e.g. means) or other basic estimates (e.g. regression coefficient) AND variation (e.g. standard deviation) or associated estimates of uncertainty (e.g. confidence intervals)
☒	☐	For null hypothesis testing, the test statistic (e.g. *F*, *t*, *r*) with confidence intervals, effect sizes, degrees of freedom and *P* value noted *Give P values as exact values whenever suitable.*
☒	☐	For Bayesian analysis, information on the choice of priors and Markov chain Monte Carlo settings
☒	☐	For hierarchical and complex designs, identification of the appropriate level for tests and full reporting of outcomes
☒	☐	Estimates of effect sizes (e.g. Cohen's *d*, Pearson's *r*), indicating how they were calculated

Our web collection on statistics for biologists contains articles on many of the points above.

Software and code

Policy information about availability of computer code

Data collection	Raw microscopy data was acquired using µManager (Version 2.0-gamma) (Edelstein, A., Amodaj, N., Hoover, K., Vale, R. & Stuurman, N. Curr. Protoc. Mol. Biol. 14.20 (2010))
Data analysis	Custom analysis software Picasso was used to process raw super-resolution data. The software is open source and was described in detail in the following publication: Nature Protocols volume 12, pages 1198–1228 (2017) doi:10.1038/nprot.2017.024 Origin Pro 2019b was used for data fitting and plotting.

For manuscripts utilizing custom algorithms or software that are central to the research but not yet described in published literature, software must be made available to editors/reviewers. We strongly encourage code deposition in a community repository (e.g. GitHub). See the Nature Research guidelines for submitting code & software for further information.

Data

Policy information about availability of data

All manuscripts must include a data availability statement. This statement should provide the following information, where applicable:

- Accession codes, unique identifiers, or web links for publicly available datasets
- A list of figures that have associated raw data
- A description of any restrictions on data availability

All raw data are available upon request from the authors.

Field-specific reporting

Please select the one below that is the best fit for your research. If you are not sure, read the appropriate sections before making your selection.

☒ Life sciences ☐ Behavioural & social sciences ☐ Ecological, evolutionary & environmental sciences

For a reference copy of the document with all sections, see nature.com/documents/nr-reporting-summary-flat.pdf

Life sciences study design

All studies must disclose on these points even when the disclosure is negative.

Sample size	The sample size in case of quantitative DNA origami experiments was defined by the density of DNA Origami structures on the coverslip and the limited field of view of image acquisition
Data exclusions	No data were excluded.
Replication	All replications were successful.
Randomization	No grouping of experiments or samples were performed
Blinding	Blinding is not applicable to the study since no grouping was performed

Reporting for specific materials, systems and methods

We require information from authors about some types of materials, experimental systems and methods used in many studies. Here, indicate whether each material, system or method listed is relevant to your study. If you are not sure if a list item applies to your research, read the appropriate section before selecting a response.

Materials & experimental systems

n/a	Involved in the study
☐	☒ Antibodies
☐	☒ Eukaryotic cell lines
☒	☐ Palaeontology
☒	☐ Animals and other organisms
☒	☐ Human research participants
☒	☐ Clinical data

Methods

n/a	Involved in the study
☒	☐ ChIP-seq
☒	☐ Flow cytometry
☒	☐ MRI-based neuroimaging

Antibodies

Antibodies used	1) Anti-Vimentin (Cell Signaling Technology, Cat: 5741S, Clone: D21H3, Dilution: 1:100) 2) Anti-α-Tubulin (Synaptic systems, Cat: 302211, Clone: 3A2, Dilution: 5 µg/ml) 3) Anti-c-Met (Thermo Fisher Scientific, Cat: 700261, Clone: 22H22L13, Dilution: 1:100) 4) Anti-ErbB3 (BioLegend, Cat: 324702, Clone: 1B4C3 , Dilution: 1:100) 6)Donkey Anti-Mouse IgG (Jackson Immunosearch, Cat: 715-005-151, polyclonal, Dilution: 10 µg/ml) 7) Donkey Anti-Rabbit IgG (Jackson Immunosearch, Cat: 711-005-152, polyclonal, Dilution: 10 µg/ml)) 8) FluoTag-Q anti GFP, unlabeled (Nanotag, Cat: N0301, Clone: 1H1, Dilution: 50 nM) 9) FluoTag-Q anti-tagFP, unlabled (Nanotag, N0501, Clone: 1H7, Dilution: 50 nM) 10) FluoTag-Q anti-mouse IgG kLC, unlabeled (Nanotag, custom, Clone: 1A23 , Dilution: 50 nM) 11) FluoTag-Q anti-rabbit IgG, unlabeled (Nanotag, custom, Clone: 10E10, Dilution: 50 nM)
Validation	All antibodies were validated for IF and human species reactivity by the manufacturer according to their websites.

Eukaryotic cell lines

Policy information about cell lines

Cell line source(s)	U-2 OS-CRISPR-Nup96-mEGFP cells were obtained from the Ellenberg and Ries lab (Reference: https://doi.org/10.1038/s41592-019-0574-9. SKOV3 GFP-HER2 RFP-EGFR cells were purchased from Sigma Aldrich.
Authentication	The cell lines were not authenticated.
Mycoplasma contamination	All cell lines have been tested negative for mycoplasma contamination.

Commonly misidentified lines (See ICLAC register)	No commonly misidentified cell lines were used.

nature methods

SUPPLEMENTARY INFORMATION

https://doi.org/10.1038/s41592-020-0869-x

In the format provided by the authors and unedited.

Up to 100-fold speed-up and multiplexing in optimized DNA-PAINT

Sebastian Strauss[1,2] **and Ralf Jungmann**[1,2] ✉

[1]Faculty of Physics and Center for Nanoscience, Ludwig Maximilian University, Munich, Germany. [2]Max Planck Institute of Biochemistry, Martinsried, Germany. ✉e-mail: jungmann@biochem.mpg.de

Supplementary Information

Up to 100-fold speedup and multiplexing in optimized DNA-PAINT

Sebastian Strauss[1,2] and Ralf Jungmann[1,2]

[1]Faculty of Physics and Center for Nanoscience, Ludwig Maximilian University, Munich, Germany. [2]Max Planck Institute of Biochemistry, Martinsried, Germany. Correspondence should be addressed to R.J. (jungmann@biochem.mpg.de).

Supplementary Figure 1	**Origami structures used for speed quantification**
Supplementary Figure 2	**τ_b vs. τ_d scatter plots for R sequences**
Supplementary Figure 3	**Hybridization kinetics of 5xR1 sequence under three different buffer conditions**
Supplementary Figure 4	**Overview image of 6-color 20-nm grid origami imaging**
Supplementary Table 1	**Apparent mean k_{on} values in $(Ms)^{-1}$ calculated from data shown in Extended Data Figure 2 Supplementary Figure 2**
Supplementary Table 2	**Imager strand sequences**
Supplementary Table 3	**Biotinylated DNA staple strands**
Supplementary Table 4	**Staple strand extensions for 1 binding site experiments**
Supplementary Table 5	**DNA-PAINT sequence extensions of staple strands for 20-nm-grid experiments**
Supplementary Table 6	**List of used antibodies and nanobodies and respective applied dilutions/concentrations**
Supplementary Table 7	**Docking site sequences for antibody and nanobody conjugation**
Supplementary Table 8	**Imaging parameters**
Supplementary Table 9	**Imager concentrations for data shown in Supplementary Figures 4 and 5**
Supplementary Table 10	**Calculated NeNa values for selected DNA-PAINT measurements**
Supplementary References	

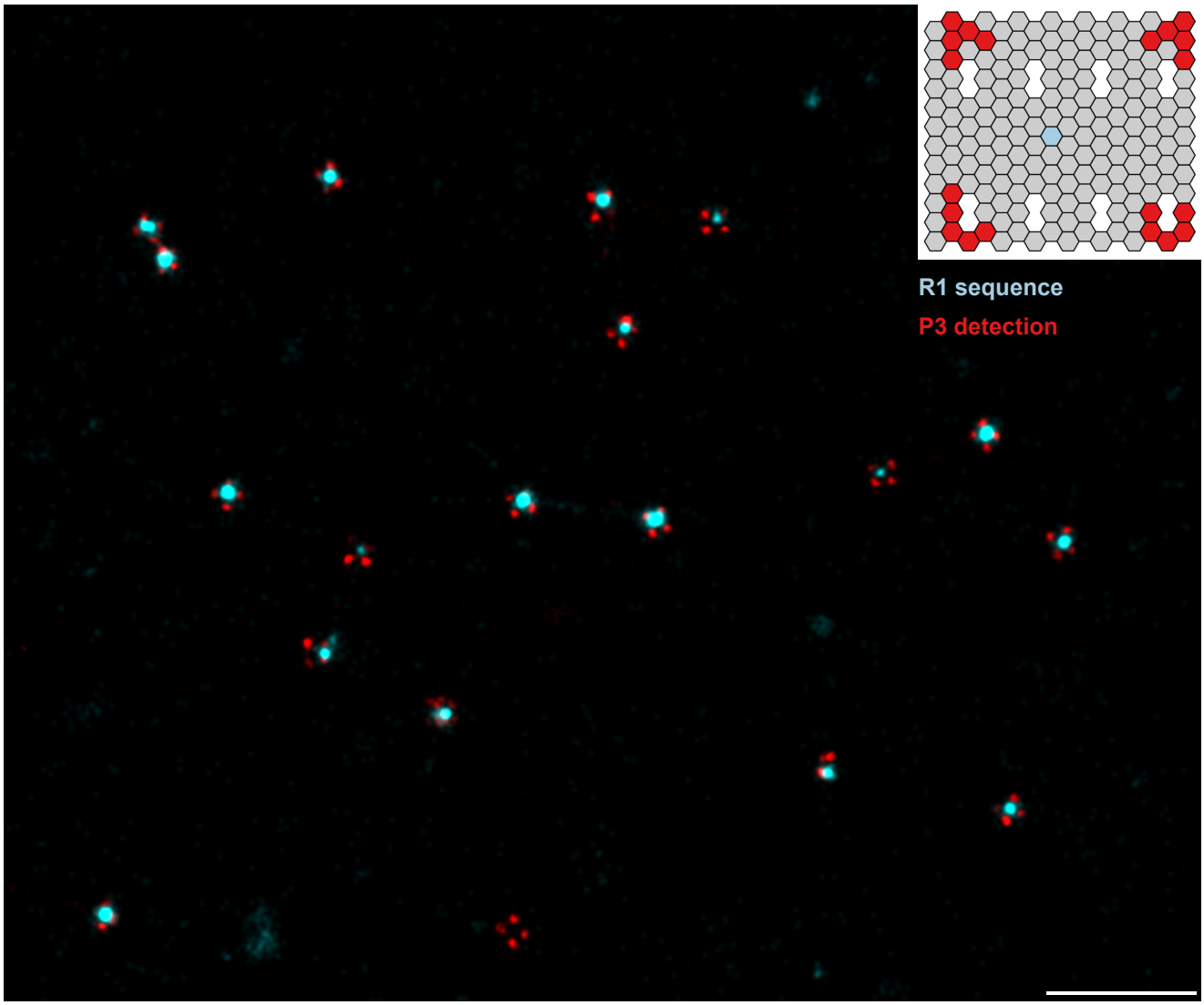

Supplementary Figure 1 | Origami structures used for speed quantification. Origami structures were designed to carry a single DNA-PAINT sequence in the center (cyan color), which is either 1xR1, 3xR1, 5xR1, or 10xR1, targeted with a Cy3B-labeled imager strand. All four origami species were measured in the same sample. The Cy3B localizations were linked to single binding events. Brightness of the cyan spots thus scales linearly with the number of binding events. For unbiased detection of DNA origami, P3 extensions (red color) in the corners are visualized using a P3 ATTO 655 imager strand. After alignment, the P3 signal was used to select DNA origami structures and kinetic properties from the data obtained in the Cy3B channel were calculated from these picked regions (Figure 1e). The same origami design was also used for data in Supplementary Figure 2. Scale bar: 500 nm. (Integration time: 100 ms, 30 000 frames, 1.5 nM R1 Cy3B, Excitation intensity: 17 W/cm^2).

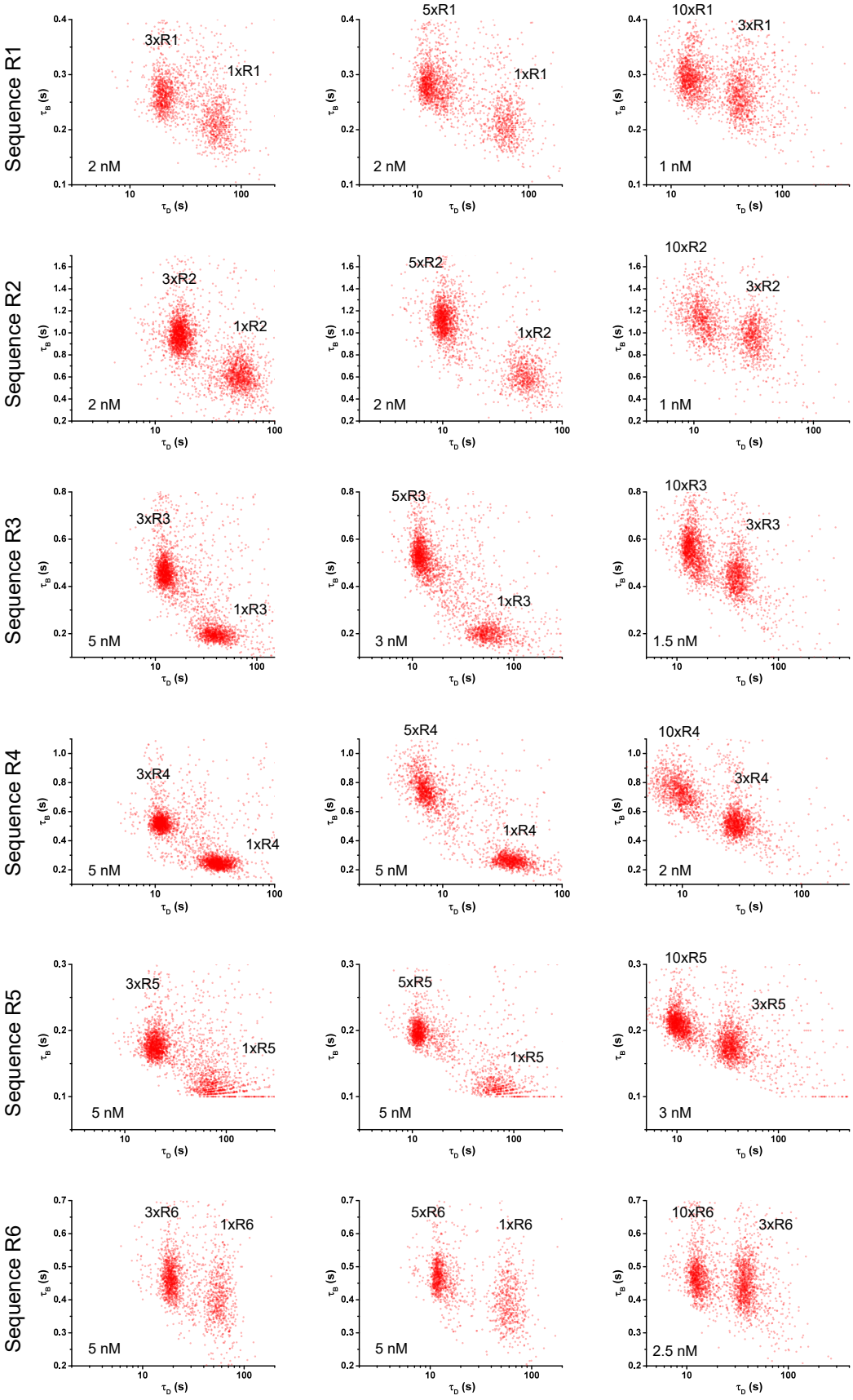

Supplementary Figure 2 | τ_b vs. τ_d scatter plots for R sequences. Pairwise comparison of docking sites with different number of repeats for all 6 motifs (1x vs. 3x; 1x vs. 5x; 3x vs. 10x). Each point depicts the calculated mean τ_b and τ_d values of a single binding site.

Scatter plots of each measurement reveal two distinct populations. Increasing number of repeats lead to decreased dark time, as expected. We note that also bright times are increased, which is most likely due to increased binding stability caused by neighboring unpaired bases on the docking strand. Note that higher motif repeats were performed with reduced imager strand concentrations to avoid multiple binding events.

4

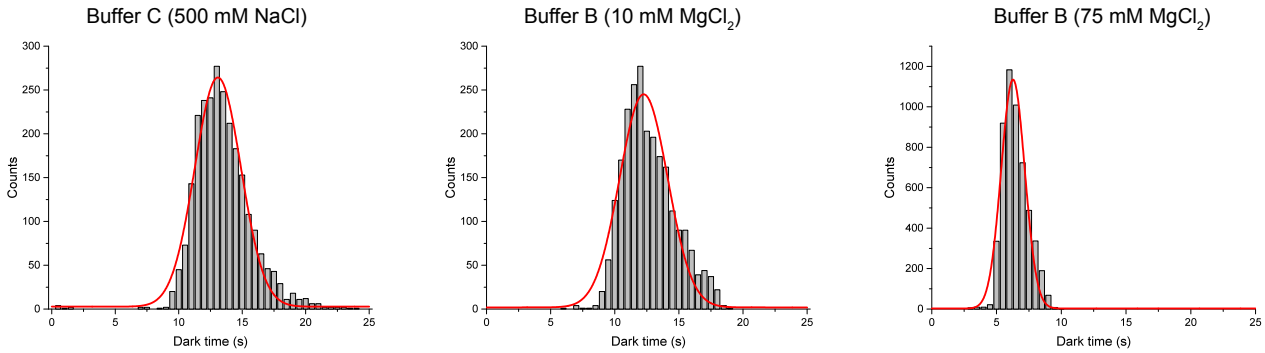

Supplementary Figure 3 | Hybridization kinetics of 5xR1 sequence under three different buffer conditions. The mean dark time (τ_D) distributions obtained for different buffer conditions were fitted with a Gaussian function. Buffer B and C showed similar τ_d values for the 5xR1 sequence ($\tau_d = 12\ s\ \pm 2\ s$ and $\tau_d = 13\ s\ \pm 2\ s$, respectively). Increasing the $MgCl_2$ concentration to 75 mM decreases the dark time by a factor of two ($\tau_d = 6.3\ s\ \pm 0.9\ s$), as reported earlier[1]. Number of analyzed origami structures: Buffer B: n = 2936, Buffer C: n = 3228, Buffer B (75 mM $MgCl_2$): n = 5953. (Integration time: 100 ms, 10 000 frames, 2 nM R1 Cy3B, Excitation intensity: 15 W/cm^2).

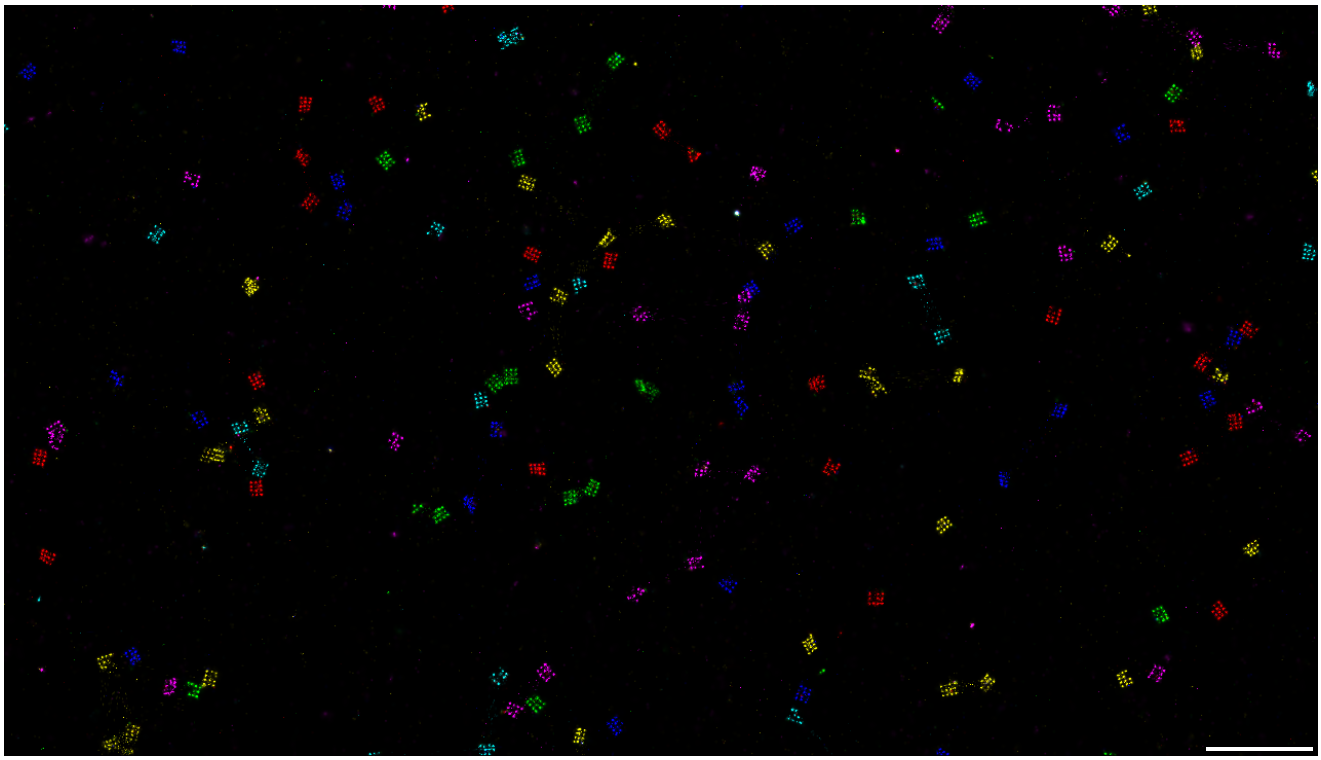

Supplementary Figure 4 | Overview image of 6-color 20-nm grid origami imaging. 6-color Exchange-PAINT imaging of 20-nm-grid origami structures that carry R1–R6 docking sites. Respective signals show no crosstalk to each other, highlighting their orthogonality. Data is shown as linked localizations. Scale bar: 500 nm. (Integration time: 100 ms, 10 000 frames, Imager concentrations: R1–4: 1 nM, R5–6: 2 nM, Excitation intensity: 120 W/cm^2). The experiment was repeated two times independently with similar results.

Supplementary Table 1 | Apparent mean k_{on} values in $(Ms)^{-1}$ calculated from data shown in Extended Data Figure 2 and Supplementary Figure 2

Sequence	1x	3x	5x	10x
R1	$7.8 * 10^6$	$23 * 10^6$	$37 * 10^6$	$65 * 10^6$
R2	$9.3 * 10^6$	$30 * 10^6$	$44 * 10^6$	$77 * 10^6$
R3	$5.4 * 10^6$	$16 * 10^6$	$27 * 10^6$	$46 * 10^6$
R4	$5.5 * 10^6$	$17 * 10^6$	$26 * 10^6$	$47 * 10^6$
R5	$2.6 * 10^6$	$9.5 * 10^6$	$17 * 10^6$	$32 * 10^6$
R6	$3.3 * 10^6$	$10 * 10^6$	$16 * 10^6$	$30 * 10^6$

Supplementary Table 2 | Imager strand sequences

Imager name	Sequence	3'-mod	Vendor
R1	AGGAGGA	Cy3B	Eurofins Genomics
R1_6nt	GGAGGA	Cy3B	Metabion
R2	TGGTGGT	Cy3B	Eurofins Genomics
R2_6nt	GGTGGT	Cy3B	Eurofins Genomics
R3	GAGAGAG	Cy3B	Metabion
R3_2	AGAGAGA	Cy3B	Metabion
R4	TGTGTGT	Cy3B	Metabion
R4_6nt	GTGTGT	Cy3B	Metabion
R5	GAAGAAG	Cy3B	Metabion
R6	TTGTTGTT	Cy3B	Metabion
R6_7nt	TGTTGTT	Cy3B	Metabion
P3	AATGAAGA	ATTO 655	Metabion

Supplementary Table 3 | List of biotinylated DNA staple strands

No	Position	Name	Sequence	Mod
1	C02	18[63]20[56]BIOTIN	ATTAAGTTTACCGAGCTCGAATTCGGGAAACCTGTCGTGC	5'-Biotin
2	C09	4[63]6[56]BIOTIN	ATAAGGGAACCGGATATTCATTACGTCAGGACGTTGGGAA	5'-Biotin
3	G02	18[127]20[120]BIOTIN	GCGATCGGCAATTCCACACAACAGGTGCCTAATGAGTG	5'-Biotin
4	G09	4[127]6[120]BIOTIN	TTGTGTCGTGACGAGAAACACCAAATTTCAACTTTAAT	5'-Biotin
5	K02	18[191]20[184]BIOTIN	ATTCATTTTTGTTTGGATTATACTAAGAAACCACCAGAAG	5'-Biotin
6	K09	4[191]6[184]BIOTIN	CACCCTCAGAAACCATCGATAGCATTGAGCCATTTGGGAA	5'-Biotin
7	O02	18[255]20[248]BIOTIN	AACAATAACGTAAAACAGAAATAAAAATCCTTTGCCCGAA	5'-Biotin
8	O09	4[255]6[248]BIOTIN	AGCCACCACTGTAGCGCGTTTTCAAGGGAGGGAAGGTAAA	5'-Biotin

Supplementary Table 4 | Staple strand extensions for 1 binding site experiments

Name	Sequence (first two bases as spacers)
R1	TT $\mathbf{(TCC)_n}$ TCCT
R2	AA $\mathbf{(ACC)_n}$ ACCA
R3	TC $\mathbf{(CT)_n}$ CTCTC
R4	CA $\mathbf{(AC)_n}$ ACACA
R5	CC $\mathbf{(CTT)_n}$ CTTC
R6	AA $\mathbf{(AAC)_n}$ AACAA

Supplementary Table 5 | DNA-PAINT sequence extensions of staple strands for 20-nm-grid experiments

Name	Sequence
1xR1	TCCTCCT
5xR1	TCCTCCTCCTCCTCCTCCT
5xR2	ACCACCACCACCACCACCA
7xR3	CTCTCTCTCTCTCTCTCTC
7xR4	ACACACACACACACACACA
5xR5	CTTCTTCTTCTTCTTCTTC
5xR6	AACAACAACAACAACAACAA

Supplementary Table 6 | List of used antibodies and nanobodies and respective applied dilutions/concentrations

Name	Vendor	Catalog number	Dilution/Concentration
Anti-Vimentin (rabbit monoclonal IgG)	Cell Signaling Technology	5741S	1:100
Anti-α-Tubulin (mouse monoclonal IgG)	Synaptic systems	302211	5 µg/ml
Anti-c-Met (monoclonal Rabbit IgG)	Thermo Fisher Scientific	700261	1:100
Anti-ErbB3 (monoclonal mouse IgG2a)	BioLegend	324702	1:100
Donkey Anti-Mouse IgG	Jackson Immunosearch	715-005-151	10 µg/ml
Donkey Anti-Rabbit IgG	Jackson Immunosearch	711-005-152	10 µg/ml
FluoTag-Q anti GFP (unlabeled, C-terminal ectopic cysteine)	Nanotag Biotechnologies	N0301	50 nM
FluoTag-Q anti-tagFP (unlabeled, C-terminal ectopic cysteine)	Nanotag Biotechnologies	N0501	50 nM
FluoTag-Q anti-mouse IgG kLC (unlabeled, C-terminal ectopic cysteine)	Nanotag Biotechnologies	Custom	50 nM
FluoTag-Q anti-rabbit IgG (unlabeled, C-terminal ectopic cysteine)	Nanotag Biotechnologies	Custom	50 nM

Supplementary Table 7 | Docking site sequences for antibody and nanobody conjugation

Nanobody/Antibody	Handle Name	Sequence	5'-mod	Vendor
GFP	5xR1	TCCTCCTCCTCCTCCTCCT	C-3 azide	Metabion
tagFP	5xR2	ACCACCACCACCACCACCA	C-3 azide	Metabion
Rabbit IgG	7xR3	CTCTCTCTCTCTCTCTCTC	C-3 azide	Metabion
Mouse kappa chain	7xR4	ACACACACACACACACACA	C-3 azide	Metabion
Mouse IgG polyclonal	2xR3	CTCTCTCTC	C-3 azide	Metabion
Rabbit IgG polyclonal	2xR4	ACACACACA	C-3 azide	Metabion

Supplementary Table 8 | Imaging parameters

Dataset	Parameters	Buffer	Power
Figure 1 c and d **Extended Data Figure 1**	100 ms, 40 000 frames, 500 pM, R1	C	125 W/cm^2
Figure 1 e, Supplementary Figure 1	100 ms, 30 000 frames, 1.5 nM, R1	C	17 W/cm^2
Extended Data Figures 2 and 3, **Supplementary Figure 2**	100 ms, 20 000 frames, 1–5 nM, R1–6 P3: 150 ms, 7 000 frames, 2–3 nM	C	15 W/cm^2 (560 nm) 300W/cm^2 (640nm)
Supplementary Figure 3	100 ms, 10 000 frames, 1 nM R1	C/B10/B75	15 W/cm^2
Figure 2 d, Extended Data Figure 6	100 ms, 40 000 frames, 200 pM	C + PCA/PCD/Tx	650 W/cm^2
Extended Data Figure 4, **Supplementary Figure 4**	100 ms, 10 000 frames, R1–4 (1 nM), R5 + 6 (2 nM)	C	120 W/cm^2
Figure 2 b and c **Extended Data Figure 5**	50 ms, 5500 frames R1_6nt (5 nM), R2_6nt (2 nM), R3_2 (5 nM), R4_6nt (5 nM), R5 (10 nM), R6_6nt (10 nM)	C + PCA/PCD/Tx	650 W/cm^2
Figure 2 e, Extended Data Figure 7	100 ms, 40 000 frames, R1, 250 pM	C + PCA/PCD/Tx	180 W/cm^2
Extended Data Figure 8	100 ms, 20 000 frames, R3+4, 50 pM	C	200 W/cm^2
Figure 2 f and g **Extended Data Figure 9**	100 ms Her2: R1, 1 nM, 20 000 frames EGFR: R2_6nt, 0.5nM. 40 000 frames c-Met: R3, 1 nM, 20 000 frames ErbB3: R4, 1 nM, 20 000 frames	C + PCA/PCD/Tx	200 W/cm^2
Extended Data Figure 10	100 ms, 20 000 frames, R3, 3 nM	C + PCA/PCD/Tx	25 W/cm^2

Supplementary Table 9 | Imager concentrations and number of analyzed origami structures (n) for data shown in Extended Data Figures 2 and 3 and Supplementary Figure 2

Dataset	1x and 3x		1x and 5x		1x and 10x	
	Concentration	n	Concentration	n	Concentration	n
R1	2 nM R1	2216	2 nM R1	2473	1 nM R1	2633
R2	2 nM R2	3548	2 nM R2	2565	1 nM R2	1938
R3	5 nM R3	3282	3 nM R3	3073	1.5 nM R3	3101
R4	5 nM R4	3247	5 nM R4	2582	2 nM R4	2585
R5	5 nM R5	2853	5 nM R5	2048	3 nM R5	3328
R6	5 nM R6	2220	5 nM R6	1794	2.5 nM R6	2839

Supplementary Table 10 | Calculated NeNa values for selected DNA-PAINT measurements

Dataset	Docking site / Imager	NeNa
Figure 1 c and d, Extended Data Figure 1	1xR1 / R1	3.7 nm
	5xR1 / R1	3.5 nm
Figure 2 b and c, Extended Data Figure 5	5xR1 / R1_6nt	3.8 nm
	5xR2 / R2_6nt	2.9 nm
	7xR3 / R3_2	3.8 nm
	7xR4 / R4_6nt	2.9 nm
	5xR5 / R5	3.7 nm
	5xR6 / R6_6nt	3.8 nm
Figure 2 d, Extended Data Figure 6	5xR1 / R1	1.8 nm
Figure 2 e, Extended Data Figure 7	5xR1 / R1	4.0 nm
Extended Data Figure 8	2xR3 / R3	4.5 nm
	2xR4 / R4	4.7 nm
Figure 2 f and g, Extended Data Figure 9	5xR1 / R1	5.0 nm
	5xR2 / R2_6nt	4.9 nm
	7xR3 / R3	5.6 nm
	7xR4 / R4	4.8 nm

Supplementary References

1. Schueder, F. et al. An order of magnitude faster DNA-PAINT imaging by optimized sequence design and buffer conditions. *Nat Methods* **16**, 1101-1104 (2019).

4 Outlook

In this work, SOMAmers have been established as a group of small and quantitative binders for super-resolution microscopy. Furthermore, the multiplexing capability of DNA-PAINT has been advanced with a kinetic barcoding approach. Finally, improved sequence design using repetitive overlapping binding motifs lead to significant speed improvement. Of note, kinetic barcoding and repetitive binding sites can be readily implemented without additional costs and the need for improved hardware. However, the kinetic barcoding approach in cells is challenging because it requires distinct spatial separation, thus ideally single molecule resolution, to identify unique kinetic fingerprints after post-processing. The combination of using small binders, improved repetitive binding sites with kinetic barcodes can help to increase the resolution and achieve sufficient separation for the extraction of distinct kinetic traces. Moreover, the use of repetitive binding sites can be combined with other approaches that enhance DNA-PAINT's imaging speed such as fluorogenic probes and using Argonaut protein-assisted imager strands [45, 47].

Despite these technical advances, multiplexing capabilities combined with molecular resolution are yet limited by the availability of small high-affinity binders suitable for cell labeling. So far, nanobodies, Affimers, and SOMAmers have extended the binder portfolio that had primarily consisted of antibodies. However, only a few examples out of each category have been demonstrated to work for super-resolution imaging. Therefore, a systematic screening of all available binders out of each category is necessary to build a large portfolio. Moreover, other binder categories need to be explored and tested for application in super-resolution microscopy. In the following paragraph, I will introduce two binder categories that provide promising features for potentially suitable binders: DARPins and Affibodies. Furthermore, I will propose an approach to screen labeling probes in a high-throughput fashion and with subsequent validation of preselected binders.

Designed ankyrin repeat proteins (DARPins) are a promising class of molecules to be applied as labeling probes for super-resolution microscopy. Similar to nanobodies, they are small (~33 amino acids per repeat) and display high binding affinities. DARPins are based on ankyrin repeat proteins composed of tightly packed repeats, each forming a beta turn followed by two antiparallel alpha helices [121]. An improved version, called loopDARPins, with high affinities down to 30 pM have been isolated after a single round of ribosome display, as their modified

scaffold has a larger surface to interact with a target [122]. DARPins do not contain any cysteine, proline, and glycine residues, meaning that a unique cysteine can be inserted for site-specific and quantitative modification with DNA or fluorophores. Therefore, the same labeling chemistries and purification procedures can be applied as previously described for nanobodies and Affimers [108]. Furthermore, bacterial expression and purification via metal ion chromatography are simple to perform and ensure consistent quality.

Another group of antibody mimetic based on a protein scaffold are Affibodies. Originally, the Affibody scaffold corresponded to the IgG-binding Z domain of protein A, which consists of ~56 amino acids of three alpha helices, containing 13 randomized amino acids located in two alpha helices [123]. The scaffold was then optimized, leading to the selection of highly stable and affine binders [124-126]. Affibodies have excellent properties as potential binders for super-resolution microscopy since they are small (~6 kDa), stable, and can be site-specifically modified via a unique cysteine. Figure 17 displays preliminary DNA-PAINT data using an Affibody as a binder. In this data, a commercially available affibody specific to EGFR (Abcam, ab95116) was coupled to a DNA-PAINT docking strand and incubated with untreated and EGF ligand treated cells. Since oligomerization was only observed in treated cells, we can deduce that the labeling of EGFR was specific.

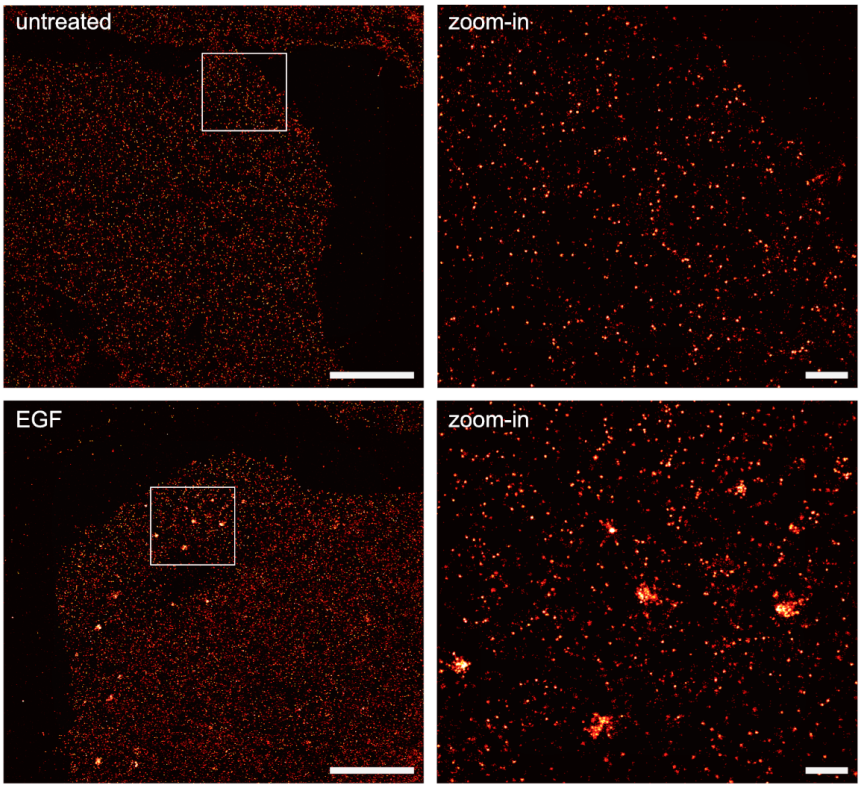

Figure 17: DNA-PAINT imaging of EGFR labeling with an Affibody. An EGFR specific Affibody was conjugated to a DNA-PAINT docking strand (5xR1) and used to stain A549 cells. In untreated cells (top row) no distinct oligomerization is detected. Upon treatment with the ligand EGF (bottom row), receptor oligomerization can be observed, indicating specific labeling by the affibody. Scale bars: 5 µm (left), 500 nm (right).

A long-term goal for highly multiplexed imaging is to establish a library of validated labeling probes. For efficient and precise validation, a systematic screening procedure needs to be established. Ideally, each binder would be tested and compared to a ground-truth control where close to 100 % of the protein of interest would be labeled. This could be accomplished using genetic-engineering approaches based on CRISPR-Cas9 to create homozygous knock-in cell lines [127]. Nanobodies against ALFA and GFP tags have been previously demonstrated as robust labeling probes with high labeling efficiencies [85, 102]. Both tags can be combined and genetically incorporated into the protein of interest to potentially obtain nearly 100 % labeling efficiency. This would enable accurate measurements of absolute labeling efficiencies of binders as well as their off-target binding. Knowing these parameters will pave the way to a more precise counting and absolute quantification of proteins. In practice, an efficient screening procedure could be carried out in two steps: First, a high-throughput binder evaluation would be performed with diffraction-limited resolution. Here, the GFP signal would be compared to the binder carrying a fluorophore. This step will also include the optimization of sample preparation protocols such as binder concentration and cell fixation conditions. In a second screening step, the qualified binders from previous selection rounds will be subjected

to DNA-PAINT super-resolution imaging. The colocalization of each binder to the GFP/ALFA-tag nanobodies will then be evaluated, ideally on a single-molecule scale. Finally, each binder will obtain an evaluation score to quantify the labeling efficiency and binding specificity.

5 References

1. Jablonski, A., *Efficiency of Anti-Stokes Fluorescence in Dyes*. Nature, 1933, **131**(3319), 839-840.
2. Lakowicz, J.R., *Fluorophores*, in *Principles of Fluorescence Spectroscopy*. 2006, Springer US: Boston, MA, 63-95.
3. Cooper, M., et al., *Cy3B: improving the performance of cyanine dyes.* J Fluoresc, 2004, **14**(2), 145-150.
4. Abbe, E., *Beiträge zur Theorie des Mikroskops und der mikroskopischen Wahrnehmung.* Archiv für Mikroskopische Anatomie, 1873, **9**, 413-468.
5. Rayleigh, *XXXI. Investigations in optics, with special reference to the spectroscope.* The London, Edinburgh, and Dublin Philosophical Magazine and Journal of Science, 1879, **8**(49), 261-274.
6. Rayleigh, *XV.On the theory of optical images, with special reference to the microscope.* The London, Edinburgh, and Dublin Philosophical Magazine and Journal of Science, 1896, **42**(255), 167-195.
7. Fish, K.N., *Total internal reflection fluorescence (TIRF) microscopy.* Curr Protoc Cytom, 2009, **Chapter 12**, Unit12 18.
8. Funatsu, T., et al., *Imaging of single fluorescent molecules and individual ATP turnovers by single myosin molecules in aqueous solution.* Nature, 1995, **374**(6522), 555-559.
9. Axelrod, D., *Chapter 9 Total Internal Reflection Fluorescence Microscopy*, in *Fluorescence Microscopy of Living Cells in Culture Part B. Quantitative Fluorescence Microscopy—Imaging and Spectroscopy*. 1989, Elsevier, 245-270.
10. Tokunaga, M., et al., *Single molecule imaging of fluorophores and enzymatic reactions achieved by objective-type total internal reflection fluorescence microscopy.* Biochem Biophys Res Commun, 1997, **235**, 47-53.
11. Burghardt, T.P., *Measuring incidence angle for through-the-objective total internal reflection fluorescence microscopy.* J Biomed Opt, 2012, **17**(12), 126007.

12. Tokunaga, M., et al., *Highly inclined thin illumination enables clear single-molecule imaging in cells.* Nat Methods, 2008, **5**(2), 159-161.

13. Hell, S.W. and Wichmann, J., *Breaking the diffraction resolution limit by stimulated emission: stimulated-emission-depletion fluorescence microscopy.* Opt Lett, 1994, **19**(11), 780-782.

14. Klar, T.A., et al., *Fluorescence microscopy with diffraction resolution barrier broken by stimulated emission.* Proc Natl Acad Sci U S A, 2000, **97**(15), 8206-8210.

15. Huang, B., et al., *Super-resolution fluorescence microscopy.* Annu Rev Biochem, 2009, **78**, 993-1016.

16. Westphal, V. and Hell, S.W., *Nanoscale resolution in the focal plane of an optical microscope.* Phys Rev Lett, 2005, **94**(14), 143903.

17. Yildiz, A. and Selvin, P.R., *Fluorescence imaging with one nanometer accuracy: application to molecular motors.* Acc Chem Res, 2005, **38**(7), 574-582.

18. Thompson, R.E., et al., *Precise nanometer localization analysis for individual fluorescent probes.* Biophys J, 2002, **82**(5), 2775-2783.

19. Betzig, E., et al., *Imaging intracellular fluorescent proteins at nanometer resolution.* Science, 2006, **313**(5793), 1642-1645.

20. Ando, R., et al., *Regulated fast nucleocytoplasmic shuttling observed by reversible protein highlighting.* Science, 2004, **306**(5700), 1370-1373.

21. Rust, M.J., et al., *Sub-diffraction-limit imaging by stochastic optical reconstruction microscopy (STORM).* Nat Methods, 2006, **3**(10), 793-795.

22. Heilemann, M., et al., *Subdiffraction-resolution fluorescence imaging with conventional fluorescent probes.* Angew Chem Int Ed Engl, 2008, **47**(33), 6172-6176.

23. Balzarotti, F., et al., *Nanometer resolution imaging and tracking of fluorescent molecules with minimal photon fluxes.* Science, 2017, **355**(6325), 606-612.

24. Gwosch, K.C., et al., *MINFLUX nanoscopy delivers 3D multicolor nanometer resolution in cells.* Nat Methods, 2020, **17**(2), 217-224.

25. Kao, H.P. and Verkman, A.S., *Tracking of single fluorescent particles in three dimensions: use of cylindrical optics to encode particle position.* Biophysical Journal, 1994, **67**(3), 1291-1300.

26. Huang, B., et al., *Three-dimensional super-resolution imaging by stochastic optical reconstruction microscopy.* Science, 2008, **319**(5864), 810-813.

27. Sharonov, A. and Hochstrasser, R.M., *Wide-field subdiffraction imaging by accumulated binding of diffusing probes.* Proc Natl Acad Sci U S A, 2006, **103**(50), 18911-18916.

28. Jungmann, R., et al., *Single-molecule kinetics and super-resolution microscopy by fluorescence imaging of transient binding on DNA origami.* Nano Lett, 2010, **10**(11), 4756-4761.

29. Dai, M., et al., *Optical imaging of individual biomolecules in densely packed clusters.* Nat Nanotechnol, 2016, **11**(9), 798-807.

30. Schnitzbauer, J., et al., *Super-resolution microscopy with DNA-PAINT.* Nat Protoc, 2017, **12**(6), 1198-1228.

31. SantaLucia, J., Jr. and Hicks, D., *The thermodynamics of DNA structural motifs.* Annu Rev Biophys Biomol Struct, 2004, **33**, 415-440.

32. Alberty, R.A. and Hammes, G.G., *Application of the Theory of Diffusion-controlled Reactions to Enzyme Kinetics.* The Journal of Physical Chemistry, 2002, **62**(2), 154-159.

33. Jungmann, R., et al., *Multiplexed 3D cellular super-resolution imaging with DNA-PAINT and Exchange-PAINT.* Nat Methods, 2014, **11**(3), 313-318.

34. Agasti, S.S., et al., *DNA-barcoded labeling probes for highly multiplexed Exchange-PAINT imaging.* Chem Sci, 2017, **8**(4), 3080-3091.

35. Beater, S., et al., *Simple and aberration-free 4color-STED--multiplexing by transient binding.* Opt Express, 2015, **23**(7), 8630-8638.

36. Schueder, F., et al., *Universal Super-Resolution Multiplexing by DNA Exchange.* Angew Chem Int Ed Engl, 2017, **56**(14), 4052-4055.

37. Wang, Y., et al., *Rapid Sequential in Situ Multiplexing with DNA Exchange Imaging in Neuronal Cells and Tissues.* Nano Lett, 2017, **17**(10), 6131-6139.

38. Jungmann, R., et al., *Quantitative super-resolution imaging with qPAINT.* Nat Methods, 2016, **13**(5), 439-442.

39. Jayasinghe, I., et al., *True Molecular Scale Visualization of Variable Clustering Properties of Ryanodine Receptors.* Cell Rep, 2018, **22**(2), 557-567.

40. Auer, A., et al., *Fast, Background-Free DNA-PAINT Imaging Using FRET-Based Probes.* Nano Lett, 2017, **17**(10), 6428-6434.

41. Lee, J., et al., *Accelerated super-resolution imaging with FRET-PAINT.* Mol Brain, 2017, **10**, 63.

42. Lee, J., et al., *Accelerated FRET-PAINT microscopy.* Mol Brain, 2018, **11**, 70.

43. Schickinger, M., et al., *Tethered multifluorophore motion reveals equilibrium transition kinetics of single DNA double helices.* Proc Natl Acad Sci U S A, 2018, **115**(32), E7512-E7521.

44. Schueder, F., et al., *An order of magnitude faster DNA-PAINT imaging by optimized sequence design and buffer conditions.* Nat Methods, 2019, **16**(11), 1101-1104.

45. Filius, M., et al., *High-Speed Super-Resolution Imaging Using Protein-Assisted DNA-PAINT.* Nano Lett, 2020, **20**(4), 2264-2270.

46. Cui, T.J., et al., *Argonaute bypasses cellular obstacles without hindrance during target search.* Nat Commun, 2019, **10**, 4390.

47. Chung, K.K.H., et al., *Fluorogenic probe for fast 3D whole-cell DNA-PAINT.* PrebioRxiv, 2020, DOI: 10.1101/2020.04.29.066886.

48. Watson, J.D. and Crick, F.H., *Molecular structure of nucleic acids; a structure for deoxyribose nucleic acid.* Nature, 1953, **171**(4356), 737-738.

49. Narayana, N. and Weiss, M.A., *Crystallographic analysis of a sex-specific enhancer element: sequence-dependent DNA structure, hydration, and dynamics.* J Mol Biol, 2009, **385**(2), 469-490.

50. Seeman, N.C., *Nucleic acid junctions and lattices.* J Theor Biol, 1982, **99**(2), 237-247.

51. Chen, J.H. and Seeman, N.C., *Synthesis from DNA of a molecule with the connectivity of a cube.* Nature, 1991, **350**(6319), 631-633.

52. Rothemund, P.W., *Folding DNA to create nanoscale shapes and patterns.* Nature, 2006, **440**(7082), 297-302.

53. Douglas, S.M., et al., *Self-assembly of DNA into nanoscale three-dimensional shapes.* Nature, 2009, **459**(7245), 414-418.

54. Wagenbauer, K.F., et al., *Gigadalton-scale shape-programmable DNA assemblies.* Nature, 2017, **552**(7683), 78-83.

55. Douglas, S.M., et al., *Rapid prototyping of 3D DNA-origami shapes with caDNAno.* Nucleic Acids Research, 2009, **37**(15), 5001-5006.

56. Steinhauer, C., et al., *DNA origami as a nanoscopic ruler for super-resolution microscopy.* Angew Chem Int Ed Engl, 2009, **48**(47), 8870-8873.

57. Schmied, J.J., et al., *Fluorescence and super-resolution standards based on DNA origami.* Nat Methods, 2012, **9**(12), 1133-1134.

58. Schmied, J.J., et al., *DNA origami nanopillars as standards for three-dimensional superresolution microscopy.* Nano Lett, 2013, **13**(2), 781-785.

59. Dey, S., et al., *DNA origami.* Nature Reviews Methods Primers, 2021, **1**, 13.

60. Schlichthaerle, T., et al., *DNA nanotechnology and fluorescence applications.* Curr Opin Biotechnol, 2016, **39**, 41-47.

61. Prendergast, F.G. and Mann, K.G., *Chemical and physical properties of aequorin and the green fluorescent protein isolated from Aequorea forskalea.* Biochemistry, 1978, **17**(17), 3448-3453.

62. Shaner, N.C., et al., *A guide to choosing fluorescent proteins.* Nat Methods, 2005, **2**(12), 905-909.

63. Keppler, A., et al., *Labeling of fusion proteins of O6-alkylguanine-DNA alkyltransferase with small molecules in vivo and in vitro.* Methods, 2004, **32**(4), 437-444.

64. Keppler, A., et al., *Labeling of fusion proteins with synthetic fluorophores in live cells.* Proc Natl Acad Sci U S A, 2004, **101**(27), 9955-9959.

65. Los, G.V., et al., *HaloTag: a novel protein labeling technology for cell imaging and protein analysis.* ACS Chem Biol, 2008, **3**(6), 373-382.

66. Mahen, R., et al., *Comparative assessment of fluorescent transgene methods for quantitative imaging in human cells.* Mol Biol Cell, 2014, **25**(22), 3610-3618.

67. Wood, A.J., et al., *Targeted genome editing across species using ZFNs and TALENs.* Science, 2011, **333**(6040), 307.

68. Ran, F.A., et al., *Genome engineering using the CRISPR-Cas9 system.* Nat Protoc, 2013, **8**(11), 2281-2308.

69. Whelan, D.R. and Bell, T.D., *Image artifacts in single molecule localization microscopy: why optimization of sample preparation protocols matters.* Sci Rep, 2015, **5**, 7924.

70. Im, K., et al., *An Introduction to Performing Immunofluorescence Staining*, in *Methods in Molecular Biology*. 2019, Springer New York, 299-311.

71. Opazo, F., et al., *Aptamers as potential tools for super-resolution microscopy.* Nat Methods, 2012, **9**(10), 938-939.

72. Gupta, S., et al., *Rapid histochemistry using slow off-rate modified aptamers with anionic competition.* Appl Immunohistochem Mol Morphol, 2011, **19**(3), 273-278.

73. Carrington, G., et al., *Exploiting nanobodies and Affimers for superresolution imaging in light microscopy.* Mol Biol Cell, 2019, **30**(22), 2737-2740.

74. Harris, L.J., et al., *Refined structure of an intact IgG2a monoclonal antibody.* Biochemistry, 1997, **36**(7), 1581-1597.

75. Uhlen, M., et al., *A human protein atlas for normal and cancer tissues based on antibody proteomics.* Mol Cell Proteomics, 2005, **4**(12), 1920-1932.

76. Thul, P.J., et al., *A subcellular map of the human proteome.* Science, 2017, **356**(6340), eaal3321.

77. Rousseaux, J., et al., *Optimal conditions for the preparation of Fab and F(ab')2 fragments from monoclonal IgG of different rat IgG subclasses.* J Immunol Methods, 1983, **64**, 141-146.

78. Hamers-Casterman, C., et al., *Naturally occurring antibodies devoid of light chains.* Nature, 1993, **363**(6428), 446-448.

79. Beghein, E. and Gettemans, J., *Nanobody Technology: A Versatile Toolkit for Microscopic Imaging, Protein-Protein Interaction Analysis, and Protein Function Exploration.* Front Immunol, 2017, **8**, 771.

80. Pleiner, T., et al., *Nanobodies: site-specific labeling for super-resolution imaging, rapid epitope-mapping and native protein complex isolation.* Elife, 2015, **4**, e11349.

81. Gonzalez-Sapienza, G., et al., *Single-Domain Antibodies As Versatile Affinity Reagents for Analytical and Diagnostic Applications.* Front Immunol, 2017, **8**, 977.

82. Platonova, E., et al., *Single-molecule microscopy of molecules tagged with GFP or RFP derivatives in mammalian cells using nanobody binders.* Methods, 2015, **88**, 89-97.

83. Ries, J., et al., *A simple, versatile method for GFP-based super-resolution microscopy via nanobodies.* Nat Methods, 2012, **9**(6), 582-584.

84. Virant, D., et al., *A peptide tag-specific nanobody enables high-quality labeling for dSTORM imaging.* Nat Commun, 2018, **9**, 930.

85. Gotzke, H., et al., *The ALFA-tag is a highly versatile tool for nanobody-based bioscience applications.* Nat Commun, 2019, **10**, 4403.

86. Sograte-Idrissi, S., et al., *Circumvention of common labelling artefacts using secondary nanobodies.* Nanoscale, 2020, **12**(18), 10226-10239.

87. Pleiner, T., et al., *A toolbox of anti-mouse and anti-rabbit IgG secondary nanobodies.* J Cell Biol, 2018, **217**(3), 1143-1154.

88. Tuerk, C. and Gold, L., *Systematic evolution of ligands by exponential enrichment: RNA ligands to bacteriophage T4 DNA polymerase.* Science, 1990, **249**(4968), 505-510.

89. Ellington, A.D. and Szostak, J.W., *In vitro selection of RNA molecules that bind specific ligands.* Nature, 1990, **346**(6287), 818-822.

90. Ni, S., et al., *Recent Progress in Aptamer Discoveries and Modifications for Therapeutic Applications.* ACS Appl Mater Interfaces, 2021, **13**(8), 9500-9519.

91. Wang, T., et al., *Three decades of nucleic acid aptamer technologies: Lessons learned, progress and opportunities on aptamer development.* Biotechnol Adv, 2019, **37**, 28-50.

92. Gold, L., et al., *Aptamer-based multiplexed proteomic technology for biomarker discovery.* PLoS One, 2010, **5**(12), e15004.

93. Ramaraj, T., et al., *Antigen-antibody interface properties: composition, residue interactions, and features of 53 non-redundant structures.* Biochim Biophys Acta, 2012, **1824**(3), 520-532.

94. Rohloff, J.C., et al., *Nucleic Acid Ligands With Protein-like Side Chains: Modified Aptamers and Their Use as Diagnostic and Therapeutic Agents.* Mol Ther Nucleic Acids, 2014, **3**, e201.

95. Jankowski, W., et al., *Modified aptamers as reagents to characterize recombinant human erythropoietin products.* Sci Rep, 2020, **10**, 18593.

96. Berman, H.M., et al., *The Protein Data Bank.* Nucleic Acids Research, 2000, **28**, 235-242.

97. Gelinas, A.D., et al., *Crystal structure of interleukin-6 in complex with a modified nucleic acid ligand.* Journal of Biological Chemistry, 2014, **289**(12), 8720-8734.

98. Sehnal, D.a.R., Alexander and Koca, Jaroslav and Burley, Stephen and Velankar, Sameer, *Mol*: Towards a Common Library and Tools for Web Molecular Graphics*, J.B.a.M.K.a.B. Sommer, Editor. 2018, The Eurographics Association.

99. Gomes de Castro, M.A., et al., *Aptamers provide superior stainings of cellular receptors studied under super-resolution microscopy.* PLoS One, 2017, **12**(2), e0173050.

100. Sograte-Idrissi, S., et al., *Nanobody Detection of Standard Fluorescent Proteins Enables Multi-Target DNA-PAINT with High Resolution and Minimal Displacement Errors.* Cells, 2019, **8**, 48.

101. Nieves, D.J., et al., *tagPAINT: covalent labelling of genetically encoded protein tags for DNA-PAINT imaging.* R Soc Open Sci, 2019, **6**(12), 191268.

102. Thevathasan, J.V., et al., *Nuclear pores as versatile reference standards for quantitative superresolution microscopy.* Nat Methods, 2019, **16**(10), 1045-1053.

103. Schlichthaerle, T., et al., *Direct Visualization of Single Nuclear Pore Complex Proteins Using Genetically-Encoded Probes for DNA-PAINT.* Angew Chem Int Ed Engl, 2019, **58**(37), 13004-13008.

104. Moore, R.P. and Legant, W.R., *Improving probes for super-resolution.* Nat Methods, 2018, **15**(9), 659-660.

105. Kalkhof, S. and Sinz, A., *Chances and pitfalls of chemical cross-linking with amine-reactive N-hydroxysuccinimide esters.* Anal Bioanal Chem, 2008, **392**, 305-312.

106. Agard, N.J., et al., *A strain-promoted [3 + 2] azide-alkyne cycloaddition for covalent modification of biomolecules in living systems.* J Am Chem Soc, 2004, **126**(46), 15046-15047.

107. Mukhortava, A. and Schlierf, M., *Efficient Formation of Site-Specific Protein-DNA Hybrids Using Copper-Free Click Chemistry.* Bioconjug Chem, 2016, **27**(7), 1559-1563.

108. Schlichthaerle, T., et al., *Site-Specific Labeling of Affimers for DNA-PAINT Microscopy.* Angew Chem Int Ed Engl, 2018, **57**(34), 11060-11063.

109. Wals, K. and Ovaa, H., *Unnatural amino acid incorporation in E. coli: current and future applications in the design of therapeutic proteins.* Front Chem, 2014, **2**, 15.

110. Guimaraes, C.P., et al., *Site-specific C-terminal and internal loop labeling of proteins using sortase-mediated reactions.* Nat Protoc, 2013, **8**(9), 1787-1799.

111. Yin, J., et al., *Genetically encoded short peptide tag for versatile protein labeling by Sfp phosphopantetheinyl transferase.* Proc Natl Acad Sci U S A, 2005, **102**(44), 15815-15820.

112. Femino, A.M., et al., *Visualization of single RNA transcripts in situ.* Science, 1998, **280**(5363), 585-590.

113. Raj, A., et al., *Imaging individual mRNA molecules using multiple singly labeled probes.* Nat Methods, 2008, **5**(10), 877-879.

114. Orjalo, A., et al., *Stellaris™ fluorescence in situ hybridization (FISH) probes: a powerful tool for mRNA detection.* Nature Methods, 2011, **8**(10), i-ii.

115. Beliveau, B.J., et al., *Versatile design and synthesis platform for visualizing genomes with Oligopaint FISH probes.* Proc Natl Acad Sci U S A, 2012, **109**(52), 21301-21306.

116. Beliveau, B.J., et al., *Single-molecule super-resolution imaging of chromosomes and in situ haplotype visualization using Oligopaint FISH probes.* Nat Commun, 2015, **6**(1), 7147.

117. Beliveau, B.J., et al., *In Situ Super-Resolution Imaging of Genomic DNA with OligoSTORM and OligoDNA-PAINT*, in *Methods in Molecular Biology*. 2017, Springer New York, 231-252.

118. Strauss, S., et al., *Modified aptamers enable quantitative sub-10-nm cellular DNA-PAINT imaging.* Nat Methods, 2018, **15**(9), 685-688.

119. Wade, O.K., et al., *124-Color Super-resolution Imaging by Engineering DNA-PAINT Blinking Kinetics.* Nano Lett, 2019, **19**(4), 2641-2646.

120. Strauss, S. and Jungmann, R., *Up to 100-fold speed-up and multiplexing in optimized DNA-PAINT.* Nat Methods, 2020, **17**(8), 789-791.

121. Li, J., et al., *Ankyrin repeat: a unique motif mediating protein-protein interactions.* Biochemistry, 2006, **45**(51), 15168-15178.

122. Schilling, J., et al., *From DARPins to LoopDARPins: Novel LoopDARPin Design Allows the Selection of Low Picomolar Binders in a Single Round of Ribosome Display.* Journal of Molecular Biology, 2014, **426**(3), 691-721.

123. Nord, K., et al., *Binding proteins selected from combinatorial libraries of an alpha-helical bacterial receptor domain.* Nature Biotechnology, 1997, **15**(8), 772-777.

124. Feldwisch, J., et al., *Design of an optimized scaffold for affibody molecules.* J Mol Biol, 2010, **398**(2), 232-247.

125. Kronqvist, N., et al., *Combining phage and staphylococcal surface display for generation of ErbB3-specific Affibody molecules.* Protein Eng Des Sel, 2011, **24**(4), 385-396.

126. Frejd, F.Y. and Kim, K.T., *Affibody molecules as engineered protein drugs.* Exp Mol Med, 2017, **49**(3), e306.

127. Koch, B., et al., *Generation and validation of homozygous fluorescent knock-in cells using CRISPR-Cas9 genome editing.* Nat Protoc, 2018, **13**(6), 1465-1487.

Acknowledgements

First, I would like to thank Ralf Jungmann, for accepting me as a PhD student and being a great mentor. It was exciting to work on these projects and improving the DNA-PAINT technique.

I want to thank Veit Hornung for being my internal supervisor at the faculty of chemistry and pharmacy of the LMU.

Many thanks to all Jungmann lab members for a motivating work atmosphere and all your support. I have learned a lot from you guys.

- Thanks to the microscope crew, Alexander, Florian, Maximilian, Mahipal, Eduard and Jürgen, for keeping the microscopes in their best possible states
- Thanks to Maximilian and Jörg for writing and maintaining the Picasso data analysis software that has made data analysis so convenient
- Thanks to Thomas and Alexandra for the fun time in the cool room and the great help with the binder conjugations
- Thanks to Alexandra and Jürgen for proofreading my thesis

I would like to thank all my fantastic collaborators, especially Shashi and Nebojsa for sharing the SOMAmer reagents and your support on the project. Thank you, Alex, for the amazing coffee and the fun exchange imaging sessions with the Leica microscope.

I also want to thank the QBM graduate school for the support and organizing workshops and retreats.

Thank you, Melissa, for the wonderful time in the last years and for your understanding when I sometimes spent long days in the lab.

Finally, I want to thank my family for your support throughout my entire life and for constantly believing in me.